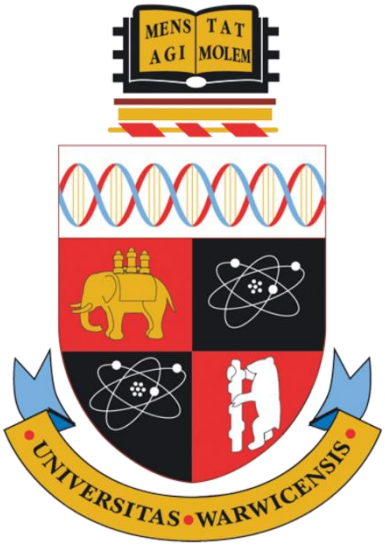

Post-Modification Strategies for Polymeric Cyclic Peptide Nanotubes

Tammie Rose Barlow

A thesis submitted in partial fulfilment of the requirements for the degree of

Doctor of Philosophy in Chemistry

Department of Chemistry

University of Warwick

July 2017

The more you know, the more you know you don't know.

- Aristotle

It is finished.

- Jesus Christ

Table of Contents

List of Figures

List of Tables

List of Schemes

Abbreviations

4,4′-Azobis(4-cyanovaleric acid)	ACVA
Atomic force microscopy	AFM
Atom transfer radical polymerisation	ATRP
Butyl acrylate	BA
Bromo ethyl acrylate	BEA
deuterated chloroform	$CDCl_3$
Cyclic peptide	CP
cyclic peptide [poly(bromo ethyl acrylate)]$_2$	CP-[pBEA_n]$_2$
cyclic peptide [poly(thioglucose ethyl acrylate)] $_2$	CP-[p*Glu*EA_n]$_2$
cyclic peptide [poly(thioglycerol ethyl acrylate)] $_2$	CP-[p*Glu*EA_n]$_2$
cyclic peptide [poly(trimethyl ammonium ethyl acrylate)] $_2$	CP-[p$TMAEA_n$]$_2$
cyclic peptide [poly(trimethyl phosphonium ethyl acrylate)] $_2$	CP-[p$TMPEA_n$]$_2$
(4-Cyano pentanoic acid)yl ethyl trithiocarbonate	CPAETC
Cyclic Peptide Nanotube	CPNT
Chain Transfer Agent	CTA
Copper Azide Alkyne Cycloaddition	CuAAC
Dichloromethane	DCM
N,*N*-Diisopropylethylamine	DIPEA
Dynamic Light Scattering	DLS
Dimethylamino pyridine	DMAP
Dimethylformamide	DMF
Dimethylsulfoxide	DMSO
4-(4,6-Dimethoxy-1,3,5-triazin-2-yl)-4-methylmorpholinium	DMTMM
Degree of Polymerisation	DP
1-Ethyl-3-(3-dimethylaminopropyl)carbodiimide	EDC
Electrospray Ionisation Time of Flight	ESI ToF
Ethanol	EtOH

Fourier Transform Infrared Spectroscopy	FTIR
O-(Benzotriazole-1-yl)-*N,N,N',N*'-tetramethyluronium	HBTU
Hexafluoro-2-propanol	HFIP
High-performance liquid chromatography	HPLC
Infrared	IR
Association constant	K_a
Layer-by-layer	LbL
Leucine	Leu
Lysine	Lys
Methanol	MeOH
Megahertz	MHz
Number Average Molecular Weight	M_n
Molecular Weight	M_w
Molecular Weight Cut Off	MWCO
Avogadro's Number	*N*a
Number of Aggregation	N_{agg}
N-acryloyl morpholine	NAM
NIST Centre for Neutron Research	NCNR
N-hydroxysuccinimide	NHS
N-hydroxysuccinimide-(4-cyano pentanoic acid)yl ethyl Trithiocarbonate	NHS-CPAETC
N-isopropyl acrylamide	NiPAAm
National Institute of Standards and Technology	NIST
N-methyl morpholine	NMM
Nitroxide-mediated radical polymerisation	NMP
Nuclear Magnetic Resonance	NMR
Nanotube	NT
poly(azido ethyl acrylate)	pAEA
poly(bromo ethyl acrylate)	pBEA
Phosphate buffered saline	PBS

polyethylene glycol	PEG
poly(ethylene glycol) methyl ether acrylate	PEGA
poly(ethylene oxide)	PEO
poly(2-ethyl-2-oxazoline)	pEtOx
poly(thioglycerol ethyl acrylate)	p*Gly*EA
poly(methyl methacrylate)	pMMA
polystyrene	PS
poly(trimethyl ammonium ethyl acrylate)	pTMAEA
poly(trimethyl phosphonium ethyl acrylate)	pTMPEA
poly (thiophenol ethyl acrylate)	pTPEA
Wave vector	q
Reversible Addition Fragmentation chain-Transfer	RAFT
Reversible Deactivation Radical Polymerisations	RDRP
Radius of gyration	R_g
Hydrodynamic radius	R_h
Refractive Index	RI
Rayleigh ratio	R_θ
Small Angle Neutron Spectroscopy	SANS
Size Exclusion Chromatography	SEC
Single-Electron Transfer Living Radical Polymerisation	SET-LRP
Static Light Scattering	SLS
Solid Phase Peptide Synthesis	SPPS
Transmission electron microscopy	TEM
Trifluoro acetic acid	TFA
Tetrahydrofuran	THF
Triisopropylsilane	TIPS
Tryptophan	Trp
Ultra Violet-Visible	UV-Vis
Refractive Index	η

Acknowledgements

I can manage to write a thesis, and yet I can't seem to find the words to start thanking the many people who have helped me through these last few years! Hopefully I won't forget anyone, but if you feel left out, then you know you've helped.

First of all, I'd like to thank my supervisor Professor Sébastien Perrier, for giving me the opportunity of a life-time to move across the world to study in England! Without this opportunity I would be stuck in Sydney, with stunning weather, surrounded by beaches, family and friends. Fortunately, I was sent to Coventry where I have made wonderful friends and colleagues, travelled the world, and under your guidance have become the scientist I am today. Thank you for your unfailing ability to sell me my own project (even when it's going terribly wrong) and for patiently enduring the tearful breakdowns throughout my degree.

To my Chemistry teachers throughout the years: Ms Cheong and Mr Harris in high school, and at university, to Professor Kate Jolliffe, your enjoyable organic puzzles drew me to you as a supervisor. Thank you for giving me an opportunity all those years ago, without it, I would never be where I am today.

When I first began my degree in 2013, I had no friends on this side of the world. Fortunately, I landed in a wonderful group that became my friends and family over here. To my fellow soon to be doctors Liam and Sophie, thank you for always being there, for the copious amounts of beer and wine all over Australia and Europe and (to Junliang as well) thank you for being the best friends you could ever hope to have in your year with you!

In this time, so many wonderful post-docs have come and gone. Dr Johannes "Hanney" Brendel, thank you for being a wonderful friend and teacher. Without your ideas and support (and beer) my project would have taken a completely different path. Dr Sylvain Catrouillet, thank you for teaching me about scattering and how to maximise nap time. I will never forget your love of wrestling or sweet dance moves. Dr Raoul "Rourou" Peltier, while I've only known you a much shorter time, you've really managed to pack in the

fun times (you and your gorgeous fam too)! Your guidance and shenanigans are always appreciated. Ximo, you are a wonderful man, thank you for bringing sunshine and smiles into my life when you're around. Ming, thank you for teaching me all about cyclic peptides and for your unwavering enthusiasm for the pub on a Thursday afternoon. Dr Guillaume "GG" Gody, a masssiiiiiifff thank you for teaching me so much about RAFT, even if you never understood a word I was saying. Matthias, it's always a pleasure to be with you and your wonderful little family. Dr Ed, you are an incredible proof-reader and without you, this thesis wouldn't be what it is; thank you so much! Dr Kempe, thanks for all the spicy soup and the QCM chips. Dr Jon Newland, while I know you're not *my* post-doc, but thanks for teaching me how to keep it real as a PhD student.

To my loyal (to varying degrees) tea crew! May the summoning spoon ring on in your hearts. To the Perrier group, each and every one of you have been a pleasure to meet and work with these past years, thank you for your friendly faces each day in the corridor. To my football homies, thanks for all the laughs and bruises. To George, thank you for always smiling and cheering me up, even when it's 1 am and we're both still working.

I also met many students here who have become some of my best friends. Liam and Sophie for helping me make a home with you guys. Sophie, thanks for reminding me to save the trees when I print, to try to eat less meat, and to never be greedy around the cupcakes. To Julia, for the insanely delicious baking, and providing such tempting cupcakes and lunch leftovers. To Cookie, thank you for always being such a cheerful, happy-go-lucky guy and for always keeping us on our toes in the office. To the chatty rays of sunshine that are Julia and Aggie, it is always a pleasure seeing your smiling faces wandering into the office, I love your enthusiasm for life, tea and talking.

To Anthony's family, Tracey, Tina, Nanny, Ollie, Tash, Phil and *co.* thank you for welcoming me into your family and your lives. You have always made me feel completely welcomed and loved. The Sunday dinners were always great for a catch-up, and gave me a second family, while I've been so far away from my own.

To Anthony, without you I honestly don't know how I would have survived this far. Thank you for your constant patience and unwavering love. Thank you for holding me when I was upset because nothing had worked, for encouraging me whenever I thought I

was too stupid to be here, for convincing me I could do this when I felt like I couldn't and for reminding me there's so much more to life than a degree. I know it can't have been easy putting up with me, but I am so, so grateful that you did.

To my family, to my Mummy and Daddy, to my big blister Beth, to my Auntie Splat and John, to Nanna, to Chris and little Joshie (who I can't wait to meet!), to Jenny, Damien, Arwen and Poppy: I don't have the words to describe how difficult it has been not being able to be with you. Not a day has gone by that I haven't thought of you and missed you, and wished I could show you the life I have built here. Thank you for always believing in me. Thank you to my wonderful parents for loving me and supporting me completely and unconditionally, no matter which strange activity I take up. But in particular to my mum, thank you so much for coming to see me all the way over here. I know how hard you must have worked to get here to come and see me. I miss you all every day and I can't wait to see you all again soon!

Declaration

This thesis is submitted to the University of Warwick in support of my application for the degree of Doctor of Philosophy. It has been composed by myself and has not been submitted in any previous application for any degree. The experimental work contained in this thesis is original research carried out by the author, unless stated otherwise, in the Department of Chemistry at the University of Warwick.

The work presented was carried out by the author except in the following instances:

Chapter 5: XTT assays, cell uptake studies and fluorescence corrections were conducted by Dr. Raoul Peltier (University of Warwick, School of Life Science).

Date: _____ _____

Tammie Barlow

List of Publications

Parts of this thesis have been published by the author:

1. Poly(bromoethyl acrylate): A Reactive Precursor for the Synthesis of Functional RAFT Materials. **Barlow, T. R.**; Brendel, J. C.; Perrier, S. *Macromolecules* **2016,** 49, (17), 6203-6212.
2. Tunable Length of Cyclic Peptide–Polymer Conjugate Self-Assemblies in Water. Catrouillet, S.; Brendel, J. C.; Larnaudie, S.; **Barlow, T**.; Jolliffe, K. A.; Perrier, S. *ACS Macro Letters* **2016,** 5, (10), 1119-1123.
3. An Orthogonal Reaction Sequence for the Synthesis of Sugar-Coated Cyclic Peptide Nanotubes. **Barlow, T. R.**; Brendel, J. C.; Jolliffe, K. A.; Perrier, S. *Submitted for publication.*
4. The Effect of Ionic Strength on the Self-Assembly of Highly Charged Polyelectrolyte-Cyclic Peptide Conjugates. **Barlow, T. R.**; Brendel, J. C.; Mansfield, E. D. H.; Rogers, S. E.; Jolliffe, K. A.; Perrier, S. *Submitted for publication.*
5. Effect of Charge versus Self-Assembly on the Cellular Uptake of Cyclic Peptide-Polymer Nanotubes. **Barlow, T. R.**; Peltier, R.; Jolliffe, K. A.; Perrier, S. *In preparation.*

Abstract

Self-assembly is a powerful process by which complex architectures can be achieved from single monomer units for a diverse range in applications from drug delivery to nano-electronics, an excellent example of which is self-assembled cyclic peptide nanotubes. The addition of polymers greatly enhances the potential applications of cyclic peptide nanotubes, however, there lacks a fundamental understanding on how this affects assembly, and whether it can be controlled by environmental manipulation. Additionally, there are few synthetic methods by which it is possible to access more complex polymeric architectures without the need for complex conjugation strategies.

As such the present work aims to further develop a scope of synthetic possibilities for polymeric cyclic peptide nanotubes, generating materials by which it is possible to probe the self-assembly properties of these complex supramolecular systems. Initially the polymerisation of poly(bromo ethyl acrylate) (BEA) is explored *via* reversible addition-fragmentation chain transfer polymerisation (RAFT) and the post-modification possibilities this reactive polymeric precursor provides. From this, a library of polymer materials from a pBEA precursor *via* nucleophilic substitution with a range of nucleophiles can be generated.

From this, the reactive pBEA polymers are combined with self-assembling cyclic peptides, without any unwanted side reactions. The self-assembly of these CP-pBEA conjugates was characterised in solution by SANS and SLS. From the CP-pBEA conjugates, it is possible to generate a range of materials, and the self-assembly of various nanotubular systems can be studied. These materials include a glycopolymer conjugate that forms sugar coated nanotubes in water, as determined by SANS, and displays interesting lectin binding properties. Furthermore, synthesis of highly charged polyelectrolyte-peptide conjugates was be carried out. The self-assembly of these polyelectrolyte conjugates could be readily manipulated by controlling the ionic strength of the solution.

Finally, the cell-penetration of charged copolymers of poly(poly(ethylene glycol) methyl ether acrylate) (pPEGA) conjugates were studied to determine whether charge or self-assembly has a greater effect on cellular uptake. It was identified that self-assembly results in far greater *in vitro* cell penetration than for charged analogues.

This thesis in its entirety reflects a thorough design strategy for the synthesis of complex materials; from the development of novel synthetic strategies and post-polymerisation modifications, through to supramolecular characterisation and a finally demonstration of the materials as an application for drug delivery *in vitro*.

1

Introduction

Self-assembly is a powerful tool for the synthesis of complex materials. By carefully tailoring individual building blocks, supramolecular forces can be used to do the synthetic heavy-lifting for the difficult task of creating demanding and otherwise challenging structures. As such, a diverse range of morphologies can be formed including micelles, vesicles, nanotubes, and lamellar sheets. Nanotubular structures in particular have gained a lot of attention recently, for the interesting properties that arise from their shape.[1-6] Since their discovery in the 1990s, carbon nanotubes have championed the field of nanotube research,[7-9] with a lot of attention paid to their unique structural, mechanical and electronic properties. With the introduction of carbon nanotube synthesis in the early 1990s,[10] the interest in nanotubes has vastly increased. Unfortunately, poor solubility, toxicity, and lack of size uniformity is a major drawback for any specific biomedical applications. Many of the problems facing fullerene based nanotubular structures can fortunately be overcome by employing organic nanotubes that more closely mimic nature such as carbohydrates, lipids and polymer-based nanotubes. These nanotubes generally span the width region between 10 - 1000 nm; a scale that is inaccessible to top-down microfabrication techniques, nor carbon nanotube fabrication methods.[11] Thus the study and synthesis of polymeric based bottom-up self-assembly processes is essential to obtain functional nanostructures. As is so often the case, science can take inspiration from nature for the synthesis of organic nanotubes and supramolecular materials. Tobacco mosaic

virus for example, exists as a tubular structure comprising unimeric coat proteins that self-assemble into a rod-like helical structure around a single strand of RNA.[11, 12] Nanotubular structures have advantages over other nanoparticle architectures in biological systems, due to their anisotropy resulting in increased circulation times and altered internalisation kinetics *vs* spherical and cubic nanoparticles.[5, 6, 13, 14]

There are a number of intermolecular interactions by which supramolecular self-assembly can be guided, including van der Waals, electrostatic, π-π, and hydrogen bonding to name but a few.[15] Of these, hydrogen bonds are particularly noteworthy due to the directionality of their interaction, enabling intricate supramolecular assemblies. Though hydrogen bonds are weak (**Figure 1.1**),[16, 17] they are key to a number of biological interactions including DNA and RNA strand recognition, and protein folding. The cumulative strength of multiple hydrogen bonds in concert with other weak attractive forces, can lead to strong and stable complex architectures.[17, 18]

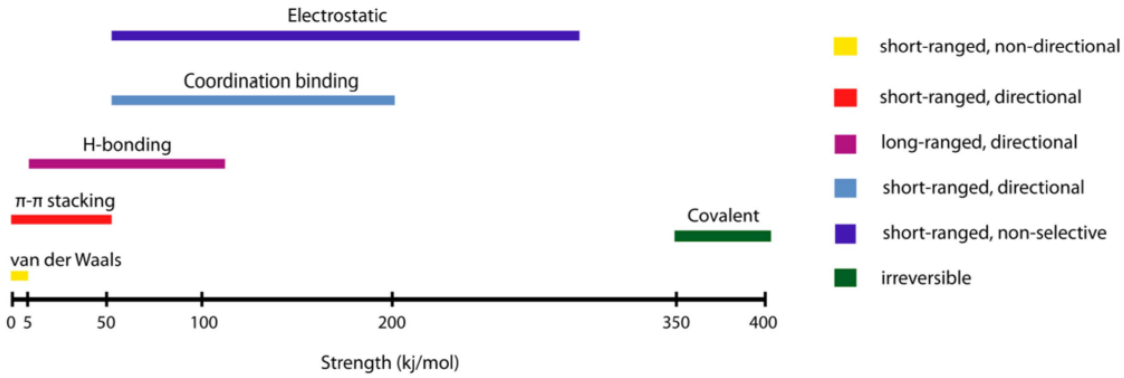

Figure 1.1: A comparison of the strength and properties of noncovalent interactions involved in self-assembly. Adapted from Guler *et al.*[17]

Numerous bio-molecules have been used in the preparation of nanotubes including DNA, lipids, carbohydrates, and peptides.[11] Of these examples, peptides in particular are an attractive building block due to the ease with which the sequence can be modified and tailored towards a specific application. Alteration of the amino acid sequence in linear peptides allows for tuning the function and efficacy of the obtained material; a prime example of which is Gramicidin. Gramicidin A is perhaps one of the best know examples of linear peptides coiling into nanotubular structures of β-helices.[19] Comprising

alternating L- and D- amino acids, Gramicidin has been extensively studied for its membrane transport properties.[20] Studies have revealed that it is highly sensitive to structural alterations, and varying a single amino acid in the peptide sequence (Gramicidin A, B, and C variants) results in a subtly different supramolecular conformation, leading to different membrane interactions.[19]

1.1 Self-assembling Cyclic Peptides

β-sheet forming cyclic peptides are a remarkable example of synthetic nanotube forming materials. By tailoring the chemical structure of the cyclic peptide, the properties of the supramolecular structure can be altered. In this way the building blocks can be adjusted to tailor the nanotube properties to meet the requirements for the desired application. Self-assembling cyclic peptides have thus become of particular interest as nanomaterial scaffolds in a range of fields from biomedical applications such as antimicrobials,[21-23] biosensors,[24] to nanoelectronics.[25-28]

1.1.1 Self-Assembly

The potential of cyclic peptides comprised of alternating L- and D- α-amino acids to self-assemble was first realised by De Santis and co-workers in 1974.[29] In their theoretical study, they found that the backbone C=O and N-H bonds point in opposite directions and were nearly parallel to the symmetry of the ring (**Scheme 1.1**). They postulated that the direction of the backbone amide bonds would lead to inter-annular stabilisation that may result in a contiguous parallel or antiparallel β-sheet structure. It wasn't until 1993 that the first self-assembling cyclic peptide was synthesised by Ghadiri *et al*;[30] whereby they assembled the *cyclo*[-D-Ala-L-Glu-D-Ala-L-Gln-]$_2$ peptide into nanotubes by controlled acidification. Their characterisation of the nanotubes by electron diffraction[30, 31] suggested that the nanotubes formed an antiparallel β-sheet-like structure with an inter-unit spacing of 4.73 Å. Subsequent molecular dynamics[32] and dimerisation studies[33-36] corroborate that an antiparallel β-sheet structure is the most energetically favourable conformation by 0.8 kcal· mol^{-1} over the parallel arrangement.[34]

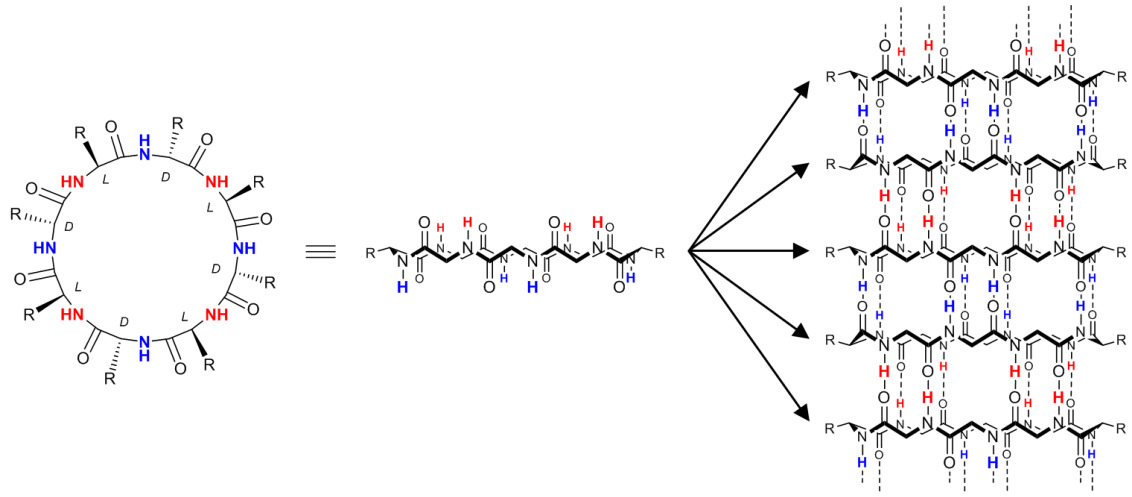

Scheme 1.1: Scheme highlighting the directionality of the amide bonds in the backbone of CPs of alternating L/D α-amino acids in an octapeptide. Hydrogen bonding allows CP units to self-assemble in an antiparallel β-sheet conformation.

In recent work by Silk *et al.*, the first crystal structure of any continuous nanotube, rather than a simple *N*-alkylated CP-dimer, was analysed.[37] In their work, the authors crystallised two cyclic octapeptides of alternating D- and L- α-amino acids comprising similar peptide sequences (**Scheme 1.2**). Remarkably, despite the similarity in the peptide sequence, the crystal structure revealed that the leucine bearing CPs formed nanotubes *via* an antiparallel β-sheet assembly, with CPs adopting two different conformations to facilitate stacking (**Scheme 1.2A**). The alanine bearing CP, however was present in only a single conformation, and adopted a parallel assembly (**Scheme 1.2B**). Despite the parallel conformation being a less favourable structure, the literature on Cyclic Peptide Nanotubes (CPNTs) has always assumed that nanotube formation is antiparallel. The antiparallel assumption has been based on computational modelling and model systems of *N*-methylated CP structures, however this new work highlights the importance of studying the continuous hydrogen bonded network. These crystal structures clearly demonstrate that assembly *via* parallel stacking is possible, despite being less energetically favourable, and should be considered as a mechanism for CPNT formation in future.

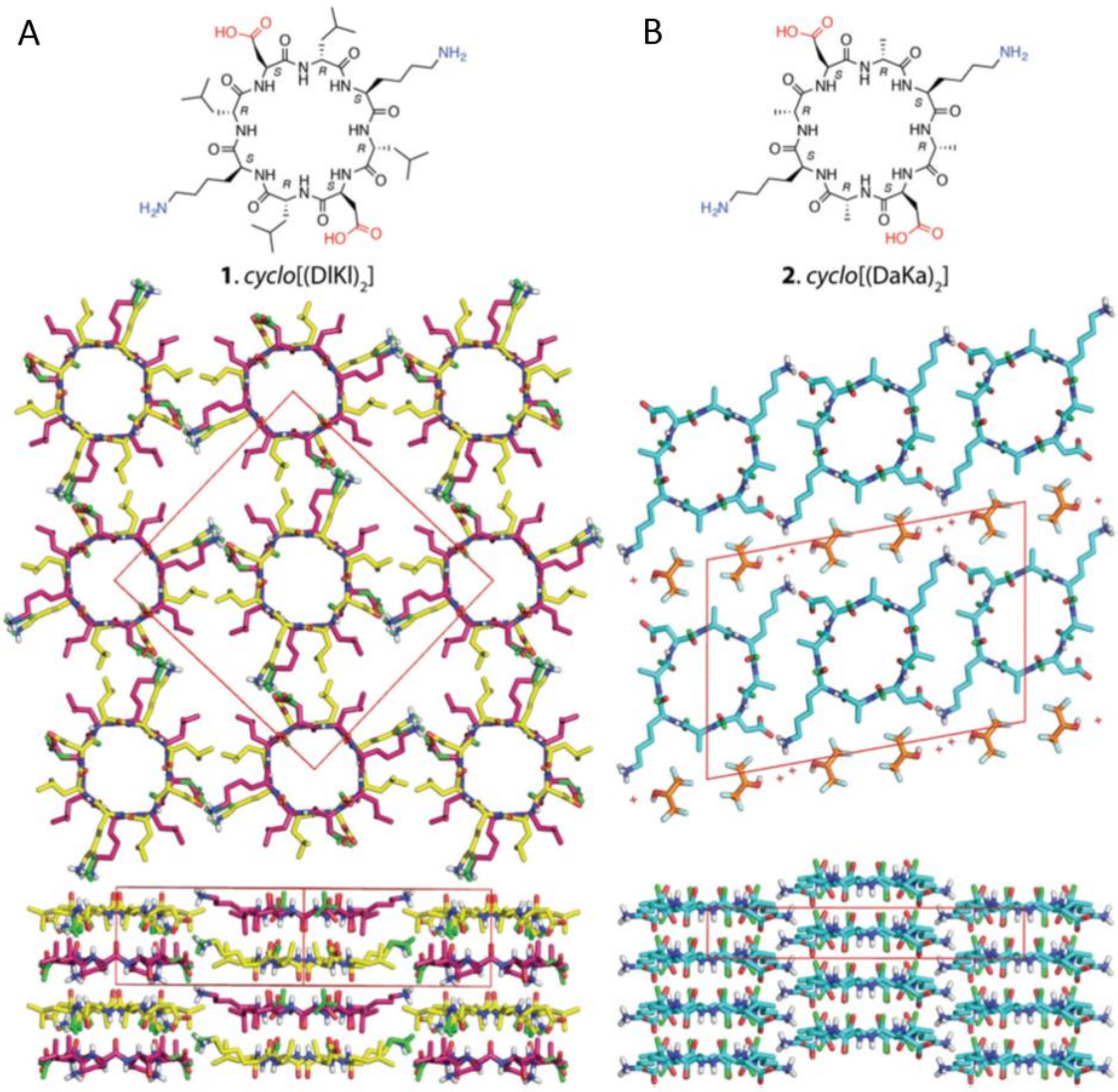

Scheme 1.2: X-ray crystal structures of peptide nanotubes. (a) Antiparallel nanotubes formed by *cyclo*[(DlKl)$_2$]. Two conformations of the peptide are present (pink and yellow). Adjacent nanotubes are oriented head-to-tail. (b) Parallel nanotubes of *cyclo*[(DaKa)$_2$] formed by a single peptide conformer. Adjacent nanotubes are parallel to one another and form sheets separated by HFIP molecules (orange). Adapted from Silk *et al.*[37]

In either case for a parallel or antiparallel β-sheet assembly, the orientation of the backbone amide bonds forces the amino acid side chains to extend pseudo-equatorially from the periphery of the CP ring (**Scheme 1.1**). Following self-assembly into a nanotubular structure, the amino acid side chains thus form the external functionality of the nanotube (**Scheme 1.3**). The versatility of CPs as a supramolecular building block

arise from the ability to manipulate the peptide sequence, thereby controlling the supramolecular properties. By substituting different amino acids, whether naturally occurring or synthetic, into the peptide chain the properties of the nanotube can be tailored to a desired application. The inclusion of hydrophobic amino acids, such as tryptophan for example, has been used to improve lipid membrane interaction,[22, 32, 38-42] and charged residues such as glutamic acid, aspartic acid, and lysine have been included to induce electrostatic charge that can control assembly.[28, 30] These charged systems have also been analysed for potential antimicrobial activities.[21, 23, 43] Control of the peptide sequence is pivotal to control the properties of the nanotube including the size of the pore, the internal and external functionality, as well as the extent of hydrogen bonding in the nanotube such as by *N*-alkylation of the peptide backbone.

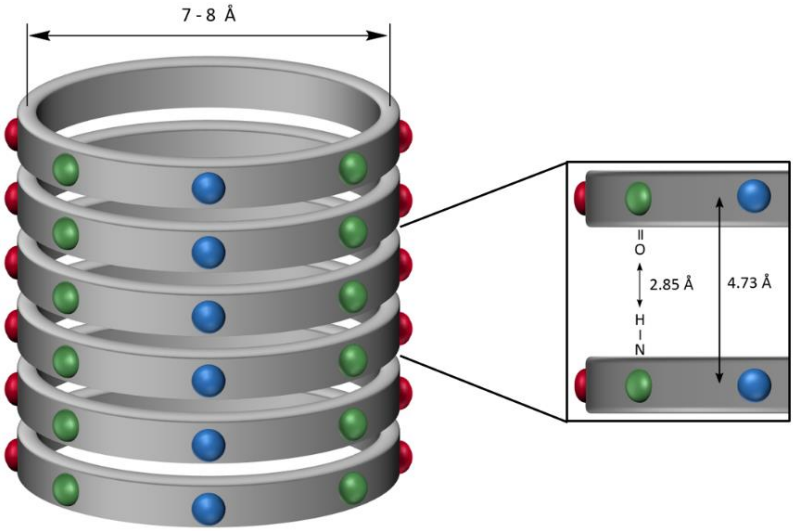

Scheme 1.3: Schematic representation of the assembly of a cyclic octapeptide comprising alternating L- and D- α-amino acids, displaying the dimensions of the internal pore. Red, green and blue protrusions from the circumference of the ring represent the amino acid side chains extending equatorially from the ring. The inset highlights the sequence-dependent inter-ring distances including the hydrogen-bond length (≈ 2.85 Å) and inter-axial distance (≈ 4.73 Å).

1.1.2 Cyclic peptides comprising non-natural amino acids

Numerous attempts have been made at controlling the extended hydrogen bonding network in self-assembling CPs. This has primarily been achieved using strategic *N*-alkylation of the amide backbone.[33, 35, 36, 44, 45] By incorporating *N*-methyl or *N*-alkyl residues of the same stereochemistry, the hydrogen bonding on a single face of the CP is blocked and self-assembly is limited to dimerisation (**Scheme 1.4**). This model system improves solubility and provides an insight into the thermodynamics and association constants of different peptide sequences. The equilibrium dimerisation constant, K_a, of CP dimers can be readily studied by concentration dependent ^{1}H NMR studies in deuterated chloroform and is a far simpler task than the study of the association constant of non-alkylated analogues. Dimerisation constants measured for *N*-alkylated D,L-α-octapeptides comprising Ala and Phe are among the highest reported, between 2,500 – 3,000 M^{-1}.[33, 34, 44] The low association constant suggests that the CPs interact *via* a cooperative mechanism. While computational approaches have brought insight to the self-assembly process,[46-48] understanding nanotube formation and controlling the length and self-assembly of cyclic peptide nanotubes (CPNTs) remains challenging.

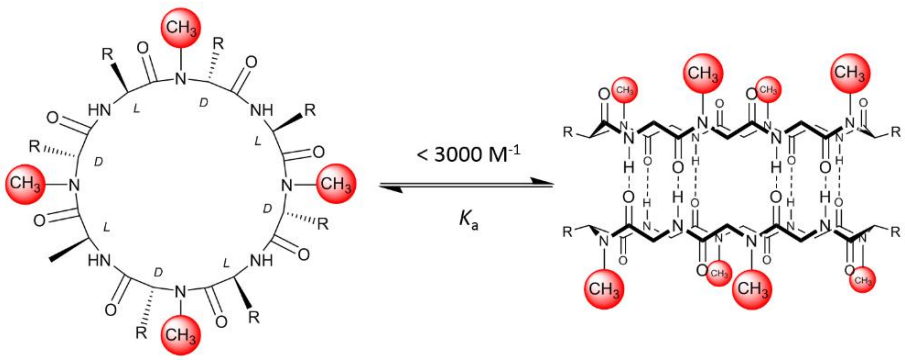

Scheme 1.4: Schematic representation of the antiparallel β-sheet dimer composed of D,L-α-octapeptides with strategically *N*-alkylated amino acids blocking the hydrogen bonding from one face.

CPs comprising alternating D,L α-amino acids (*cyclo*[-D-Ala-L-Glu-D-Ala-L-Gln-]$_2$) were the first CP sequences reported, however since then, a number of sequences capable of self-assembly into nanotubular structures have been discovered. Peptide structures with

sequence lengths ranging from 6 amino acids,[49, 50] through to 10[51, 52] and 12 α-residues have been reported.[53] Additionally, sequences in which some or all of the α-amino acids have been replaced with β-[54, 55] and cyclic γ-residues[56-59] have also been explored (**Scheme 1.5**). These structures result in nanotubes with a larger internal pore diameter, however successful nanotube formation is linked to ability of the CP to adopt a rigid ring conformation. Inclusion of γ-residues has been found to increase the strength of the assemblies formed despite decreasing the hydrogen bonding interaction,[56, 60] with association constants as high as 5.3×10^5 M^{-1},[33, 34] several orders of magnitude higher than many α-peptides. In addition, the cyclic nature of these γ-residues lends additional structural rigidity to the backbone when compared to α-CPs. As such, the internal diameters available to this system are far greater than for α-CPs, due to the additional rigidity of the peptide and their ability to form favourable intermolecular hydrogen bonds. Alteration of the amino acid sequence modifies the internal pore size of the CPNT in addition to the amino acid side chains providing the external properties of the nanotube.

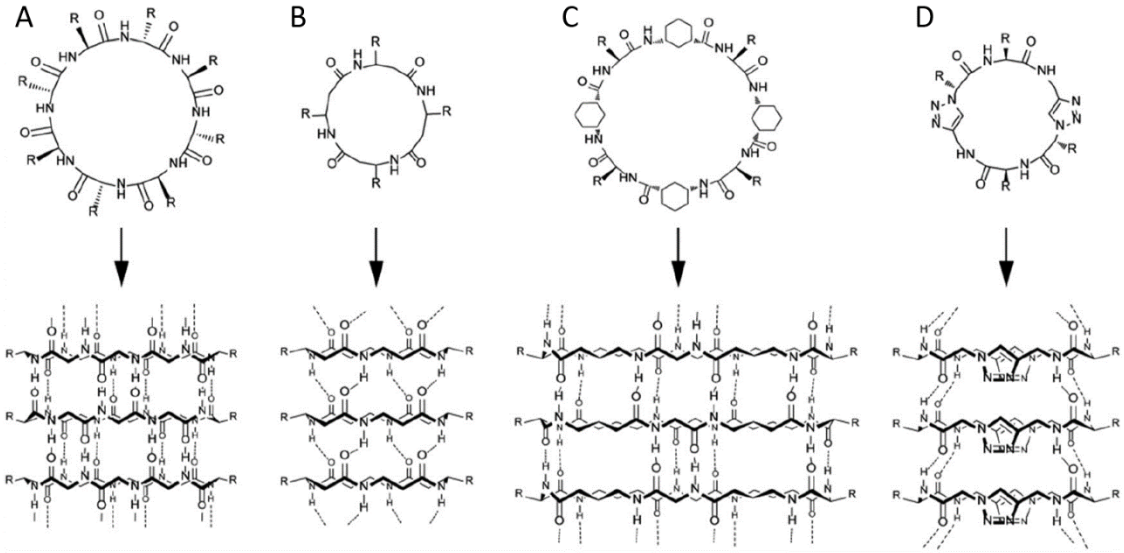

Scheme 1.5: Classes of cyclic peptides that assemble into nanotubes through β-sheet interactions: (A) CPs comprising alternating D, L α- residues; (B) CPs incorporating β-residues; (C) CPs with both α- and γ-residues and; (D) self-assembling heterocyclic peptides by incorporation of ε-amino acids. Adapted from Chapman *et al.*[61]

1.1.3 External properties of the nanotubes

It is clear in that the ability to tailor the peptide sequence of CPs is fundamental to their practicality as nanomaterial scaffolds. Given that the side-chains extend equatorially from the ring of the peptide, it is possible to control the functionality of the periphery of the nanotube. Adaptation of the amino acid sequence has led to a range of studies of structure activity relationships for applications such as ion-channels[38, 39, 45, 51, 52, 62] and antimicrobials.[21-23, 43, 50] The effect of peptide composition, including both natural and non-natural amino acids, on lipid bilayer interactions was studied by Danial *et al*.[42] They found that CPs of different structures formed different pores within lipid bilayers (**Figure 1.1**). This research, along with other earlier studies, focused heavily on lipid bilayer interaction, with a view to understanding the mechanism by which these CPs disrupt membranes. As such, they could be used as an exciting new class of antimicrobial materials.[21-23, 42, 43, 50]

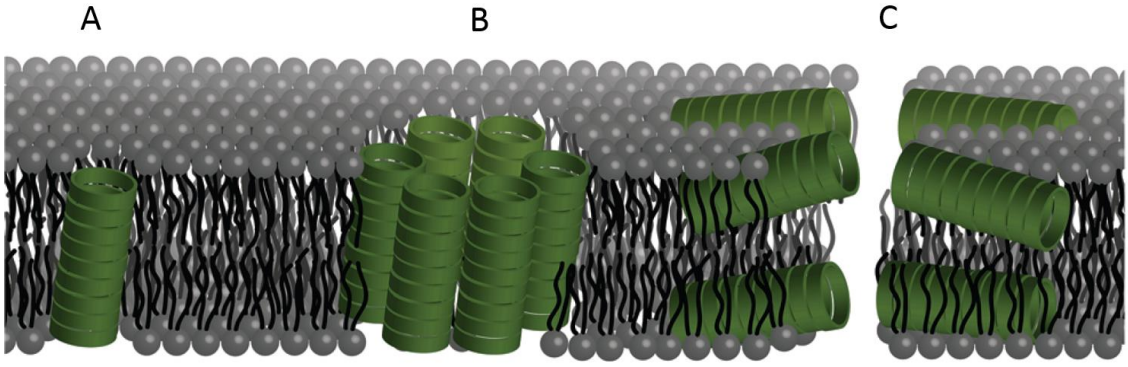

Figure 1.2: Illustration showing the different possible modes of bilayer channel formation. Formation of cyclic peptide channels in a lipid bilayer can occur as (A) a unimeric pore, (B) a barrel stave or (C) through a bilayer or carpet-like disruption. Adapted from Danial *et al*.[42]

The orientation of the amino acid side chains has also been exploited to great effect for conjugation of both small and large molecules to CPs. By incorporating a reactive amino acid, such as the amine-bearing residue lysine, into the CP sequence, ligation of desirable materials can be readily achieved. This addition provides further functionality to the resulting nanotubes and allows for more control over the overall assembly. The primary

focus of conjugating molecules to the exterior of the nanotubes has been to tailor the CPNT properties towards specific applications, such as drug delivery, ion channel mimics, and electron transport. Indeed, various macrocyclic and polycyclic conjugates have been synthesised for their electron transport properties including a 1,4,5,8-naphthalenetetracarboxylic diimide (NDI) conjugate.[25] These CP-NDI conjugates displayed strong fluorescence properties which facilitated the study of the peptide orientation and conformation upon assembly. The additional attractive forces of π-π stacking between the NDI units resulted in nanotubes hundreds of nanometres long with an extended electronically-delocalised state.[25] This system provides a very good example on how the addition of a molecule to the exterior of the nanotube can greatly enhance its physico-chemical properties, and therefore expand on the range of applications for these systems. In addition to controlling the peptide sequence, macromolecular conjugation is another primary focus of CPNT research, since the first instance of polymer-peptide nanotubes by Biesalski *et al*. in 2005 and is discussed at length in Section 1.2.

1.1.4 Controlling Assembly and Orientation

Controlling the self-assembly of CPNTs has been a key area of research, primarily focused on limitation of backbone hydrogen bonding, through strategic *N*-alkylation or electrostatic interactions introduced by charged amino acid residues,[63] as in the seminal work by Ghadiri *et al*. using controlled acidification.[30] A good example of successful control of both nanotube orientation and length was demonstrated by Mizrahi and co-workers; who exploited different peptide sequences as a means of controlling the orientation of the nanotube on a gold surface in order to assess electron transport properties.[28] They designed a series of three CPs for layer by layer (LbL) assembly; one for initial deposition on a gold surface, and a second and third (incorporating glutamic acid and lysine residues) to introduce negative and positive charges respectively (**Figure 1.3**). The first CP included diametrically opposing cysteines for attachment to the gold electrode, in addition to the lysine residues to provide a point for charge interactions for additional layers. Assembly was induced by interlayer electrostatic interaction, with subsequent layer deposition alternating between negative glutamic acid bearing CPs (**Figure 1.3**, red ring) and positively charged lysine bearing CPs (**Figure 1.3**, blue ring).

LbL deposition is an interesting and successful approach to controlling NT length, however use of this system in solution severely limits the potential applications including cell-uptake and drug delivery.

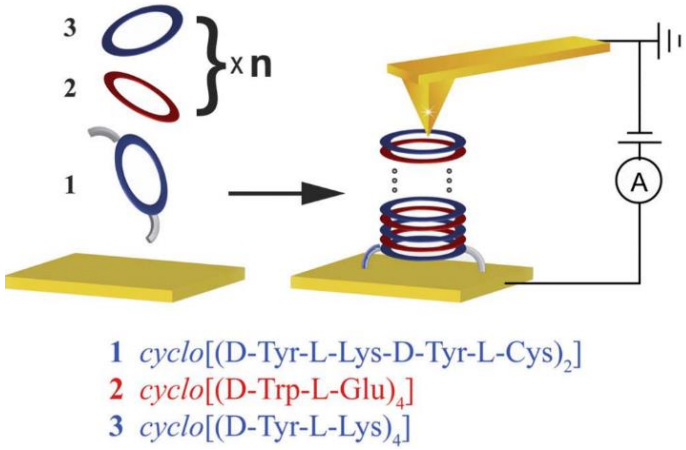

Figure 1.3: Schematic of the LbL assembly approach used by Mizrahi *et al*. Blue/red represents positively/negatively charged CPs respectively. The grey ‘‘arm’’ represents the cysteine side chains used to tether CPs to the gold surface. Note: AFM tip not to scale. Adapted from Mizrahi *et al*.[28]

The structure of the peptide can have a drastic effect on its ability to self-assemble into nanotubes. Various structures and conformations have been extensively studied in order to understand the driving forces behind this process, which has paved way for future research looking into functionalised nanotubes as a way of expanding potential applications.

1.2 Cyclic Peptide-Polymer Conjugates

Polymer-conjugates of these self-assembling CPs have garnered considerable interest of late, due to the wide range of functionalities that can be imparted by polymeric species. Biesalski *et al*. first synthesised polymer conjugates with self-assembling cyclic peptides *via* a divergent approach in 2005. They synthesised a cyclic octapeptide with three atom transfer radical polymerisation (ATRP) initiating groups attached at the side-chains of Lys residues, from which they polymerised NIPAAm.[64] While this divergent approach is

a successful synthetic approach, more recent advances have focused on convergent methods, which presents fewer limitations on reaction conditions and simpler characterisation methods.[65, 66]

Larnaudie *et al.* recently highlighted that both a convergent approach, grafting polymers to the CP core; and a divergent approach, polymerising from the CP core, results in similar materials, however convergent synthesis facilitates full characterisation of all structures including the peptide, polymer and resultant nanotube.[66] Employing a convergent approach to CPNT synthesis has led to many recent advances, including the creation of water-soluble conjugates,[66, 67] stimuli responsive conjugates,[41, 67-69] and more complex asymmetrical Janus-like NTs (Section 1.2.1).[70]

The convergent approach to the synthesis of polymer conjugated CPNTs was first employed by Börner and co-workers,[71] who used an 1-ethyl-3-(3-dimethylaminopropyl)carbodiimide (EDC) mediated condensation reaction to couple two poly(*n*-butyl acrylate) (pBA) arms with two lysine residues on a D, L-α-octapeptide core. The resulting nanotubes showed similar dimensions to those obtained by the divergent approach mentioned previously, with lengths of up to 300 nm and widths of ~5 nm in the dry state by AFM.[71] More recently, a highly efficient conjugation method for the attachment of 2, 3, and 4 arms to cyclic octapeptides has been demonstrated by Chapman *et al. via* copper catalysed azide–alkyne cycloaddition (CuAAC) chemistry (**Scheme 1.6**).[72-74] Alkyne groups were installed on the α-chain end of polymers by reversible addition–fragmentation chain transfer (RAFT) polymerisation, mediated by an alkyne functional chain transfer agent (CTA). The lysine groups on the cyclic peptides were transformed into azides and incorporated into the peptide sequence by solid phase peptide synthesis (SPPS).

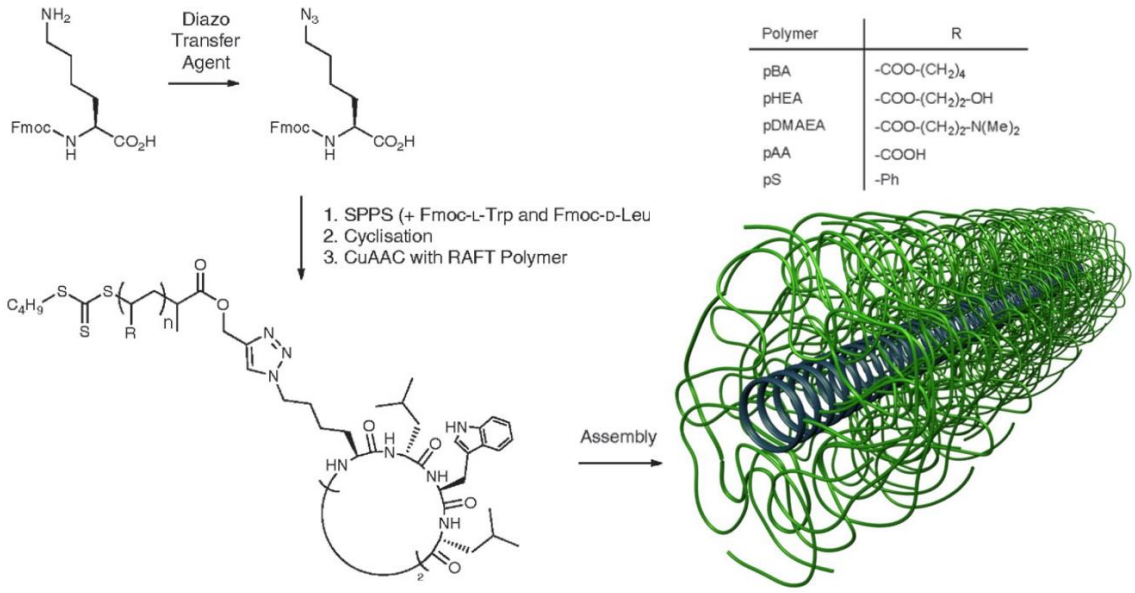

Scheme 1.6: Convergent approach to cyclic peptide–polymer nanotubes *via* CuAAC. Adapted from Chapman *et al.*[72]

CuAAC "click" reactions such as these are ideal as a peptide-polymer coupling strategy,[75] as it uses functional groups that are orthogonal to both free radical polymerisation and peptide chemistries, in addition to being synthetically simple to introduce into both polymer and peptide. A library of peptide-polymer nanotubes has been synthesised by the CuAAC mediated convergent approach, including conjugates of poly(butyl acrylate),[73, 76] poly(dimethylaminoethyl acrylate),[72] poly(acrylic acid),[67] poly(styrene) (PS),[72] and poly(hydroxyethyl acrylate).[72, 74, 77] While the synthesis of CPNTs by CuAAC is attractive, due to its highly efficient and orthogonal nature to the chemistries involved, the presence of copper has been highlighted as problematic for applications such as drug-delivery due to the toxicity of free metal ions, and some copper complexes,[77] requiring careful selection of the copper catalyst employed.[78, 79] In addition to the potentially cytotoxic nature of copper, it is also know to quench the fluorescence of dyes such as calcein,[80] leading to potential problems in fluorescent labelled materials for cell-uptake studies. The synthesis of CP-polymers *via* copper-free conjugation techniques has led to the development of orthogonal conjugation strategies providing access to complex architectures.[70]

Attaching polymer arms to the CP core results in a number of changes to the properties of the nanotubes. For example, the steric bulk of the polymer arms limits the extent of hydrogen bonding, resulting in far shorter assemblies with no apparent lateral/inter-tube aggregation. In addition to altered nanotube dimensions, the CP-polymer nanotubes adopt enhanced solubility properties, more similar to those of the conjugated polymer arms. Functionalisation with PEG for example greatly enhances the aqueous solubility of the peptides, and provides a route for *in vivo* and *in vitro* applications. Another important factor is the length and graft density of the conjugated polymer chains on nanotube assembly. Biesalski *et al*. assessed the impact of polymer mass and graft density on the length and diameter of the nanotubes in the dry state.[81] From AFM measurements they determined that as polymer molar mass increased, nanotube length decreased. More recently this has been demonstrated in solution, using Small Angle Neutron Scattering (SANS) to highlight that polymer length and graft density can have a significant impact on nanotube length.[76]

While many strides have been taken towards understanding the effect of polymer length and steric interactions on nanotube assembly, the reality is that the effects on self-assembly are more complicated than simply the polymer size. Factors such as the steric bulk of the monomer in addition to the solvent necessary to solvate the nanotube add further layers of complexity to the study of self-assembly. In a study by Koh *et al*.,[82] they demonstrated that in highly hydrogen-bonding competitive solvents such as TFA, DMSO and DMF, the solvent competes with the backbone hydrogen-bonding necessary for self-assembly, resulting in essentially unimeric species with scattering barely above the background in SANS. Analysis of the same pBA_{30} conjugates in chloroform and THF resulted in extended cylindrical structures with a length > 2100 Å. In 1:9 v/v mixtures of $[D_1]$TFA/$[D_8]$THF and $[D_1]$TFA/$CDCl_3$, 10 % TFA was sufficient to diminish NT length to 100 - 300 Å, highlighting how detrimental solvent hydrogen-bonding competitivity can be to CPNTs. Thus far the polymeric CPs described have focused on fundamental synthesis and characterisation of the self-assembly. However some recent examples in the literature include preparation of functional nanotubular materials as well as interesting architectures *via* strategic orthogonal chemistries.

1.2.1 Complex Architectures and Functionality

In addition to CuAAC, there are examples in the literature on the use of different synthetic strategies to create more complex systems and materials. For example, Xu *et al*. have also followed a convergent methodology for the synthesis of CP-polymer conjugates, conjugating low molecular weight polymers of poly(ethylene oxide) (PEO), PS and pMMA to cyclic D, L α-octapeptides (**Figure 1.4**).[83, 84] They annealed the various peptide-polymer conjugates with block-copolymers of pBA-*b*-pMMA that form hexagonally packed cylindrical micro domains which are normally orientated to the surface of the thin film. They found that CP-PEO conjugates in particular were selectively sequestered into the cylindrical micro domains, within which the conjugates self-assembled forming nano-channels in the free-standing block copolymer film (**Figure 1.4**). The nanoporous channels were tested for gas permeability with carbon dioxide and neopentane, and it was found that gas permeance was higher for the smaller CO_2 molecules than the larger neopentane molecules.[83]

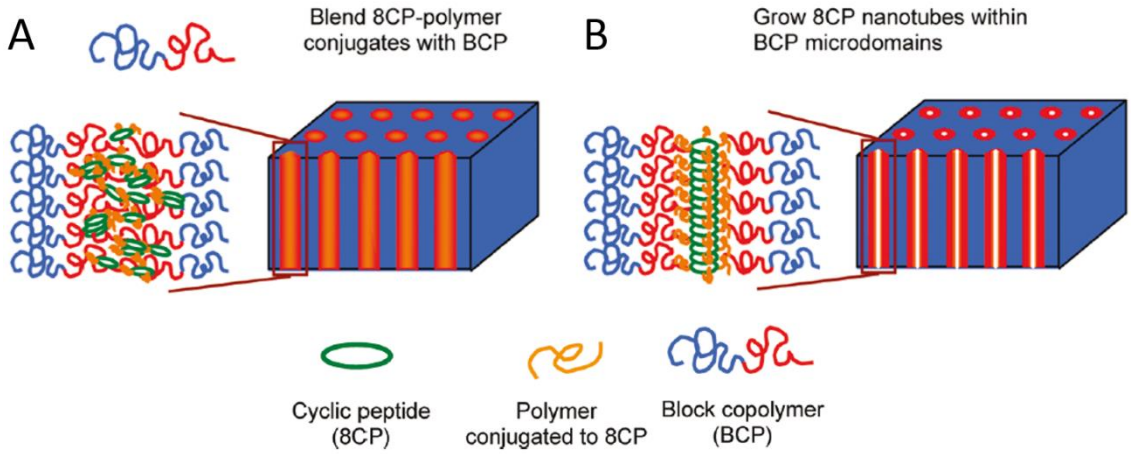

Figure 1.4: Schematic showing the directed co-assembly CP-polymer conjugates. (A) CP-polymer conjugates are first blended with block copolymers, (B) which results in formation of nanopores within microporous domains. Adapted from Xu *et al.*[83]

Polymer addition not only allows for enhanced applications of CPNTs, it provides a unique method by which the self-assembly can be manipulated. Since their discovery, researchers have aimed to control the self-assembly of CP-polymer nanotubes to generate

well-defined, uniform nanotubular materials. The initial paper by Biesalski and co-workers[64] mention steric repulsion of the polymer arms as a potential mechanism by which the nanotube length could be controlled. pH driven electrostatic repulsion is an attractive method for controlling nanotube assembly and has been used for unfunctionalised CP systems (*vide supra*). Incorporation of pH and temperature responsive polymer arms have also proven effective for controlling CPNT assembly.[67-69] Chapman *et al*. studied thermoresponsive conjugates of CPs with poly(2-ethyl-2-oxazoline) (pEtOx).[69] Poly(2-oxazoline)s with ethyl side chains are known to exhibit molecular weight dependent LCST behaviours,[85] and conjugates of CP-pEtOx were also found to display a lower critical solution temperature LCST in water. Below the LCST transition, or cloud point temperature, the polymer is hydrophilic and water soluble. However due to the unfavourable entropy of mixing, as the temperature increases the polymer becomes hydrophobic and thus insoluble in water.[69] The addition of the CP to pEtOx resulted in different LCST behaviour to the native polymer, presumably due to the presence of a sterically hindered polymer environment around the CP core that modify the hydrogen bonding and hydrophobic interactions in the polymeric corona of the nanotube.

Addition of ionisable groups on conjugated polymer arms has also been identified as an effective way to manipulate polymeric CPNT assembly. Another study by Chapman *et al*. made use of poly (acrylic acid) conjugates (pAA),[67] and Catrouillet *et al*. used poly(dimethyl amino ethyl methacrylate) (pDMAEMA) conjugates,[68] to control NT assembly, by manipulating the pH of the solutions, in both cases assessing self-assembly by SANS. For CP-pAA conjugates, assembly into cylinders occurred when the pAA arms were in an uncharged state at pH 3, as observed by SANS and supported by DLS measurements, with assembly greatly diminished at pH 11. Catrouillet and co-workers demonstrated the reversibility of assembly of CP-pDMAEMA conjugates in their SANS study.[68] At pH 9 the CP-pDMAEMA conjugates were uncharged and formed NTs with a length of 68 Å and number of aggregation (N_{agg}) of 14.6. By controlled acidification with DCl down to pH 2, assembly was disrupted resulting in highly charged, unimeric species. Addition of NaOD brought the pH back up to 9, resulting in reformation of the

nanotubular assemblies with the accompanying increase in scattering intensity and comparable length of 59 Å and N_{agg} of 13.

Another example of exacting control of the polymer nanotube architecture is the orthogonal synthesis of asymmetrical Janus-like CPNTs by Danial *et al*.[70] They employed a two-step convergent strategy using consecutive orthogonal conjugation reactions that provided high-yielding conversions without the necessity of synthesising complex amino acids or linkers. They used a CuAAC/thiol-ene addition sequence, as well as a consecutive active-ester/thiol-ene sequence (**Figure 1.5A**) to synthesise Janus tubes both with and without copper. They discovered that the ligation relay employed had a significant impact on the conjugation efficiency of each technique. They found that CuAAC followed by thiol-ene resulted in quantitative conversion to the asymmetrical two arm product. However when the thiol-ene/CuAAC relay was employed, conjugation efficiencies were between 60-80% for thiol-ene addition, due to the limited solubility of the CP core in DMF. The Janus nature of the conjugate was assessed by 2D NMR, DSC and pore formation was observed in lipid bilayers. 2D NMR was used to observe the proton interactions between the asymmetrical polymer arms and DSC was employed to observe the changes in the T_g for conjugates of mixed corona (**Figure 1.5B**) and conjugates of Janus-like demixed corona (**Figure 1.5C**). The authors go on to assess the properties of the Janus NTs as nanopores following the well-established technique in which a fluorescent dye is encapsulated in large unilamellar vesicles (LUVs). As copper is known to quench fluorescence,[80] the Janus NTs were recreated *via* an activated ester/thiol-ene ligation relay to avoid the CuAAC. From the calcein dye release profile of Janus *vs*. non-Janus NTs, they determined that Janus NTs form a macropore in LUVs as depicted in **Figure 1.5D**, as the calcein molecule is too large to fit through a unimeric pore, such as in **Figure 1.2A**. Their work-demonstrated the complex architectures accessible using self-assembling CPNTs and is an interesting bottom-up approach for the fabrication of new nanotubular materials.

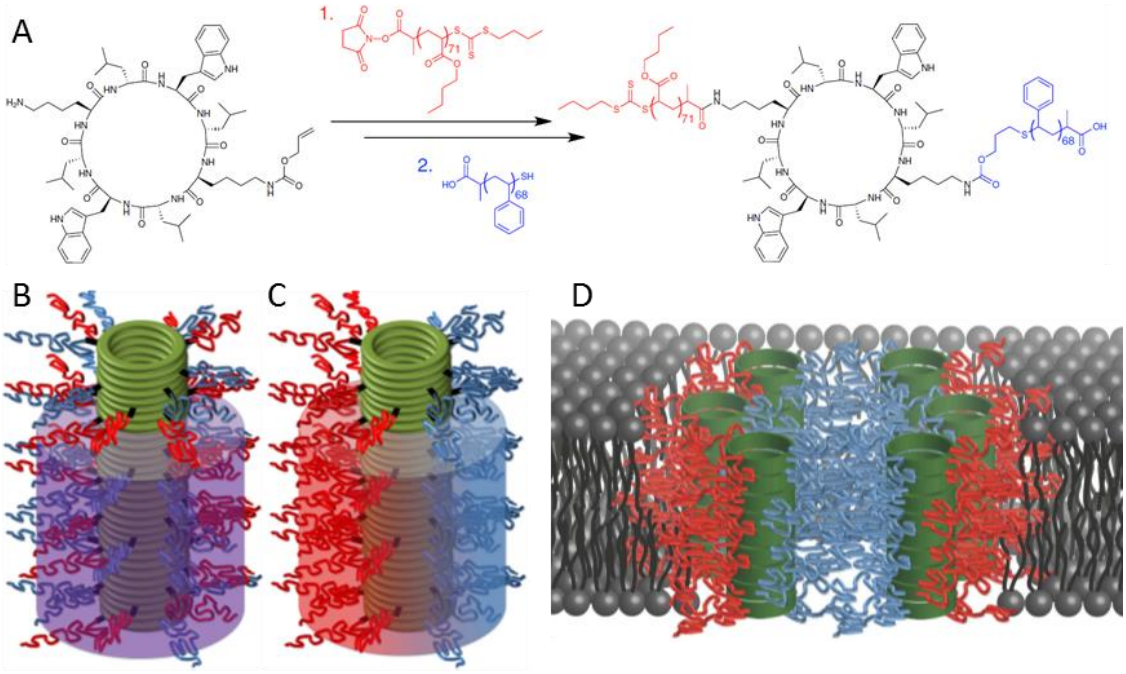

Figure 1.5: (A) Synthesis of Janus conjugate [pBA_{71}]-CP-[$pSty_{68}$], (B) asymmetrical conjugates with a "mixed" corona comprising two miscible polymers (PS and pCHA), (C) depiction of the "demixed" corona of a Janus nanotube arising from micro-phase separation of immiscible polymers (PS and pBA), and (D) schematic representation of the pore formed by Janus conjugates in a lipid bilayer. Adapted from Danial et al.[70]

These studies highlight the interesting yet complex nature of hydrogen bond directed self-assembly of CPNTs, and while significant progress towards functionalising CP-polymer NTs has been made, there are few examples of fine control by manipulating the polymer corona.

1.3 Motivation for this work

Complex functionality can be difficult to incorporate into linear polymers, let alone complex polymeric architectures or polymer conjugates. In the various studies of CP-polymer conjugates generated by either convergent or divergent approaches, it is clear that the vast majority of polymers used are simple polymers generated from direct polymerisation of the desired monomers by RDRP techniques such as ATRP and RAFT polymerisations. Incorporation of complex functionalities onto nanotubular architectures

remains to be explored. From these studies, it is clear that a more comprehensive view on the self-assembly process is required. The addition of polymers greatly enhances the potential applications of CPNTs, however, as discussed, there lacks a fundamental understanding on how this affects assembly, and whether it can be controlled by environmental manipulation. Additionally, there are few synthetic methods by which it is possible to access more complex polymeric architectures.

As such, the aim of this thesis is to address these limitations, focusing on the synthesis and characterisation of polymeric CPNTs, and finally to demonstrate the bio-applications of these materials. Initially, a synthetic strategy by which complex functionalities can be introduced into the polymer arms of CPNTs will be developed. To this end the post-modification of an alkyl halide monomer will be explored, to determine the materials that can be made *via* this strategy. Following on from this, the viability of conjugating a reactive polymer to the CP will be explored, to determine the orthogonality of the reactive polymer to the peptide chemistry. Once a successful synthetic strategy is established, a library of materials polymeric materials of varying functionalities will be generated *via* substitution of the precursor alkyl halide conjugate with different nucleophiles. The self-assembly properties of each of the functional materials will be studied by a combination of scattering techniques including SLS and SANS. Finally, based on this fundamental ground work, a series of polymer conjugates will be prepared to assess the cellular interactions and uptake of these materials as potential biomaterials.

1.4 References

1. Albanese, A.; Tang, P. S.; Chan, W. C. W., The Effect of Nanoparticle Size, Shape, and Surface Chemistry on Biological Systems. In *Annual Review of Biomedical Engineering, Vol 14*, Yarmush, M. L., Ed. Annual Reviews: Palo Alto, 2012; Vol. 14, pp 1-16.

2. Elsabahy, M.; Wooley, K. L. *Chemical Society Reviews* **2012,** 41, (7), 2545-2561.

3. Banerjee, A.; Qi, J.; Gogoi, R.; Wong, J.; Mitragotri, S. *Journal of Controlled Release* **2016,** 238, 176-185.

4. Rathgeber, S.; Pakula, T.; Wilk, A.; Matyjaszewski, K.; Beers, K. L. *The Journal of Chemical Physics* **2005,** 122, (12), 124904.

5. Li, Y.; Kroger, M.; Liu, W. K. *Nanoscale* **2015,** 7, (40), 16631-16646.

6. Truong, N. P.; Whittaker, M. R.; Mak, C. W.; Davis, T. P. *Expert Opin. Drug Deliv.* **2015,** 12, (1), 129-142.

7. Iijima, S. *Nature* **1991,** 354, (6348), 56-58.

8. Iijima, S.; Ichihashi, T. *Nature* **1993,** 363, (6430), 603-605.

9. Tasis, D.; Tagmatarchis, N.; Bianco, A.; Prato, M. *Chemical Reviews* **2006,** 106, (3), 1105-1136.

10. Tenne, R.; Margulis, L.; Genut, M.; Hodes, G. *Nature* **1992,** 360, (6403), 444-446.

11. Shimizu, T.; Masuda, M.; Minamikawa, H. *Chemical Reviews* **2005,** 105, (4), 1401-1444.

12. Namba, K.; Pattanayek, R.; Stubbs, G. *Journal of Molecular Biology* **1989,** 208, (2), 307-325.

13. Mullner, M.; Dodds, S. J.; Nguyen, T. H.; Senyschyn, D.; Porter, C. J. H.; Boyd, B. J.; Caruso, F. *Acs Nano* **2015,** 9, (2), 1294-1304.

14. Gratton, S. E. A.; Ropp, P. A.; Pohlhaus, P. D.; Luft, J. C.; Madden, V. J.; Napier, M. E.; DeSimone, J. M. *Proceedings of the National Academy of Sciences* **2008,** 105, (33), 11613-11618.

15. García-Fandiño, R.; Amorín, M.; Granja, J. R., *Supramolecular Chemistry: From Molecules to Nanomaterials*. John Wiley & Sons, Ltd: 2012.

16. Steed, J. W.; Atwood, J. L., *Supramolecular Chemistry*. John Wiley & Sons, Ltd: 2009.

17. Melis Sardan, E.; Goksu, C.; Mohammad Aref, K.; Mustafa, O. G. *Nanotechnology* **2016,** 27, (40), 402002.

18. Busseron, E.; Ruff, Y.; Moulin, E.; Giuseppone, N. *Nanoscale* **2013,** 5, (16), 7098-7140.

19. Kelkar, D. A.; Chattopadhyay, A. *Biochimica et Biophysica Acta (BBA) - Biomembranes* **2007,** 1768, (9), 2011-2025.

20. Hladky, S. B.; Haydon, D. A. *Biochimica et Biophysica Acta (BBA) - Biomembranes* **1972,** 274, (2), 294-312.

21. Fernandez-Lopez, S.; Kim, H. S.; Choi, E. C.; Delgado, M.; Granja, J. R.; Khasanov, A.; Kraehenbuehl, K.; Long, G.; Weinberger, D. A.; Wilcoxen, K. M.; Ghadiri, M. R. *Nature* **2001,** 412, (6845), 452-455.

22. Rodriguez-Vazquez, N.; Ozores, H. L.; Guerra, A.; Gonzalez-Freire, E.; Fuertes, A.; Panciera, M.; Priegue, J. M.; Outeiral, J.; Montenegro, J.; Garcia-Fandino, R.; Amorin, M.; Granja, J. R. *Current topics in medicinal chemistry* **2014,** 14, (23), 2647-61.

23. Motiei, L.; Rahimipour, S.; Thayer, D. A.; Wong, C.-H.; Ghadiri, M. R. *Chemical Communications* **2009**, (25), 3693-3695.

24. Motesharei, K.; Ghadiri, M. R. *Journal of the American Chemical Society* **1997,** 119, (46), 11306-11312.

25. Horne, W. S.; Ashkenasy, N.; Ghadiri, M. R. *Chemistry* **2005,** 11, (4), 1137-44.

26. Ashkenasy, N.; Horne, W. S.; Ghadiri, M. R. *Small* **2006,** 2, (1), 99-102.

27. Takahashi, R.; Wang, H.; Lewis, J. P. *Journal of Physical Chemistry B* **2007,** 111, (30), 9093-9098.

28. Mizrahi, M.; Zakrassov, A.; Lerner-Yardeni, J.; Ashkenasy, N. *Nanoscale* **2012,** 4, (2), 518-524.

29. De Santis, P.; Morosett, S.; Rizzo, R. *Macromolecules* **1974,** 7, (1), 52-58.

30. Ghadiri, M. R.; Granja, J. R.; Milligan, R. A.; McRee, D. E.; Khazanovich, N. *Nature* **1993,** 366, (6453), 324-327.

31. Hartgerink, J. D.; Granja, J. R.; Milligan, R. A.; Ghadiri, M. R. *Journal of the American Chemical Society* **1996,** 118, (1), 43-50.

32. Engels, M.; Bashford, D.; Ghadiri, M. R. *Journal of the American Chemical Society* **1995,** 117, (36).

33. Ghadiri, M. R.; Kobayashi, K.; Granja, J. R.; Chadha, R. K.; McRee, D. E. *Angew. Chem.-Int. Edit. Engl.* **1995,** 34, (1), 93-95.

34. Kobayashi, K.; Granja, J. R.; Ghadiri, M. R. *Angew. Chem.-Int. Edit. Engl.* **1995,** 34, (1), 95-98.

35. Clark, T. D.; Kobayashi, K.; Ghadiri, M. R. *Chemistry-a European Journal* **1999,** 5, (2), 782-792.

36. Clark, T. D.; Ghadiri, M. R. *Journal of the American Chemical Society* **1995,** 117, (49), 12364-12365.

37. Silk, M. R.; Newman, J.; Ratcliffe, J. C.; White, J. F.; Caradoc-Davies, T.; Price, J. R.; Perrier, S.; Thompson, P. E.; Chalmers, D. K. *Chemical Communications* **2017,** 53, (49), 6613-6616.

38. Kim, H. S.; Hartgerink, J. D.; Ghadiri, M. R. *Journal of the American Chemical Society* **1998,** 120, (18), 4417-4424.

39. Clark, T. D.; Buehler, L. K.; Ghadiri, M. R. *Journal of the American Chemical Society* **1998,** 120, (4), 651-656.

40. Suga, T.; Osada, S.; Kodama, H. *Bioorganic & Medicinal Chemistry* **2012,** 20, (1), 42-46.

41. Danial, M.; Tran, C. M. N.; Jolliffe, K. A.; Perrier, S. *Journal of the American Chemical Society* **2014,** 136, (22), 8018-26.

42. Danial, M.; Perrier, S.; Jolliffe, K. A. *Organic & Biomolecular Chemistry* **2015,** 13, (8), 2464-73.

43. Horne, W. S.; Wiethoff, C. M.; Cui, C.; Wilcoxen, K. M.; Amorin, M.; Ghadiri, M. R.; Nemerow, G. R. *Bioorganic & Medicinal Chemistry* **2005,** 13, (17), 5145-5153.

44. Clark, T. D.; Buriak, J. M.; Kobayashi, K.; Isler, M. P.; McRee, D. E.; Ghadiri, M. R. *Journal of the American Chemical Society* **1998,** 120, (35), 8949-8962.

45. Sanchez-Ouesada, J.; Isler, M. P.; Ghadiri, M. R. *Journal of the American Chemical Society* **2002,** 124, (34), 10004-10005.

46. Benjamin, A.; Keten, S. *The Journal of Physical Chemistry B* **2016,** 120, (13), 3425-3433.

47. Vijayaraj, R.; Van Damme, S.; Bultinck, P.; Subramanian, V. *Physical Chemistry Chemical Physics* **2012,** 14, (43), 15135-15144.

48. Koh, M. L. Self assembly of (N-methylated cyclic peptide)-polymer conjugates. University of Sydney, 2013.

49. Sun, X.; Lorenzi, G. P. *Helvetica Chimica Acta* **1994,** 77, (6), 1520-1526.

50. Fletcher, J. T.; Finlay, J. A.; Callow, M. E.; Callow, J. A.; Ghadiri, M. R. *Chemistry – A European Journal* **2007,** 13, (14), 4008-4013.

51. Granja, J. R.; Ghadiri, M. R. *Journal of the American Chemical Society* **1994,** 116, (23), 10785-10786.

52. Sánchez-Quesada, J.; Sun Kim, H.; Ghadiri, M. R. *Angewandte Chemie International Edition* **2001,** 40, (13), 2503-2506.

53. Khazanovich, N.; Granja, J. R.; McRee, D. E.; Milligan, R. A.; Ghadiri, M. R. *Journal of the American Chemical Society* **1994,** 116, (13), 6011-6012.

54. Fujimura, F.; Hirata, T.; Morita, T.; Kimura, S.; Horikawa, Y.; Sugiyama, J. *Biomacromolecules* **2006,** 7, (8), 2394-2400.

55. Fujii, S.; Morita, T.; Umemura, J.; Kimura, S. *Thin Solid Films* **2006,** 503, (1-2), 224-229.

56. Brea, R. J.; Vázquez, M. E.; Mosquera, M.; Castedo, L.; Granja, J. R. *Journal of the American Chemical Society* **2007,** 129, (6), 1653-1657.

57. Brea, R. J.; Castedo, L.; Granja, J. R.; Herranz, M. A.; Sanchez, L.; Martin, N.; Seitz, W.; Guldi, D. M. *Proc. Natl. Acad. Sci. U. S. A.* **2007,** 104, (13), 5291-5294.

58. Hourani, R.; Zhang, C.; van der Weegen, R.; Ruiz, L.; Li, C. Y.; Keten, S.; Helms, B. A.; Xu, T. *Journal of the American Chemical Society* **2011,** 133, (39), 15296-15299.

59. Horne, W. S.; Stout, C. D.; Ghadiri, M. R. *Journal of the American Chemical Society* **2003,** 125, (31), 9372-9376.

60. Brea, R. J.; Castedo, L.; Granja, J. R. *Chemical Communications* **2007**, (31), 3267-3269.

61. Chapman, R.; Danial, M.; Koh, M. L.; Jolliffe, K. A.; Perrier, S. *Chemical Society reviews* **2012,** 41, (18), 6023-41.

62. Ghadiri, M. R.; Granja, J. R.; Buehler, L. K. *Nature* **1994,** 369, (6478), 301-304.

63. Sun, L.; Fan, Z.; Wang, Y.; Huang, Y.; Schmidt, M.; Zhang, M. *Soft Matter* **2015,** 11, (19), 3822-3832.

64. Couet, J.; Jeyaprakash, J. D.; Samuel, S.; Kopyshev, A.; Santer, S.; Biesalski, M. *Angewandte Chemie-International Edition* **2005,** 44, (21), 3297-3301.

65. Dehn, S.; Chapman, R.; Jolliffe, K. A.; Perrier, S. *Polym. Rev.* **2011,** 51, (2), 214-234.

66. Larnaudie, S. C.; Brendel, J. C.; Jolliffe, K. A.; Perrier, S. *Journal of Polymer Science Part A: Polymer Chemistry* **2016,** 54, (7), 1003-1011.

67. Chapman, R.; Warr, G. G.; Perrier, S.; Jolliffe, K. A. *Chemistry-a European Journal* **2013,** 19, (6), 1955-1961.

68. Catrouillet, S.; Brendel, J. C.; Larnaudie, S.; Barlow, T.; Jolliffe, K. A.; Perrier, S. *ACS Macro Letters* **2016,** 5, (10), 1119-1123.

69. Chapman, R.; Bouten, P. J. M.; Hoogenboom, R.; Jolliffe, K. A.; Perrier, S. *Chemical Communications* **2013,** 49, (58), 6522-6524.

70. Danial, M.; My-Nhi Tran, C.; Young, P. G.; Perrier, S.; Jolliffe, K. A. *Nature Communications* **2013,** 4, 2780.

71. ten Cate, M. G. J.; Severin, N.; Borner, H. G. *Macromolecules* **2006,** 39, (23), 7831-7838.

72. Chapman, R.; Jolliffe, K. A.; Perrier, S. *Polym. Chem.* **2011,** 2, (9), 1956-1963.

73. Poon, C. K.; Chapman, R.; Jolliffe, K. A.; Perrier, S. *Polym. Chem.* **2012,** 3, (7), 1820-1826.

74. Chapman, R.; Jolliffe, K. A.; Perrier, S. *Aust. J. Chem.* **2010,** 63, (8), 1169-1172.

75. Barner-Kowollik, C.; Du Prez, F. E.; Espeel, P.; Hawker, C. J.; Junkers, T.; Schlaad, H.; Van Camp, W. *Angewandte Chemie International Edition* **2011,** 50, (1), 60-62.

76. Chapman, R.; Koh, M. L.; Warr, G. G.; Jolliffe, K. A.; Perrier, S. *Chemical Science* **2013,** 4, (6), 2581-2589.

77. Blunden , B. M.; Chapman, R.; Danial, M.; Lu, H.; Jolliffe, K. A.; Perrier , S.; Stenzel, M. H. *Chemistry – A European Journal* **2014,** 20, (40), 12745-12749.

78. Kennedy, D. C.; McKay, C. S.; Legault, M. C. B.; Danielson, D. C.; Blake, J. A.; Pegoraro, A. F.; Stolow, A.; Mester, Z.; Pezacki, J. P. *Journal of the American Chemical Society* **2011,** 133, (44), 17993-18001.

79. Hong, V.; Steinmetz, N. F.; Manchester, M.; Finn, M. G. *Bioconjugate chemistry* **2010,** 21, (10), 1912-1916.

80. Knöpfel, M.; Smith, C.; Solioz, M. *Biochemical and Biophysical Research Communications* **2005,** 330, (3), 645-652.

81. Couet, J.; Biesalski, M. *Small* **2008,** 4, (7), 1008-1016.

82. Koh, M. L.; FitzGerald, P. A.; Warr, G. G.; Jolliffe, K. A.; Perrier, S. *Chemistry – A European Journal* **2016,** 22, (51), 18419-18428.

83. Xu, T.; Zhao, N. N.; Ren, F.; Hourani, R.; Lee, M. T.; Shu, J. Y.; Mao, S.; Helms, B. A. *Acs Nano* **2011,** 5, (2), 1376-1384.

84. Zhang, C.; Xu, T. *Nanoscale* **2015,** 7, (37), 15117-15121.

85. Hoogenboom, R.; Thijs, H. M. L.; Jochems, M. J. H. C.; van Lankvelt, B. M.; Fijten, M. W. M.; Schubert, U. S. *Chemical Communications* **2008**, (44), 5758-5760.

2

RAFT Polymerisation and Post-modification of poly(bromo ethyl acrylate)

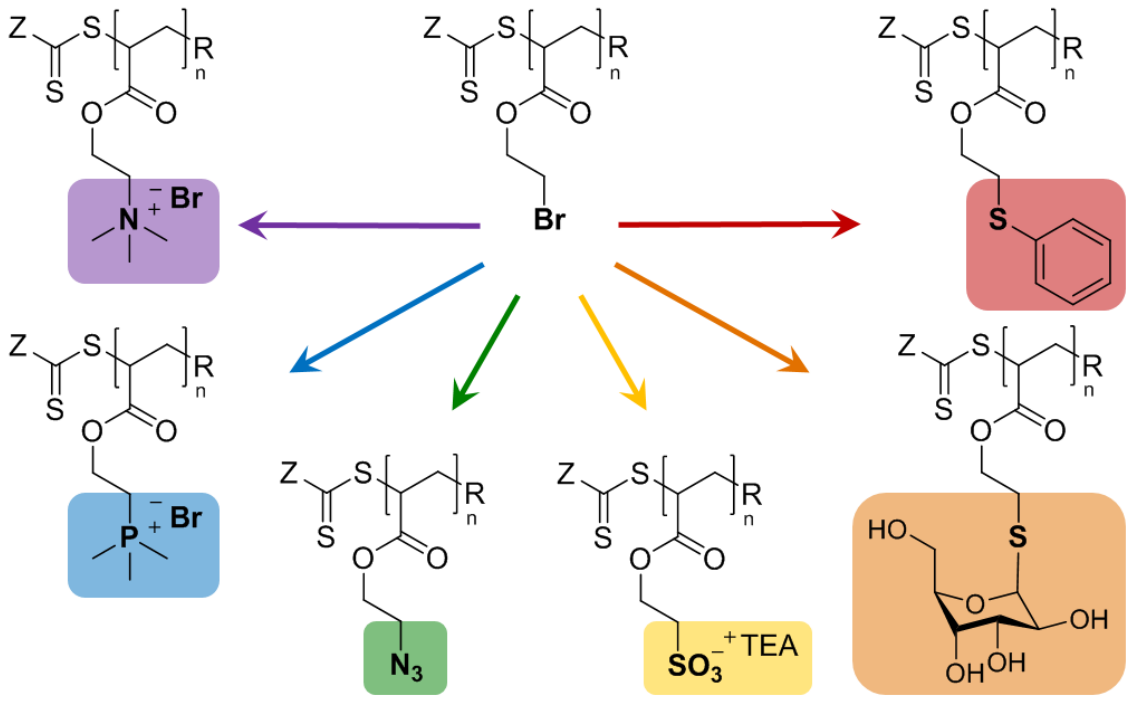

Post-polymerisation modification has become a powerful tool to create a diverse range of functional materials. However, simple nucleophilic substitution reactions on halogenated monomers remains relatively unexplored. Here is summarised the synthesis of

poly(bromoethyl acrylate) (pBEA) by reversible addition fragmentation chain transfer (RAFT) polymerisation to generate a highly reactive polymer precursor for post-polymerisation nucleophilic substitution. RAFT polymerisation of BEA generated well-defined homopolymers and block copolymers over a range of molecular weights. The alkyl bromine containing homo- and block copolymer precursors were readily substituted by a range of nucleophiles in good to excellent conversion under mild and efficient reaction conditions without the need of additional catalysts. The broad range of nucleophilic species that are compatible with this post modification strategy enable the facile synthesis of complex functionalities, from permanently charged polyanions to hydrophobic polythioethers to glycopolymers. This chapter describes the synthesis and characterisation of all post-functionalised polymeric materials used in subsequent chapters.

2.1 Introduction

Synthesis of complex polymers with desirable functionalities, well-defined and controlled architectures is a core target of modern polymer science. The development of several "living" or controlled polymerisation methods, and in particular reversible deactivation radical polymerisation (RDRP), has paved the way for precise control over molecular weights, polymer architecture and end-group functionality.[1-5] However, inclusion of desirable material properties, in addition to well-controlled polymerisation is limited by the range of chemical functionalities accessible to these polymerisation techniques.[6-8] In light of this, post-modification of a reactive polymer precursor provides an attractive approach to overcoming this limitation, enabling synthesis of diversely functional materials, without subjecting them to detrimental polymerisation conditions.[9-13]

A variety of post-polymerisation methods have previously been explored,[6-9] including copper-catalysed azide/alkyne click (CuAAC),[14-16] Diels-Alder cycloadditions[17-20] and active ester couplings.[10, 21-23] These methods enable the introduction of complex functional groups, targeting applications ranging from drug delivery to organic electronics.[19, 24, 25] In addition to these more established post-modification methods, is a

simple yet relatively un-explored reaction – nucleophilic substitution of alkyl halides. Thus far it is primarily metal catalysed polymerisations that have exploited this versatile handle to introduce functionality.[13, 26-28] One reason for the limited use of this method in RDRPs may be the susceptibility of alkyl halides to abstraction by radicals, an attribute that is exploited in iodine transfer polymerisations.[29, 30] Controlled radical polymerisations have thus far primarily made use of the monomer vinylbenzyl chloride, however control of this styrene type monomer requires extensive optimisation for successful polymerisation, often at the cost of very low conversions and yields.[31, 32] As an alternative to overcome this limitation, Monnereau *et al.* used a two-step method by substituting a poly(hydroxyethyl acrylate) generated by ATRP with trimethylsilyl bromide to give the desired polybrominated product.[12] However, the issues described above leave the direct polymerisation of simple alkyl halide monomers relatively unexplored, despite convenient monomer synthesis and a wide range of nucleophiles available for substitution of the precursor. The few examples reported using alkyl bromide monomers by RDRP methods, have primarily targeted the synthesis of ammonium based polycations[33-35] or azide modifications in degradable copolymers.[36, 37] While these bromo containing RDRP polymers were employed effectively to introduce complex functionality, it is fascinating to note that these substitutions focused solely on nitrogen based nucleophiles, which represent but a fraction of the diverse range of potential substitutions achievable with alkyl halide monomers.

In this contribution, the efficiency of polymerising bromoethyl acrylate (BEA) using the reversible addition-fragmentation chain transfer (RAFT) process is demonstrated. The versatility of the resulting BEA polymer in subsequent nucleophilic substitution reactions to generate a library of polymers of diverse and complex functionalities was shown. RAFT polymerisation provides a robust system that is both facile and convenient, yet remains tolerant to a broad range of functional groups and monomer varieties.[1] BEA combines the ease of acrylate polymerisations with the high electrophilicity of a carbon adjacent to the bromine group, while the reactivity towards radicals remains low. Kinetic studies of the polymerisation shed light on the control and the retention of the active chain end.

The obtained reactive precursor polymer was subsequently used in a range of post-polymerisation substitutions, to generate a library of functional polyacrylates. To demonstrate the versatility of the method, a wide variety of nucleophiles that differ in size, polarity and charge was used. An important characteristic of these reactions is the full conversion of the bromine group under very mild reaction conditions. In addition to these modifications, it was further illustrated the potential for functionalisation of pBEA by formation of block-copolymers followed by substitution to create self-assembled copolymer structures from a single reactive polymer precursor.

2.2 Results and Discussion

2.2.1 RAFT Homopolymerisation

For RAFT polymerisation of BEA, (4-cyano pentanoic acid)yl ethyl trithiocarbonate (CPAETC) was used as the chain transfer agent (CTA) and dioxane as the solvent. To confirm the control of radical polymerisation of BEA, kinetics of the polymerisation were followed by ^{1}H NMR and SEC (DMF, 0.1% LiBr). After an induction period of approximately 30 min, the pseudo first-order rate plot (**Figure 2.1A**) approaches linearity. The increase in M_n with monomer conversion is linear and dispersity of the polymer remains narrow ($Đ < 1.2$), thus indicating a controlled radical polymerisation.[38-40] At longer polymerisation times (> 2 h) the kinetic plot deviates from linearity and is more closely approximated by a third order polynomial, however the SEC traces (**Figure 2.1C**) still show a narrow dispersity (**Figure 2.1B**) indicating the polymerisation remains controlled. The downturn in the kinetic rate plot (**Figure 2.1A**) is due to a decrease in the total radical concentration during polymerisation.[41] Despite 85% of the initiator ACVA remaining at 2 h, radical generation by the initiator was less than the amount of radicals undergoing termination reactions, indicating potential unwanted side reactions such as radical abstraction by the pendant bromines.[5, 42] By limiting the polymerisation time to the period in which the rate is closest to linear, it is possible to avoid unnecessary termination products that may occur at longer reaction times, ensuring a reduction in the number of dead chains present. It should also be noted, that the molecular weights obtained by SEC (**Figure 2.1D**) consistently underestimate M_n due to calibration of the

SEC using poly(methyl methacrylate) standards, however dispersity and molecular weight distribution remain representative. Furthermore, the M_n by NMR cannot be calculated for kinetic samples due to the ethyl end on the CTA *Z* group overlapping with the backbone polymer peaks (at ~1.2 ppm), and the dioxane solvent peak interfering with the peak at ~3.35ppm, giving incorrect integrations and erroneous M_n NMRs.

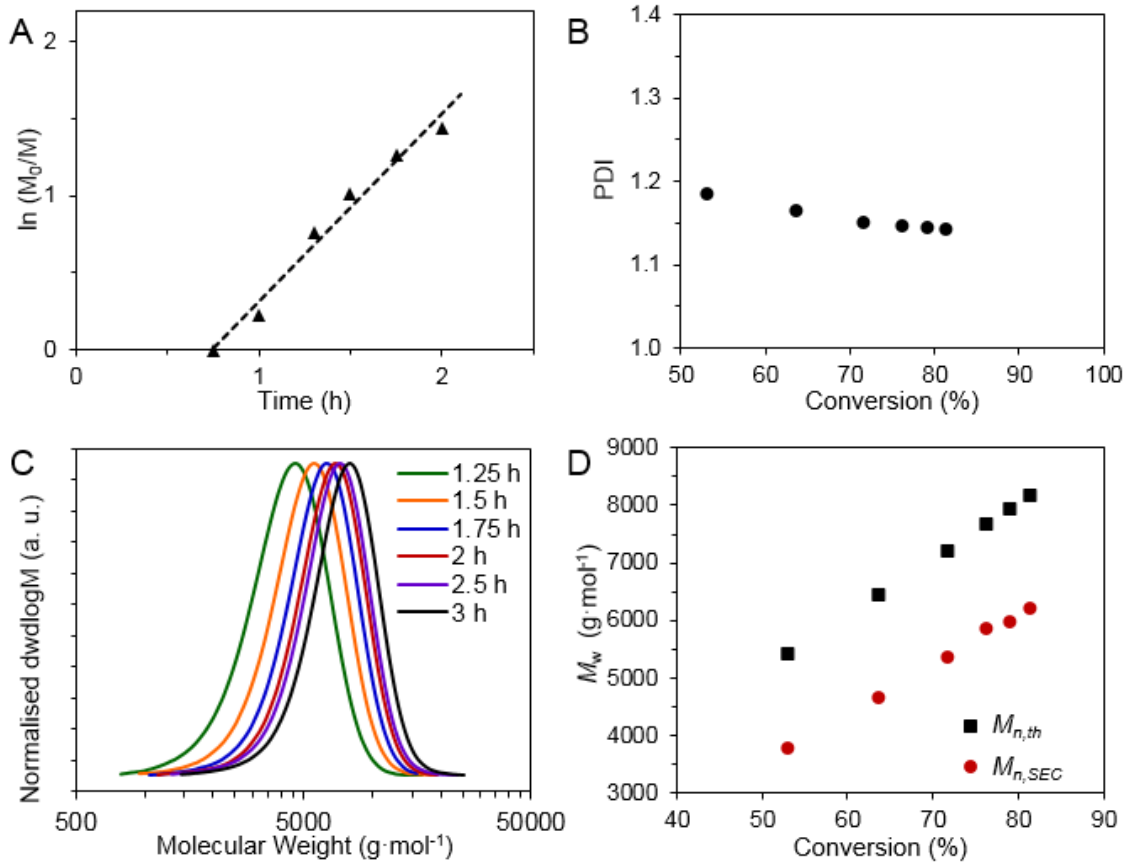

Figure 2.1: Kinetic data for pBEA targeting DP 50. (A) Kinetic plot for the RAFT polymerisation of pBEA as determined by ^{1}H NMR spectroscopy. Dashed line indicates linearity. (B) Plot of polymer dispersity vs. conversion. (C) SEC traces of kinetic samples. (D) Theoretical M_n vs. M_n from SEC values.

Based on these kinetics a range of polymer DPs were targeted by varying the monomer/CTA ratio, the results of which are summarised in (**Table 2.1**). The prepared polymers were purified by precipitation using either methanol or diethyl ether and were obtained in high yield. In all cases high conversions (> 75 %) were obtained with short

polymerisation times (2 h) and a low consumption of initiator (< 2 %).[43, 44] These results clearly demonstrate the ease of polymerising the halogenated monomer BEA using RAFT.

Table 2.1: Summary of BEA RAFT homopolymerisation

$[M]_0/[CTA]_0$	$[CTA]_0/[I]_0$	Conv.[a] (%)	$M_{n,th}$[b] (g·mol^{-1})	$M_{n,NMR}$[c] (g·mol^{-1})	$M_{n,SEC}$[d] (g·mol^{-1})	$Đ$
13	10	94	2200	2500	1800	1.12
25	10	96	5000	4700	4200	1.10
50	10	94	8000	8300	6500	1.12
100	10	90	16500	16800	15100	1.10
200	10	78	26200	28000	24600	1.17

[a] Determined from ^{1}H NMR.
[b] Calculated from conversion and characteristics of the parent polymer.
[c] Calculated from ^{1}H NMR end group analysis. [d] From SEC analysis (DMF LiBr, pMMA-Std.).

2.2.2 RAFT block copolymerisation

Based on the promising previous results, the formation of block copolymers comprising BEA monomer was further investigated, to demonstrate that the RAFT chain ends are still present and functional. The advantage of RAFT polymerisation is that it enables facile synthesis of well-defined block copolymers, by chain extending the remaining trithiocarbonate end-group moiety. To examine this "livingness" of the precipitated homopolymer, pBEA was chain extended using the hydrophobic monomer butyl acrylate (BA). The polymerisation of the second pBA block was achieved in an analogous fashion to BEA homopolymerisation, but instead the BEA polymer was utilised as a macro-CTA (**Scheme 2.1**). The shift in the SEC trace to high molecular weights clearly demonstrates the successful chain extension of the pBEA with pBA, however a low molecular weight shoulder can be observed, which corresponds to the macro-CTA (**Figure 2.2A**). Calculating the initiator decomposition under our reaction conditions, it would be expected that the number of dead chains in the system to be below 2 %.[43, 44] Considering the highly reactive nature of the monomer due to the bromine group, additional loss of the CTA end-group cannot be fully excluded. Nevertheless, more than 90% of the chains

reinitiate and the SEC traces of the second block were in good agreement with theoretically expected values for the block copolymer (**Figure 2.2A**).

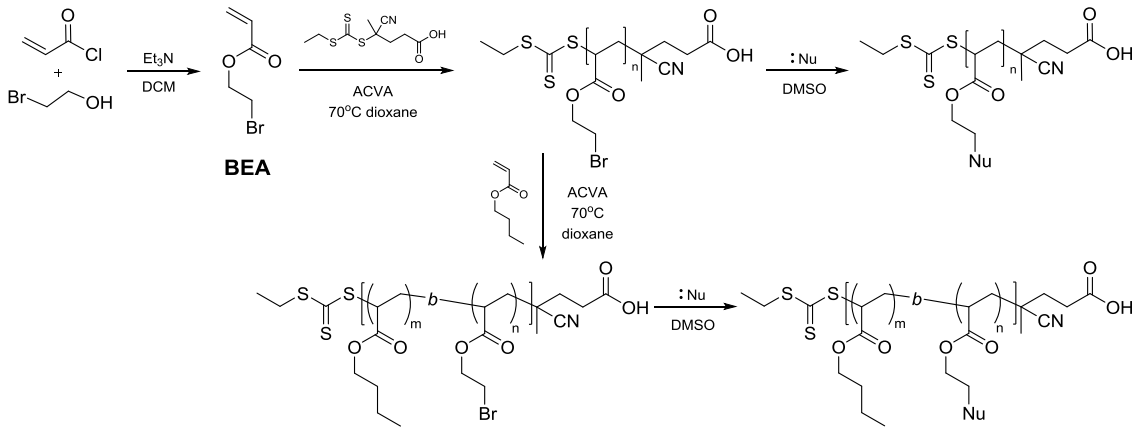

Scheme 2.1: Scheme of entire synthesis, beginning with monomer synthesis, RAFT homo and block copolymerisation of BEA and nucleophilic substitution of pBEA precursors.

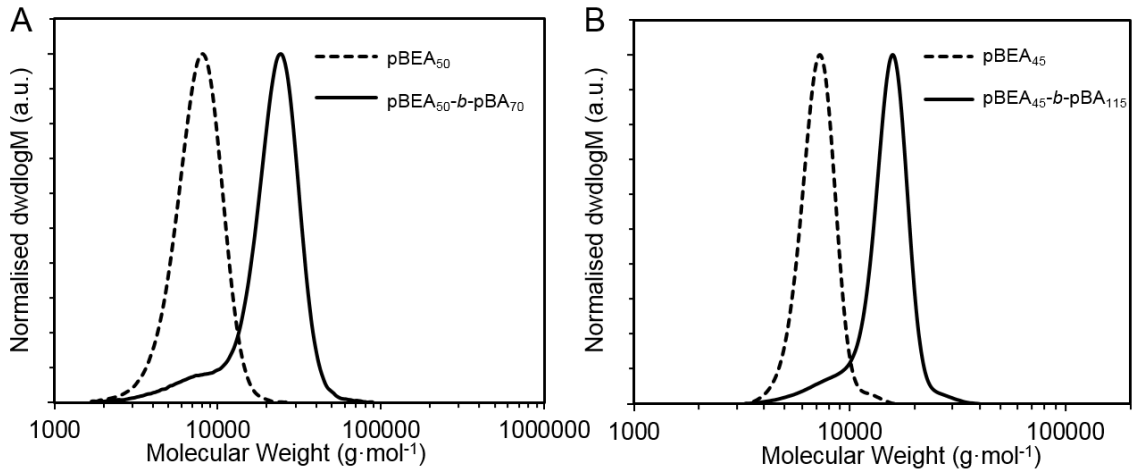

Figure 2.2: Chain extension of: (A) $pBEA_{50}$ macro-CTA (**A1**) with pBA_{70} and (B) $pBEA_{45}$ macro-CTA (**A2**) polymerised to 75% conversion, and subsequent chain extension with pBA_{115}.

To eliminate the possibility of the shoulder being formed by side-reactions at high conversion in the polymerisation of the pBEA macro-CTA, conversion of the macro-CTA polymerisation was limited to 75%, before repeating the chain extension with pBA. The low molecular weight shoulder remained (**Figure 2.2B**), despite limiting conversion of

the first block, suggesting that poor re-initiation of the macro-CTA is the cause of the shoulder. Formation of well-defined block copolymers requires that the first block have an R-group with a similar or greater leaving ability, than that of the second polymer radical.[45, 46] In this case, despite both blocks being formed of acrylates, the polymer side chain appears to have influenced the stability of the macro-radical.[43] The pBEA likely forms a macro-radical of lower stability than that formed by pBA, resulting in an adduct radical that partitions in favour of the starting materials, which causes the broadening of the molecular weight distribution, indicative of the remaining macro-CTA seen in **Figure 2.2A**. In addition to the previous polymer sequence, the chain extension of a pBA macro-CTA with BEA monomer was examined. Using similar conditions, a well-defined block copolymer, with a symmetrical, monomodal SEC trace (**Figure 2.3**) can be observed. These results support the hypothesis that pBA forms a more stable macro-radical, resulting in a better defined block-copolymer due to complete re-initiation of the macro-CTA. Thus it can be demonstrated that BEA is suitable for the formation of pure block copolymers without any apparent side reactions with the bromine group, however synthesis does require planning of the block order and consideration of the second block macro-radical stability.

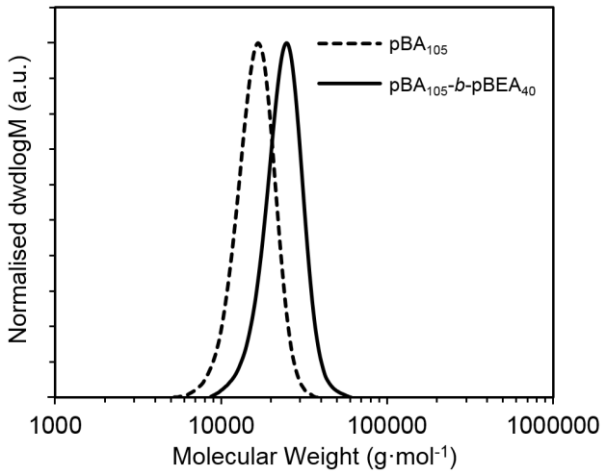

Figure 2.3: Chain extension of pBA_{105} macro-CTA **A3** with $pBEA_{40}$.

2.2.3 Post-polymerisation Modification

After demonstrating the successful polymerisation of BEA, the reactivity of this precursor in nucleophilic substitutions testing a range of nucleophiles was investigated. Since pBEA consists of primary alkyl halides, it would be assumed that it would readily undergo an S_N2 reaction with various nucleophilic species. As such, testing to see if very high conversions (> 95 %) could be reached in the absence of side reactions, both of which are crucial for an effective post-polymerisation modification, was studied. To investigate the versatility, 5 different types of nucleophiles were selected: amines, phosphines, azides, sulfites and thiols (**Scheme 2.2**). The substitutions of pBEA were conveniently followed by ^{1}H NMR, by observing the shifts on the ethyl acrylate pendant arms both before and after substitution.

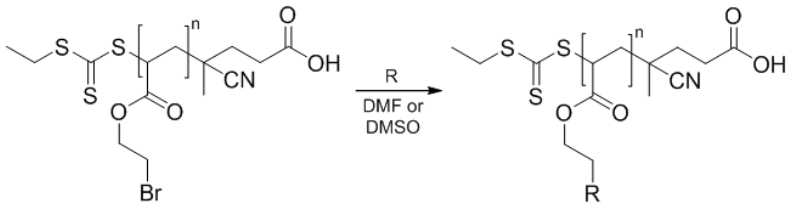

R =	Nucleophile	R =	Nucleophile
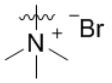	Trimethyl amine	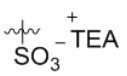	Tetraethyl ammonium sulfite
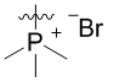	Trimethyl phosphine		Sodium azide
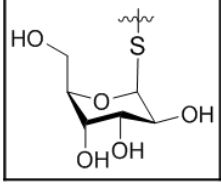	β-D-Thioglucose	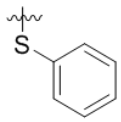	Thiophenol

Scheme 2.2: Summary of the substitutions achieved with $pBEA_{50}$ precursor.

As a first example, the substitution of the bromine by thiophenol (**Figure 2.4**) was examined. Thio-bromo substitutions have previously been reported to be rapid and efficient reactions to introduce end-group functionality.[47-52] However, thio-bromo

substitutions have not been thoroughly explored for main chain functionalisation of polymers by controlled radical polymerisation.

Thiophenol was selected to representatively probe substitution efficacy, since the appearance of aromatic protons in the ^{1}H NMR (~7.1 ppm) are well separated from any peaks in the pBEA precursor simplifying the comparison. Initially the substitution was attempted using only 2 equiv. of thiophenol. Surprisingly, less than 5% conversion was observed after 3 h as indicated by the ^{1}H NMR spectra (**Figure 2.14A**). In a subsequent reaction 2 equiv. of the sterically hindered base *N*,*N*-Diisopropylethylamine (DIPEA) was added to deprotonate the thiol, thereby increasing its nucleophilicity. This change resulted in a quantitative conversion to the desired polythiophenol product, as determined by a shift of proton signals from 4.34 and 3.65 ppm, to 4.08 and 3.09 ppm respectively, as well as the appearance of aromatic signals at ~7.1 ppm in ^{1}H NMR (**Figure 2.4B** and **Figure 2.14**), and the SEC trace also shifts to higher M_w (**Figure 2.4A**). Purification was conveniently achieved by precipitation in methanol. Comparison of the elemental analysis of the precursor pBEA with the polythiophenol product further demonstrates that the final product is pure and free from unreacted bromine sites. Remarkably, the ability to limit or promote reactivity by a change of pH offers the unique potential to combine this reaction with other thiol targeting conjugations such as the radical thiol-ene "click" and Michael addition to an acceptor.

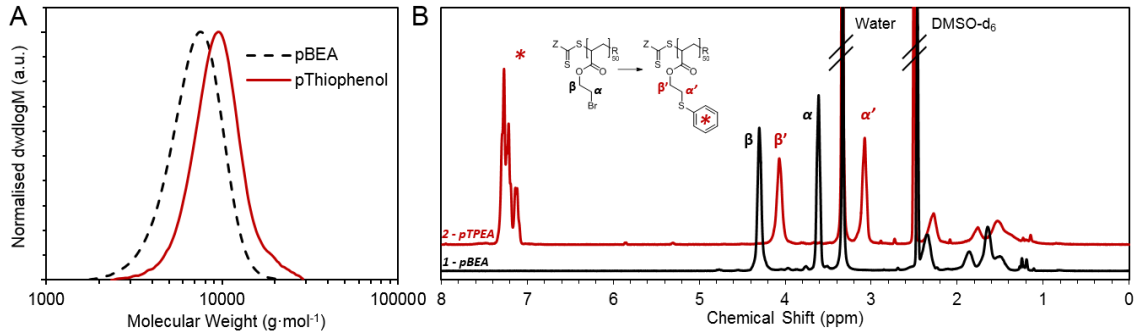

Figure 2.4: (A) SEC trace of precursor $pBEA_{50}$ (**1**), and post-substitution $pTPEA_{50}$, showing the similarity in distribution (B) ^{1}H NMR in DMSO-d_6 indicating the shifts of the pendant ethyl acrylate chain for protons α and β of $pBEA_{50}$ (**1**) and protons α' and β' of $pTPEA_{50}$.

Another highly desirable functionality to introduce is the azide group, which provides a potent platform for further post-modification reactions.[6, 53, 54] The direct synthesis of polyazides requires polymerisation of azido monomers at low temperatures,[55, 56] and numerous steps involve handling the toxic and potentially explosive azido derivatives. In this case, 2 equiv. of sodium azide were used and the reaction proceeded smoothly at room temperature, yielding full conversion after 16 h, with the excess sodium azide conveniently removed by precipitation in a brine/water mixture. Conversion was readily observed by the shift in the ^{1}H NMR (**Figure 2.5B**), 4.34 and 3.65 ppm, to 4.17 and 3.54 ppm in DMSO-d_6, and the appearance of a strong signal at 2200 cm^{-1} in the IR spectrum (**Figure 2.5A**) that corresponds to the $-N_3$ stretch frequency. This post-modification strategy for the synthesis of polyazides circumvents the use of highly reactive azido monomers, yet still readily provides the desired polymer.

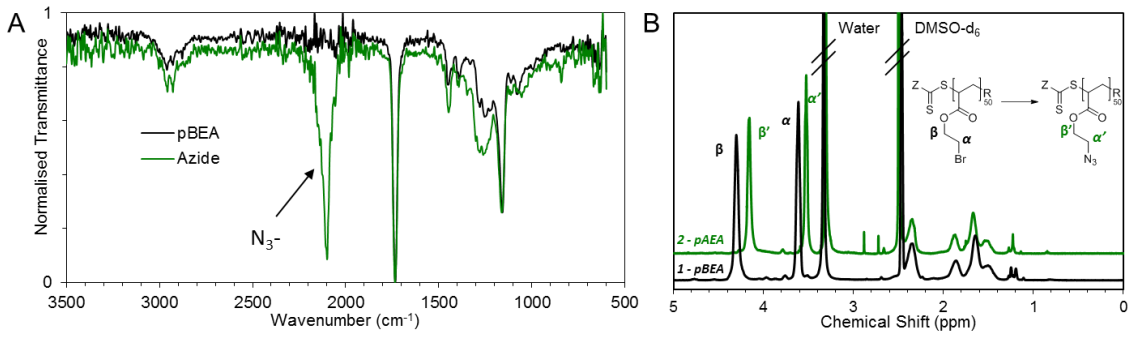

Figure 2.5: (A) IR overlay showing the absorbance of the $pBEA_{50}$ (**1**) vs. $pAEA_{50}$ (B) ^{1}H NMR in DMSO-d_6 indicating the shifts of the pendant ethyl acrylate chain for protons α and β of $pBEA_{50}$ (**1**) and protons α' and β' of $pAEA_{50}$.

Another example where direct synthesis by controlled radical polymerisation is very demanding is the preparation of polyelectrolytes.[57] The usual method of synthesis requires either protection of the ionic group or use of water as the polymerisation medium rendering it incompatible with hydrophobic co-monomers. The use of BEA as a precursor enables the synthesis of random and block copolymers in a hydrophobic environment before subsequent modification to give the polyelectrolyte.[58, 59] Cationic polyelectrolytes were prepared *via* quarternisation with trimethyl amine or trimethyl phosphine. Tertiary amines are known to be strong nucleophiles, however, sterically demanding groups

encumber reaction on the amine as in the case of the sterically hindered DIPEA. Strong nucleophiles are also able to cleave trithiocarbonates, resulting in a free thiol at the terminus of polymer chains, as in the case of aminolysis.[60] However, generally this requires a substantial excess of nucleophile to cleave all chain ends, and the nucleophile is likely to react preferentially with the alkyl halide than with the trithiocarbonate. For the less hindered trimethyl amine, the reaction proceeded rapidly to yield quantitative conversion of the bromine group (**Figure 2.10**) and a highly charged polyelectrolyte is obtained. Following this, the structurally and nucleophilically similar reaction of trimethyl phosphine with the bromine precursor was undertaken. This reaction was carried out under identical conditions to that of trimethyl amine and provided a particularly hygroscopic, polycationic polymer species (**Figure 2.11**).

As previously mentioned this post modification route facilitates preparation of well-defined ionic copolymers starting from hydrophobic monomers. To demonstrate the versatility of this method, the substitution reaction on the previously described block copolymers pBA-*b*-pBEA using trimethyl amine was tested. Similar to the corresponding homopolymers the reaction proceeds smoothly. The obtained pTMAEA-*b*-pBA block copolymer enables the formation of micellar structures, due to the opposing polarity of polyelectrolyte and pBA blocks. Dispersing the copolymer in water gives a highly turbid solution, which was analysed using DLS and zeta-potential. The results confirm the formation of uniform micelles with a positive surface charge (**Table 2.5**).

In contrast to cationic polymers, strong anionic polyelectrolytes such as poly sulfonates are so far only accessible *via* the direct polymerisation of the respective sulfonate monomers, which require either stringent reaction conditions or protecting group strategies. Surveying the literature on preparation of sulfonates, it was discovered that sulfite salts are known to be excellent nucleophiles (the Strecker reaction), that have thus far been neglected for decades likely due to the limited solubility of these salts in organic solvent.[61, 62] Based on a recent report,[26] the tetraethyl ammonium salt starting from dimethyl sulfite was synthesised; a salt that displays superior solubility in polar organic solvents such as methanol or DMSO. With this material in hand, the substitution efficiency of the sulfite on the bromine polymer was tested. Astonishingly, this reaction

rapidly generates the desired sulfonate polymer in quantitative yield without any need for further optimisation (**Figure 2.6**). The success of this reaction highlights the strong nucleophilic character of sulfites and the preparation of alkyl ammonium salts drastically improves their solubility in organic media, which is crucial for such polymer analogous reactions.

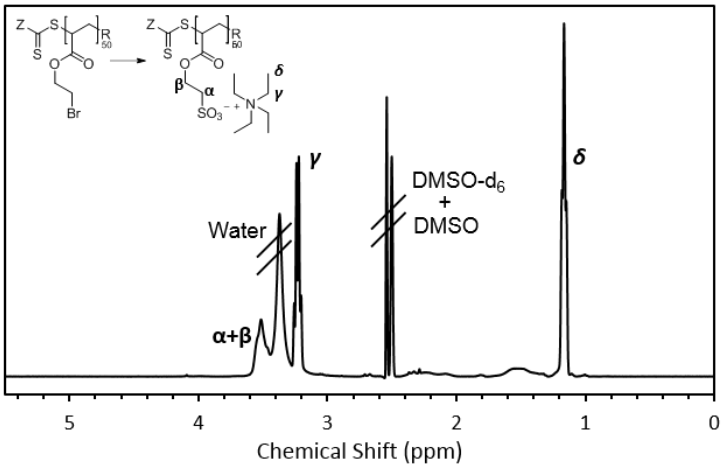

Figure 2.6: ^{1}H NMR in DMSO-d_6 of tetraethyl ammonium sulfonate polymer from $pBEA_{50}$

Finally, more biological relevant polymers were studied. Glycopolymers have recently attracted considerable attention due to their exclusive binding properties to surface proteins.[63] The direct polymerisation of the respective glycomonomers still remains a challenge, and thus far the most common routes are *via* polymerisation of protected sugar monomers[64] or post modification such as using CuAAC or activate ester strategies.[14, 22, 65, 66] Nevertheless, these attachments create additional linker groups such as triazoles that may impact on binding affinity.[67, 68] The presented substitution of BEA does not create such expansive linkers. Given the success of the thio-bromo substitution using thiophenol, the commercially available thiolated sugar, β-thioglucose sodium salt was used. Anticipating that the thiolate anion would be sufficiently nucleophilic for the substitution, the reaction was conducted in the absence of any additional base. As confirmed by ^{1}H NMR (**Figure 2.15**), substitution was quantitative after 48 h, using only 1.5 molar excess of the sugar, at room temperature. The SEC trace (**Figure 2.16**) indicates there was some end group removal of the RAFT agent that caused minor disulfide

formation resulting in a shoulder at high molecular weight. Any additional sugar starting material was then easily and rapidly separated from the obtained glycopolymer, by centrifugal filtration. Considering the convenient synthesis of the precursor polymer by RAFT, the availability of various thiosaccharides, and the efficiency of the substitution, this synthesis represents a cost effective and scalable route towards accessible and well-defined glycopolymers. Furthermore, by proceeding without catalysts nor protecting groups, and under very mild conditions, this is a protocol that could be widely applicable due to the ease of characterisation of the precursor, which with limited synthetic effort could rapidly generate a library of glycopolymers.

Table 2.2: Summary of pBEA substitutions and structural characteristics of polymers and derivatives.

Nucleophile	Conv.[a]	DP	$M_{n,th}$[b] pBEA	$M_{n,SEC}$[c] pBEA	$M_{n,th}$[b] Substituted	$M_{n,SEC}$[c] Substituted	M_w/M_n[c]
Trimethyl amine	>99%	50	8000	6500	10600	-	-
Trimethyl amine	>99%	100	16500	15100	24200	-	-
Trimethyl phosphine	88%	50	8000	6500	11300	-	-
TEA sulfite	>99%	50	8000	6500	13600	6500	1.21
TEA sulfite	>99%	150	26200	24600	45100	18200	1.34
Sodium azide	>99%	50	8000	6500	7200	6800	1.16
β-D-Thioglucose	>99%	50	8000	6500	15100	21400	1.16
Thiophenol	>99%	50	8000	6500	10800	9500	1.18
Trimethyl amine	>99%	50-*b*-70	22800	24600	21200	-	-
Trimethyl phosphine	>99%	50-*b*-70	22800	24600	22100	-	-

[a] Determined from ^{1}H NMR
[b] Calculated from the conversion and characteristics of the parent polymer
[c] From SEC analysis

2.3 Conclusion

This work demonstrates that nucleophilic substitutions of a halogen side group polymer, a reaction that has been widely disregarded in polymer science to date, enables access to highly reactive and yet well-defined homopolymers. These polymers can be synthesised without the need of stringent polymerisation conditions nor at the cost of polymer yield. Here is demonstrated a convenient and versatile synthesis of an alkylbromo polymer, pBEA that can be readily synthesised under RAFT conditions. A series of pBEA

polymers were synthesised with varied molecular weights (2.0 – 26.2 kg mol $^{-1}$) and narrow dispersities (PDI = 1.10 – 1.17). Chain extension of these macro-CTAs proved that the majority of the chain ends remain active and no significant side reactions were observed despite the high reactivity of the bromine groups. The versatility of pBEA in nucleophilic substitutions for efficient production of a diverse library of functional polymers is shown. Therefore a variety of nucleophiles were examined including well known nitrogen based substituents such as azides or tertiary amines, but also the unreported sulfites and sugars were tested. Across all these nucleophilic species the substitution of pBEA proceeded with almost quantitative conversion (> 88%). A major advantage of this simple substitution are the mild conditions employed, *i.e.* room temperature and no need for additional catalysts.

In combination with the good control provided by RAFT, this strategy enables the synthesis of well-defined, highly charged polycations, permanently charged polyanions, stable polythiol ethers, a highly reactive polyazide and even synthetically demanding glycopolymers with minimal synthetic effort. In particular, the substitution using thiols is not limited to the demonstrated materials, but can certainly be extended to encompass other available thiolates. Considering the potential to create libraries of various materials with minimal effort and originating from a single precursor polymer, the presented synthesis route represents a unique and versatile tool for material science. All these materials were later grafted to a cyclic peptide core to study the self-assembly process.

2.4 Experimental

2.4.1 Materials

Triethylamine, dioxane and DMSO were purchased from Fisher Scientific. 4,4-Azobis(4-cyanovaleric acid) (ACVA) was purchased from MP Biomedicals. All other compounds were purchased from Sigma-Aldrich. All chemicals were used as received. All solvents were bought from commercial sources and used as received.

2.4.2 Instrumentation

^{1}H NMR spectra were recorded on a Bruker AV-300, HD-300 or AV-400 in $CDCl_3$, D_2O or DMSO-d_6. Shift values (δ) are reported in ppm. The residual proton signal of the solvent was used as an internal standard ($CDCl_3$ δ_H 7.26, D_2O δ_H 4.79, DMSO-d_6 δ_H 2.50). Size exclusion chromatography (SEC) was carried out on a Polymer Laboratories PL-GPC 50 Plus. All anionic polymers were analysed on a Polymer Laboratories PL-GPC 50 Plus system using a PL aquagel-OH guard column (5μm, 7.5 × 50 mm) followed by two PL aquagel-OH 30 columns (7.5 × 300 mm). Water (0.1 M $NaNO_3$) was used as eluent at 1.0 mL min^{-1} at 30 °C. All other polymers were analysed on a Polymer Laboratories PL-GPC 50 Plus system using a PolarGel-M guard column (7.5 × 50 mm) followed by two PolarGel-M columns (7.5 × 300 mm). DMF (0.1% LiBr) was used as eluent at 1.0 mL· min^{-1} at 50 °C. Commercial narrow linear poly(methyl methacrylate) standards in range of 2.0 × 10^2 g mol^{-1} to 1.0 × 10^6 g mol^{-1} were used to calibrate the DMF SEC system. Analyte samples were filtered through polytetrafluoroethylene (PTFE) membrane with either 0.2 μm or 0.45 μm pore size before injection (100 μL). Centrifugal filtration was carried out using Vivaspin® 20, 3,000 MWCO centrifuge tubes. Experimental $M_{n,SEC}$ and $Đ$ values of synthesised polymers were determined using Agilent GPC software. Elemental analyses for CHN were carried out on a CE440 CHN Elemental Analyser, and Bromine was analysed using classical oxygen flask methods by Warwick Analytical Service.

2.4.3 (4-cyano pentanoic acid)yl ethyl trithiocarbonate (CPAETC)

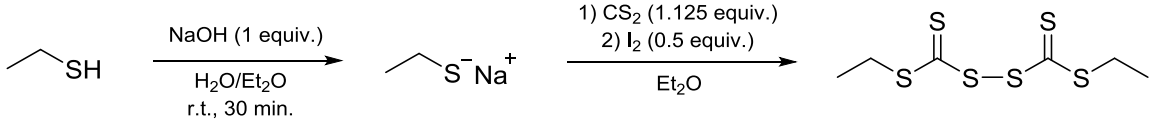

CPAETC was synthesised according to previously published procedures.[69, 70] A solution of ethanethiol (5 mL, 69.3 mmol) was suspended in diethyl ether (50 mL) under strong stirring at room temperature, to which a 27 wt % aqueous solution of sodium hydroxide (~10 g, containing 2.704 g, 69.3 mmol of NaOH) was added. The clear, colourless

solution was stirred for 30 min., then treated with carbon disulfide (4.6 mL, 76.2 mmol) to give an orange solution. After further 30 min stirring, diethyl ether (15 mL) was added and the product reacted with a slow addition of iodine (4.8 g, 37.8 mmol). After 1.5 h, diethyl ether (30 mL) was added and the ether phase washed twice with an aqueous sodium thiosulfate solution (50 mL) and once with water (50 mL). The ether phase was dried over magnesium sulfate, filtered, and the solvent removed under reduced pressure to give the intermediate product bis-(ethylsulfanylthiocarbonyl) disulfide as an orange oil. This was used unpurified in the subsequent step. ^{1}H-NMR (400 MHz, $CDCl_3$, ppm): δ = 3.31 (4H, *t*, -CH_2-S), 1.36 (6H, *m*, -CH_3).

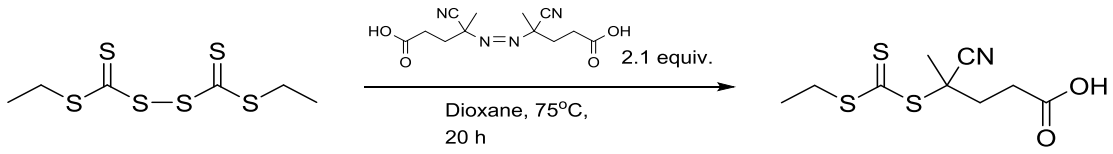

To a solution of bis-(ethylsulfanylthiocarbonyl) disulfide (2.27 g, 8.3 mmol) in dioxane (25 mL), 4,4`-Azobis(4-cyanovaleric acid) (4.6 g, 16.4 mmol) was added and the mixture was stirred for 20 h at 75 °C. Solvent was removed under reduced pressure, and the product purified by silica gel column chromatography (eluent: n-Hexane/EtOAc, 50/50) to afford the expected compound as a dark orange oil (1.51 g, 5.8 mmol, 70 % yield) that solidified on refrigeration. ^{1}H-NMR (400 MHz, $CDCl_3$, ppm): δ = 3.35 (2H, *t*, -CH_2-S), 2.71-2.67 (*m*, 2H, -CH_2-), 2.58-2.36 (2*m*, 2H, -CH_2-), 1.89 (3H, *s*, -CH_3-), 1.36 (3H, *t*, -CH_3); ^{13}C-NMR (100 MHz, $CDCl_3$, ppm): δ = 216.9, 177.3, 118.9, 46.2, 33.4, 31.4, 29.5, 24.8, 12.7; MS (ESI): $[M+Na]^+$ calculated: 286.0, found: 285.9.

2.4.4 Synthesis of 2-bromoethyl acrylate (BEA)

BEA monomer was adapted from previously reported procedures.[33, 71] In a typical reaction, 2-bromoethanol (67 g, 38 mL, 0.54 mol) was dissolved in CH_2Cl_2 (300 mL) to which triethylamine (82.2 mL, 59.7 g, 0.59 mol) was added under a nitrogen atmosphere, and the reaction cooled to 0 °C. Acryloyl chloride (53.4 g, 47.9 mL, 0.59 mol) in CH_2Cl_2 (30 mL) was subsequently added dropwise over an hour with stirring. The reaction was allowed to warm to room temperature overnight with continued stirring. Upon

completion, the reaction mixture was filtered, the solid residue washed with CH_2Cl_2, and the organic layer washed with water (2 × 100 mL) then brine (2 × 100 mL). The organic layer was dried over anhydrous $MgSO_4$, filtered and the solvent removed *via* rotary evaporation. The product was purified by distillation under reduced pressure (~1 mBar, 39 - 40 ^oC) to give 2-bromoethyl acrylate as a clear colourless liquid in 80% yield. ^1H NMR (300 MHz, 293 K, $CDCl_3$, δ): 6.46 (dd, *J* = 17.3, 1.5 Hz, 1 H, C=C*H*$_2$), 5.62 (dd, *J* = 17.3, 10.4 Hz, 1 H, CH_2=C*H*-), 5.89 (dd, *J* = 10.5, 1.4 Hz, 1 H, C=C*H*$_2$), 4.47 (t, *J* = 6.1 Hz, 2 H, -OC*H*$_2$CH$_2$-), 3.55 (t, *J* = 6.2 Hz, 2 H, -CH$_2$C*H*$_2$Br) ppm; ^{13}C-NMR (100 MHz, $CDCl_3$, ppm): δ = 165.52, 131.63, 127.82, 63.83, 28.60; Boiling Point: 41 - 43 ^oC (0.68 mmHg).

2.4.5 RAFT polymerisation of BEA

Polymers were synthesised by the following general method. A small vial was charged with magnetic stirrer; (4-cyano pentanoic acid)yl ethyl trithiocarbonate (0.0535 g, 0.203 mmol), BEA (2.0 g, 11.17 mmol), ACVA (5.69 mg, 0.0203 μmol) and 1,3,5-trioxane (~5 mg) as an internal standard. The mixture was dissolved in dioxane (2 mL) and the vial sealed with a rubber septum and deoxygenated by a stream of bubbled nitrogen for 10 min. The vial was then suspended in a preheated oil bath at 70 ^oC and allowed to stir for 3 h. Upon completion the solution was cooled to room temperature, opened to air and precipitated in diethyl ether to give compound **1**. ^1H-NMR (400 MHz, DMSO-d_6, ppm): δ = 4.34 (*m*, 2*n*H), 3.65 (*m*, 2*n*H), 2.39-1.54 (4*m*, 3*n*H), 1.29 (*t*, 3H); ^1H-NMR (300 MHz, $CDCl_3$, ppm): δ = 4.41 (*m*, 2*n*H), 3.55 (*m*, 2*n*H), 2.45 (*m*, *n*H), 2.03 (*m*, 0.5*n*H), 1.76 (*m*, *n*H), 1.59 (*m*, 0.5*n*H), 1.36 (*t*, 3H); ^{13}C-NMR (100 MHz, $CDCl_3$, ppm): δ = 63.75, 41.24, 34.89, 28.90, 25.61, 24.05, 12.80; IR (thin film) ν_{max} 2962, 2929, 1733, 1444, 1386, 1280, 1244, 1219, 1161, 1084 cm^{-1}. For further details see **Table 2.3**. See **Figure 2.2** for typical SECs in DMF (0.1 % LiBr): A1: $pBEA_{50}$, M_n = 7000 g·mol^{-1}, M_w = 7800 g·mol^{-1}, $Đ$ = 1.12.

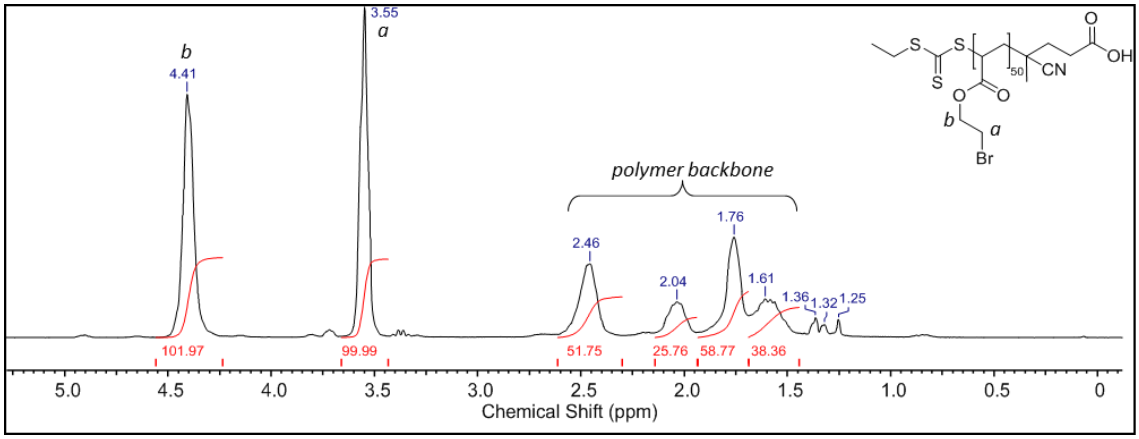

Figure 2.7: ^{1}H NMR in $CDCl_3$ of $pBEA_{50}$.

2.4.6 RAFT block copolymerisation of p(BEA)-b-p(BA)

Block-copolymers were synthesised by the following general method. A small vial was charged with magnetic stirrer, $pBEA_{50}$ (compound A1 **Table 2.3**) homopolymer macro-chain transfer agent (macro-CTA) (0.243 g, 0.026 mmol), BA (0.4 g, 3.121 mmol), ACVA (0.73 mg, 0.0026 μmol) and 1,3,5-trioxane (~5 mg) as an internal standard. The mixture was dissolved in dioxane (0.4 mL) and the vial sealed with a rubber septum and deoxygenated by a stream of bubbled nitrogen for 10 min. The vial was then suspended in a preheated oil bath at 70 °C and allowed to stir for 2 h. Upon completion the solution was cooled to room temperature, opened to air and precipitated in methanol. ^{1}H-NMR (400 MHz, $CDCl_3$, ppm): δ = 4.41 (*m*, 2*n*H), 3.96 (*m*, 2*m*H), 3.55 (*m*, 2*n*H), 2.45 (*m*, *n*H), 2.27 (*m*, *m*H), 2.03 (*m*, 0.5*n*H), 1.89 (*m*, 0.5*m*H), 1.76 (*m*, *n*H), 1.60 (br *d*, [2*m*H + 0.5*n*H]), 1.36 (br *d*, [2*m*H + 3H]), 0.93 (br *t*, 3*m*H). For further details of conditions see **Table 2.4**. See **Figure 2.2**A for a typical SEC in DMF (0.1 % LiBr): $pBEA_{50}$-*b*-pBA_{70}: M_n = 18200 g·mol^{-1}, M_w = 22700 g·mol^{-1}, $Đ$ = 1.25.

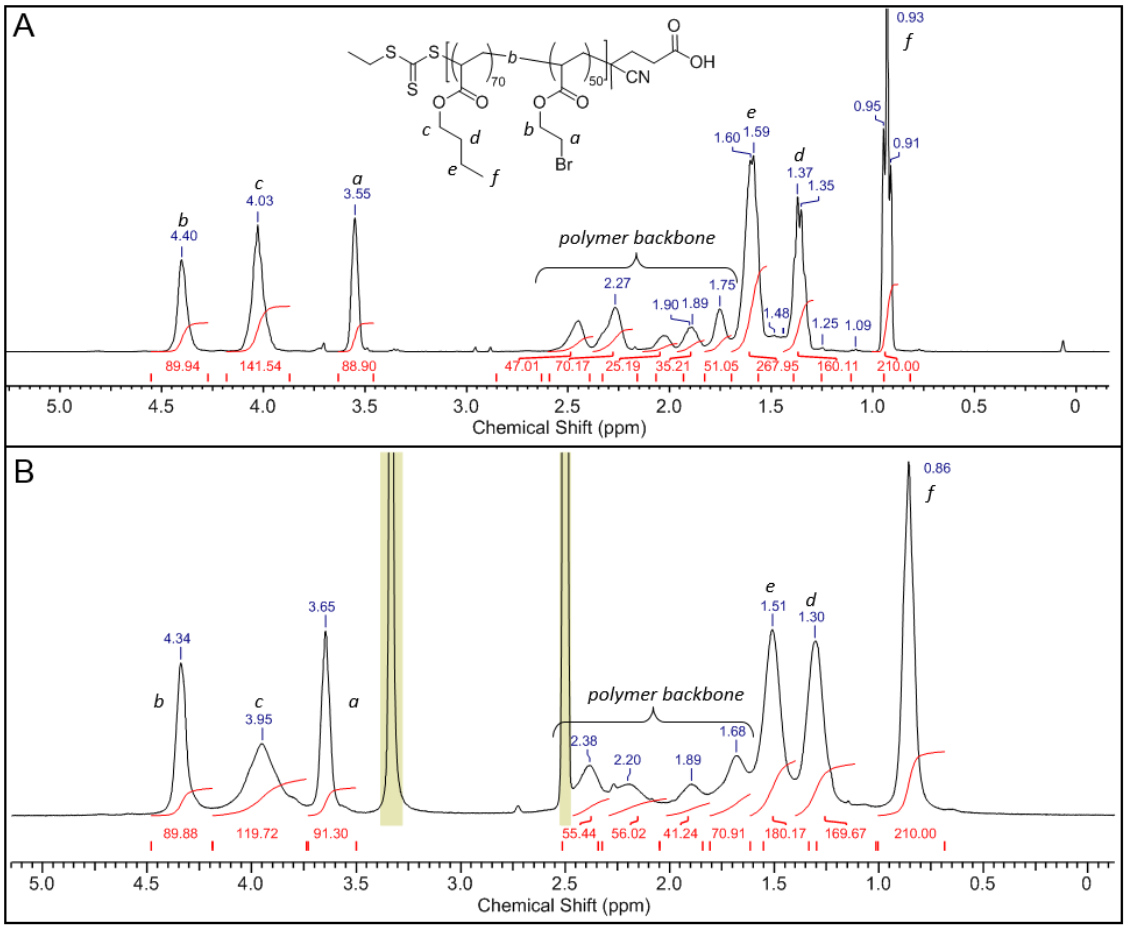

Figure 2.8: ^{1}H NMR pBEA$_{50}$-*b*-pBA$_{70}$ (from macro-CTA **A1**) in (A) in $CDCl_3$ and (B) DMSO-d_6.

2.4.7 RAFT polymerisation of BA

Polymers were synthesised by the following general method. A small vial was charged with magnetic stirrer; (4-cyano pentanoic acid)yl ethyl trithiocarbonate (0.0137 g, 0.052 mmol), BA (1.0 g, 7.80 mmol), ACVA (1.46 mg, 0.0052 μmol) and 1,3,5-trioxane (~5 mg) as an internal standard. The mixture was dissolved in dioxane (1 mL) and the vial sealed with a rubber septum and deoxygenated by a stream of bubbled nitrogen for 10 min. The vial was then suspended in a preheated oil bath at 70 ºC and allowed to stir for 2 h. Upon completion the solution was cooled to room temperature, opened to air and precipitated in diethyl ether. ^{1}H-NMR (300 MHz, $CDCl_3$, ppm): δ = 4.01 (*m*, 2*m*H), 2.29 (*m*, *m*H), 1.89 (*m*, 0.5*m*H), 1.60 (br *m*, 2*m*H), 1.39 (br *m*, 2*m*H), 0.94 (br *t*, 3*m*H). For

more details see **Table 2.3**. Anal. calcd. for $C_{259}H_{363}Br_{50}NO_{102}S_3$: C 33.76%, H 3.97%, N 0.15%, Br 43.36%. Found: C 34.19%, H 4.04%, N 0.14%, Br 45.14%. For further details see **Table 2.3**. See **Figure 2.3** for a typical SEC in DMF (0.1 % LiBr): A3 : pBA-$_{105}$: M_n = 15400 g·mol^{-1}, M_w = 16600 g·mol^{-1}, $Đ$ = 1.08.

2.4.8 RAFT block copolymerisation of p(BA)-b-p(BEA)

Block-copolymers were synthesised by the following general method. A small vial was charged with magnetic stirrer, pBA$_{115}$ (compound A3 **Table 2.3**) homopolymer macro-chain transfer agent (macro-CTA) (0.502 g, 0.037 mmol), BEA (0.4 g, 2.23 mmol), ACVA (1.04 mg, 0.0037 µmol) and 1,3,5-trioxane (~5 mg) as an internal standard. The mixture was dissolved in dioxane (0.4 mL) and the vial sealed with a rubber septum and deoxygenated by a stream of bubbled nitrogen for 10 min. The vial was then suspended in a preheated oil bath at 70 ºC and allowed to stir for 2 h. Upon completion the solution was cooled to room temperature, opened to air and precipitated in methanol. ^{1}H-NMR (300 MHz, $CDCl_3$, ppm): δ = 4.38 (*m*, 2*n*H), 4.01 (*m*, 2*m*H), 3.52 (*m*, 2*n*H), 2.43 (*m*, *n*H), 2.25 (*m*, *m*H), 1.99 (*m*, 0.5*n*H), 1.87 (*m*, 0.5*m*H), 1.73 (*m*, *n*H), 1.57 (br *m*, [2*m*H + 0.5*n*H]), 1.35 (br *m*, [2*m*H + 3H]), 0.91 (br *t*, 3*m*H). For further details see **Table 2.4**. See **Figure 2.3** for a typical SEC in DMF (0.1 % LiBr): pBA$_{105}$-*b*-pBEA$_{40}$: M_n = 22800 g·mol^{-1}, M_w = 24600 g·mol^{-1}, $Đ$ = 1.08.

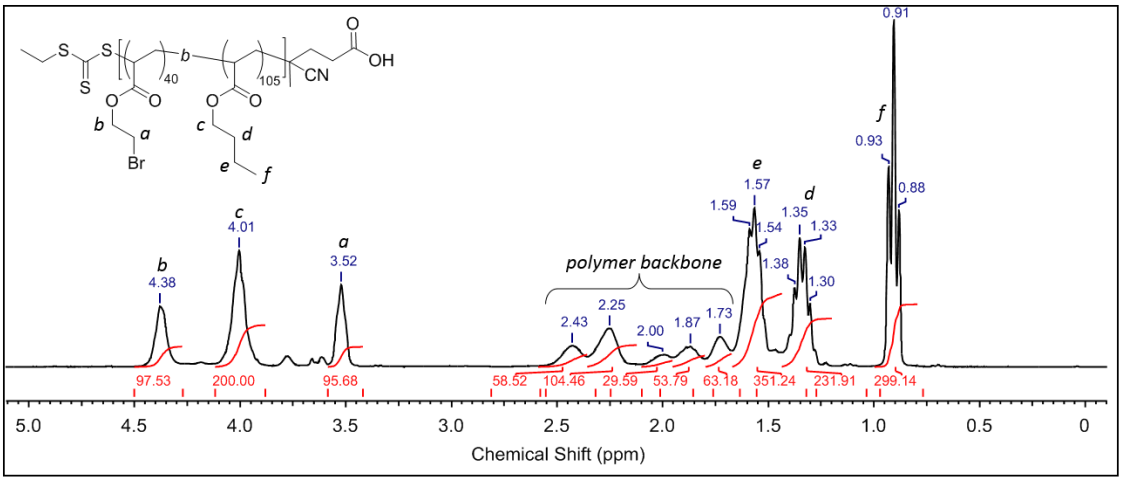

Figure 2.9: ^{1}H NMR in $CDCl_3$ of pBA$_{105}$-*b*-pBEA$_{40}$ from macro-CTA **A3**.

Table 2.3: Summary of RAFT homopolymerisation for use as macro-CTAs.

Polymer	Monomer	$\frac{[M]_0}{[CTA]_0}$	$\frac{[CTA]_0}{[I]_0}$	Conv.[a] (%)	$M_{n,th}$[b] (g·mol^{-1})	$M_{n,SEC}$[c] (g·mol^{-1})	Đ
A1	BEA	55	10	92	9100	7100	1.12
A2	BEA	61	10	75	7800	7000	1.09
A3	BA	150	10	74	13900	15400	1.08

[a] Determined from ^{1}H NMR.

[b] Calculated from the conversion and characteristics of the parent polymer.

[c] From SEC analysis (DMF LiBr, pMMA-Std.).

Table 2.4: Summary of RAFT chain extensions.

Macro CTA	Block 1 monomer	Block 2 monomer	$\frac{[M]_0}{[CTA]_0}$	$\frac{[CTA]_0}{[I]_0}$	Conv.[a] (%)	$M_{n,th}$[b] (g·mol^{-1})	$M_{n,SEC}$[c] (g·mol^{-1})	Đ
A1	BEA	BA	120	10	64	22000	18200	1.25
A2	BEA	BA	150	10	70	23000	15900	1.20
A3	BA	BEA	60	10	68	20700	22800	1.08

[a] Determined from ^{1}H NMR.

[b] Calculated from the conversion and characteristics of the parent polymer.

[c] From SEC analysis (DMF LiBr, pMMA-Std.).

2.4.9 Post-polymerisation substitutions of homopolymers

2.4.9.1 Substitution with Trimethyl amine

Typical reaction of trimethyl amine with pBEA: $pBEA_{50}$ (0.10 g, 12.6 μmol) was suspended in 3 mL of DMSO in a small vial with stirrer bar, to which was added 2 equiv. of trimethyl amine (4.2 M in ethanol, 300 μL, 1.26 mmol) and stirred for 24 h under a N_2 atmosphere. Upon completion, the solution was diluted with H_2O, purified by dialysis and lyophilised to give the desired poly(trimethyl ammonium bromide ethyl acrylate). ^{1}H-NMR (300 MHz, DMSO-d_6, ppm): δ = 4.53 (*m*, 2*n*H), 3.91 (*m*, 2*n*H), 3.34 (br *m*,

9*n*H), 2.41-1.61 (4*m*, 3*n*H); ^{13}C-NMR (75 MHz, $CDCl_3$, ppm): δ = 175.19, 64.46, 59.02, 54.02, 38.74.

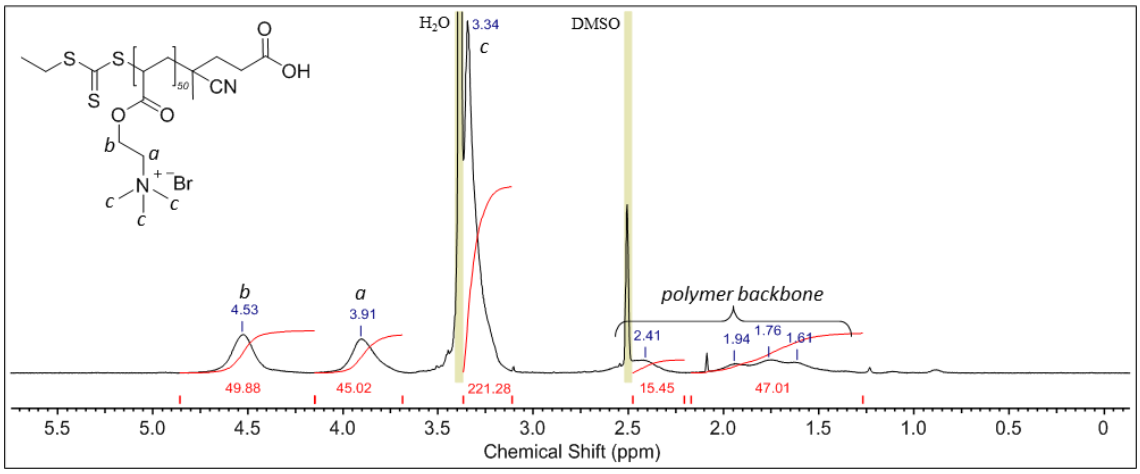

Figure 2.10: ^{1}H NMR in DMSO-d_6 of product from trimethyl amine substitution of $pBEA_{50}$.

2.4.9.2 Substitution with Trimethyl phosphine

Typical reaction of trimethyl phosphine with pBEA: $pBEA_{50}$ (0.10 g, 12.6 μmol) was suspended in 2.5 mL of DMSO in a small vial with stirrer bar, to which was added 2 equiv. of trimethyl phosphine (1 M in THF, 1.30 mL, 1.30 mmol) and stirred for 24 h under a N_2 atmosphere. Upon completion, the solution was diluted with H_2O, purified by dialysis and lyophilised to give the desired poly(trimethyl phosphonium bromide ethyl acrylate). ^{1}H-NMR (300 MHz, DMSO-d_6, ppm): δ = 4.33 (*m*, 2*n*H), 2.80 (*m*, 2*n*H), 2.30 (*m*, *n*H), 2.04 (br *m*, 9*n*H), 1.75-1.50 (2*m*, 2*n*H); ^{13}C-NMR (75 MHz, $CDCl_3$, ppm): δ = 174.21, 71.76, 70.26, 64.71, 58.60, 8.98, 8.26.

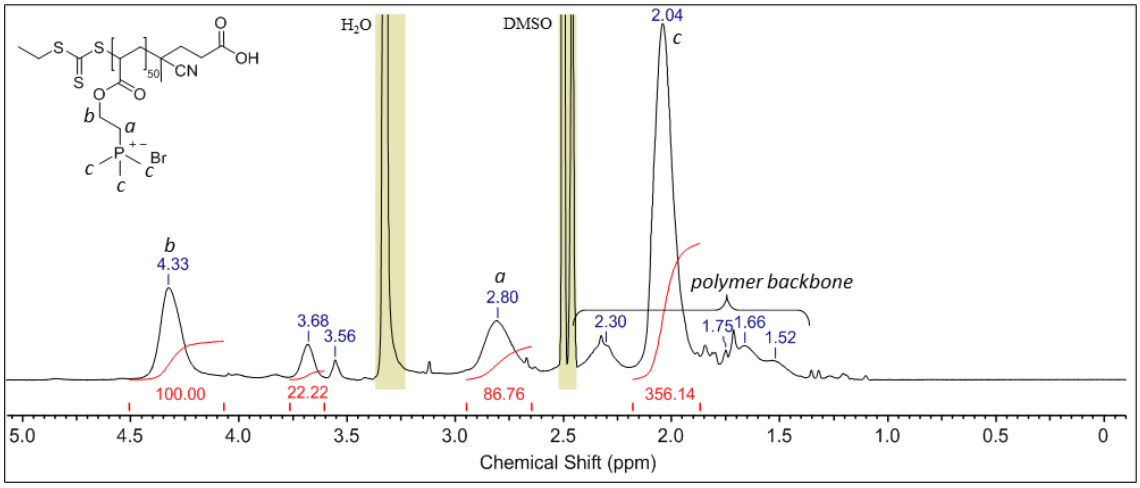

Figure 2.11: ^{1}H NMR in DMSO-d_6 of product from trimethyl phosphine substitution of $pBEA_{50}$.

2.4.9.3 Substitution with Tetraethyl ammonium sulfite

Typical synthesis of tetraethyl ammonium sulfite salt: In a small vial 1 equiv. of dimethylsulfite (0.197 mL, 2.32 mmol) and 1.9 equiv. of tetraethyl ammonium hydroxide (1.5 M solution in methanol, 2.936 mL, 4.04 mmol) are combined and stirred vigorously for 5 h. The turbid solution of tetraethyl ammonium sulfite in methanol is used directly in the substitution of pBEA.

Typical reaction of tetraethyl ammonium sulfite with pBEA: $pBEA_{50}$ (0.10 g, 12.6 µmol) was suspended in 2 mL of DMSO in a small vial with stirrer bar, to which was added 5 equiv. of tetraethyl ammonium sulfite (0.75 M in methanol, 3.72 mL, 5.87 mmol) and stirred for 24 h under a N_2 atmosphere. Upon completion, the solution was diluted with H_2O, purified by dialysis and lyophilised to give the desired poly(ethyl acrylate tetraethyl ammonium sulfonate). ^{1}H-NMR (400 MHz, DMSO-d_6, ppm): δ = 3.55-3.47 (*m*, 2*n*H), 3.23 (*q*, 8*n*H), 2.35-1.32 (4*m*, 3*n*H), 1.16 (*t*, 12*n*H). See **Figure 2.12** for typical SEC traces in water (0.1 M $NaNO_3$): $pEASTEA_{50}$ M_n = 6500 g·mol^{-1}, M_w = 7900 g·mol^{-1}, $Đ$ = 1.21.

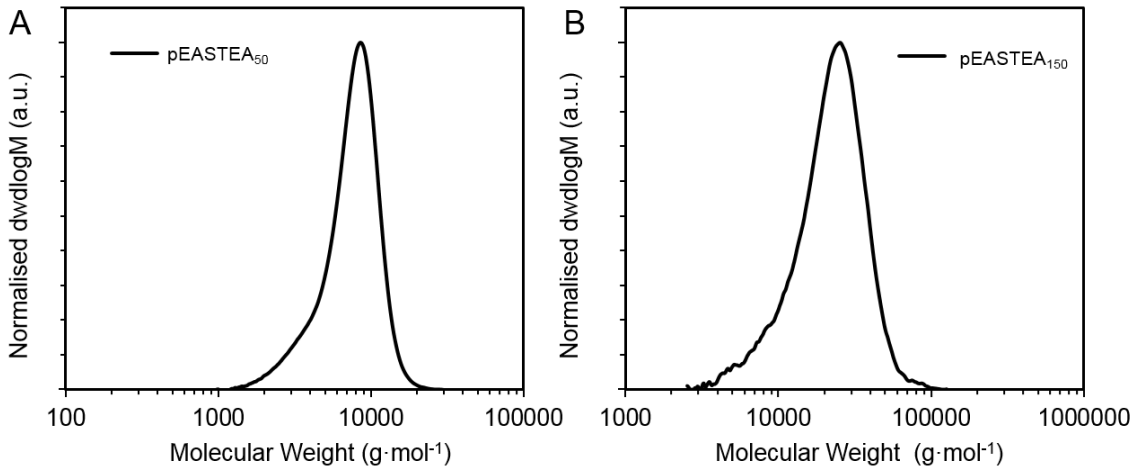

Figure 2.12: SEC trace of product of tetraethyl ammonium sulfite substitution of $pBEA_{50}$ and $pBEA_{150}$.

2.4.9.4 Substitution with Sodium azide

$pBEA_{50}$ (0.05 g, 6.17 μmol) was suspended in 1 mL of DMF in a small vial with stirrer bar, to which was added sodium azide (0.0426 g, 0.49 mmol) in DMF 1.5 mL and stirred for 24 h under a N_2 atmosphere. Upon completion, the solution was precipitated in a 1:1 brine/water mixture, the precipitate was washed with water and dried under a stream of nitrogen to give the desired poly(azido ethyl acrylate). ^{1}H-NMR (300 MHz, DMSO-d_6, ppm): δ = 4.17 (*m*, 2*n*H), 3.54 (*m*, 2*n*H), 2.36-1.54 (4*m*, 3*n*H); IR (thin film) ν_{max} 2958, 2929, 2098, 1733, 1444, 1392, 1302, 1278, 1263, 1162 cm^{-1}. See **Figure 2.13** for a typical SEC trace in DMF (0.1 % LiBr): $pAEA_{50}$ M_n = 6800 g·mol^{-1}, M_w = 7800 g·mol^{-1}, $Đ$ = 1.16.

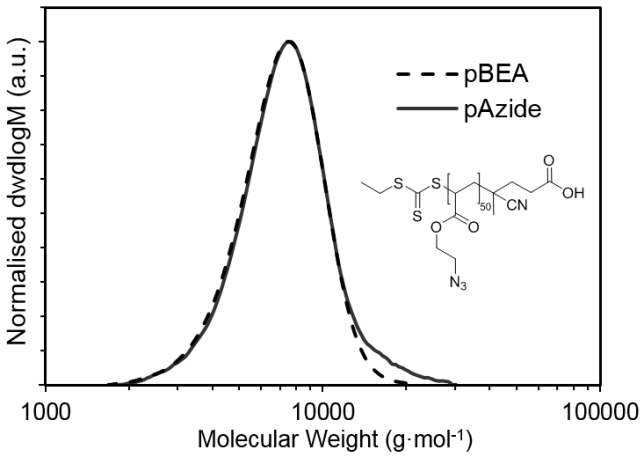

Figure 2.13: SEC trace of product of sodium azide substitution of $pBEA_{50}$.

2.4.9.5 Substitution with Thiophenol

$pBEA_{50}$ (0.04 g, 5.44 μmol) was suspended in 1.5 mL of DMF in a small vial with stirrer bar, to which was added 2 equiv. of thiophenol (50 μL, 0.49 mmol) and DIPEA (77.9 μL, 0.45 mmol) and stirred for 24 h under a N_2 atmosphere. Upon completion, the solution was precipitated in methanol and dried under vacuum to give the desired poly(thiophenol ethyl acrylate). ^{1}H-NMR (300 MHz, DMSO-d_6, ppm): δ = 7.26-7.11 (*m*, 5*n*H), 4.06 (*m*, 2*n*H), 3.07 (*m*, 2*n*H), 2.27-1.39 (4*m*, 3*n*H); ^{13}C-NMR (75 MHz, $CDCl_3$, ppm): δ = 174.18, 174.09, 135.07, 129.74, 129.11, 129.69, 126.54, 67.99, 63.03, 62.90, 41.34, 32.07, 31.97, 25.62; Anal. calcd. for $C_{559}H_{613}NO_{102}S_{53}$: C 62.88%, H 5.79%, N 0.13%. Found: C 60.13%, H 5.62%, N 0.15%. See **Figure 2.14** for ^{1}H-NMR spectra in $CDCl_3$. See **Figure 2.4A** for a typical SEC trace in DMF (0.1 % LiBr): $pTPEA_{50}$ M_n = 8700 g·mol^{-1}, M_w = 9900 g·mol^{-1}, $Đ$ = 1.13.

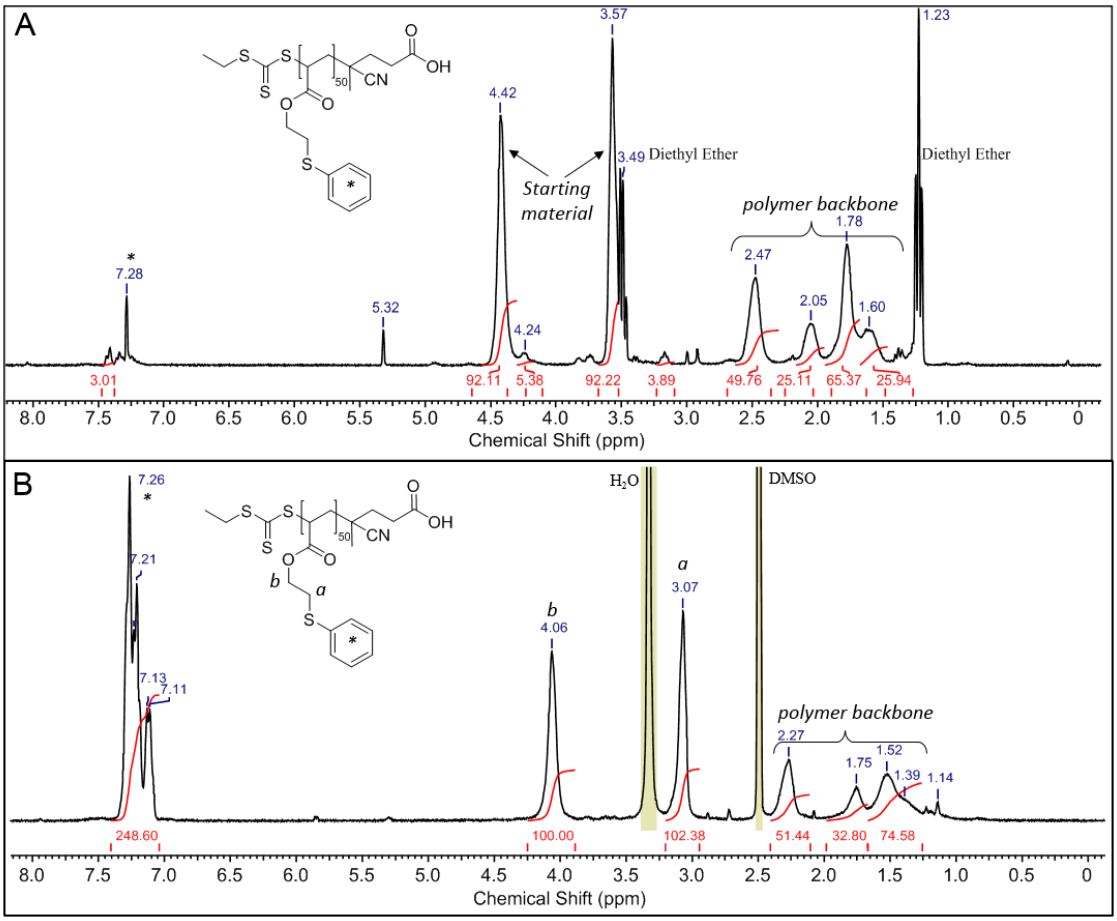

Figure 2.14: ^{1}H NMR in $CDCl_3$ of thiophenol substitutions of $pBEA_{50}$ conducted: (A) without base and (B) in the presence of DIPEA.

2.4.9.6 Substitution with 1-β-D-Thioglucose

$pBEA_{50}$ (0.014 g, 1.7 µmol) was suspended in 1 mL of DMSO in a small vial with stirrer bar, to which was added 1.5 equiv. of β-D-thioglucose sodium salt (21.8 mg, 0.1 mmol) and stirred for 24 h under a N_2 atmosphere. Upon completion, the solution was diluted with H_2O, purified by centrifugal filtration (3000 MWCO) and lyophilised to give the desired poly(β-D-thioglucose ethyl acrylate). ^{1}H-NMR (400 MHz, D_2O, ppm): δ = 4.57 (*d*, *n*H), 4.34(*br m*, 2*n*H), 3.89 (*d*, *n*H), 3.72 (*br d*, *n*H), 3.45 (*br m*, 3*n*H), 3.34 (*br t*, *n*H), 3.05 (*br m*, *n*H), 2.99 (*br m*, *n*H), 2.42 (*br m*, *n*H), 2.00 (*br m*, 0.5*n*H), 1.79 (*br m*, *n*H), 1.64 (*br m*, 0.5*n*H); ^{13}C-NMR (75 MHz, $CDCl_3$, ppm): δ = 176.17, 85.47, 79.93, 77.26,

72.35, 69.47, 64.71, 61.04, 38.71, 28.53. See **Figure 2.16** for a typical SEC trace in DMF (0.1 % LiBr): pTPEA$_{50}$ M_n = 21400 g·mol^{-1}, M_w = 24900 g·mol^{-1}, $Đ$ = 1.16.

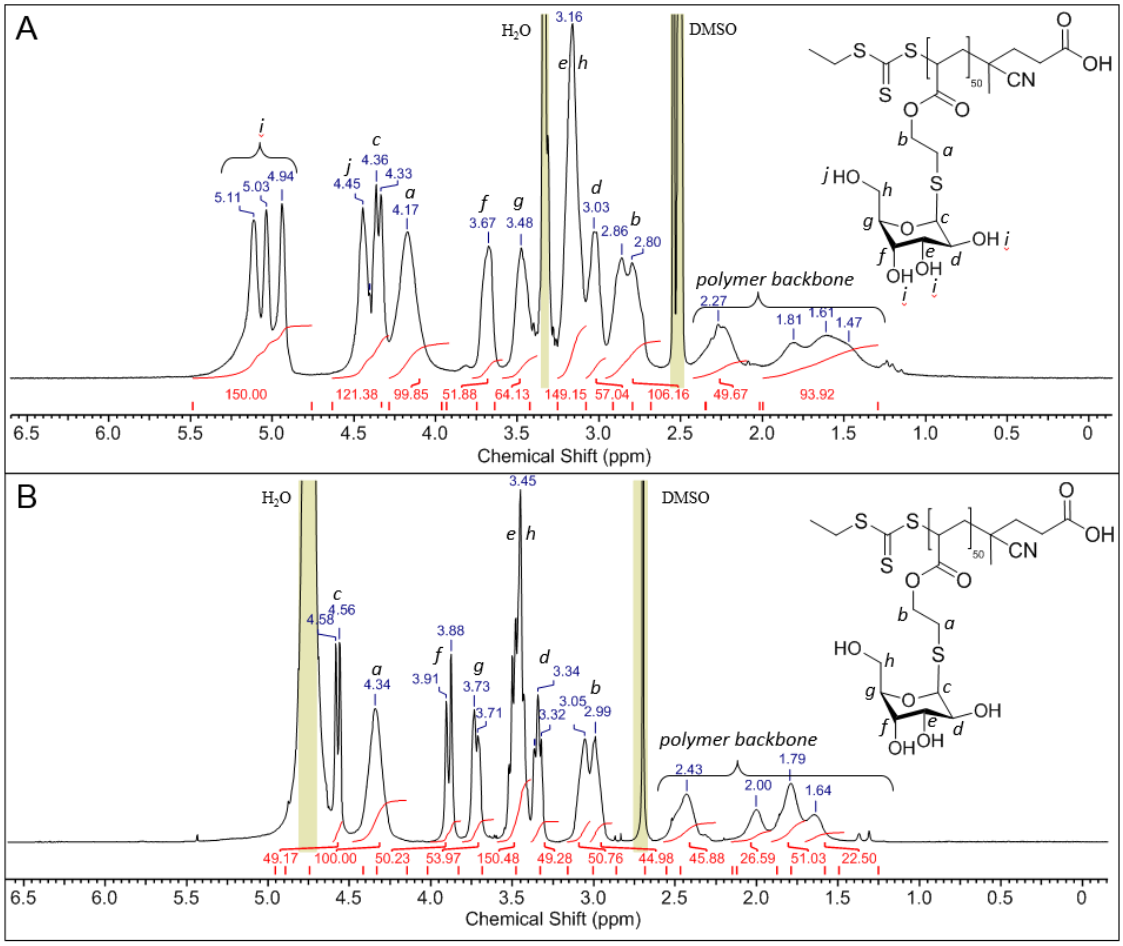

Figure 2.15: ^{1}H NMR of p*Glu*EA$_{50}$ in (A) DMSO-d$_6$ and (B) D$_2$O.

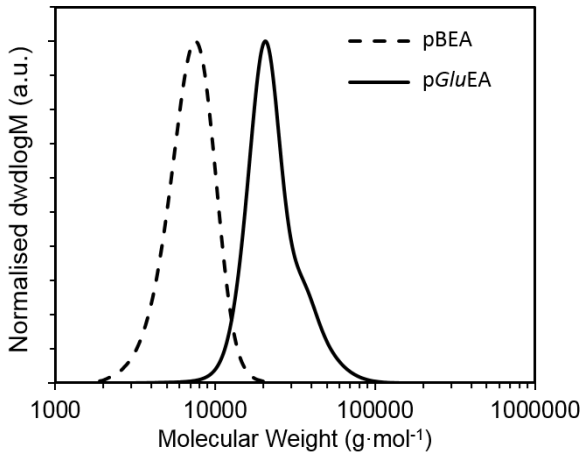

Figure 2.16: SEC trace of product of 1-β-D-thioglucose substitution of $pBEA_{50}$.

2.4.10 Post-polymerisation substitutions of block-copolymers

Block co-polymers of pBEA were substituted in the same manner as the homopolymers (*vide supra*).

2.4.10.1 Substitution with Trimethyl amine

Block co-polymers of pBEA were substituted in the same manner as the homopolymers (*vide supra*). ^{1}H-NMR (400 MHz, DMSO-d_6, ppm): δ = 4.36 (*m*, 2*n*H), 3.96 (*m*, [2*m*H + 2*n*H]), 2.19 (*m*, *m*H), 2.05 (*m*, [*m*H + 0.5*n*H]), 1.95 (*m*, *n*H), 1.77 (*m*, [0.5*m*H + *n*H]), 1.53 (br *d*, [2*m*H + 2*n*H]), 1.32 (br *d*, [2*m*H + *n*H]), 0.87 (br *t*, 3*m*H).

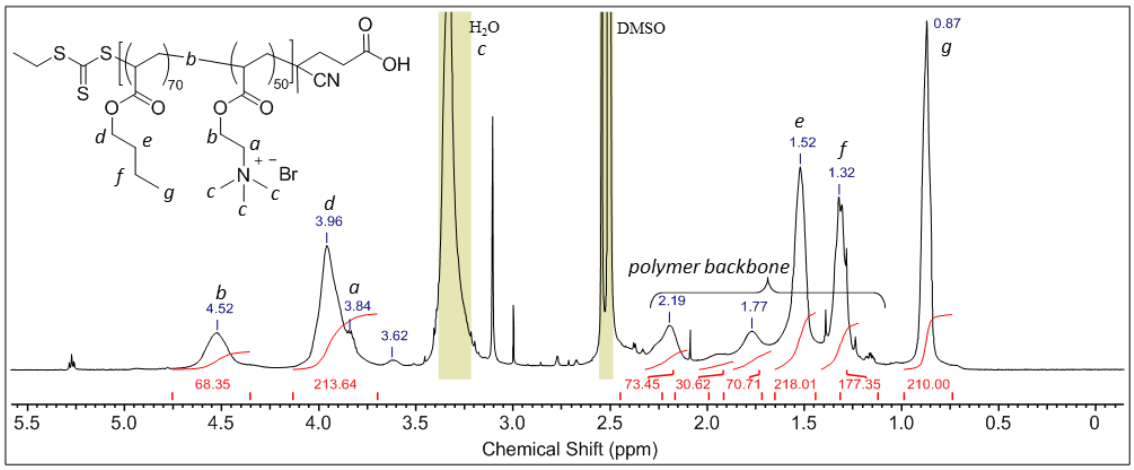

Figure 2.17: ^{1}H NMR in DMSO-d_6 of product from trimethyl amine substitution of $pBEA_{50}$-*b*-pBA_{70}.

2.4.10.2 Substitution with Trimethyl phosphine

Block co-polymers of pBEA were substituted in the same manner as the homopolymers (*vide supra*). ^{1}H-NMR (400 MHz, DMSO-d_6, ppm): δ = 4.36 (*m*, 2*n*H), 3.97 (*m*, 2*m*H), 3.70 (*m*, 2*n*H), 2.80 (*m*, *n*H), 2.19 (*m*, *m*H), 2.05 (br *m*, 9*n*H]), 1.78 (*m*, [0.5*m*H + 2*n*H]), 1.53 (br *d*, [2*m*H + 2*n*H]), 1.32 (br *d*, [2*m*H + *n*H]), 0.87 (br *t*, 3*m*H).

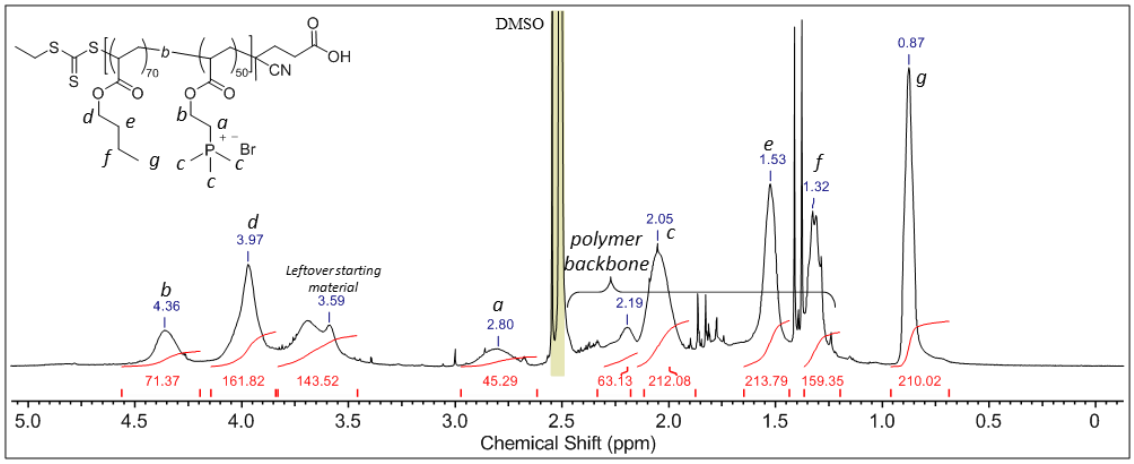

Figure 2.18: ^{1}H NMR in DMSO-d_6 of product from trimethyl phosphine substitution of $pBEA_{50}$-*b*-pBA_{70}.

Table 2.5: DLS and Zeta Potential of block copolymers after substitution with trimethyl amine (pTMAEA) and trimethyl phosphine (pTMPEA).

Sample	Charged Type	Filtered	Size (d.nm)	PDI	Zeta Potential (mV)
pTMAEA	N^+	No	163	0.272	44.6
	N^+	Yes	137	0.202	
pTMPEA	P^+	No	127	0.264	38.26
	P^+	Yes	124	0.205	

2.5 References

1. Braunecker, W. A.; Matyjaszewski, K. *Progress in Polymer Science* **2007,** 32, (1), 93-146.

2. Szwarc, M., Living polymers and mechanisms of anionic polymerization. In *Living Polymers and Mechanisms of Anionic Polymerization*, Springer Berlin Heidelberg: 1983; Vol. 49, pp 1-177.

3. Anastasaki, A.; Nikolaou, V.; Nurumbetov, G.; Wilson, P.; Kempe, K.; Quinn, J. F.; Davis, T. P.; Whittaker, M. R.; Haddleton, D. M. *Chemical Reviews* **2015,** 116, (3), 835-77.

4. Patten, T. E.; Xia, J.; Abernathy, T.; Matyjaszewski, K. *Science* **1996,** 272, (5263), 866-868.

5. Gody, G.; Maschmeyer, T.; Zetterlund, P. B.; Perrier, S. *Nat Commun* **2013,** 4.

6. Günay, K. A.; Theato, P.; Klok, H.-A., History of Post-Polymerization Modification. In *Functional Polymers by Post-Polymerization Modification*, Wiley-VCH Verlag GmbH & Co. KGaA: 2012; pp 1-44.

7. Gunay, K. A.; Theato, P.; Klok, H. A. *J. Polym. Sci. Pol. Chem.* **2013,** 51, (1), 1-28.

8. Gauthier, M. A.; Gibson, M. I.; Klok, H.-A. *Angewandte Chemie International Edition* **2009,** 48, (1), 48-58.

9. Wong, L.; Boyer, C.; Jia, Z.; Zareie, H. M.; Davis, T. P.; Bulmus, V. *Biomacromolecules* **2008,** 9, (7), 1934-1944.

10. Nuhn, L.; Overhoff, I.; Sperner, M.; Kaltenberg, K.; Zentel, R. *Polym. Chem.* **2014,** 5, (7), 2484-2495.

11. Eberhardt, M.; Théato, P. *Macromol. Rapid Commun.* **2005,** 26, (18), 1488-1493.

12. Appukuttan, V. K.; Dupont, A.; Denis-Quanquin, S.; Andraud, C.; Monnereau, C. *Polym. Chem.* **2012,** 3, (10), 2723-2726.

13. Ashok Kothapalli, V.; Shetty, M.; de los Santos, C.; Hobbs, C. E. *Journal of Polymer Science Part A: Polymer Chemistry* **2016,** 54, (1), 179-185.

14. Abdelkader, O.; Moebs-Sanchez, S.; Queneau, Y.; Bernard, J.; Fleury, E. *Journal of Polymer Science Part A: Polymer Chemistry* **2011,** 49, (6), 1309-1318.

15. Li, G.; Wang, H.; Zheng, H.; Bai, R. *Journal of Polymer Science Part A: Polymer Chemistry* **2010,** 48, (6), 1348-1356.

16. Sumerlin, B. S.; Tsarevsky, N. V.; Louche, G.; Lee, R. Y.; Matyjaszewski, K. *Macromolecules* **2005,** 38, (18), 7540-7545.

17. Bousquet, A.; Barner-Kowollik, C.; Stenzel, M. H. *Journal of Polymer Science Part A: Polymer Chemistry* **2010,** 48, (8), 1773-1781.

18. Inglis, A. J.; Sinnwell, S.; Stenzel, M. H.; Barner-Kowollik, C. *Angewandte Chemie International Edition* **2009,** 48, (13), 2411-2414.

19. Kim, T.-D.; Luo, J.; Tian, Y.; Ka, J.-W.; Tucker, N. M.; Haller, M.; Kang, J.-W.; Jen, A. K. Y. *Macromolecules* **2006,** 39, (5), 1676-1680.

20. Liu, P. S.; Song, J. *J. Polym. Sci. Pol. Chem.* **2016,** 54, (9), 1268-1277.

21. Gunay, K. A.; Schuwer, N.; Klok, H.-A. *Polym. Chem.* **2012,** 3, (8), 2186-2192.

22. Gibson, M. I.; Fröhlich, E.; Klok, H.-A. *Journal of Polymer Science Part A: Polymer Chemistry* **2009,** 47, (17), 4332-4345.

23. Kakuchi, R.; Theato, P. *Polym. Chem.* **2014,** 5, (7), 2320-2325.

24. Brendel, J. C.; Liu, F.; Lang, A. S.; Russell, T. P.; Thelakkat, M. *ACS Nano* **2013,** 7, (7), 6069-6078.

25. Mammen, M.; Dahmann, G.; Whitesides, G. M. *Journal of Medicinal Chemistry* **1995,** 38, (21), 4179-4190.

26. Brendel, J. C.; Schmidt, M. M.; Hagen, G.; Moos, R.; Thelakkat, M. *Chemistry of Materials* **2014,** 26, (6), 1992-1998.

27. Zhai, L.; Pilston, R. L.; Zaiger, K. L.; Stokes, K. K.; McCullough, R. D. *Macromolecules* **2003,** 36, (1), 61-64.

28. Sugiyama, K.; Azuma, H.; Watanabe, T.; Ishizone, T.; Hirao, A. *Polymer* **2003,** 44, (15), 4157-4164.

29. David, G.; Boyer, C.; Tonnar, J.; Ameduri, B.; Lacroix-Desmazes, P.; Boutevin, B. *Chemical Reviews* **2006,** 106, (9), 3936-3962.

30. Zetterlund, P. B.; Kagawa, Y.; Okubo, M. *Chemical Reviews* **2008,** 108, (9), 3747-3794.

31. Couture, G.; Améduri, B. *European Polymer Journal* **2012,** 48, (7), 1348-1356.

32. Zheng, Z.; Ling, J.; Müller, A. H. E. *Macromol. Rapid Commun.* **2014,** 35, (2), 234-241.

33. Gu, Y.; Lodge, T. P. *Macromolecules* **2011,** 44, (7), 1732-1736.

34. Cotanda, P.; Sudre, G.; Modestino, M. A.; Chen, X. C.; Balsara, N. P. *Macromolecules* **2014,** 47, (21), 7540-7547.

35. Meek, K. M.; Elabd, Y. A. *Macromolecules* **2015,** 48, (19), 7071-7084.

36. Hedir, G. G.; Bell, C. A.; O'Reilly, R. K.; Dove, A. P. *Biomacromolecules* **2015,** 16, (7), 2049-2058.

37. Hedir, G. G.; Pitto-Barry, A.; Dove, A. P.; O'Reilly, R. K. *Journal of Polymer Science Part A: Polymer Chemistry* **2015,** 53, (23), 2699-2710.

38. Moad, G.; Barner-Kowollik, C., The Mechanism and Kinetics of the RAFT Process: Overview, Rates, Stabilities, Side Reactions, Product Spectrum and Outstanding Challenges. In *Handbook of RAFT Polymerization*, Wiley-VCH Verlag GmbH & Co. KGaA: 2008; pp 51-104.

39. Moad, G.; Rizzardo, E.; Thang, S. H. *Aust. J. Chem.* **2009,** 62, (11), 1402-1472.

40. Moad, G.; Rizzardo, E.; Thang, S. H. *Aust. J. Chem.* **2012,** 65, (8), 985-1076.

41. Gody, G.; Maschmeyer, T.; Zetterlund, P. B.; Perrier, S. *Macromolecules* **2014,** 47, (2), 639-649.

42. Martin, L.; Gody, G.; Perrier, S. *Polym. Chem.* **2015,** 6, (27), 4875-4886.

43. Stenzel, M. H., Complex Architecture Design via the RAFT Process: Scope, Strengths and Limitations. In *Handbook of RAFT Polymerization*, Wiley-VCH Verlag GmbH & Co. KGaA: 2008; pp 315-372.

44. de Lambert, B.; Charreyre, M.-T.; Chaix, C.; Pichot, C. *Polymer* **2007,** 48, (2), 437-447.

45. Chong, Y. K.; Le, T. P. T.; Moad, G.; Rizzardo, E.; Thang, S. H. *Macromolecules* **1999,** 32, (6), 2071-2074.

46. Tang, C.; Kowalewski, T.; Matyjaszewski, K. *Macromolecules* **2003,** 36, (23), 8587-8589.

47. Rosen, B. M.; Lligadas, G.; Hahn, C.; Percec, V. *Journal of Polymer Science Part A: Polymer Chemistry* **2009,** 47, (15), 3931-3939.

48. Rosen, B. M.; Lligadas, G.; Hahn, C.; Percec, V. *Journal of Polymer Science Part A: Polymer Chemistry* **2009,** 47, (15), 3940-3948.

49. Xu, J.; Tao, L.; Boyer, C.; Lowe, A. B.; Davis, T. P. *Macromolecules* **2010,** 43, (1), 20-24.

50. Chen, S.; Ströhl, D.; Binder, W. H. *ACS Macro Letters* **2015,** 4, (1), 48-52.

51. Tsarevsky, N. V.; Matyjaszewski, K. *Macromolecules* **2002,** 35, (24), 9009-9014.

52. Tsarevsky, N. V.; Sumerlin, B. S.; Matyjaszewski, K. *Macromolecules* **2005,** 38, (9), 3558-3561.

53. Lutz, J.-F. *Angewandte Chemie International Edition* **2007,** 46, (7), 1018-1025.

54. Goldmann, A. S.; Glassner, M.; Inglis, A. J.; Barner-Kowollik, C. *Macromol. Rapid Commun.* **2013,** 34, (10), 810-849.

55. Ladmiral, V.; Legge, T. M.; Zhao, Y.; Perrier, S. *Macromolecules* **2008,** 41, (18), 6728-6732.

56. Li, Y.; Yang, J.; Benicewicz, B. C. *Journal of Polymer Science Part A: Polymer Chemistry* **2007,** 45, (18), 4300-4308.

57. Laschewsky, A. *Current Opinion in Colloid & Interface Science* **2012,** 17, (2), 56-63.

58. Kolomanska, J.; Johnston, P.; Gregori, A.; Fraga Dominguez, I.; Egelhaaf, H.-J.; Perrier, S.; Rivaton, A.; Dagron-Lartigau, C.; Topham, P. D. *RSC Advances* **2015,** 5, (82), 66554-66562.

59. Sumerlin, B. S.; Lowe, A. B.; Thomas, D. B.; Convertine, A. J.; Donovan, M. S.; McCormick, C. L. *Journal of Polymer Science Part A: Polymer Chemistry* **2004,** 42, (7), 1724-1734.

60. Willcock, H.; O'Reilly, R. K. *Polym. Chem.* **2010,** 1, (2), 149-157.

61. Strecker, A. *Justus Liebigs Annalen der Chemie* **1868,** 148, (1), 77-90.

62. Reed, R. M.; Tartar, H. V. *Journal of the American Chemical Society* **1935,** 57, (3), 570-571.

63. Eissa, A.; Cameron, N., Glycopolymer Conjugates. In *Bio-synthetic Polymer Conjugates*, Schlaad, H., Ed. Springer Berlin Heidelberg: 2013; Vol. 253, pp 71-114.

64. von der Ehe, C.; Rinkenauer, A.; Weber, C.; Szamosvari, D.; Gottschaldt, M.; Schubert, U. S. *Macromolecular Bioscience* **2016,** 16, (4), 508-521.

65. Becer, C. R.; Babiuch, K.; Pilz, D.; Hornig, S.; Heinze, T.; Gottschaldt, M.; Schubert, U. S. *Macromolecules* **2009,** 42, (7), 2387-2394.

66. Burns, J. A.; Gibson, M. I.; Becer, C. R., Glycopolymers via Post-Polymerization Modification Techniques. In *Functional Polymers by Post-Polymerization Modification*, Wiley-VCH Verlag GmbH & Co. KGaA: 2012; pp 237-265.

67. Maheshwari, R.; Levenson, E. A.; Kiick, K. L. *Macromolecular Bioscience* **2010,** 10, (1), 68-81.

68. Zwicker, V. E.; Liu, X.; Yuen, K. K. Y.; Jolliffe, K. A. *Supramolecular Chemistry* **2016,** 28, (1-2), 192-200.

69. Larnaudie, S. C.; Brendel, J. C.; Jolliffe, K. A.; Perrier, S. *Journal of Polymer Science Part A: Polymer Chemistry* **2016,** 54, (7), 1003-1011.

70. Barlow, T. R.; Brendel, J. C.; Perrier, S. *Macromolecules* **2016,** 49, (17), 6203-6212.

71. Bara, J. E.; Lessmann, S.; Gabriel, C. J.; Hatakeyama, E. S.; Noble, R. D.; Gin, D. L. *Industrial & Engineering Chemistry Research* **2007,** 46, (16), 5397-5404.

3

An Orthogonal Reaction Sequence for the Synthesis of Sugar-Coated Cyclic Peptide Nanotubes

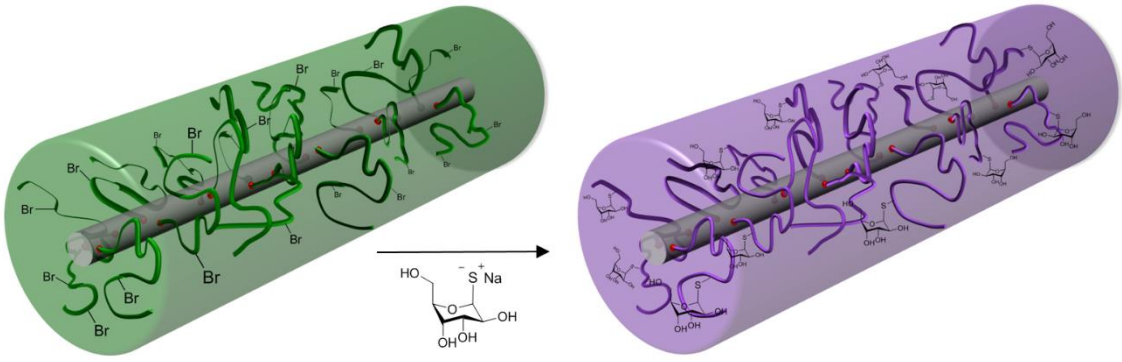

Self-assembly is a versatile technique for the creation of complex supramolecular materials, however synthesis of the precursors can be difficult when challenging functionalities are required. Post-modification of polymers is a versatile tool for the incorporation of synthetically demanding moieties in a material. Herein sugar-coated nanotubes were synthesised *via* an orthogonal peptide-polymer conjugation and

substitution strategy. Firstly, reactive polymer arms of poly(bromo ethyl acrylate) (pBEA) were conjugated onto a self-assembling cyclic-peptide core, applying a strategy using activated esters which react considerably faster and thus avoiding any unwanted side reactions. These robust precursor conjugates are then transformed using a thio-bromo "click" reaction with thioglucose to create sugar-coated nanotubes. Using Small Angle Neutron Scattering (SANS) and Static Light Scattering (SLS) the self-assembly of the precursor CP-pBEA and CP-glycopolymer conjugates was analysed in solution. Despite the rather large substituents on the polymer arms, in particular for the glycosylated materials, these conjugates form tubular assemblies that increase in size with decreasing lengths of the polymer chains.

3.1 Introduction

Introduction of complex functional groups, such as sugars, limits the ligations options available. Completely orthogonal reaction sequences become necessary, factoring in both polymer and CP reactivities and solubilities, yet remain robust and highly efficient under these conditions. In many cases the only route is *via* extensive protecting group strategies resulting in laborious syntheses. An elegant solution to the synthesis of materials incorporating two complex functionalities is post-modification. Post-polymerisation modification has proved a powerful tool in polymer chemistry,[1-4] in particular for glycopolymers,[5] offering numerous modification possibilities, involving mild conditions. We have recently reported on the polymerisation of bromo ethyl acrylate (BEA),[6] a reactive halogen-bearing polymer that we have previously employed for the synthesis of complex polymeric materials *via* post-modification, requiring only mild conditions to create a diverse library of materials by nucleophilic substitution.

Scattering techniques offer a powerful tool by which supramolecular materials may be characterised in solution. These techniques such as Small Angle Neutron Scattering (SANS) and Static Light Scattering (SLS) rely on the measurement of the scattered intensity at an angle, θ, by a particle irradiated with an incident beam at a wavelength, λ_0 (**Figure 3.1**).

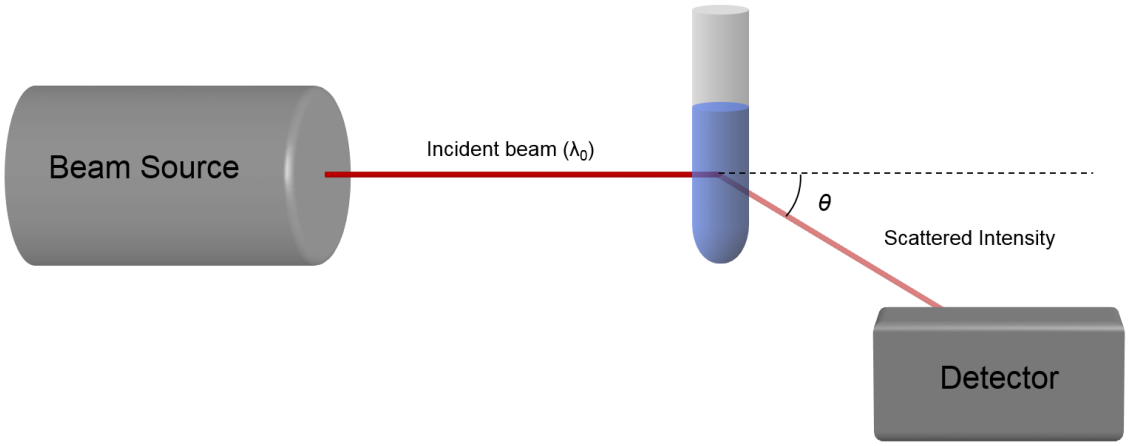

Figure 3.1: The principle of scattering.

The wave vector, q, can be defined by eq. 1:

$$q = \frac{4\pi \sin\frac{\theta}{2}}{\lambda_0} \quad \text{(SANS)} \qquad q = \frac{4\pi n \sin\frac{\theta}{2}}{\lambda_0} \quad \text{(SLS)} \qquad (1)$$

where θ is the scattered angle, λ is the incident beam wavelength and n is the refractive index of the solvent.

The inverse of the wave vector, q^{-1}, is proportional to the size of the window of observation; the bigger the wave vector, the smaller the window of observation. By varying the position of the detector, and therefore the value of θ; or changing the wavelength of the incident beam, such as using light or neutrons, information can be obtained over a range of sizes. As such, SANS and SLS are complementary techniques, as highlighted in **Figure 3.2**, with which detailed information can be obtained about supramolecular structures in solution.

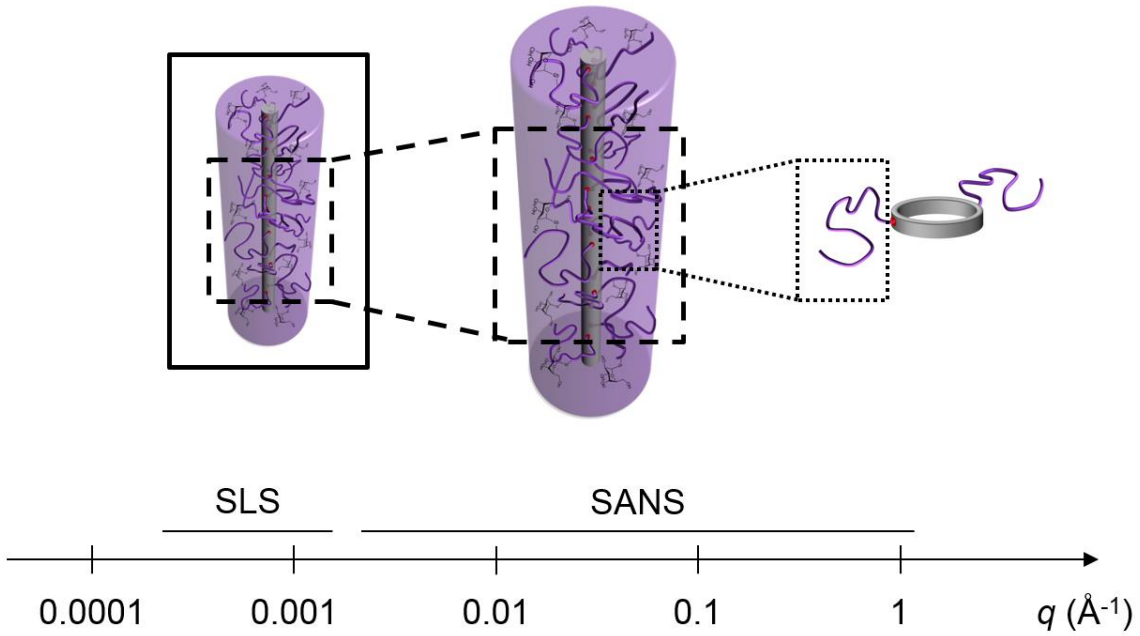

Figure 3.2: Relationship between *q*-range and size of the window of observation showing the complementarity of SLS and SANS.

Herein, we outline the preparation of CP-polymer conjugates, comprising self-assembling cyclic peptides and pBEA of two polymer lengths. The conjugation was monitored by size exclusion chromatography (SEC) and the resulting materials were analysed by NMR to evaluate the orthogonality of the reactive pendant bromines to the activated ester end group used for conjugation. The self-assembly properties of the resulting CP-pBEA conjugates were analysed by using SANS and SLS. These reactive halogen-bearing polymer-conjugates are then transformed by post-modification, using nucleophilic substitution to install thioglucose moieties for the synthesis of glycopolymer-conjugates. The self-assembly properties of these sugar-coated nanotubes was also assessed by SANS.

3.2 Results and Discussion

3.2.1 Synthetic Strategy

There are two primary synthetic methods for the preparation of cyclic-peptide polymer-nanotubes. The divergent method, whereby the polymer is grown from the peptide

provides several advantages in terms of reaction conditions and purification, however characterisation of the constituent polymer and peptide is challenging.[7] Alternatively, a convergent approach, that attaches a pre-formed polymeric chain to the peptide, is achieved using site specific and high yielding conjugation methods, enabling full characterisation of the polymer, peptide and conjugate.[8, 9] Fortunately, conjugation chemistry has progressed in recent years such that there are a number of suitable options available, including copper(I)-catalysed azide-alkyne cycloaddition (CuAAC),[10-13] isocyanate,[14-16] or activated ester-amide coupling.[17-21] Using efficient ligation protocols in concert with controlled radical polymerisation techniques such as RAFT polymerisation,[22] polymers of narrow dispersity with well-defined end-groups can be created with little synthetic effort. By manipulating polymer chain lengths and graft densities on the CP, some measure of control of the nanotube length and radius can be achieved.[23]

Due to the reactive nature of pBEA, the ligation method employed must be orthogonal to nucleophilic substitution in order to limit the possibility of side reactions, and the polymerisation and substitution of these polymers was discussed in Chapter 2. Recently, successful strategies for the synthesis of well-defined CP polymer-conjugates *via* activated ester amide bond formation have been developed.[8, 24] This synthetic route incorporates an *N*-hydroxysuccinamidyl (NHS) ester at the α-chain end by employing a chain transfer agent (CTA), with the -NHS pre-installed on the R-group prior to polymerisation. Also identified was that the speed and extent of conjugation strongly depends on the steric hindrance at the α-position of the activated ester, with primary esters resulting in more rapid conjugation than secondary.[8] The CTA NHS-CPAETC bears a primary ester that results in rapid and efficient conjugation, with complete ligation achieved within 24 h to ~90 % efficiency. Since CPAETC has been shown to effectively control polymerisation of BEA,[6] the NHS- modified CPAETC was thus used to polymerise BEA, providing well-defined polymers of narrow dispersity (**Table 3.1**). The cyclic-peptide core, *cyclo*[(L-Lys-D-Leu-L-Trp-D-Leu-)$_2$], was designed to bear two lysine residues for use as polymer tethers (**Scheme 3.1**),[8] to which NHS-pBEA$_n$ polymers

were reacted to form an amide bond, giving the desired CP-[pBEA$_n$]$_2$ conjugates (**Scheme 3.1**).

Table 3.1: Details of NHS-pBEA polymers synthesised.

Polymer	DP	$[M]_0$ / $[CTA]_0$	$[CTA]_0$ / $[I]_0$	Conversion χ [a] (%)	$M_{n,th}$ [b] (g·mol^{-1})	$M_{n,SEC}$ [c] (g·mol^{-1})	$Đ$
NHS-pBEA$_{10}$	10	11	10	94	2000	1800	1.12
NHS-pBEA$_{25}$	25	27	10	92	4400	3900	1.10

[a] *Conversion determined by ^{1}H-NMR*
[b] *Theoretical number-average molecular weight*
[c] *DMF SEC, DRI detector, PMMA standards, number-average molecular weight*

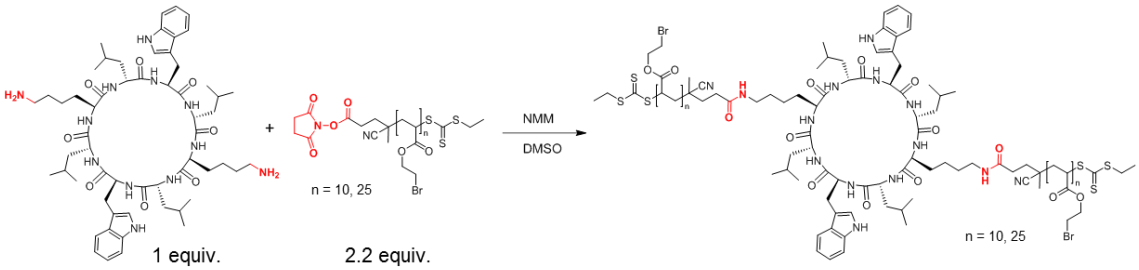

Scheme 3.1: Reaction scheme of pBEA conjugations to a self-assembling cyclic peptide.

Use of NHS-CPAETC as the CTA for BEA polymerisation resulted in NHS-pBEA polymers that underwent rapid conjugation with the CP. Ligation was complete within 24 h using only a 1.1 equiv. of polymer per lysine, with conjugation efficiencies between 86 - 94 % (**Table A3.1**), similar to those calculated for conjugation of non-reactive polymers.[8] Primary amines are effective nucleophiles, capable of reacting not only once, but multiple times with alkyl halides; as the subsequent secondary and tertiary amines are produced, these intermediates then substitute further equivalents of the alkyl halide. Due to the nucleophilicity of the amines on the lysine residue, there is the potential of a side reaction on the pendant bromines on the polymer arms. Substituting the bromine would result in a shift of the adjacent protons in the ^{1}H NMR spectrum, however no such substitution was observed by ^{1}H NMR (**Figure 3.3** - b and c). The analysis by SEC provides an even higher sensitivity for potential side reactions, as the multiple binding

sites on the reactive polymer would certainly result in larger chains and crosslinking. Therefore the SEC traces should show at least a high molecular weight shoulder in the case of side reactions. The absence of any shift by protons b and c in **Figure 3.3**, in addition to the absence of any higher molar mass shoulders in the SEC analysis of the conjugation reaction (**Figure 3.4**), indicates that the pendant bromines on CP-[pBEA$_n$]$_2$ remain mostly intact. This suggests that the lysine -NH$_2$ reactivity towards the activated ester is far more expedient than the halide substitution. To remove the remaining excess polymer, conjugates were purified by preparatory scale SEC in THF. Interestingly, short polymer-conjugates had better separation and fewer mixed fractions than conjugates with long polymer arms, due to the self-assembly increasing the gap between polymer and nanotube molecular weights. Conjugates were analysed by IR to estimate the inter-ring stacking distance, using Krimm's analysis of the amide A N-H stretch in the region of 3225 to 3280 cm^{-1}.[25] The peak arising at 3267 cm^{-1} in **Figure A3.3** can be correlated to an NH···O bond distance of 2.97 Å, consistent with previous literature on self-assembling CP-polymer conjugates, resulting in an inter subunit spacing of 4.71 Å.[9, 26 27]

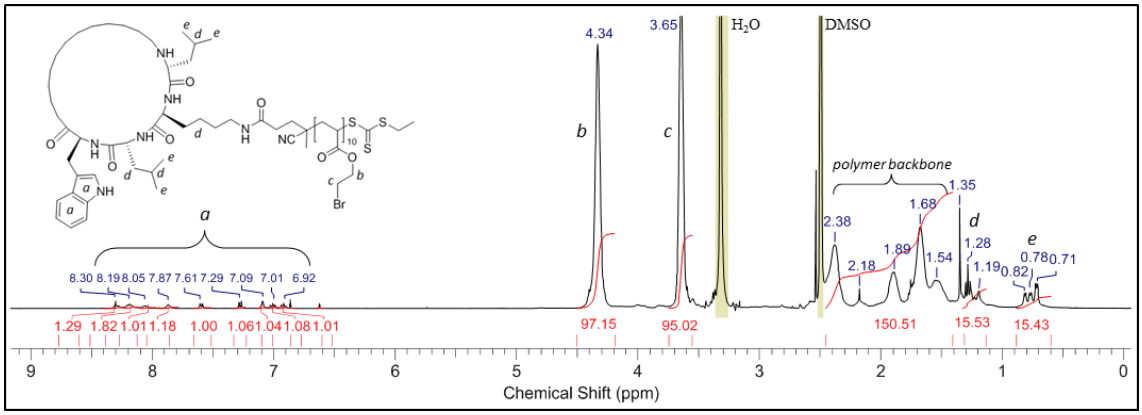

Figure 3.3: ^{1}H NMR of CP-[pBEA$_{25}$]$_2$ in DMSO-d$_6$.

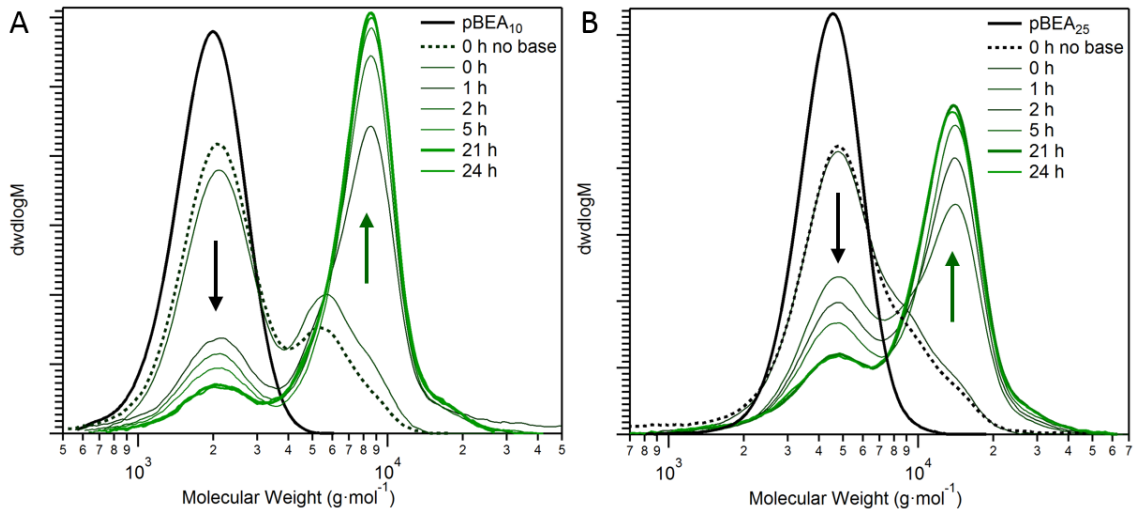

Figure 3.4: SEC chromatograms of conjugation reactions with varying polymer lengths: (A) DP 10 and (B) DP 25. The black arrows highlight the decreasing polymer peaks and the green arrow to the increasing 2-arm conjugate peak.

The rate of reaction of pBEA conjugations, particularly in the early stages of reaction, depended on the length of polymer chain. This is likely due to the reduced steric hindrance at short polymer chain ends resulting in a faster reaction rate. This trend can be clearly observed in **Figure 3.4A** and **B**, CP-[$pBEA_{10}$]$_2$ and CP-[$pBEA_{25}$]$_2$ respectively, where the reaction has begun prior to the addition of base which should start the reaction. Close inspection of **Figure 3.4A** and **B** reveals that three populations are present during the early stages of conjugation; the polymer peak as well as two shoulders emerging towards high molecular weight. To better understand the species present, the SEC RI response of CP-[$pBEA_{25}$]$_2$ was converted to a number average MW as outlined by Zetterlund *et al*[15, 28] and deconvolved by fitting to a Log-normal distribution (**Figure 3.5** and **Table A3.2**) in a manner similar to Monteiro *et al* for polymer-polymer couplings.[29] From the deconvolution it is clear that three species are present, corresponding to the starting polymer, the 1-arm intermediate and the 2-arm final product. Over the first 3.5 h of reaction, the apparent percentage of 1-arm species remains constant at ~10 %, while the two-arm conjugate peak increases rapidly (**Table A3.2**). The constant quantity of 1-arm species indicates that the addition of one polymer arm to a CP lysine does not impede the second polymer arm addition to the second CP Lysine. This high reactivity, despite

increased steric hindrance, suggests there is little opportunity for nucleophilic attack by the lysine amine due to rapid consumption by the NHS mediated coupling. The shift in molecular weight by SEC for all conjugations is greater than double the molecular weight of the free polymer (**Figure 3.4**). Since self-assembly is suppressed in hydrogen bonding competitive solvents, such as the DMF eluent used for SEC, this suggests the CP core has a large impact on the hydrodynamic volume by SEC.

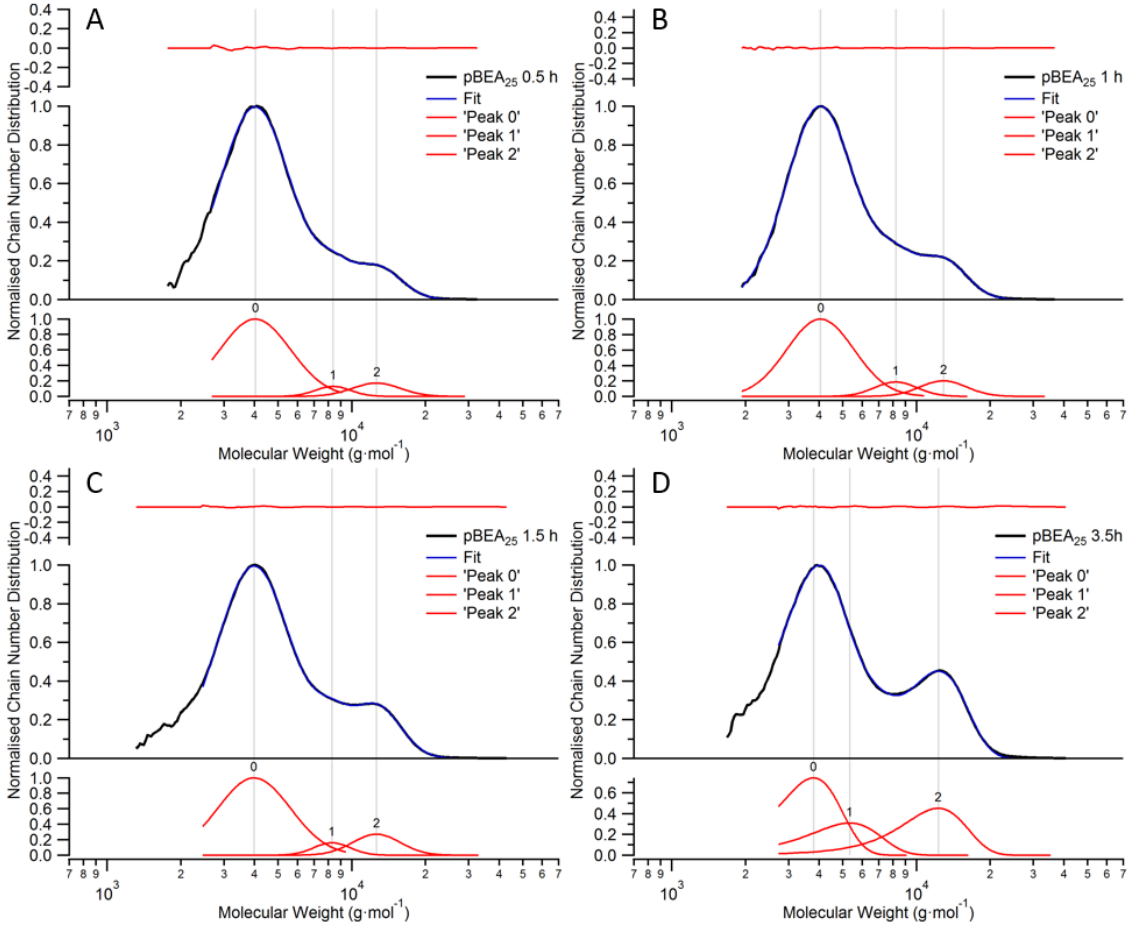

Figure 3.5: Deconvolution number average molecular weight distributions of CP-[pBEA$_{25}$]$_2$ conjugation at (A) 0.5 h, (B) 1 h, (C) 1.5 h, (D) 3.5 h.

3.2.2 Post-polymerisation modification

Synthesis of glycopolymers by direct polymerisation of glycomonomers can be synthetically demanding, often requiring protecting group chemistry and extensive

optimisation. Post-modification is thus an attractive strategy for glycopolymer synthesis that is achievable by a number of different "click" strategies; including copper-catalysed azide-alkyne cycloaddition (CuAAC)[30-32] and thiol based reactions including thiol-ene[33] or thiol-halide.[34, 35] Thiols are excellent nucleophiles for the substitution of bromine, and have often been exploited for end-group modification and are frequently referred to as "click" reactions.[36-39] Thiol-halogen substitution is an attractive synthetic strategy for glycopolymers leading to near quantitative yield with sufficiently activated halides without the requirement of a metal catalyst making it an ideal strategy to yield compounds suitable for drug delivery applications.[5] To synthesise the desired sugar-coated nanotube, sugar moieties could be introduced by nucleophilic substitution on the bromine using a thiolate salt of glucose. Substitution of pBEA can be achieved under very mild conditions,[6] ensuring that side reactions on the peptide core remain unlikely. 1-β-D-Thioglucose sodium salt is readily available commercially, and the thiolate salt negates the necessity of base during the reaction, minimising potential aminolysis of RAFT end groups.

Nucleophilic substitution of CP-[pBEA$_n$]$_2$ conjugates was achieved in DMSO at room temperature with 1.5 equiv. of thioglucose with full conversion to the desired glycopolymer conjugate (CP-[p*Glu*EA$_n$]$_2$) achieved in 24 h. CP-[p*Glu*EA$_n$]$_2$ conjugates were purified by centrifugal filtration and substitution was confirmed by ^{1}H NMR (**Figure 3.6**). As has previously shown, p*Glu*EA$_{50}$ is readily soluble in DMF,[6] whereas CP-[p*Glu*EA$_n$]$_2$ conjugates were not, thus prohibiting analysis by SEC. The next step following the synthesis of these sugar-coated nanotubes, was to determine their self-assembly properties in solution.

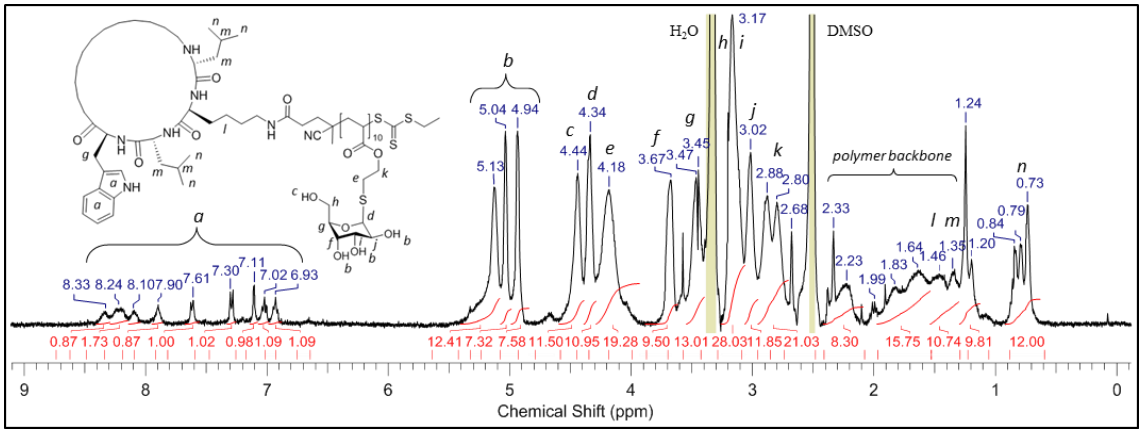

Figure 3.6: ^{1}H NMR of CP-[p*Glu*EA$_{10}$]$_2$ in DMSO-d$_6$.

3.2.3 Self-Assembly properties of CP-polymer conjugates

SANS is a powerful technique for the characterisation of supramolecular systems, as it allows direct assessment of any structural changes such as in response to stimuli or from processes applied to the sample. SANS measurements were taken over a large *q* range, resulting in a comprehensive molecular study on a broad length scale. The *q*-range probed can be further increased by using SLS, a complementary technique to SANS whereby using light rather than neutrons over wider scattering angles, further information including molecular weight and number of aggregation can be extrapolated. By measuring the scattering profiles of CP-polymer conjugates by SANS and SLS, and fitting the data to a series of form factors, it is possible to get an understanding on the overarching structures within the system, and how the polymer arm type and length affects self-assembly. From the work of Biesalski and Couet,[40] as well as Chapman and Koh,[23] it is anticipated that as polymer arm length increases, nanotube length will decrease; with conjugates of long polymers resulting in short, wide nanotubes, and conjugates of short polymers resulting in long, narrow nanotubes. As such the data obtained by SANS was fitted to a series of form factors to gain an understanding on the behaviour of the conjugates in solution. All data were analysed using the form factors available in the NIST SANS analysis package for Igor Pro.[41, 42] First the data were fit to a Guinier-Porod model,[55] which is an empirical model applicable to objects of arbitrary shape which gives an estimate of the radius of gyration, R_g, and a dimension variable, *s*.

The dimension variable is indicative of the shape of the object; $s = 0$ indicates the structure is a 3D spherical object, $s = 1$ indicates the object has an elongated or 2D symmetry such as a rod or cylinder, and $s = 2$ indicates the object has a 1D symmetry such as for lamellae or platelets, with values in between suggesting an intermediate shape. From the Guinier-Porod analysis, subsequent form factors were used including Cylinder and a summative Gaussian Coil-Cylinder model to get the dimension of the nanotubes.

3.2.4 Assembly of pBEA-conjugates

The SANS profile of CP-[pBEA$_{10}$]$_2$ at low-q has an extended q^{-1} region that is characteristic of cylindrical structures. Guinier-Porod analysis of CP-[pBEA$_{10}$]$_2$ suggests a rod-like nanotube is formed in THF-d$_8$ (**Table 3.2** and **Figure A3.5A**) from the obtained s value of 0.90 (**Table 3.2**). When the CP-[pBEA$_{10}$]$_2$ sample in THF-d$_8$ was filtered through a 0.5 μm syringe filter, the scattering profile changed dramatically, with a marked decrease in scattering intensity at low-q ($q < 0.025$ Å^{-1}, **Figure A3.5B**) and an increase in scattering at intermediate-q values ($q > 0.025$ Å^{-1}). The profile of filtered CP-[pBEA$_{10}$]$_2$ when analysed by the Guinier-Porod model resulted in a dimension variable of $s = 0.54$. Since an s value between 0 and 1 indicates an intermediate shape between a cylinder and a sphere, CP-[pBEA$_{10}$]$_2$ after filtration adopts an elongated sphere or ellipsoidal shape in solution. This change in morphology is likely due to the shear forces of filtration disrupting self-assembly, breaking up the longest assemblies, resulting in a greater proportion of intermediate length nanotubes.

The scattering profile of CP-[pBEA$_{25}$]$_2$ has a lower overall intensity than the CP-[pBEA$_{10}$]$_2$ samples with a plateau at $q < 0.02$ Å^{-1}. Guinier-Porod modelling of CP-[pBEA$_{25}$]$_2$ predicts a spherical object, with an s value of 0.013 (**Table 3.2**). The R_g estimated by Guinier-Porod modelling increased along with polymer arm length, yet remained independent of the shape given by the estimated dimension parameter. From this it can be concluded that the R_g determined by Guinier-Porod modelling is the cross-sectional radius of the nanotube, rather than a representation of the overall molecule, which is consistent with the work by Pesek *et al.* on polymer bottlebrushes.[43, 44]

Table 3.2: Results of the Guinier-Porod analysis for Dimension Variable, s, and Radius of Gyration, R_g for CP-[pBEA$_n$]$_2$ conjugates.

Compound	S	R_g (Å)
CP-[pBEA$_{10}$]$_2$	0.90 ± 0.0040	22.8 ± 0.13
CP-[pBEA$_{10}$]$_2$ Filtered	0.54 ± 0.0065	26.5 ± 0.21
CP-[pBEA$_{25}$]$_2$	0.013 ± 0.0064	36.6 ± 0.15

While Guinier-Porod analysis suggests spherical objects, the data could not be fit to a sphere model. Instead the data were fit to cylinder based models, which gives qualitative information about the sample by incorporating scattering length densities of the conjugate and solvent. Due to the supramolecular nature of our assemblies, there exist two regions that must be well described by the form factor; both the low-q region (q < 0.02 Å^{-1}), corresponding to large molecules and intermolecular aggregation, and the intermediate q region (0.02 Å^{-1} < q < 0.1 Å^{-1}), corresponding to the polymer arms of the supramolecular brush-like nanotubes (**Figure 3.2**). To adequately account for both regions in the SANS profiles, a summative model of the Cylinder and the Gaussian-Coil models in the Igor Pro software package was used to fit the data giving an improved fit over the Cylinder only model (**Figure A3.7**).[41]

The CP-[pBEA$_{10}$]$_2$ profile displays an extended q^{-1} region at q < 0.02 Å^{-1}, a feature that is characteristic of elongated supramolecular structures. Cylinder-Gaussian Coil modelling of CP-[pBEA$_{10}$]$_2$ gives a nanotube radius of 31.8 Å and a length of 1480 Å (**Table 3.3** and **Figure 3.7**). Since the q^{-1} region extends beyond the q-range probed by SANS, it is not possible to determine the exact length of CP-[pBEA$_{10}$]$_2$ nanotubes without SLS. The filtered CP-[pBEA$_{10}$]$_2$ (**Figure 3.7** and **Figure A3.6B**) modelled by the Cylinder-Gaussian Coil fit resulted in a similar radius of 32.9 Å, however the estimated length was reduced to only 259 Å (**Table 3.3**) which is significantly shorter than the nanotube length prior to filtration. This reduction in length further strengthens the hypothesis that the force of filtration decreases nanotube length. However it remains to be seen whether filtration accelerates equilibration to a thermodynamically favourable length or if it results in artificially shortened nanotubes. Analysis of CP-[pBEA$_{25}$]$_2$ estimated a radius of 46.5 Å

consistent with the longer polymer chain, and the estimated length was only 50.7 Å. This aspect ratio of nanotube radius and length is consistent with the spherical dimension variable estimated by Guinier-Porod analysis, suggesting short nanotubes.

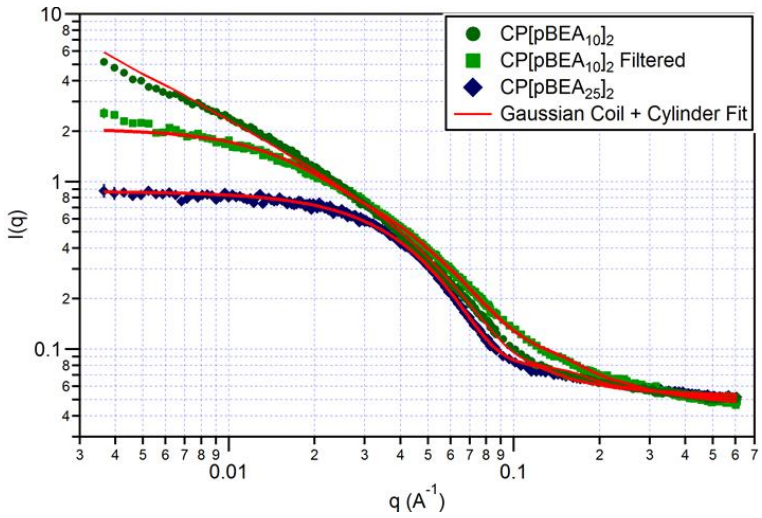

Figure 3.7: SANS profiles of CP-[pBEA$_n$]$_2$ conjugates at 10 mg · mL^{-1} in THF-d$_8$: CP-[pBEA$_{10}$]$_2$ before (green circles) and after (green squares) filtration and CP-[pBEA$_{25}$]$_2$ (blue diamonds). Data were fit to a Cylinder-Gaussian Coil model (red lines).

Table 3.3: Parameters estimated from fitting to Cylinder-Gaussian Coil model.

Sample	Radius (Å)	Length (Å)	R_g (Å)	N_{agg}
CP-[pBEA$_{10}$]$_2$	31.8 ± 0.075	1480 ± 77	15.5 ± 0.0033	314.8 ± 16
CP-[pBEA$_{10}$]$_2$ Filtered	32.9 ± 0.14	259.4 ± 2.8	19.5 ± 0.0032	55.2 ± 0.6
CP-[pBEA$_{25}$]$_2$	46.5 ± 0.32	50.7 ± 1.3	44.0 ± 0.0079	10.8 ± 0.28

To further investigate the effect of filtration and equilibration time of the pBEA conjugates, an additional two conjugates, CP-[pBEA$_{15}$]$_2$ and CP-[pBEA$_{29}$]$_2$, were synthesised for characterisation by SLS (**Figures A3.12 - 15**). SLS data were collected before and after filtration, as well as after several days of equilibration time (**Table 3.4**), to calculate the number of aggregation (N_{agg}). For CP-[pBEA$_{15}$]$_2$, the N_{agg} obtained by SLS was 287, equivalent to ~ 1351 Å. After filtration the N_{agg} dropped to 175, and following 10 days of equilibration the N_{agg} was only 55 (**Table 3.4**). The diminution of

the N_{agg} with filtration by SLS is consistent with SANS data, suggesting that filtration breaks up large aggregates, however this does not represent the final, and most thermodynamically stable assembly. With additional equilibration time, the solvent will continue to permeate to the core, disrupting aggregation further, until the CP-assemblies attain a more thermodynamically favourable state, which for CP-[pBEA$_{15}$]$_2$ in THF is 257 Å (N_{agg} = 55) as analysed by SLS. For CP-[pBEA$_{29}$]$_2$, the conjugate with longer polymer arms before filtration, the N_{agg} is 8.1. Following filtration the N_{agg} drops to 5.6 with additional equilibration time resulting in an increase in the N_{agg} to 9.8. This trend corroborates the hypothesis that the force of filtration disrupts the length of the nanotubes formed, shortening the length of assemblies. Additional equilibration time then enables CPs to assemble or disassemble to a more favourable length. These data are consistent with previous literature on these systems that demonstrated that graft density, and polymer length affect the length of self-assemblies.

Table 3.4: N_{agg} of CP-[pBEA$_n$]$_2$ conjugates before and after filtration, and after 10 days equilibration time.

Compound	Before Filtration	After Filtration	Equilibration
CP-[pBEA$_{10}$]$_2$	315	55	-
CP-[pBEA$_{15}$]$_2$	287	175	55
CP-[pBEA$_{25}$]$_2$	11	-	-
CP-[pBEA$_{29}$]$_2$	8.1	5.6	9.8

3.2.5 Assembly of Sugar-Conjugates

To assess the self-assembly of glycopolymer-conjugates in D_2O, both CP-[p*Glu*EA$_{10}$]$_2$ and CP-[p*Glu*EA$_{25}$]$_2$ were analysed by SANS. At 5 mg· mL^{-1} the scattering profile of CP-[p*Glu*EA$_{10}$]$_2$ increases towards low-q with a short region of q^{-1} scattering indicating that cylindrical structures are present in solution. Guinier-Porod analysis of CP-[p*Glu*EA$_{10}$]$_2$ estimates a dimension variable, s, of 0.51 that suggests an elongated sphere or ellipsoidal morphology in solution. At the same concentration, CP-[p*Glu*EA$_{25}$]$_2$ has a lower intensity over all q-values than CP-[p*Glu*EA$_{10}$]$_2$, suggesting that the assemblies formed are smaller. Guinier-Porod modelling estimated an s value of 0.19, suggesting a more spherical ellipsoid morphology than for CP-[p*Glu*EA$_{10}$]$_2$. The

estimated R_g values increase with polymer arm length, from 20.1 Å to 26.8 Å for CP-[p*Glu*EA$_{10}$]$_2$ and CP-[p*Glu*EA$_{25}$]$_2$ respectively (**Figure A3.11**), consistent with an R_g arising from the cross-sectional radius of the nanotube. In both cases the CP-[p*Glu*EA$_n$]$_2$ conjugates adopt ellipsoidal morphologies in solution, with shorter polymer arms resulting in higher aspect ratio nanotubes, consistent with that found for CP-[pBEA$_n$]$_2$ conjugates (*vide supra*) and previous work.[23] Since neither data set could be satisfactorily fit to a sphere model, the data were instead fit to a Cylinder (**Figure A3.10B**) and a Cylinder-Gaussian Coil model (**Table 3.6** and **Figure A3.10A**). Fitting of the data with the Cylinder-Gaussian Coil model gave radii of 23.8 Å and 26.8 Å for CP-[p*Glu*EA$_{10}$]$_2$ and CP-[p*Glu*EA$_{25}$]$_2$ respectively; similar to the R_g values estimated by the Guinier-Porod model. The estimated length of CP-[p*Glu*EA$_{10}$]$_2$ was 148.7 Å (N_{agg} = 32) and for CP-[p*Glu*EA$_{25}$]$_2$ the length was 135.1 Å (N_{agg} = 29).

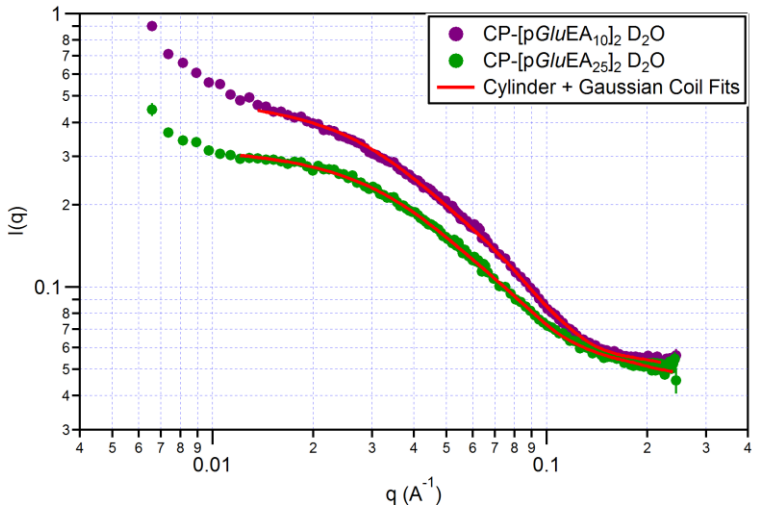

Figure 3.8: SANS profiles of CP-[p*Glu*EA$_{10}$]$_2$ (purple circles) and CP-[p*Glu*EA$_{25}$]$_2$ (green circles) scattering profiles at 5 mg· mL^{-1} in D_2O. Data were fit to a Cylinder-Gaussian Coil model (red lines).

Table 3.5: Summary of Guinier-Porod model fits for CP-[p*Glu*EA$_n$]$_2$ in D_2O.

Sample	*S*	R_g (Å)
CP-[p*Glu*EA$_{10}$]$_2$	0.50 ± 0.0047	20.3 ± 0.093
CP-[p*Glu*EA$_{25}$]$_2$	0.19 ± 0.012	26.8 ± 0.34

Table 3.6: Summary of Cylinder-Gaussian Coil model fits for CP-[p*Glu*EA$_n$]$_2$ in D_2O.

Sample	Radius (Å)	Length (Å)	R_g (Å)	N_{agg}
CP-[p*Glu*EA$_{10}$]$_2$	23.8 ± 0.28	148.7 ± 1.7	25.5 ± 0.0063	31.6 ± 0.36
CP-[p*Glu*EA$_{25}$]$_2$	26.8 ± 0.76	135.1 ± 3.0	32.2 ± 0.014	28.7 ± 0.63

Previous studies on the effect of polymer length and graft density have identified that increased steric bulk limits self-assembly in these systems.[23, 40] In addition to steric effects, charge is capable of reversibly disrupting self-assembly in pH responsive polymer-conjugates.[45] Indeed a number of factors have been identified that can affect the self-assembly of β-sheet forming CPs including; hydrogen-bond competitivity of the solvent, solvent access to the core, in addition to the steric effects of the polymer arms.[23, 40, 46] Considering the steric bulk of the glucose unit, the extent of self-assembly of CP-[p*Glu*EA$_n$]$_2$ conjugates is surprising and that the sugar-conjugates are able to assemble in water, a highly hydrogen bonding competitive solvent, is even more so. Linear glycopolymers are capable of both intra- and inter-molecular hydrogen bonding between the carbohydrate hydroxyl units, as well as with several proteins, in addition to their selective targeting of cell receptors, a property making them attractive for use as gene therapy candidates.[47, 48] The attractive hydrogen bonding forces between glucose moieties in this case works to promote nanotube self-assembly. Despite the bulky nature of the glucose monomer unit, the hydrogen bonding provided by the numerous hydroxyl units overcomes the steric repulsion, resulting in remarkably long sugar-nanotubes of ~140 Å in a highly hydrogen-bonding competitive environment.

3.2.6 Lectin binding studies

Biological events are often related to the interaction between carbohydrates and lectins. Lectins are binding proteins with high stereo-specificity for carbohydrates. A monomeric saccharide shows low affinity for its natural ligand, whereas multivalent interactions between a single lectin with one or more carbohydrate units are highly prevalent in nature;[49, 50] and this "cluster-effect"[32] strongly influences the design of well-defined glycopolymer architectures.

A critical requirement for the application of glycopolymers in targeted drug delivery, is their ability to selectively bind to lectins, which is an important method for targeting cancerous cells that over-express lectins. To examine the binding efficacy of the glycopolymer conjugates, turbidimetry assays were performed for both CP-[p*Glu*EA$_n$]$_2$ conjugates using the lectin Concanavalin A (Con A). Con A comprises aggregates of 25 g·mol^{-1} size. At pH 5 to 5.6 it exists as a dimer in solution, while at pH ≥ 7 Con A predominantly aggregates into tetramers.[51] The rate of clustering was monitored in real-time by measuring the absorbance at λ = 420 nm for 30 min after mixing the lectin and polymer solutions. The change in turbidity is related to the rate of receptor-receptor associations caused by the sugar-units of the polymers. The slope of the steepest portion of the initial curve was used to represent the clustering rate (s^{-1}).[52] The initial values of the curves relate to the formation of isolated Con A-polymer clusters, with later values correlating to interactions between the clusters. The formation of cross-linked clusters of higher order increases over time, thus analysis is limited to the section of the curve after the initial time points with high noise. The results of the Con A binding studies for CP-[p*Glu*EA$_n$]$_2$ conjugates are summarised in **Figure 3.9** and **Figure 3.10**.

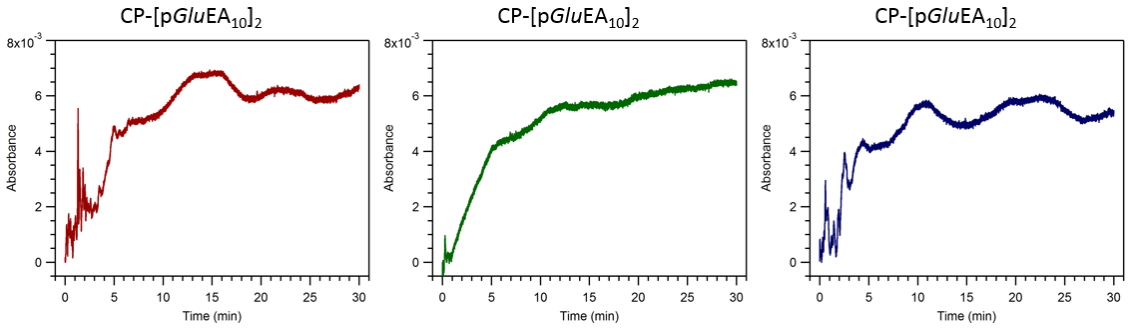

Figure 3.9: Absorbance (λ = 420 nm) curves after adding 100 µL of 1 mg· mL^{-1} solution of Con A in HBS buffer to the solution of the polymer CP-[p*Glu*EA$_{10}$]$_2$ (50 µM per sugar unit, in HBS). The linear fit of the steepest portions of the curves were used to calculate the clustering rate $k = 1.31 \cdot 10^{-3}$ s^{-1}.

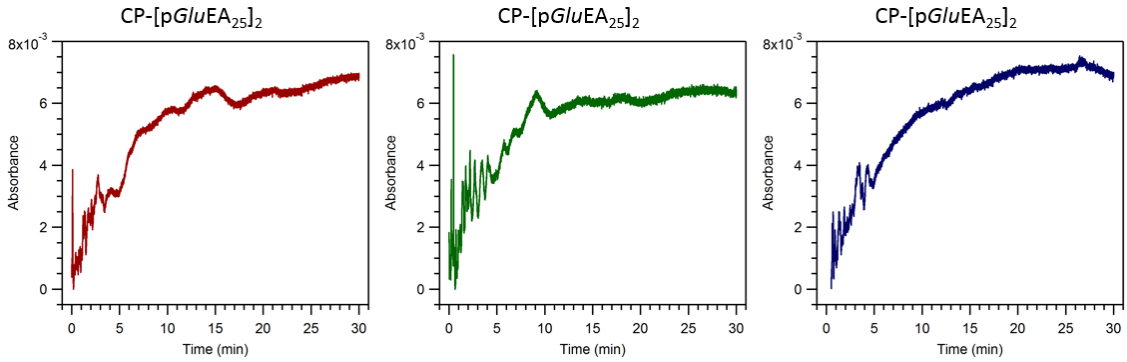

Figure 3.10: Absorbance (λ = 420 nm) curves after adding 100 µL of 1 mg· mL^{-1} solution of Con A in HBS buffer to the solution of the polymer CP-[p*Glu*EA$_{25}$]$_2$ (50 µM per sugar unit, in HBS). The linear fit of the steepest portions of the curves were used to calculate the clustering rate $k = 5.94 \cdot 10^{-4}$ s^{-1}.

Both CP-[p*Glu*EA$_n$]$_2$ conjugates exhibit a continuous, slow increase in absorbance, indicating secondary interactions such as cross-linked clusters or partially soluble conjugates. The chain length of glycopolymers is an important factor that influences lectin clustering, with longer polymer chains generally resulting in an increased rate of binding.[53] Interestingly, the clustering rate of Con A is faster for the shorter DP conjugate CP-[p*Glu*EA$_{10}$]$_2$ than for the longer conjugate CP-[p*Glu*EA$_{25}$]$_2$, in contrast to the literature.[52, 53] This inverse trend is likely due to the increased self-assembly of the DP10 conjugate that results in longer nanotubes. Once nanotube length is considered, since

shorter polymer arms tend to result in longer nanotubes in this system, it stands to reason that the inverse trend for DP dependent glycopolymer clustering will be true for this system. The rapid rate at which these sugar-coated nanotubes bind to Con A is a positive step towards the use of these interesting materials as for biological related applications.

3.3 Conclusion

Described here, is the development an orthogonal reaction sequence for the synthesis of sugar-coated nanotubes. End-functionalised BEA polymers were synthesised by RAFT polymerisation, using an NHS-modified CTA. NHS-pBEA polymers were conjugated to the self-assembling CP core without side-reactions, resulting in reactive nanotube precursors for subsequent post-modification. CP-[pBEA$_n$]$_2$ nanotubes were analysed by SANS and SLS and found to form short nanotubes in solution, with increased polymer chain length found to decrease the length of nanotube. The brominated precursor conjugates were then post-modified by a thio-bromo "click" reaction with thioglucose resulting in CP glycopolymer conjugates. These glycopolymer nanotubes were found to be rapid and effective lectin binding compounds that would make them excellent cell targeting materials. The sugar nanotubes were analysed by SANS and found to improve self-assembly over that of pBEA precursor, demonstrating that post-modification does not hinder self-assembly, but can improve it. Previous work described the synthesis of a complex new material with properties ideal for applications in cell-biology and gene-delivery. The most remarkable result is the effect of post-modification on self-assembly of DP25 conjugates. CP-[pBEA$_{25}$]$_2$ conjugates form very short assemblies of only 50.7 Å long in THF-d$_6$. Following post-modification, CP-[p*Glu*EA$_{25}$]$_2$ in D_2O formed longer tubes of 135.1 Å, in a more hydrogen bonding competitive environment. THF being a polar aprotic solvent is capable of participating in hydrogen bonding as a hydrogen bond acceptor, however remains far less competitive than water towards hydrogen bonding-directed nanotube formation. The increase in length of the DP25 conjugate following post-modification, is an excellent demonstration that post-modification does not hinder self-assembly of the cyclic-peptide. Instead, post-modification is an advantageous route for enhancing nanotube formation by incorporating functional monomer units that can

promote self-assembly, either by improving solubility, reducing steric hindrance or increasing the inter-molecular attractive-forces such as with additional hydrogen bonding or π-π stacking.

3.4 Experimental

3.4.1 Materials

Dioxane and DMSO were purchased from Fisher Scientific. 4,4-Azobis(4-cyanovaleric acid) (ACVA) was purchased from MP Biomedicals. Biobead SX-1 resin was purchased from Bio-Rad Laboratories Ltd. Cyclic peptide *cyclo*[(L-Lys-D-Leu-L-Trp-D-Leu-)$_2$] was synthesised according to published methods[8, 45] All other compounds were purchased from Sigma-Aldrich. All chemicals were used as received. All solvents were bought from commercial sources and used as received. The synthesis of BEA monomer is described in Chapter 2.

3.4.2 Instrumentation

^{1}H NMR spectra were recorded on a Bruker AV-300, HD-300 or AV-400 in $CDCl_3$, D_2O or DMSO-d_6. Shift values (δ) are reported in ppm. The residual proton signal of the solvent was used as an internal standard ($CDCl_3$ δ_H 7.26, D_2O δ_H 4.79, DMSO-d_6 δ_H 2.50). Size exclusion chromatography (SEC) was carried out on a Polymer Laboratories PL-GPC 50 Plus. All polymers were analysed on a Polymer Laboratories PL-GPC 50 Plus system using a PolarGel-M guard column (7.5 × 50 mm) followed by two PolarGel-M columns (7.5 × 300 mm). DMF (0.1% LiBr) was used as eluent at 1.0 mL min^{-1} at 50 °C. Commercial narrow linear poly(methyl methacrylate) standards in range of 2.0 × 10^2 g mol^{-1} to 1.0 × 10^6 g mol^{-1} were used to calibrate the DMF SEC system. Analyte samples were filtered through a polytetrafluoroethylene (PTFE) membrane with either 0.2 μm or 0.45 μm pore size before injection (100 μL). Centrifugal filtration was carried out using Vivaspin® 20, 3,000 or 10,000 MWCO centrifuge tubes. Preparatory scale size exclusion chromatography was carried out using Biobead S-X1 bulk media in THF. Experimental $M_{n,SEC}$ and $Đ$ values of synthesised polymers were determined using Agilent GPC software. Infrared (IR) absorption spectra were recorded on a Bruker Vector 22 FT-IR

spectrometer using attenuated total reflection of a thin film. Notable vibrational wavenumbers are recorded in cm^{-1}. PTFE 0.2 μm syringe filters were obtained from Fisherbrand for filtration of samples in organic solvents. Pall Gelman GHP Acrodisc 0.2 μm syringe filters were obtained from Sigma-Aldrich for filtration of aqueous samples.

3.4.3 Synthesis of Linear Peptide

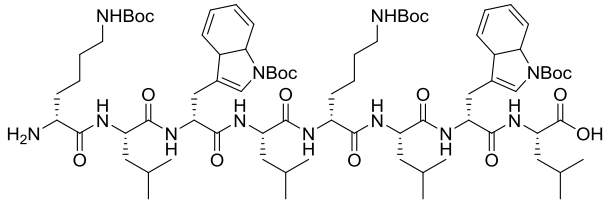

Synthesis of the linear peptide H2N-L-Lys(Boc)-D-Leu-L-Trp(Boc)-D-Leu-L-Lys(Boc)-D-Leu-L-Trp(Boc)-D-Leu-COOH was achieved using solid phase synthesis adapted from previously published procedures:[8, 23, 45, 54, 55] Under anhydrous conditions, 2-clorotrityl chloride resin (0.5 g, loading capacity 1.1 mmol· g^{-1}) was swelled in CH_2Cl_2 (4 mL) for 30 min in a 10 mL sinter-fitted syringe. The CH_2Cl_2 was filtered off and a solution of Fmoc-D-Leu-OH (2 eq. relative to resin capacity, 0.776 g, 2.2 mmol) and DIPEA (4 eq./amino acid, 1.14 g, 8.8 mmol) in CH_2Cl_2 (8 mL) was added to the resin and gently agitated for 2 h. The resulting loaded resin was washed with CH_2Cl_2 (3 × 5 mL), followed by a solution of CH_2Cl_2/MeOH/ DIPEA (17:2:1, 2 × 5 mL × 5 min) to cap any remaining unreacted sites and finally with CH_2Cl_2 (3 × 5 mL), DMF (3 × 5 mL) and CH_2Cl_2 (3 × 5 mL). The resin was drained and dried under vacuum and used for further solid phase peptide synthesis.

The loaded resin (0.2507 g, 0.218 mmol) was transferred to a sintered syringe, and swollen in CH_2Cl_2 for 30 min. The CH_2Cl_2 was filtered off then the peptide washed with DMF (3 × 5 mL) before treatment with a solution of 20 % piperidine in DMF (3 × 5 mL × 5 min) to remove the Fmoc group. These initial Fmoc deprotection solutions were collected for resin loading determination. The resin was drained and immediately washed

sequentially with DMF (3 × 5 ml), CH_2Cl_2 (3 × 5 mL) and DMF (3 × 5 mL). The resulting amine was used immediately in peptide couplings.

The Fmoc deprotection solutions were combined and made up to 25 mL with 20% piperidine in DMF. An aliquot of this solution was diluted 200-fold and the concentration of the fulvene-piperidine adduct was assessed using UV-Vis absorption (301 nm, ε = 7800 $M^{-1} \cdot cm^{-1}$) to give the resin loading (1.15 mmol g^{-1}).

For subsequent coupling reactions, solutions containing the Fmoc-amino acid (3 eq., 0.653 mmol), HBTU (3.1 eq., 0.675 mmol) and DIPEA (6 eq., 1.307 mmol) in DMF (2 mL) were prepared, bubbled with N_2 for 15 min drawn to suspend the resin and agitated for 3 h. After additions, the resin was washed with sequentially with DMF (5 × 5 mL), CH_2Cl_2 (5 × 5 mL) and DMF (5 × 5 mL).

Deprotection and addition steps were repeated to obtain the desired octapeptide. After completion of the amino acid coupling reactions and removal of the final Fmoc protecting group using 20 % piperidine in DMF, the peptide was cleaved from the resin using a solution of 20 % HFIP in CH_2Cl_2 (3 × 8 mL; 10 min each). The resin was washed with CH_2Cl_2 (3 × 4 mL) and the filtrate was concentrated *in vacuo* to yield the linear peptide as an off-white solid. Yield 0.40 g (quantitative). ^{1}H-NMR (400 MHz, TFA-d, ppm): δ = 8.07 (m, 2H, Trp), 7.54-7.22 (m, 8H, Trp), 5.11 (m, 2H, H_α Trp), 4.68-4.48 (m, 5H, H_α Leu and H_α Lys), 4.21 (m, 1H, H_α Lys *N*-end), 3.32-3.03 (m, 8H, CH_2 Trp and CH_2-NH Lys), 2.07-0.86 (m, 60H, CH_2-CH_2-CH_2 Lys, CH_2-CH Leu, $C(CH_3)_3$ Boc), 0.85-0.58 (m, 24H, CH_3 Leu), NH signals not observed. MS (ESI): $[M+H]^+$ calculated: 1498.9, found 1498.9.

3.4.4 Cyclisation of Linear Peptide

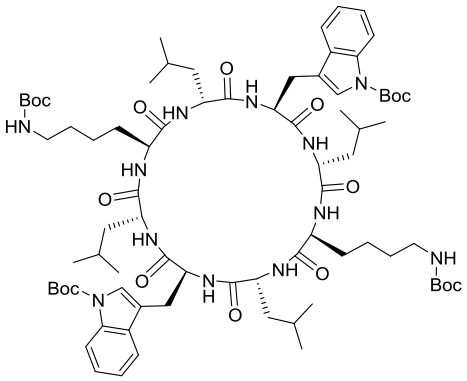

Linear peptides were cyclised by head-to-tail coupling under dilute conditions.[8, 23, 45, 54, 55] Under anhydrous conditions linear peptide (0.200 g, 0.127 mmol) was dissolved in DMF (20 mL) and deoxygenated *via* a bubbled N_2 stream for 20 min. DMTMM·BF_4 (1.2 eq., 0.051 mg, 0.152 mmol) was dissolved in DMF (5 mL) and deoxygenated with N_2 for 20 min, which was then added dropwise to the linear peptide solution. The mixture was stirred under an inert atmosphere for 5 days. The DMF solution was reduced to a volume of ~ 1 mL *in vacuo* then diluted in methanol (20 mL). Aliquots of the suspension were distributed into 2 mL Eppendorf tubes and centrifuged at 10000 rpm for 4 minutes using a benchtop centrifuge. The supernatant was discarded and the pellets resuspended in methanol. These solutions were centrifuged again and the supernatant discarded. The pellets were resuspended in methanol and combined. Methanol was removed *in vacuo* to yield the Boc-protected cyclic peptide in the form of an off-white powder. Yield 73 % (138 mg, 0.093 mmol). ^{1}H-NMR (400 MHz, TFA-*d*, ppm): δ = 8.07 (m, 2H, Trp), 7.54-7.22 (m, 8H, Trp), 5.15 (m, 2H, H_α Trp), 4.79-4.52 (m, 6H, H_α Leu and H_α Lys), 3.29-2.96 (m, 8H, CH_2 Trp and C*H*$_2$-NH Lys), 2.07-0.86 (m, 60H, CH_2-CH_2-CH_2 Lys, CH_2-CH Leu, C(CH_3)$_3$ Boc), 0.85-0.58 (m, 24H, CH_3 Leu), NH signals not observed. MS (ESI) $[M+Na]^+$ calculated: 1503.89, found: 1503.8.

3.4.5 Deprotection of Cyclic Peptide

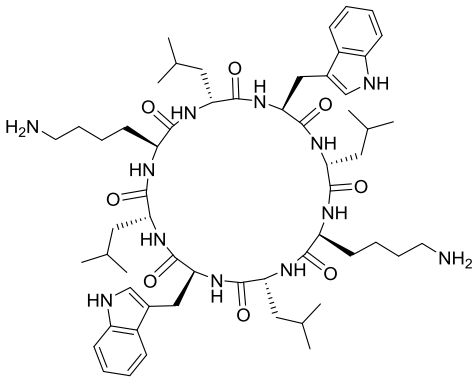

Deprotection of the cyclic peptide was achieved using previously reported procedures:[8, 23, 45, 54, 55] Boc groups were removed by treatment with TFA/TIPS/H_2O (18:1:1 v/v/v, 5 mL) for 2 h, then precipitated in ice-cold diethyl ether and the supernatant discarded (2 × 50 mL). The precipitate was resuspended in diethyl ether and isolated *via* centrifugation in Eppendorf tubes. Excess solvent was removed *in vacuo* to yield an off-white powder. Yield: 124 mg (quantitative). ^{1}H-NMR (400 MHz, TFA-d, ppm): δ = 7.64-6.60 (m, 10H, Trp), 5.16 (m, 2H, H_α Trp), 4.73 (m, 6H, H_α Leu and Hα Lys), 3.29-2.96 (m, 8H, CH_2 Trp and CH_2-NH Lys), 2.07-0.86 (m, 24H, CH_2-CH_2-CH_2 Lys, CH_2-CH Leu,), 0.85-0.58 (m, 24H, CH_3 Leu), NH signals not observed. MS (ESI) $[M+Na]^+$ calculated: 1103.67, found: 1103.5.

3.4.6 Synthesis of N-hydroxysuccinimide-(4-cyano pentanoic acid)yl ethyl trithiocarbonate (NHS-CPAETC)

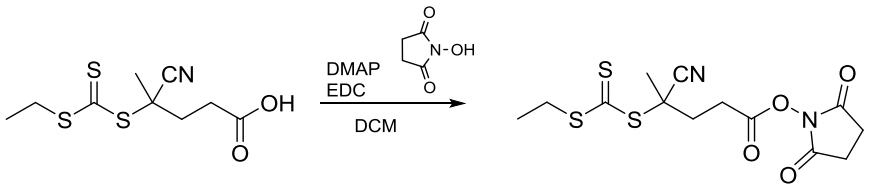

NHS-CPAETC was prepared from CPAETC (synthesised in Chapter 2) using a protocol adapted from the literature.[8, 56] CPAETC (2.3 g, 8.7 mmol) was dissolved in CH_2Cl_2 (50 mL) and stirred, followed by the addition of *N*-hydroxysuccinimide (1.2 equiv., 1.2 g,

10.5 mmol) and DMAP (0.1 g, 0.9 mmol). To this mixture, a 50 mL CH_2Cl_2 solution containing 1-ethyl-3-(3-dimethylaminopropyl)carbodiimide (EDC) (1.2 equiv., 2.26 g, 11.8 mmol) was added slowly over a period of 1 h at room temperature. The reaction was allowed to proceed at room temperature for a further 16 h yielding an orange solution. The excess EDC and DMAP was removed by washing twofold with water (200 mL) and twofold with brine (200 mL). The CH_2Cl_2 phase containing the product was dried over anhydrous $MgSO_4$, filtered and dried to ~7 mL *via* rotary evaporation. Flash silica chromatography was performed using hexane:ethyl acetate (1:1 v/v) as the eluent. The purified NHS-CPAETC (1.98 g, 5.5 mmol, 63% yield) was isolated as a yellow oil that solidified upon refrigeration. ^{1}H-NMR (400 MHz, $CDCl_3$, ppm): δ = 3.35 (*q*, *J* = 7.3 Hz, 2H, -CH_2-S), 2.95-2.91 (*m*, 2H, -CH_2-), 2.85 (*m*, 4H, NHS -CH_2-CH_2-), 2.69-2.49 (2*m*, 2H, -CH_2-), 1.88 (*s*, 3H, -CH_3-), 1.36 (*t*, *J* = 7.4 Hz, 3H, -CH_3). ^{13}C-NMR (100 MHz, $CDCl_3$, ppm): δ = 216.3, 168.8, 167.0, 118.6, 45.9, 33.1, 31.4, 26.8, 25.5, 24.7, 12.7; MS (ESI): $[M+Na]^+$ calculated: 383.0, found: 382.9.

3.4.7 RAFT Polymerisation of BEA

A typical RAFT polymerisation of BEA (**Table 3.1**): In a glass vial, NHS-CPAETC (0.0790 g, 0.219 mmol), BEA (1.0425 g, 5.82 mmol), ACVA (6.26 mg, 0.0223 mmol), 1,3,5-trioxane (0.008 g, internal ^{1}H NMR standard), and dioxane (1 mL) were combined along with a magnetic stirrer and the vial sealed with a rubber septum. The vial and solution were deoxygenated with nitrogen for 10 min, then put in an oil bath at 70 ^{o}C and allowed to stir until the desired conversion was reached (~3 h). Conversion of monomer to polymer was followed by taking kinetic samples with a degassed syringe and analysed by ^{1}H NMR. Upon completion, the polymer ($pBEA_{25}$) was rapidly cooled to room temperature, opened to air and precipitated with diethyl ether (40 mL). ^{1}H-NMR (400 MHz, 293 K, DMSO-d_6, ppm): δ = 4.34 (*m*, 2*n*H), 3.65 (*m*, 2*n*H), 2.82 (*s*, 4H), 2.39 (*m*, *n*H), 1.91 (*m*, 0.5*n*H), 1.68 (*m*, *n*H), 1.55 (*m*, 0.5*n*H), 1.28 (*t*, 3H); ^{1}H-NMR (300 MHz, 293 K, $CDCl_3$, ppm): δ = 4.40 (*m*, 2*n*H), 3.55 (*m*, 2*n*H), 2.85 (*s*, 4H), 2.47 (*m*, *n*H), 2.03 (*m*, 0.5*n*H), 1.76 (*m*, *n*H), 1.57 (*m*, 0.5*n*H), 1.36 (*t*, 3H). ^{13}C-NMR (100 MHz, $CDCl_3$, ppm): δ = 173.99, 63.75, 41.24, 34.89, 28.90, 25.61, 24.05, 12.80

3.4.8 Conjugation of Polymer to Cyclic Peptide

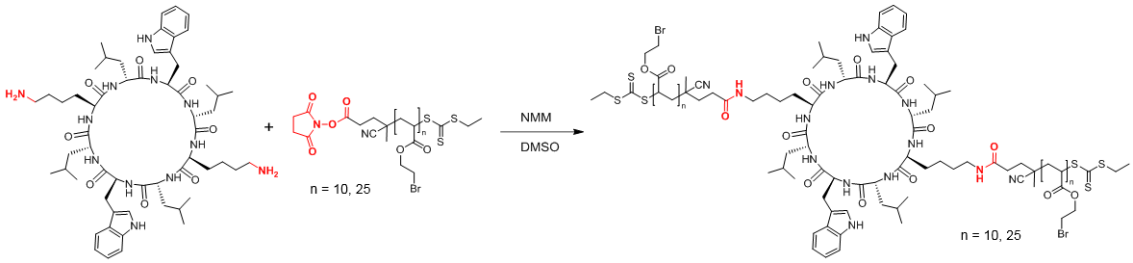

Cyclic peptide *cyclo*[(L-Lys-D-Leu-L-Trp-D-Leu-)$_2$] (1 equiv. 21.84 mg, 0.0202 mmol) and NHS-pBEA$_{25}$ (2.1 equiv. 0.2056 g, 0.04361 mmol) were suspended in DMSO (1 mL) to which *N*-methylmorpholine (NMM) (6 equiv. 13.32 µL, 0.121 mmol) was added and stirred for 24 h. Upon completion (as monitored by SEC), the conjugate was precipitated in diethyl ether. The conjugate was then dissolved in THF and purified by preparative size exclusion. ^{1}H-NMR (400 MHz, 293 K, DMSO-d$_6$, ppm): δ = 8.31 (br *m*, 2H, Trp), 8.19 (br *m*, 4H, Trp), 8.06 (br *m*, 2H, Trp), 7.87 (br *m*, 2H, Trp), 7.60 (*d*, 2H, Trp), 7.28 (*d*, 2H, Trp), 7.10 (*s*, 2H, Trp), 7.01 (*t*, 2H, Trp), 6.92 (*t*, 2H, Trp), 4.34 (*m*, 2*n*H, C<u>H</u>$_2$-Br), 3.65 (*m*, 2*n*H, C<u>H</u>$_2$-CH$_2$-Br), 2.39-1.54 (4*m*, 3*n*H, polymer backbone), 1.29 (*t*, 3H, -C<u>H</u>$_3$), 0.81-0.72 (*m*, 24H, Leu), no other peptide peaks were detectable.

3.4.9 Substitution with 1-β-D-Thioglucose

CP-[pBEA$_{25}$]$_2$ (0.0561 g, 0.0112 mmol) was suspended in DMSO (1 mL) in a small vial with stirrer bar. Separately, 1-β-D-Thioglucose sodium salt (1.5 equiv. per bromine, 0.0922 g, 0.419 mmol) was dissolved in DMSO (1 mL), then added to the CP-[pBEA$_{25}$]$_2$ solution and stirred for 24 h under a N_2 atmosphere. Upon completion, the reaction mixture was diluted in water and excess sugar removed by centrifugal filtration (10,000 MWCO) and lyophilised to give the desired poly(β-D-thioglucose ethyl acrylate) conjugate (CP-[p*Glu*EA$_{25}$]$_2$). ^{1}H-NMR (400 MHz, 293 K, DMSO-d$_6$, ppm): δ = 8.33 (*m*, 2H, Trp), 8.24 (*m*, 4H, Trp), 8.10 (*m*, 2H, Trp), 7.90 (*m*, 2H, Trp), 7.61 (*d*, 2H, Trp), 7.30 (*d*, 2H, Trp), 7.11 (*s*, 2H, Trp), 7.02 (*t*, 2H, Trp), 6.93 (*t*, 2H, Trp), 5.13 (*m*, 10H, -O<u>H</u>), 5.04 (*m*, 10H, -O<u>H</u>), 4.94 (*m*, 10H, -O<u>H</u>), 4.44 (*m*, 10H, CH$_2$-O<u>H</u>), 4.34 (*m*, 10H, CH$_2$-S-C<u>H</u>), 4.18 (*m*, C<u>H</u>$_2$-S-), 3.67 (*m*, 10H, CH-C<u>H</u>-CH), 3.46 (*m*, 10H, CH-C<u>H</u>-O), 3.17 (*m*, 30H, CH-C<u>H</u>-CH and C<u>H</u>$_2$-OH), 3.02 (*m*, 10H, CH-C<u>H</u>-CH), 2.88 - 2.80 (*d* of *m*, 10H,

$C\underline{H}_2$-CH_2-S-), 2.30 - 1.46 (4 *m*, 30H, polymer backbone), 1.35 (*m*, 10H -C<u>H</u> Leu), 0.84 - 0.70 (br *m*, 12H, Leu), no other peptide peaks were observed. See **Figure 3.3** for ^{1}H-NMR in DMSO-d_6 and **Figure 3.11** for ^{1}H-NMR in D_2O.

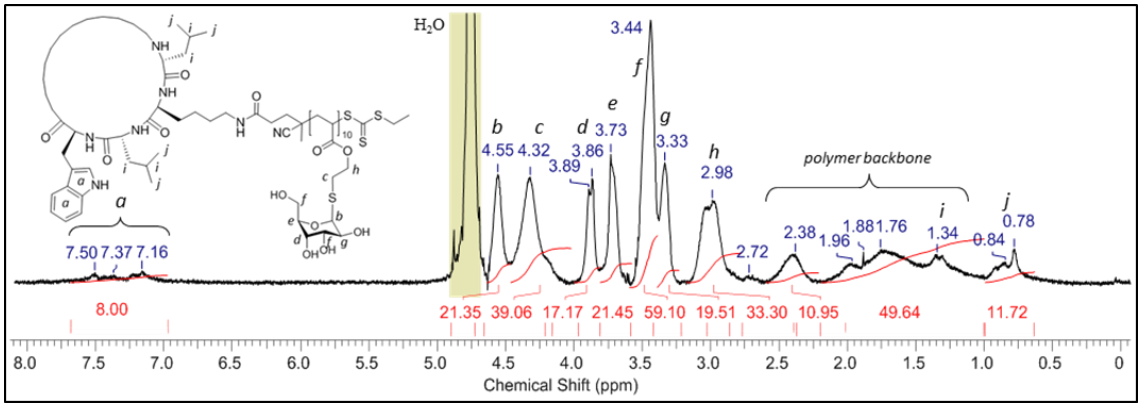

Figure 3.11: ^{1}H NMR of CP-[p*Glu*EA_{25}]$_2$ in D_2O.

3.4.10 Turbidimetry Assay

The aggregation studies with Con A were conducted as previously reported.[52] Con A was fully dissolved in HBS buffer to a concentration of 1 mg·mL^{-1}. 1 mL of a 50 μM (50 μM per sugar unit) stock solution of the polymer in HBS buffer was added to a quartz cuvette, which was placed in the UV-Vis spectrometer. 100 μL of the Con A stock solution was injected with a pipette to the bottom of the cuvette, then mixed briefly with pipette suction. The absorbance of the mixture was immediately recorded at λ = 420 nm for 30 min every 0.5 s. All experiments were completed in triplicate. The interaction rate was calculated by using the slope of the linear fit of the steepest portion and averaged over the three measurements.

3.4.11 Small Angle Neutron Scattering

SANS was carried out on the Sans2d small-angle diffractometer at the ISIS Pulsed Neutron Source (STFC Rutherford Appleton Laboratory, Didcot, U.K.).[57, 58] A collimation length of 4 m and incident wavelength range of 1.75 – 16.5 Å was employed, in order to provide a *q*-range of 0.0045 – 1.00 Å^{-1}.

q is defined as;

$$q = \frac{4\pi \sin\frac{\theta}{2}}{\lambda}$$

where θ is the scattered angle and λ is the incident neutron wavelength.

Data were measured simultaneously on two 1 m^2 detectors. The small-angle detector was 4 m from the sample and offset vertically 60 mm and sideways 100 mm. The wide-angle detector was positioned 2.4 m from the sample, offset sideways by 980 mm and rotated to face the sample. The beam diameter was 8 mm.

Each raw scattering data set was corrected for the detector efficiencies, sample transmission, and background scattering in D_2O or THF; and converted into a scattering cross-section ($\partial\Sigma/\partial\Omega$ vs. q) using instrument-specific software.[59] These data were placed on an absolute scale ($Å^{-1}$) using the scattering from a standard sample (a solid blend of hydrogenous and perdeuterated polystyrene) in accordance with established procedures.[60]

3.4.12SANS Sample Preparation

To ensure comparability between samples of different polymer arm lengths, all CP-[pBEA$_n$]$_2$ samples were made up to 10 mg· mL^{-1} in THF-d_8, and CP-[p*Glu*EA$_n$]$_2$ samples were made up to 5 mg· mL^{-1} in D_2O. Following analysis of CP-[pBEA$_{10}$]$_2$, this sample was then filtered with 0.5 μm PTFE syringe filters and rerun shortly after.

3.4.13SANS Analysis

SANS data were analysed in the NIST NCNR analysis macro using Igor pro 6.36.[41]

Data was analysed by a series of form factors, including sphere, ellipsoid, Gaussian coil, cylinder, flexible cylinder, and polyelectrolyte until the fit χ^2 values were minimised. The fit parameters are outlined in the Appendix.

3.4.14Static Light Scattering

The change in refractive index with concentration, $\partial n/\partial C$, was determined by measuring the refractive index (RI) of pBEA$_{50}$ over a range of concentrations in THF. RI measurements were taken on a Shodex RI detector operating at a wavelength of 632 nm.

The $\partial n/\partial C$ was calculated from the gradient of the RI *vs*. conc. multiplied by the RI of the solvent (THF = 1.407), divided by the RI constant of the instrument (1 194 000) to give 0.0729 for $pBEA_{50}$.

Light scattering measurements were obtained using an ALV-CGS3 system operating with a vertically polarised laser at wavelength of 632 nm. Measurements were taken at constant temperature (20 °C) over a range of scattering wave vectors, q ($q = 4\pi n \sin(\theta/2)/\lambda$, where θ is the scattered angle, λ is the incident light wavelength and n the refractive index of the solvent).

The Rayleigh ratio, R_θ, was determined using equation (2),

$$R_\theta = \frac{I_{solution}(\theta) - I_{solvent}(\theta)}{I_{toluene}(\theta)} \cdot \left(\frac{n_{solvent}}{n_{toluene}}\right)^2 \cdot R_{toluene} \qquad (2)$$

where $I_{solution}$, $I_{solvent}$ and $I_{toluene}$ are the scattering intensities of the solution, solvent and reference (toluene) respectively, n is the refractive index (n_{water} = 1.333, n_{THF} = 1.407, $n_{toluene}$ = 1.496) and $R_{toluene}$ the Rayleigh ratio of toluene ($R_{toluene} = 1.35 \times 10^{-5}$ cm^{-1} for λ = 632.8 nm).

The optical constant, K, is defined by equation (3), where N_a is Avogadro number and $\partial n/\partial C$ is the change in refractive index with concentration.

$$K = \frac{4\pi^2 {n_{solvent}}^2}{\lambda^4 N_a} \left(\frac{\partial n}{\partial C}\right)^2 \qquad (3)$$

In all cases it was verified that the apparent radius of gyration of the systems verified $q \times R_g < 1$. Thus the Zimm approximation can be used to give equation (4). Plotting KC/R_θ as a function of q^2 for each concentration yielded the apparent radius of gyration, R_g, of the scattering object and the apparent molecular weight extrapolated to zero angle, M_a. Representative plots are shown in the Appendix to Chapter 3.

$$\frac{KC}{R_\theta} = \frac{1}{M_a} \cdot \left(1 + \frac{q^2 \cdot {R_g}^2}{3}\right) \qquad (4)$$

At a given concentration the Rayleigh ratio, R_θ, is related to the apparent molecular weight of the sample, given by equation (4). It is only at infinite dilutions, where the interactions between scattering particles are negligible, that the apparent molecular weight is equal to

the true molecular weight.[61] Multiple concentrations were measured and linear regression was used to determine the apparent molecular weight at a concentration of 0 mg· mL^{-1}.

3.4.15SLS Sample Preparation

Samples of CP-$[pBEA_n]_2$ were prepared as a concentrated stock solution by direct dissolution at room temperature in THF. Samples for analysis were prepared by dilution of the stock solution to 0.5, 1, 2, and 5 mg· mL^{-1} and analysed by SLS without filtration on the day of preparation and ~24 h later. Samples were then filtered through Fisherbrand 0.2 μm pore size PTFE syringe filters.

3.5 References

1. Gauthier, M. A.; Gibson, M. I.; Klok, H.-A. *Angewandte Chemie International Edition* **2009,** 48, (1), 48-58.

2. Günay, K. A.; Theato, P.; Klok, H.-A., History of Post-Polymerization Modification. In *Functional Polymers by Post-Polymerization Modification*, Wiley-VCH Verlag GmbH & Co. KGaA: 2012; pp 1-44.

3. Gunay, K. A.; Theato, P.; Klok, H. A. *J. Polym. Sci. Pol. Chem.* **2013,** 51, (1), 1-28.

4. Blasco, E.; Sims, M. B.; Goldmann, A. S.; Sumerlin, B. S.; Barner-Kowollik, C. *Macromolecules* **2017**.

5. Burns, J. A.; Gibson, M. I.; Becer, C. R., Glycopolymers via Post-Polymerization Modification Techniques. In *Functional Polymers by Post-Polymerization Modification*, Wiley-VCH Verlag GmbH & Co. KGaA: 2012; pp 237-265.

6. Barlow, T. R.; Brendel, J. C.; Perrier, S. *Macromolecules* **2016,** 49, (17), 6203-6212.

7. Couet, J.; Jeyaprakash, J. D.; Samuel, S.; Kopyshev, A.; Santer, S.; Biesalski, M. *Angewandte Chemie-International Edition* **2005,** 44, (21), 3297-3301.

8. Larnaudie, S. C.; Brendel, J. C.; Jolliffe, K. A.; Perrier, S. *Journal of Polymer Science Part A: Polymer Chemistry* **2016,** 54, (7), 1003-1011.

9. Chapman, R.; Danial, M.; Koh, M. L.; Jolliffe, K. A.; Perrier, S. *Chemical Society reviews* **2012,** 41, (18), 6023-41.

10. Dehn, S.; Chapman, R.; Jolliffe, K. A.; Perrier, S. *Polym. Rev.* **2011,** 51, (2), 214-234.

11. Delaittre, G.; Guimard, N. K.; Barner-Kowollik, C. *Accounts of Chemical Research* **2015,** 48, (5), 1296-1307.

12. Rostovtsev, V. V.; Green, L. G.; Fokin, V. V.; Sharpless, K. B. *Angewandte Chemie-International Edition* **2002,** 41, (14), 2596-9.

13. Brendel, J. C.; Liu, F.; Lang, A. S.; Russell, T. P.; Thelakkat, M. *ACS Nano* **2013,** 7, (7), 6069-6078.

14. Gody, G.; Rossner, C.; Moraes, J.; Vana, P.; Maschmeyer, T.; Perrier, S. *Journal of the American Chemical Society* **2012,** 134, (30), 12596-12603.

15. Gody, G.; Roberts, D. A.; Maschmeyer, T.; Perrier, S. *Journal of the American Chemical Society* **2016,** 138, (12), 4061-4068.

16. Brendel, J. C.; Gody, G.; Perrier, S. *Polym. Chem.* **2016,** 7, (35), 5536-5543.

17. Anderson, G. W.; Zimmerman, J. E.; Callahan, F. M. *Journal of the American Chemical Society* **1964,** 86, (9), 1839-1842.

18. Bathfield, M.; D'Agosto, F.; Spitz, R.; Charreyre, M.-T.; Delair, T. *Journal of the American Chemical Society* **2006,** 128, (8), 2546-2547.

19. Roth, P. J.; Wiss, K. T.; Zentel, R.; Theato, P. *Macromolecules* **2008,** 41, (22), 8513-8519.

20. Li, H.; Bapat, A. P.; Li, M.; Sumerlin, B. S. *Polym. Chem.* **2011,** 2, (2), 323-327.

21. Vanparijs, N.; Maji, S.; Louage, B.; Voorhaar, L.; Laplace, D.; Zhang, Q.; Shi, Y.; Hennink, W. E.; Hoogenboom, R.; De Geest, B. G. *Polym. Chem.* **2015,** 6, (31), 5602-5614.

22. Chiefari, J.; Chong, Y. K.; Ercole, F.; Krstina, J.; Jeffery, J.; Le, T. P. T.; Mayadunne, R. T. A.; Meijs, G. F.; Moad, C. L.; Moad, G.; Rizzardo, E.; Thang, S. H. *Macromolecules* **1998,** 31, (16), 5559-5562.

23. Chapman, R.; Koh, M. L.; Warr, G. G.; Jolliffe, K. A.; Perrier, S. *Chemical Science* **2013,** 4, (6), 2581-2589.

24. Danial, M.; My-Nhi Tran, C.; Young, P. G.; Perrier, S.; Jolliffe, K. A. *Nature Communications* **2013,** 4, 2780.

25. Lautié, A.; Froment, F.; Novak, A. *Spectroscopy Letters* **1976,** 9, (5), 289-299.

26. Koh, M. L.; Jolliffe, K. A.; Perrier, S. *Biomacromolecules* **2014,** 15, (11), 4002-4011.

27. Ghadiri, M. R.; Granja, J. R.; Milligan, R. A.; McRee, D. E.; Khazanovich, N. *Nature* **1993,** 366, (6453), 324-327.

28. Zetterlund, P. B.; Kagawa, Y.; Okubo, M. *Chemical Reviews* **2008,** 108, (9), 3747-3794.

29. Monteiro, M. J. *European Polymer Journal* **2015,** 65, 197-201.

30. Ladmiral, V.; Mantovani, G.; Clarkson, G. J.; Cauet, S.; Irwin, J. L.; Haddleton, D. M. *Journal of the American Chemical Society* **2006,** 128, (14), 4823-4830.

31. Chen, G.; Tao, L.; Mantovani, G.; Geng, J.; Nyström, D.; Haddleton, D. M. *Macromolecules* **2007,** 40, (21), 7513-7520.

32. Geng, J.; Lindqvist, J.; Mantovani, G.; Haddleton, D. M. *Angewandte Chemie International Edition* **2008,** 47, (22), 4180-4183.

33. Chen, G.; Amajjahe, S.; Stenzel, M. H. *Chemical Communications* **2009**, (10), 1198-1200.

34. Boyer, C.; Bousquet, A.; Rondolo, J.; Whittaker, M. R.; Stenzel, M. H.; Davis, T. P. *Macromolecules* **2010,** 43, (8), 3775-3784.

35. Becer, C. R.; Babiuch, K.; Pilz, D.; Hornig, S.; Heinze, T.; Gottschaldt, M.; Schubert, U. S. *Macromolecules* **2009,** 42, (7), 2387-2394.

36. Rosen, B. M.; Lligadas, G.; Hahn, C.; Percec, V. *Journal of Polymer Science Part A: Polymer Chemistry* **2009,** 47, (15), 3931-3939.

37. Rosen, B. M.; Lligadas, G.; Hahn, C.; Percec, V. *Journal of Polymer Science Part A: Polymer Chemistry* **2009,** 47, (15), 3940-3948.

38. Xu, J.; Tao, L.; Boyer, C.; Lowe, A. B.; Davis, T. P. *Macromolecules* **2010,** 43, (1), 20-24.

39. Ashok Kothapalli, V.; Shetty, M.; de los Santos, C.; Hobbs, C. E. *Journal of Polymer Science Part A: Polymer Chemistry* **2016,** 54, (1), 179-185.

40. Couet, J.; Biesalski, M. *Small* **2008,** 4, (7), 1008-1016.

41. Kline, S. *Journal of Applied Crystallography* **2006,** 39, (6), 895-900.

42. Hammouda, B. *Journal of Applied Crystallography* **2010,** 43, (4), 716-719.

43. Pesek, S. L.; Li, X.; Hammouda, B.; Hong, K.; Verduzco, R. *Macromolecules* **2013,** 46, (17), 6998-7005.

44. Pesek, S. L.; Xiang, Q.; Hammouda, B.; Verduzco, R. *Journal of Polymer Science Part B: Polymer Physics* **2017,** 55, (1), 104-111.

45. Catrouillet, S.; Brendel, J. C.; Larnaudie, S.; Barlow, T.; Jolliffe, K. A.; Perrier, S. *ACS Macro Letters* **2016,** 5, (10), 1119-1123.

46. Koh, M. L.; FitzGerald, P. A.; Warr, G. G.; Jolliffe, K. A.; Perrier, S. *Chemistry – A European Journal* **2016,** 22, (51), 18419-18428.

47. Eissa, A.; Cameron, N., Glycopolymer Conjugates. In *Bio-synthetic Polymer Conjugates*, Schlaad, H., Ed. Springer Berlin Heidelberg: 2013; Vol. 253, pp 71-114.

48. Ahmed, M.; Narain, R. *Biomaterials* **2011,** 32, (22), 5279-5290.

49. Pieters, R. J. *Organic & Biomolecular Chemistry* **2009,** 7, (10), 2013-2025.

50. Ghadban, A.; Albertin, L. *Polymers* **2013,** 5, (2), 431-526.

51. Dimick, S. M.; Powell, S. C.; McMahon, S. A.; Moothoo, D. N.; Naismith, J. H.; Toone, E. J. *Journal of the American Chemical Society* **1999,** 121, (44), 10286-10296.

52. Gou, Y.; Geng, J.; Richards, S.-J.; Burns, J.; Remzi Becer, C.; Haddleton, D. M. *Journal of Polymer Science Part A: Polymer Chemistry* **2013,** 51, (12), 2588-2597.

53. Cairo, C. W.; Gestwicki, J. E.; Kanai, M.; Kiessling, L. L. *Journal of the American Chemical Society* **2002,** 124, (8), 1615-1619.

54. Koh, M. L. Self assembly of (N-methylated cyclic peptide)-polymer conjugates. University of Sydney, 2013.

55. Danial, M.; Perrier, S.; Jolliffe, K. A. *Organic & Biomolecular Chemistry* **2015,** 13, (8), 2464-73.

56. Danial, M.; Tran, C. M. N.; Young, P. G.; Perrier, S.; Jolliffe, K. A. *Nature Communications* **2013,** 4, 13.

57. http://www.isis.stfc.ac.uk http://www.isis.stfc.ac.uk.

58. Heenan, R. K.; Rogers, S. E.; Turner, D.; Terry, A. E.; Treadgold, J.; King, S. M. *Neutron News* **2011,** 22, (2), 19-21.

59. http://www.mantidproject.org. **2015**.

60. Wignall, G. D.; Bates, F. S. *Journal of Applied Crystallography* **1987,** 20, (1), 28-40.

61. Brown, W., *Light Scattering: Principles and Development*. Clarendon Press: 1996.

4

The Effect of Ionic Strength on the Self-Assembly of Polyelectrolyte-Cyclic Peptide Conjugates

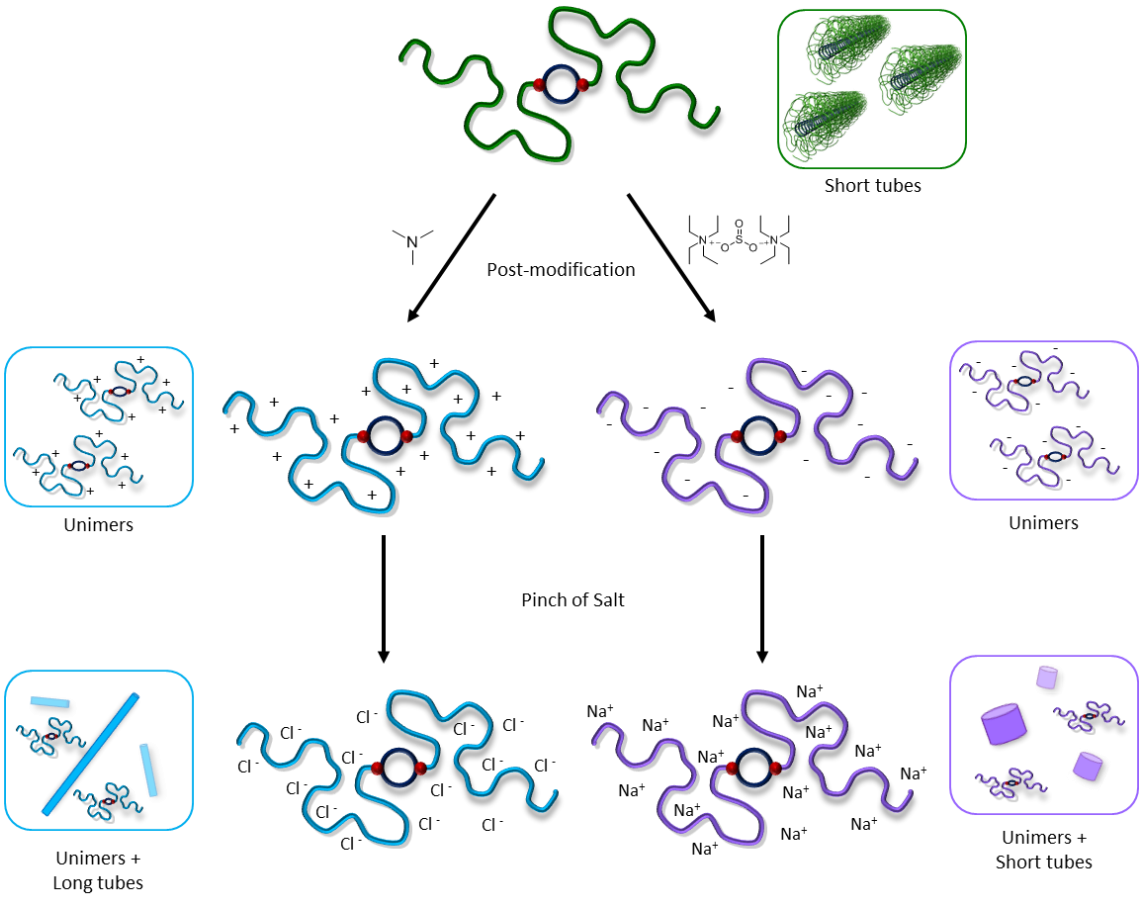

This chapter describes the synthesis and self-assembly of complex polyelectrolyte nanostructures consisting of both anionic and cationic polyelectrolyte-cyclic peptide conjugates. Using Small Angle Neutron Scattering (SANS) to follow the structure morphology in solution, it is possible to manipulate the self-assembly of the conjugates into nanotubes by varying salt concentrations. It was established that a high charge density strongly impacts the self-assembly process, and the effect can be controlled at high ionic strength; gaining valuable insight into the limitations of the system. Also demonstrated was that anionic and cationic conjugates made from an identical precursor form vastly different self-assembled structures. This study provides a fundamental insight into understanding the effect of charge on self-assembly, which is of vital importance for the design and control of charged and pH responsive conjugates as functional materials

4.1 Introduction

Despite recent advances looking at a greater diversity of polymer-conjugated nanotubes, there is still have a limited understanding of this incredibly complex supramolecular system. Water in particular is a challenging solvent due to the hydrogen bond competition between the solvent and the hydrogen-bonding necessary for nanotube formation. The hydrogen bonding between conjugates is remarkably strong for neutral, hydrophobic polymers such as poly(*n*-butyl acrylate) conjugates.[1-3] However disruption of the assemblies is readily achieved by suspending the polymer-conjugates in hydrogen-bonding competitive solvents such as DMF, DMSO or TFA.[1, 2] In such solvents, the polymer conjugates exist primarily as unimers in solution whereas, upon dilution with less competitive solvents such as THF or $CHCl_3$, the unimers begin to assemble into nanotubes. For water soluble, pH responsive polymer conjugates, including poly(dimethylamino ethyl methacrylate)[4] and poly(acrylic acid),[5] similar trends have been observed. In these cases, self-assembly is directed by pH changes, and is shown to be reversible, demonstrating that assembly can not only be controlled by pH but that the process is also reversible. Due to the hydrogen bonding capacity of water, hydrophilic polymer conjugates would likely have far shorter assemblies than could be expected in organic solvents such as methanol or THF. Thus any self-assembly occurring in water

must be sufficiently robust to overcome such a hydrogen-bond competitive environment. As demonstrated by pH controlled self-assembly studies, even the small presence of charge density on the polymer arms had a drastic impact on self-assembly.[4]

To use these promising polymeric nanotubes as drug-delivery vehicles, a thorough understanding of the self-assembly properties of polymeric nanotubes in aqueous environments must be achieved. In order to control the assembly process, it must first be possible to disassemble the nanotubes into their constituent parts: the unimeric polymer-conjugate building blocks. While attempts have been made to control nanotube assembly by using polymer-conjugates responsive to stimuli such as pH[4, 5] or temperature,[6, 7] a detailed study on the self-assembly from a disassembled state to an assembled one has yet to be carried out. Herein, cyclic-peptide polymer-conjugates bearing permanently charged polymer arms have been investigated, and an analysis on their self-assembly properties in an aqueous environment of varying ionic strength has been carried out. The polymer length, graft density, and charge density is kept constant by using a single precursor conjugate for synthesis. The samples were then studied by SANS to evaluate the morphology adopted by the conjugates in solution. By adding monovalent salt (NaCl) we incrementally increase the ionic strength of the environment, thus increasing the coulombic screening on the charged polymer arms, we can readily study the self-assembly process of charged polymer-conjugates.

4.2 Results and Discussion

4.2.1 Synthetic Strategy

This chapter looks at modified pBEA (DP25) covalently linked to a cyclic peptide. The synthesis of the polymer can be found in Chapter 2, and the conjugation strategy used was the same as in Chapter 3.

The polymer $pBEA_{25}$ was synthesised *via* RAFT polymerisation using NHS-CPAETC as a chain transfer agent following the protocols described in Chapters 2 and 3. After polymerisation, a theoretical average molecular weight of 4700 $g \cdot mol^{-1}$, corresponding to a degree of polymerisation of 25, was calculated from conversion by NMR (at 95%

monomer conversion). A narrow dispersity of 1.10 and an $M_{n,SEC}$ of 4200 were determined by SEC (**Figure 4.1**). The conjugation reaction was followed by SEC by taking samples from the reaction mixture. The polymer peak at ~4600 g · mol^{-1} (**Figure 4.1**) diminished and the peak at ~11000 g · mol^{-1} increased, indicating the reaction had gone to completion within 21 h. CP-[pBEA$_{25}$]$_2$ conjugates were purified by preparative scale size exclusion chromatography in THF to remove any excess polymer to minimise any impact on the scattering measurements. The pure CP-[pBEA$_{25}$]$_2$ conjugate had a calculated molecular weight of 10400 g· mol^{-1}, the $M_{n,SEC}$ was 12500 g· mol^{-1} with a low dispersity of 1.15 (**Figure 4.1**).

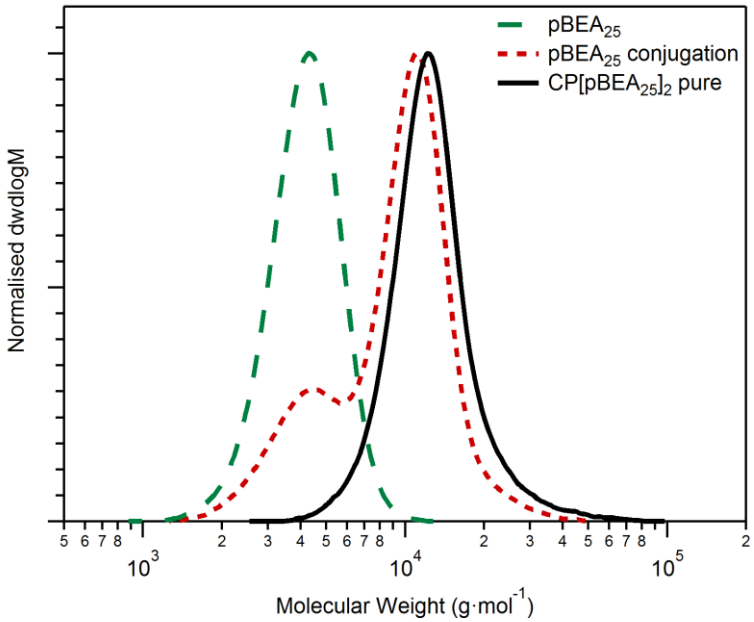

Figure 4.1: SEC chromatograms of pBEA$_{25}$ (green dashed), after CP-[pBEA$_{25}$]$_2$ conjugation is complete (red dotted) and CP-[pBEA$_{25}$]$_2$ after purification (black solid line).

Using cyclic peptide conjugates of pBEA to generate polyelectrolyte conjugates facilitates direct comparison on the effect of charge on self-assembly, while minimising structural variations that can arise during synthesis, such as different polymer lengths or inconsistent charge densities. To this end, using the CP-[pBEA$_{25}$]$_2$ conjugate was used to synthesise both cationic and anionic polyelectrolyte conjugates by nucleophilic substitution.[8] To introduce a positive charge, the bromine groups of the CP-[pBEA$_{25}$]$_2$

precursor were substituted using trimethyl amine in DMSO, to give CP-[poly(trimethyl ammonium ethyl acrylate)$_{25}$]$_2$ (CP-[(pTMAEA)$_{25}$]$_2$). The anionic charge was introduced with a tetramethyl ammonium sulfite salt in a Strecker reaction[9] in DMSO. The tetramethyl ammonium counterion used has been shown to improve sulfonated polymer solubility in polar organic solvents.[10, 11] Thus the bromine was substituted, installing the negatively charged sulfonate to give CP-[poly(ethyl acrylate sulfonate tetraethyl ammonium)$_{25}$]$_2$ (CP-[(pEASTEA)$_{25}$]$_2$).

4.2.2 SANS Analysis of Polymer-Conjugates

To guarantee full control of conjugates irrespective of pH, permanent charges were installed on the polymer arms, ensuring that any self-assembly was directed by charge shielding on the polymeric chains. SANS experiments were then used to investigate the effects of the polymer charges on conjugate self-assembly.

Here, SANS measurements were taken over a large q range (0.0045 – 1.00 Å^{-1}), resulting in a comprehensive molecular study over a broad length scale using SANS2D (ISIS, UK). The window of observation in Å^{-1} for our data is related to q by $\frac{2\pi}{q}$. The low-q range (q = < 0.025 Å^{-1}) corresponds to length scales greater than 251 Å which is the region of interest for self-assembly and intermolecular aggregation such as in supramolecular systems. The intermediate-q region, (0.025 Å^{-1} < q < 0.1 Å^{-1}), provides information on the polymer-conjugate length, shape and cross-sectional size and stiffness in the 63 - 250 Å size range. The high-q region (q > 0.1 Å^{-1}) can give information on a molecular level such as for polymer-arms of unimeric conjugates or thermal fluctuations.[12]

4.2.3 Guinier-Porod analysis

As in earlier SANS studies described in Chapter 3, the data was initially fit to a Guinier-Porod model to describe the structure of these systems in solution. Guinier-Porod modelling did not satisfactorily fit either conjugate in pure D_2O, suggesting it is unsuitable for the analysis of these samples. The s values obtained from fitting CP-[pEASTEA$_{25}$]$_2$ (**Figure A4.3**) are between 0.16 and 0.3 at all salt concentrations, which have been plotted in **Figure 4.2**, suggesting anisotropic, spherical objects or ellipsoidal

morphologies. The approximated R_g from these fits increases from 22.9 Å at 0.18 M NaCl to 30.7 Å in 5 M NaCl solution in **Figure A4.3**. Given the CP has an internal diameter of 7 Å, along with the addition of the polymer chain, could mean the peptide has the same R_g in both dimensions, indicating a more spherical object. In the case of the positively charged system, CP-[pTMAEA$_{25}$]$_2$, the dimension variable *s* ranges between 0.7 and 1.1, and is closest to 1 in 1 M and 2 M salt concentrations (*s* = 1.03 and 0.89 respectively, **Figure 4.2** and **Figure A4.6**). These greater *s* values suggest the cationic conjugates adopt a more cylindrical or rod-like morphology than the anionic conjugates. Comparing the sample with 1 M NaCl and 5 M NaCl (**Figure A4.6A** and **F**, respectively), it appears that upon increasing salt concentration, the dimension variable s decreases, suggesting the assembly is adopting a more spherical structure. R_g values obtained from the Guinier-Porod model are lower than anticipated for the supramolecular structure suggested by the dimension variable for the same fit. From this, it is possible to conclude that the R_g in this case provides an estimate of the cross-sectional radius of the cylindrical assembly, which is consistent with the studies by Verduzco and co-workers on bottlebrush polymers.[12, 13] This result is corroborated by the data presented in Chapter 3, where a similar result was found.

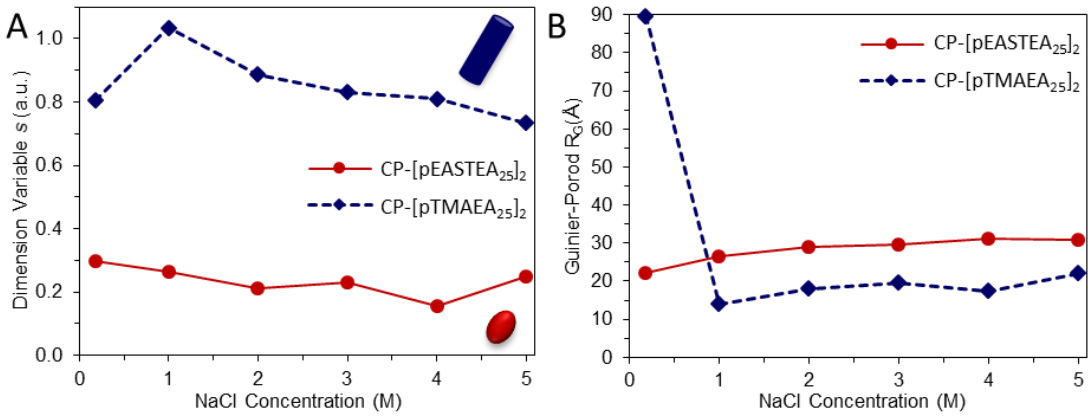

Figure 4.2: Results from Guinier-Porod Model for the Dimension Parameter, s (A) and (B) the Radius of Gyration, R_g (Fits in **Figure A4.3** and **A4.6**).

4.2.4 Polyelectrolyte conjugates in D_2O

In addition to the Guinier-Porod model, the data were also fit to both a polyelectrolyte and cylinder form factor, using the NIST macros in Igor Pro to confirm the conjugate morphologies in solution.[14] In pure D_2O, the scattering profiles shown in **Figure 4.3** are dominated by both a significant upturn at low *q* and a peak at intermediate *q* values. In pure water, it was assumed that self-assembly would be completely disrupted due to the high charge density around the polymer arms, resulting in unimers in solution. Small, uncharged unimeric polymer-conjugates are expected to have a low scattering intensity at low-*q* values, however, the upturn at low-*q* is suggestive of higher order aggregation. The scattering behaviour at low-*q* (≤ 0.25 Å^{-1}) can be fitted by a power law with an exponent between -1 and -4 which is consistent with other SANS studies on polyelectrolyte solutions.[8, 15-17] While the origin of this upturn remains controversial, it is commonly attributed to scattering arising from large multi-chain clusters of concentrated polymer domains that are present even in dilute solutions of polyelectrolytes.[15-18]

The broad maximum at intermediate-*q* (0.02 Å$^{-1} < q < 0.1$ Å^{-1}) for both positive and negative polyelectrolytes profiles (**Figure 4.3**), shows a shift towards higher *q* with increasing concentration consistent with the literature.[8, 17, 19] At middle to high, $q > 0.03$ Å^{-1}, the data for both conjugates are well described by a polyelectrolyte form factor (Borue-Erukhimovich polyelectrolyte - fits in **Figure A 4.1**). The upturn at low-*q*, < 0.025 Å^{-1}, was modelled with a power law fit that is consistent with literature on polyelectrolyte solutions,[17] giving $q^{-1.1}$ for CP-[pTMAEA$_{25}$]$_2$ and $q^{-3.7}$ for CP-[pEASTEA$_{25}$]$_2$.

The conformation of polyelectrolytes in solution are expected to fit an ellipsoidal form factor, with the polymer cross-section and length giving the radii of the ellipse.[20, 21] Modelling polyelectrolytes as ellipsoids provides additional information about the conjugate morphology by incorporating the scattering length density of the samples. This fit suggested a radius *a* of 1.8 Å and radius *b* of 30.4 Å CP-[pTMAEA$_{25}$]$_2$ (**Figure A4.2B**); and for anionic CP-[pEASTEA$_{25}$]$_2$ gave a radius *a* 2.7 Å and radius *b* of 36.8 Å (**Figure A4.2A**). In an ellipsoid fit, when the radius *b* > radius *a*, the object is an

oblate ellipsoid and of a disk-like nature, suggesting the conjugates are unimers in D_2O, with the polymer arms in an extended conformation.

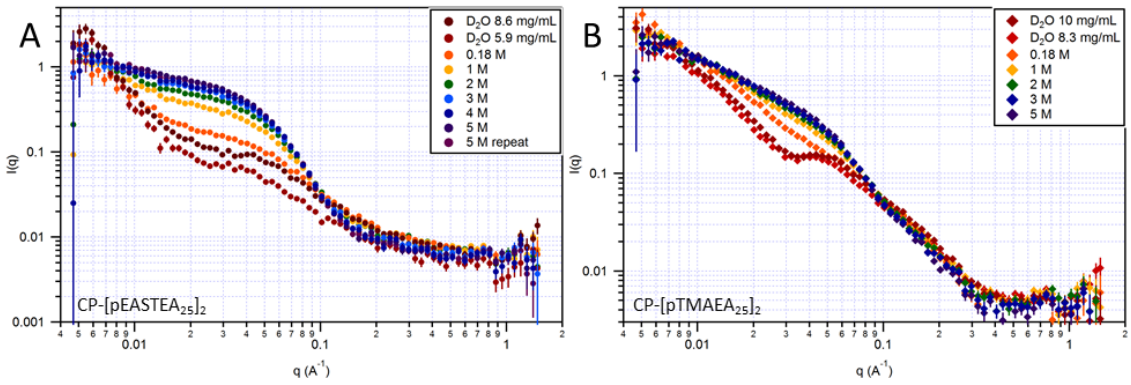

Figure 4.3: Scattering profiles of polyelectrolyte conjugates at a range of salt concentrations (A) anionic CP-[pEASTEA$_{25}$]$_2$ and (B) cationic CP-[pTMAEA$_{25}$]$_2$

From this, it is possible to conclude, by modelling of polyelectrolyte conjugates in pure D_2O, that the high charge density on the polyelectrolyte arms, competes with the intermolecular hydrogen bonding of the cyclic peptide core, hindering the supramolecular assembly to form nanotubes.

4.2.5 The Effect of Salt on Self Assembly

To control the self-assembly of the polyelectrolyte-conjugates, the addition of monovalent salt was used to screen the repulsive inter-chain interactions on the polymer arms. The use of salt in polyelectrolyte solutions is commonly used to shield long-range Coulomb interactions between particles.[22] Thus the polyelectrolyte-conjugates at increasing ionic strengths was analysed, allowing the cyclic-peptide core to drive self-assembly. To ensure consistency throughout the experiments, after each sample was run, additional salt was added to bring the solutions to the desired ionic strength, before being measured again until higher salt concentrations were achieved (5 M). 0.18 M NaCl was the lowest concentration measured, to simulate biological conditions at ion concentrations similar to biological grade phosphate buffered saline, with additional concentrations measured at 1 M through to 5 M NaCl in D_2O. While the hydrogen-bonding in polymeric cyclic-peptide nanotubes is strong,[23] a number of factors dictate the length of the nanotube

formed; inter-chain repulsion due to the high charge density on polyelectrolyte-conjugates or pH responsive systems,[4, 5] the polymer length, number of polymer arms conjugated, and bulkiness of the monomer.[1, 2, 5]

4.2.6 Analysis of Anionic Polymer Conjugates in Solution

At low ionic strength (0.18 M), the upturn in the scattering profile of CP-[pEASTEA$_{25}$]$_2$ at low-q remains steep and fits to $q^{-2.3}$, and the local maximum or shoulder at q = 0.05 Å^{-1} broadens towards low-q. The Guinier-Porod dimension variables, suggest an elongated spherical shape, however a spherical form factor was unable to be fit to the data. The polyelectrolyte model was not able to fit the data once salt concentrations are factored into the fitting parameters, due to charge shielding. In the polyelectrolyte model, the salt concentration has a major effect on the fit. For all samples with added salt, the polyelectrolyte fit was incapable of modelling the data when ionic strength was included in the fit parameters. It may be that the diffusion of salt into the polymer corona is causing different charge densities along the chain, leading to charge shielding on the outside, but not closer to the peptide core; thus adding further confounding factors not taken into account in the form factor.

The data is readily fit by a cylinder form factor however, which gives a radius of 37.7 Å and length of 2.1 Å (see **Figure A4.4B** for fits). The similarity between these results and those in D_2O suggest that the conjugates exist as unimers. In assembled cyclic-peptide nanotubes, the inter-ring distance is 4.75 Å;[24] and the Debye radius of a 0.18 M monovalent salt solution is 7.2 Å (**Table 4.3**),[25] roughly 1.5 times the inter-peptide spacing. In electrolyte solutions, the Debye length (also known as Debye radius) is the measure of the distance that the electrostatic charge effects persist, the magnitude of which depends solely on the properties of the solution and can be calculated from the ionic strength of the solution (**Table 4.3**).[25] This overlap of electrostatic repulsion would prevent the necessary hydrogen bonding between peptide subunits to occur.[26] By plotting the radius and length parameters given by the cylinder model fit (**Figure 4.4**, and **Figure A4.4** and **A4.5**), the trend with increasing ionic strength is clear. At 1 M NaCl concentrations, the length of the conjugates increases ten-fold to 23.8 Å. At this

concentration the Debye screening length is 3.0 Å, which is sufficiently reduced to allow intermolecular hydrogen bonding, permitting self-assembly to occur. As ionic strength continues to increase, so too does the length and radius, reaching a maximum at 35.6 Å and 47.1 Å respectively (**Figure A4.5D**), consistent with decreasing electrostatic repulsion facilitating assembly. The values obtained from cylindrical modelling are consistent with the Guinier-Porod values that suggest an anisotropic, spheroid object. From the inter-unit spacing and the length obtained from the cylinder model, a number of aggregation of 7.7 was calculated. The Debye radius at 5 M NaCl concentrations is 1.4 Å (**Table 4.3**), and is sufficient to screen the electrostatic interaction between polymer arms of the cyclic peptides, thus enabling hydrogen-bonding. As the negative charge on the sulfonate is screened by the sodium ions present at high salt concentrations (> 1 M) the conjugates effectively behave as neutral polymers, with steric effects governing the self-assembly over electrostatic ones. The ethyl acrylate sulfonate and the bulky tetraethyl ammonium counterion result in a very sterically hindered polymer, and the size of this monomer unit limits the assembly of the conjugates, resulting in short nanotubes.

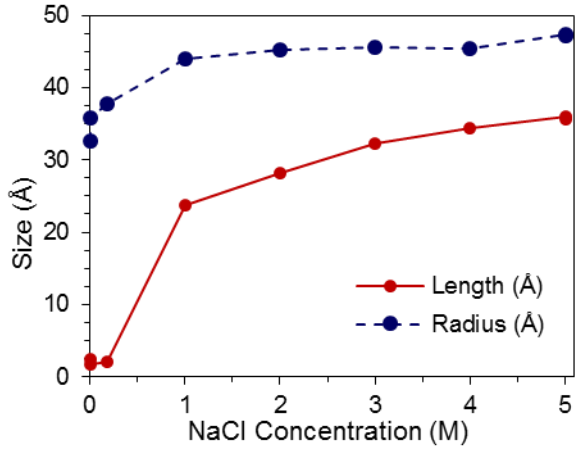

Figure 4.4: Variation in length and radius of anionic CP-[pEASTEA$_{25}$]$_2$ conjugate assemblies from cylinder model fitting (Fits in **Figure A4.4 and A4.5**). Lines between points are added to guide the eye.

4.2.7 Analysis of Cationic Polymer Conjugates in Solution

The cationic conjugate CP-[(pTMAEA)$_{25}$]$_2$ has a scattering profile that is similar to anionic CP-[(pEASTEA)$_{25}$]$_2$, with an upturn at low-q from inter-chain aggregation. However the shape of the profile is distinctly different from that of the anionic conjugate; with increasing ionic strength, there is far less change in overall shape of the curves at intermediate-q values in the region of 0.03 Å^{-1} < q < 0.2 Å^{-1}, and a distinctive q^{-1} region emerges with increased ionic strength (**Figure 4.3**). The Guinier-Porod fit suggested cylindrical rod-like structures (**Figure A4.6**), which is consistent with the extended q^{-1} domain characteristic of this shape. Thus the data were fit to a cylindrical form-factor. Only data at low-q, < 0.1 Å^{-1} corresponding to a length scale of > 63 Å, were adequately modelled by this form factor; suggesting the conjugates adopt an ordered, multi-chain array of long tubular assemblies. At high-q, however, the data were poorly fit by the cylinder model, and is instead best modelled by a Gaussian coil form factor that describes polymers in solution. Using an additive combination of the two models (**Figure A4.8**), the data could be adequately fit (**Figure A4.7**), the results of which have been plotted in **Figure 4.5**.

At low ionic strength (0.18 M NaCl), the Cylinder-Gaussian coil model, gives a radius of 11 Å and length of 198 Å (**Figure A4.7**). Here, both the radius and length increase with ionic strength to 33 Å and 284 Å respectively at 5 M NaCl, with an R_g of 40 Å. A plot of the Cylinder-Gaussian fit parameters in **Figure 4.5**, clearly shows the trend that the radius remains relatively stable and the length of the assemblies increases with ionic strength. This is consistent with the decreasing Debye length. At 1 M NaCl, the Debye radius of the electrostatic charge is 3 Å (**Table 4.3**), enabling inter-peptide hydrogen bonding. As the Debye radius decreased to 1.4 Å in 5 M NaCl, the maximum length of 284 Å was reached, corresponding to a number of aggregation of 60. For the cationic CP-[(pTMAEA)$_{25}$]$_2$ conjugates, the Cylinder-Gaussian coil model were fit to q-values ≥ 0.02 Å^{-1} (length scale of 314 Å), due to the upturn in intensity from polymer-rich aggregates commonly present in polyelectrolyte samples. For the 0.18 M sample, the length obtained from the model is unexpectedly long (200 Å), considering the Debye radius is 7.2 Å, which should be sufficient to disrupt hydrogen bonding. For this two

theories could exist, firstly, that the upturn at low-q (< 0.02 Å^{-1}) is close to q^{-1}, and may be causing the model to over-estimate the cylinder length, secondly, the Debye length and electrostatic repulsion is being overcome by the inter-unit hydrogen-bonding, and a complex equilibrium between the repulsive electrostatic and steric forces and the attractive hydrogen-bond driven self-assembly exists to finely control aggregation. As mentioned previously, the impact of steric repulsion between polymer arms can have a drastic impact on the length of the overall assembly.[1] The less bulky trimethyl ammonium ethyl acrylate monomer and counterion as compared to ethyl acrylate sulfonate leads to a lower degree of steric hindrance surrounding the peptide core.

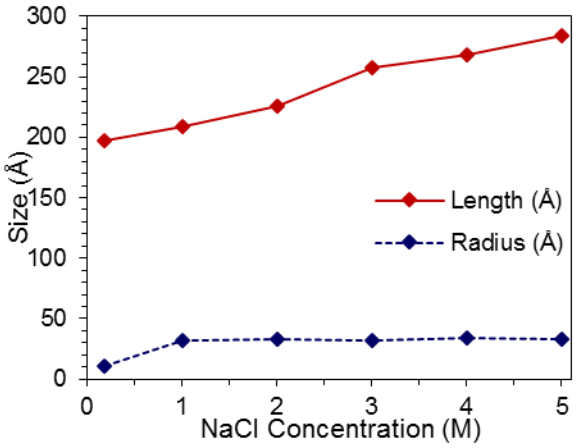

Figure 4.5: Variation in length and radius of cationic CP-[pTMAEA$_{25}$]$_2$ conjugate assemblies from Cylinder + Gaussian Coil model fitting. Lines between points are added to guide the eye.

4.3 Conclusion

Shown here is the *in situ* characterisation of polyelectrolyte-cyclic peptide conjugate self-assemblies using small angle neutron scattering. In pure D_2O, cyclic-peptide conjugates of both anionic pEASTEA and cationic pTMAEA exist as unimers. SANS scattering profiles of both conjugates were modelled to polyelectrolyte and cylinder form factors, and the results are consistent with that of single unimers in solution. The presence of unimers is due to the high electrostatic repulsion between polymer arms, preventing the inter-molecular hydrogen bond formation necessary for nanotube assembly. At high ionic

strengths, the SANS profiles of CP-[pEASTEA$_{25}$]$_2$ and CP-[pTMAEA$_{25}$]$_2$ are very different, despite being synthesised from a single precursor and having the same number of charged groups in the polymer chain. Guinier-Porod modelling revealed that CP-[pEASTEA$_{25}$]$_2$ formed an elongated spheroid structure, whereas CP-[pTMAEA$_{25}$]$_2$ formed an extended cylindrical assembly.

The scattering profile of anionic CP-[pEASTEA$_{25}$]$_2$ conjugates at high ionic strength was fit to a cylinder model, revealing that CP-[pEASTEA$_{25}$]$_2$ formed a mixture of unimeric conjugates and short stacks of peptides. The SANS profile of CP-[pTMAEA$_{25}$]$_2$ was fit with a Cylinder-Gaussian Coil combination model, which revealed that CP-[pTMAEA$_{25}$]$_2$ forms nanotubular structures of varying length in high ionic strength solutions. The difference in assembly between positively and negatively charged conjugates, despite the same polymer length, graft density and effective charge, is attributed to the difference in monomer size; with steric effects dominating the self-assembly once the electrostatic were shielded. This work presents a step towards fine control of the self-assembly of polymeric nanotubes, made possible by tuning the electrostatic repulsion between polymer arms using salt to reduce the Debye radius and electrostatic repulsion.

4.4 Experimental

4.4.1 Materials

Triethylamine, dioxane, and DMSO were purchased from Fisher Scientific (UK). 4,4-Azobis(4-cyanovaleric acid) (ACVA) was purchased from MP Biomedicals (UK). Cyclic peptide *cyclo*[(L-Lys-D-Leu-L-Trp-D-Leu-)$_2$] was synthesised within the group.[4, 27] All other compounds were purchased from Sigma-Aldrich (UK). All chemicals were used as received. All solvents were of analytical grade or higher bought from commercial sources and used as received.

4.4.2 Instrumentation

^{1}H NMR spectra were recorded on a Bruker AV-300, HD-300 or AV-400 in $CDCl_3$, D_2O or DMSO-d_6. Shift values (δ) are reported in ppm. The residual proton signal of the

solvent was used as an internal standard ($CDCl_3$ δ_H 7.26, D_2O δ_H 4.79, DMSO-d_6 δ_H 2.50). Size exclusion chromatography (SEC) was carried out on a Polymer Laboratories PL-GPC 50 Plus. All other polymers were analysed on a Polymer Laboratories PL-GPC 50 Plus system using a PolarGel-M guard column (7.5 × 50 mm) followed by two PolarGel-M columns (7.5 × 300 mm). DMF (0.1% LiBr) was used as an eluent at 1.0 mL min^{-1} at 50 °C. Commercial narrow linear poly(methyl methacrylate) standards in the range of 2.0 × 10^2 g mol^{-1} to 1.0 × 10^6 g mol^{-1} were used to calibrate the DMF SEC system. Analyte samples were filtered through a polytetrafluoroethylene (PTFE) membrane with either 0.2 μm or 0.45 μm pore size before injection (100 μL). Centrifugal filtration was carried out using Vivaspin® 20, 3,000 MWCO centrifuge tubes. Preparatory scale size exclusion chromatography was carried out using Biobead S-X1 bulk media. Experimental $M_{n,SEC}$ and $Đ$ values of synthesised polymers were determined using Agilent GPC software.

4.4.3 RAFT polymerisation of BEA

BEA was polymerised by RAFT in a similar manner as described in Chapter 2 using the conditions outlined in **Table 4.1**. See **Figure 4.1** for a typical SEC in DMF (0.1 % LiBr): $pBEA_{25}$: M_n = 3900 g·mol^{-1}, M_w = 4300 g·mol^{-1}, $Đ$ = 1.10.

Table 4.1: Details of pBEA-NHS polymerisation.

Polymer	$\frac{[M]_0}{[CTA]_0}$	$\frac{[CTA]_0}{[I]_0}$	Conv.[a] (%)	$M_{n,th}$[b] (g·mol^{-1})	$M_{n,SEC}$[c] (g·mol^{-1})	$Đ$
$pBEA_{25}$	25	10	92	4400	3900	1.10

[a] *Conversion determined by ^{1}H-NMR*

[b] *Theoretical number-average molecular weight*

[c] *DMF SEC, DRI detector, PMMA standards, number-average molecular weight*

4.4.4 Conjugation of Polymer to Cyclic Peptide

Conjugation was achieved as described in Chapter 3. See **Figure 4.1** for a typical SEC in DMF (0.1 % LiBr): CP-$[pBEA_{25}]_2$: M_n = 13500 g·mol^{-1}, M_w = 15600 g·mol^{-1}, $Đ$ = 1.15.

4.4.5 Substitution with Trimethyl amine

CP-[pBEA$_{25}$]$_2$ (0.050 g, 0.0106 mmol) was suspended in 1 mL of DMSO in a small vial with stirrer bar, to which was added 2 equiv. of trimethyl amine per bromine (4.2 M in ethanol, 133 μL, 0.559 mmol) and stirred for 24 h. Upon completion, the conjugate was precipitated in THF to give the desired poly(trimethyl ammonium bromide ethyl acrylate) conjugate (CP-[pTMAEA$_{25}$]$_2$). ^{1}H-NMR (400 MHz, 293 K, DMSO-d$_6$, ppm): δ = 8.31-6.76 (*m*, 10H, Trp), 4.53 (*m*, 2*n*H), 3.91 (*m*, 2*n*H), 3.34 (br *m*, 9*n*H), 2.41-1.61 (4*m*, 3*n*H), 0.85-0.59 (*m*, 24H, Leu), no other peptide peaks were observed.

4.4.6 Substitution with Tetraethyl ammonium sulfite

Typical synthesis of tetraethyl ammonium sulfite salt: In a small vial 1 equiv. of dimethylsulfite (0.197 mL, 2.32 mmol) and 1.9 equiv. of tetraethyl ammonium hydroxide (1.5 M solution in methanol, 2.936 mL, 4.04 mmol) were combined and stirred vigorously for 5 h. The turbid solution of tetraethyl ammonium sulfite in methanol was used directly in the substitution of pBEA.

CP-[pBEA$_{25}$]$_2$ (0.050 g, 0.0106 mmol) was suspended in 1 mL of DMSO in a small vial with stirrer bar, to which was added 5 equiv. of tetraethyl ammonium sulfite per bromine (0.75 M in methanol, 1.86 mL, 1.40 mmol) and stirred for 24 h. Upon completion, the solution was diluted with H_2O, purified by dialysis and lyophilised to give the desired poly(ethyl acrylate tetraethyl ammonium sulfonate) conjugate (CP-[pEASTEA$_{25}$]$_2$). ^{1}H-NMR (400 MHz, 293 K, DMSO-d$_6$, ppm): δ = 8.31-6.76 (*m*, 10H, Trp), 3.55-3.47 (*m*, (2 × *n*)H), 3.23 (*q*, (8 × *n*)H), 2.35-1.32 (4*m*, (3 × *n*)H), 1.16 (*t*, (12 × *n*)H) 0.85-0.59 (*m*, 24H, Leu), no other peptide peaks were observed.

4.4.7 Small Angle Neutron Scattering

SANS experiments and modelling were conducted as described in Chapter 3.

4.4.7.1 SANS Sample Preparation

To ensure comparability between different salt concentrations a single sample of polymer conjugate in D_2O was measured. After each sample was run, the additional salt was added

to bring the salt concentration to the desired level. CP-[pTMAEA$_{25}$]$_2$ (10.53 mg, 0.768 μmol) was dissolved in D_2O (1.0681 g, 8.6 mg · mL^{-1}) and the sample run. Following measurement, anhydrous NaCl was added to the sample in the cuvette and agitated until the salt was fully dissolved giving the desired salt concentration. The sample was then run again and the process repeated until 5 M solutions were reached. The quantities of NaCl added for each sample are given below in **Table 4.2**. The same procedure was used for CP-[pEASTEA$_{25}$]$_2$ (9.60 mg, 0.556 μmol) in 1.1184 g (9.9 mg· mL^{-1}) of D_2O.

Table 4.2: Quantities of NaCl added to give the desired ionic strength

Sample	mL	0.18 M (mg)	1 M (mg)	2 M (mg)	3 M (mg)	4 M (mg)	5 M (mg)
CP-[pTMAEA$_{25}$]$_2$	0.45	4.7	21.61	26.52	26.2	26.18	26.58
CP-[pEASTEA$_{25}$]$_2$	0.45	4.7	21.76	26.13	26.23	26.38	26.74

4.4.8 SANS Analysis

SANS data were analysed in the NIST NCNR analysis macro using Igor pro 6.36,[14] in a similar manner as described in Chapter 3. Data was analysed by a series of form factors, including sphere, Gaussian coil, cylinder, core-shell cylinder, flexible cylinder, and polyelectrolyte until the fit χ^2 values were minimised. The fit parameters are outlined in the Appendix to this chapter.

4.4.9 Debye Length

The Debye length was calculated at each ionic strength (**Table 4.3**) using the following equation:[25]

$$k^{-1} = \frac{0.304}{\sqrt{I}} \qquad (1)$$

where I is the ionic strength of the solution in mol· L^{-1}.

Table 4.3: Calculated values of the Debye length in nm and in Å.

NaCl Conc. (M)	Debye Length (nm)	Debye Length (Å)
0.18	0.72	7.2
1	0.30	3.0
2	0.21	2.1
3	0.18	1.8
4	0.15	1.5
5	0.14	1.4

4.5 References

1. Chapman, R.; Koh, M. L.; Warr, G. G.; Jolliffe, K. A.; Perrier, S. *Chemical Science* **2013,** 4, (6), 2581-2589.

2. Koh, M. L.; FitzGerald, P. A.; Warr, G. G.; Jolliffe, K. A.; Perrier, S. *Chemistry – A European Journal* **2016,** 22, (51), 18419-18428.

3. Danial, M.; My-Nhi Tran, C.; Young, P. G.; Perrier, S.; Jolliffe, K. A. *Nature Communications* **2013,** 4, 2780.

4. Catrouillet, S.; Brendel, J. C.; Larnaudie, S.; Barlow, T.; Jolliffe, K. A.; Perrier, S. *ACS Macro Letters* **2016,** 5, (10), 1119-1123.

5. Chapman, R.; Warr, G. G.; Perrier, S.; Jolliffe, K. A. *Chemistry-a European Journal* **2013,** 19, (6), 1955-1961.

6. Chapman, R.; Bouten, P. J. M.; Hoogenboom, R.; Jolliffe, K. A.; Perrier, S. *Chemical Communications* **2013,** 49, (58), 6522-6524.

7. Danial, M.; Tran, C. M. N.; Jolliffe, K. A.; Perrier, S. *Journal of the American Chemical Society* **2014,** 136, (22), 8018-26.

8. Vallat, P.; Catala, J. M.; Rawiso, M.; Schosseler, F. *Macromolecules* **2007,** 40, (10), 3779-3783.

9. Strecker, A. *Justus Liebigs Annalen der Chemie* **1868,** 148, (1), 77-90.

10. Brendel, J. C.; Schmidt, M. M.; Hagen, G.; Moos, R.; Thelakkat, M. *Chemistry of Materials* **2014,** 26, (6), 1992-1998.

11. Barlow, T. R.; Brendel, J. C.; Perrier, S. *Macromolecules* **2016,** 49, (17), 6203-6212.

12. Pesek, S. L.; Li, X.; Hammouda, B.; Hong, K.; Verduzco, R. *Macromolecules* **2013,** 46, (17), 6998-7005.

13. Pesek, S. L.; Xiang, Q.; Hammouda, B.; Verduzco, R. *Journal of Polymer Science Part B: Polymer Physics* **2017,** 55, (1), 104-111.

14. Kline, S. *Journal of Applied Crystallography* **2006,** 39, (6), 895-900.

15. Ermi, B. D.; Amis, E. J. *Macromolecules* **1998,** 31, (21), 7378-7384.

16. Horkay, F.; Basser, P. J.; Hecht, A.-M.; Geissler, E. *Macromolecules* **2012,** 45, (6), 2882-2890.

17. Lopez, C. G.; Rogers, S. E.; Colby, R. H.; Graham, P.; Cabral, J. T. *Journal of Polymer Science Part B: Polymer Physics* **2015,** 53, (7), 492-501.

18. Borsali, R.; Nguyen, H.; Pecora, R. *Macromolecules* **1998,** 31, (5), 1548-1555.

19. Ermi, B. D.; Amis, E. J. *Macromolecules* **1997,** 30, (22), 6937-6942.

20. Wang, D.; Lal, J.; Moses, D.; Bazan, G. C.; Heeger, A. J. *Chemical Physics Letters* **2001,** 348, (5–6), 411-415.

21. Dobrynin, A. V.; Rubinstein, M. *Progress in Polymer Science* **2005,** 30, (11), 1049-1118.

22. Schärtl, W., Light scattering from polymer solutions and nanoparticle dispersions. In *Light scattering from polymer solutions and nanoparticle dispersions*, Springer-Verlag Berlin Heidelberg: 2007.

23. Chapman, R.; Danial, M.; Koh, M. L.; Jolliffe, K. A.; Perrier, S. *Chemical Society reviews* **2012,** 41, (18), 6023-41.

24. Engels, M.; Bashford, D.; Ghadiri, M. R. *Journal of the American Chemical Society* **1995,** 117, (36).

25. Israelachvili, J. N., Chapter 14 - Electrostatic Forces between Surfaces in Liquids. In *Intermolecular and Surface Forces (Third Edition)*, Academic Press: San Diego, 2011; pp 291-340.

26. Lee, H. *Physical Chemistry Chemical Physics* **2016,** 18, (9), 6691-6700.

27. Larnaudie, S. C.; Brendel, J. C.; Jolliffe, K. A.; Perrier, S. *Journal of Polymer Science Part A: Polymer Chemistry* **2016,** 54, (7), 1003-1011.

5

Effect of Self-Assembly versus Charge on the Cellular Uptake of Cyclic Peptide-Polymer Nanotubes

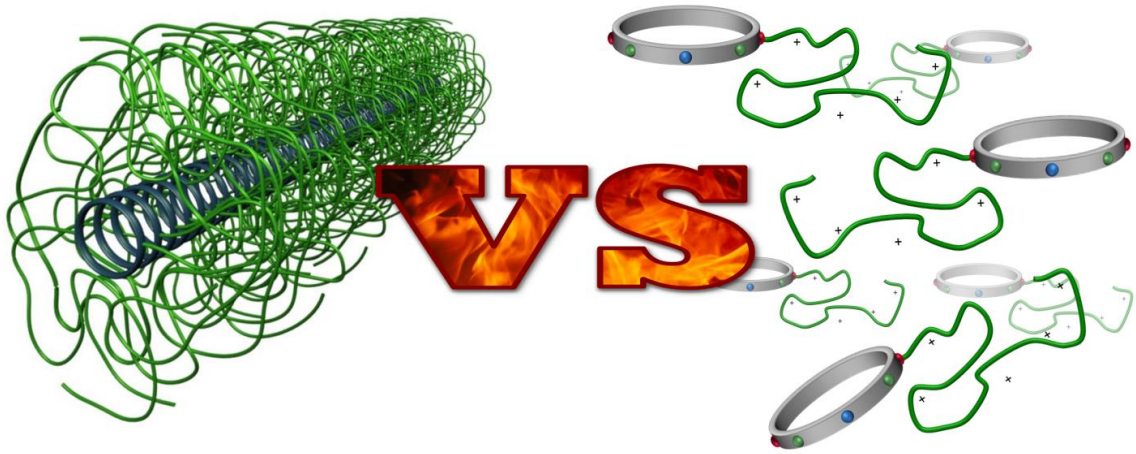

Self-assembling polymeric materials represent an exciting field in nanomedicine, especially in the field of drug delivery where they are frequently used as vectors to enhance the cellular uptake of cargo molecules. Introduction of charge has long been championed as a simple way to improve cellular uptake. However, the benefit of these charges is often incompatible with self-assembly due to the electrostatic repulsion

between individual monomer units. To better understand the importance of these two parameters, a comparison on the effect of self-assembly of cyclic-peptide polymer conjugates on cellular uptake *vs.* the effect of molecular surface charge is undertaken. Using RAFT polymerisation, the extent to which charge is introduced into each compound is carefully controlled, generating a library of statistical copolymers comprising PEGA and BEA. Using post-modification strategies, ammonium or phosphonium moieties were introduced. The introduction of charge resulted in diminished self-assembly of the cyclic peptide nanotubes, which significantly reduces cell uptake. Using these compounds, self-assembly was determined to be a greater driving force for cell-uptake than the degree of molecular surface charge. Finally, the mixing of charged and uncharged unimers demonstrates that in the case of ammonium conjugates, nanotube assembly is actively diminished by their co-assembly.

5.1 Introduction

Due to their large size and ability to carry payloads, macromolecules are well known to facilitate the transport of cargos across biological barriers and have been widely employed as cell uptake enhancers.[1] Various physical properties, including size,[2-4] charge,[5-8] hydrophilicity,[9] monomer distribution,[6, 10, 11] self-assembly properties,[12] degree of cross-linking[13] or branching[14], have all been shown to impact cellular uptake. Among them, self-assembling cyclic-peptides (CP) polymer conjugates have been shown to be particularly promising drug delivery candidates both *in vitro*[15] and *in vivo*.[16] The self-assembly of these CPs is robust to the attachment of various macromolecules including polymers[17-19] and drugs,[15] which in turn allow tuning of the physical properties (length, solubility) of the resulting conjugates. These conjugates provide a number of advantages over other nanovectors; the anisotropy of nanotubes improves circulation time,[20-22] while their supramolecular nature facilitates excretion without toxic build-up in the body as in the case of carbon nanotubes.[23] The β sheet-like self-assembly of these materials plays a key role in interaction with membranes,[24-28] which can improve cell-uptake of these materials. Despite this, the influence of physical properties on cell uptake for these systems remains largely unexplored.

Of particular interest is the introduction of positively charged residues, which are well-known to facilitate the cell uptake of macromolecules. While the presence of charged residues is expected to have a profound effect on the interaction of these conjugates with the cell membrane,[6, 29-31] it should also affect the self-assembly of these structures. While charge and self-assembly have frequently been combined in polymeric materials,[32-35] the importance of these two parameters, and in particular which is more efficient at enhancing cell uptake, remains unclear.

Herein, a charged moiety was introduced into a model self-assembling cyclic peptide-polymer conjugate, and their cell uptake assessed. Described here is a method that facilitates the incorporation of various quantities of charged residues using a post-modification strategy. We observe that for these systems, self-assembly is a greater force for improving cellular uptake than surface charge.

5.2 Results and Discussion

5.2.1 Conjugate design

Unlike previous chapters, the conjugates were designed here to comprise an asymmetrical cyclic octapeptide core with a single polymer arm conjugated at the side chain of a single Lysine residue. The polymer arm promotes solubility of the self-assembled nanotube by limiting lateral aggregation and adding some measure of control over the length of the tube by steric repulsion.[19, 36] The cyclic-peptide (CP) core comprises alternating L- and D- α-amino acids (sequence: *cyclo*-L-Lys-D-Leu-L-Trp-D-Leu-L-Trp-D-Leu-L-Trp-D-Leu-), that forms the flat, rigid ring-like conformation necessary for hydrogen bonding directed self-assembly.[37, 38]

CP-polymer conjugates comprising a poly(ethylene glycol) methyl ether acrylate (PEGA) copolymer arm with varying proportions of charge were used for this study. PEGylation is an attractive means for the preparation of polymer conjugates as it diminishes proteolytic degradation and increases bioavailability of compounds.[39-41] Conjugates of pPEGA offer additional benefits *in vivo*, with the PEG brush further diminishing enzymatic degradation and immunogenicity.[39, 41] A pPEGA arm was chosen due to its

additional synthetic flexibility over PEG;[40, 42] since it allows for further tailoring of the polymer chains to a desired sequence by using controlled radical polymerisation techniques such as RAFT polymerisation.[43-45] By this means, PEGA can be copolymerised with bromoethyl acrylate (BEA), a reactive monomer by which a range of functionalities can be included by nucleophilic substitution as discussed in previous chapters. Using this method, charged moieties can conveniently be introduced, in varying percentages, as the final step in the synthesis (Chapter 2 and 3).[46] Since macromolecules with high levels of charge typically result in highly toxic materials,[47] this approach enables the design of a library of compounds with a variation in charges, so as to improve cell uptake, without being cytotoxic. Two different cationic residues were tested; ammonium and phosphonium. On one hand, ammonium is commonly used to introduce charge due to the low cost, and straight forward syntheses of amines and amine salts. On the other hand, phosphonium analogues of these compounds are often found to have interesting cell-uptake behaviours, displaying less cytotoxicity and improved transfection efficiency.[48-51] The potential of phosphonium based polymeric materials is yet to be realised, likely due to the increased cost, toxicity and pyrophoric nature of organo phosphine reagents necessary for their production.[49, 50]

5.2.2 Synthetic strategy

Conjugates were prepared using a convergent approach in which BEA containing polymers are first prepared *via* RAFT polymerisation, then conjugated to the CP core *via* amide bond formation, as described in Chapters 2 and 3 respectively. pPEGA copolymers with DPs between 22 - 29 were successfully synthesised with conversions of 77 - 89 % and dispersities ≤ 1.13 ($p(PEGA\text{-}stat\text{-}pBEA)_{22}$: M_n = 10600 g·mol-1, M_w = 11900 g·mol-1, $Đ$ = 1.13; $p(PEGA\text{-}stat\text{-}pBEA)_{26}$: M_n = 9900 g·mol-1, M_w = 11100 g·mol-1, $Đ$ = 1.13; $p(PEGA\text{-}stat\text{-}pBEA)_{28}$: M_n = 9100 g·mol-1, M_w = 10100 g·mol-1, $Đ$ = 1.10.

Table 5.1, **Figure 5.5**). Monomer conversion was quantified by ^{1}H NMR spectroscopy, with SEC traces showing that all statistical copolymers are of comparable DP and $M_{n,SEC}$ values. Copolymers were designed to incorporate BEA at 2 %, 5 %, 10 % and 25 %, with BEA incorporation assessed by ^{1}H NMR from the shift in protons adjacent to the pendant bromine. An uncharged control polymer was also synthesised by incorporating a neutral moiety to "cap" the bromines instead. The control polymer, P1, was synthesised using the 2% statistical p(PEGA-*stat*-pBEA)$_{29}$.

The cyclic peptide was prepared using solid-phase peptide synthesis (SPPS) and cyclised using previously reported protocols (Chapter 3).[34, 52] The -NH_2 on the lysine side chain was then used as a tether for attachment of the polymer arm by amide bond formation with the polymer -NHS chain end (**Scheme 5.2**). In a previous study using BEA-CP conjugates, it was demonstrated that -NHS coupling to the Lysine residue is faster than the nucleophilic substitution on the BEA pendant bromines, as described in Chapter 3. In accordance with previous work, no trace of this S_N2 side reaction was detected by either ^{1}H NMR or SEC of the conjugates (**Figure 5.5**).

Following conjugation, compounds were tagged with a cystamidefluorescein dye prepared by amidation of carboxyfluorescein with a cystamine.HCl salt (**Scheme 5.3**).[53] A straightforward method for incorporation of a fluorescent tag is *via* substitution of bromine. To this end the cheap and commercially available carboxyfluorescein was altered, introducing a thiol moiety by forming an amide bond with cystamine. The ring opening of the lactone of fluorescein under basic conditions represented a foreseeable issue, as it makes a second carboxylic acid group available in the reaction mixture. However, due to the increased steric hindrance around the second carboxylic acid, activation of this moiety by HCTU would be unfavourable, thus making this potential side reaction unlikely.[54]

Introduction of the charge to the polymer chain was achieved post-conjugation *via* nucleophilic substitution of the bromine residues of BEA in the presence of a base. Substitution of the pBEA units was achieved by slow addition of the dye to the reaction mixture, to avoid the reformation of disulfide bonds under basic conditions. Limiting the

concentration of thiols in the presence of the base thus gave the opportunity for the resulting thiolates to attack the bromine instead. To keep the number of dye units per conjugate to a minimum, 0.25 equivalents of dye were used. Introduction of charge was done at this point *via* nucleophilic substitution of the remaining bromine units using trimethyl amine and trimethyl phosphine to yield the final conjugates containing pending ammonium groups and phosphonium groups, respectively (**Scheme 5.1**).[46] Substitution of the bromine was confirmed by ^{1}H NMR (**Figure 5.7** and **Figure 5.8**). Purification of the conjugates was achieved using centrifugal filtration in a sodium chloride solution at pH = 14 to minimise electrostatic interaction between remaining free dye and conjugates. The high salt concentration helped shield electrostatic interaction, while the high pH increased fluorescein solubility in water by deprotonating the remaining carboxylic acid moieties and opening the lactone ring. Finally, the purity of the polymers and conjugates was confirmed by HPLC using both UV and fluorescence detection (**Figure A5.1 - A5.4**).

The surface charges of both CP-polymer conjugates and control polymers was quantified *via* zeta potential measurements, the results of which are reported in **Table A5.1**. All charged polymers (P2 - P9) and conjugates (CP2 - CP9) displayed a positive trend in zeta potential compared to the neutral conjugate CP1, with the charge increases correlating to the increasing numbers of charged monomers per chain. Uncharged CP1 showed a negative zeta potential, due to the measurement being conducted in deionised water.[55] Next, self-assembly of the compounds was characterised using the absolute molecular weight (M_a) of polymer-conjugates CP1 - CP9 as determined in water by static light scattering (SLS). The results were used to calculate a number of aggregation (N_{agg}) for each conjugate as described in Section 5.4.8, and previous chapters (**Table A5.2**). CP1 was found to have a N_{agg} of approximatively 6, indicative of a short nanotube with a length of 30 Å. In contrast, CP-polymer conjugates containing positive charges were found to be mostly present as unimers in aqueous solutions, showing that introduction of even small percentages of positively charged residues in the unimers dramatically impaired the self-assembly, due to the electrostatic repulsion between the polymeric arms. These data are in agreement with those presented in Chapter 4, where the charged polymer conjugates also did not assemble in water. Measurement of the self-assembly of

these conjugates directly in cell culture media is prevented by interference from large macromolecules in measuring light scattering. Hence, for the cell culture experiments described hereafter, the N_{agg} values obtained in water *via* SLS were taken to be representative of the assembled state of the conjugates in cell media.[10]

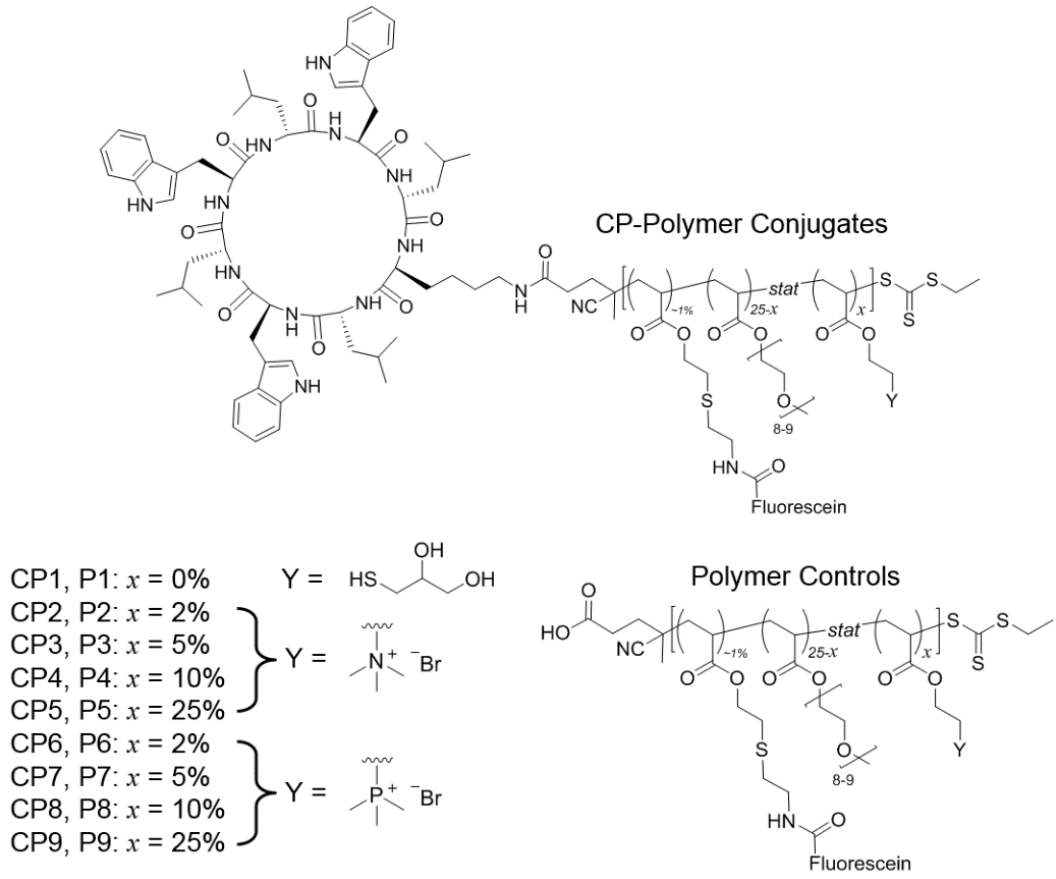

Scheme 5.1: Summary of compounds used in this study and their abbreviations.

Having determined the effect of charge on the self-assembly process, a study of the behaviour of these compounds in the presence of cells was assessed. Positively charged macromolecules, and in particular ammonium-based ones, are notoriously toxic.[47] Hence, acute cell toxicity was assessed first, using human breast adenocarcinoma (MDA-MB-231) cells as a model cell line. The results showed that, following 24 hours of incubation, all compounds were non-toxic at concentrations up to 100 μM (**Figure 5.1**). While this is expected for the uncharged P1 and CP1, the low toxicity of charged P2-9 and CP2-9 is likely due to the presence of pendant brush-like PEG chains whose steric hindrance

minimises electrostatic interactions between the positively charged groups and the negatively charged cell membrane (*vide infra*), shielding the cell from said charge.[56]

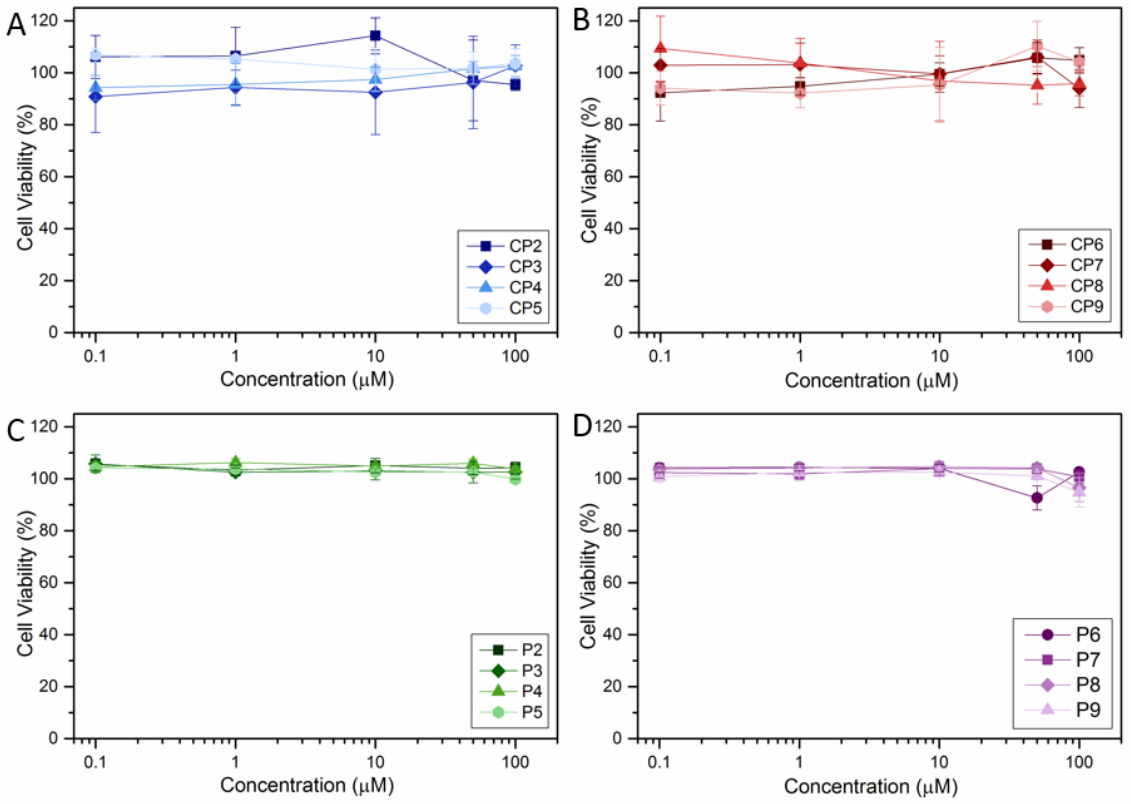

Figure 5.1: Cellular toxicity against MDA-MB-231 cells after 24 h incubation time with varying concentration of compound, as measured using XTT assay.

Next, the influence of charge on the cellular uptake of these compounds was studied. Despite using the same number of cystamide-fluorescein equivalents during the functionalisation reactions, differences in the amount of dye incorporated were observed for each polymer and conjugate. To account for these differences, the fluorescence (λ_{ex} = 488 nm, λ_{em} = 575 nm) of each compound was measured against concentrations in the linear region, and the relative values of the slopes were used to calculate correction factors, as outlined in **Table A5.2**.[57] The intracellular fluorescence of MDA-MB-231 cells incubated with 50 μM of compounds for 20 hours was quantified using flow cytometry. For each experiment, the fluorescence intensity from > 5000 live cells (n = 4) was measured. The median of these data were averaged and corrected by fluorescence

correction factors (**Table A5.2**) to give the values reported in **Figure 5.2**. Incubation of MDA-MB-231 cells with P1-9 and CP1-9 showed a positive uptake for each sample, with CP1 showing significantly higher uptake than all other compounds (**** $p < 0.0001$). Interestingly, the charged conjugates (CP2-9) and polymers (P2-9) were all internalised by the cells in a similar amount to the single PEGA chain control (CP1). In addition, no significant differences were observed between various percentages of positive charge, nor between the compounds containing ammonium or phosphonium residues.

The intracellular fluorescence results correlate with the N_{agg} data obtained *via* SLS, clearly indicating that self-assembly plays a major role on the cell-uptake of CP-polymer conjugates. In previous reports, positive charges have been highlighted as beneficial for the uptake of Lysine- or Arginine-containing macromolecules, where neutrally charged controls showed no significant cellular uptake.[6, 29, 30] While neither the uptake nor cytotoxicity mechanisms of polycations is fully understood, the enhanced uptake observed for these compounds is generally associated with the presence of electrostatic interactions between the positive charges and the negatively charged membrane of cells.[29] In the present case, increasing the amount of charge in polymers P2-9 and conjugates CP2-9 does not result in an increased uptake by the cell, thus indicating that the charged segments in the system are potentially not able to interact with the cell membranes. This phenomenon was attributed to the screening of charge by the pendant PEG chain of the polymer arms. The brush-like structure of these long chains provides steric hindrance that prevents the positive charges from coming into close contact with the cell membrane and thereby enhancing penetration. A similar phenomenon has been previously reported by Knop *et al.* who show that PEG chains form a conformational cloud that shields the charge from the cell-membrane.[39] This hypothesis is in direct accordance with the absence of toxicity observed for these compounds.

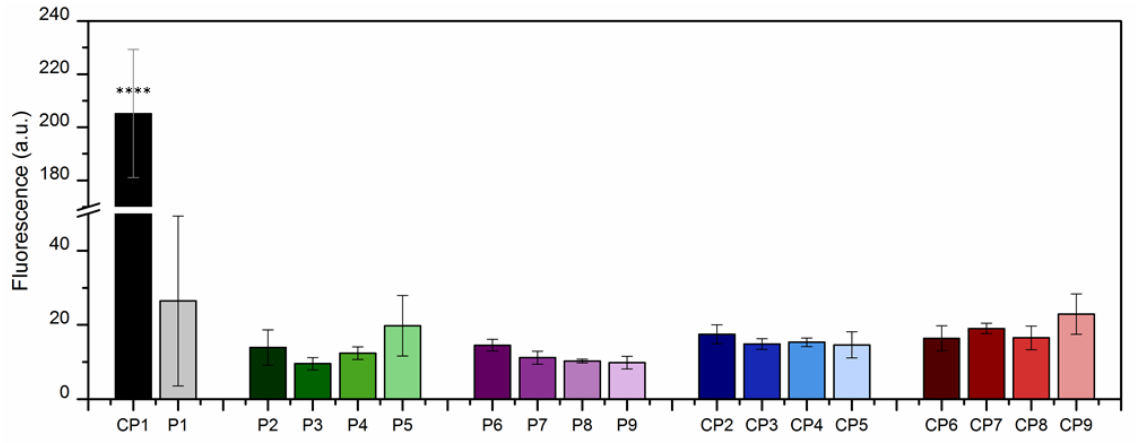

Figure 5.2: Intracellular fluorescence in MDA-MB-231 cells exposed to 50 μg· mL^{-1} of polymers P1-9, and CP-polymer conjugates CP1-9 for 20 hours, as determined using flow cytometry and fluorescence correction factors (n = 4).

Having demonstrated that self-assembly is required for the enhanced uptake of these conjugates, the importance of charge repartition within the conjugates was investigated. This was done by comparing the cellular uptake of CP2-9, for which charges are homogeneously distributed within the polymer arms, with heterogeneous mixture of charged and uncharged conjugates. By combining charged (CP5 or CP9) and non-charged (CP1) conjugates, one of three effects would be observed; co-assembly resulting in improved cellular uptake, co-assembly resulting in diminished cell-uptake, or no co-assembly resulting in simple dilution of fluorescence. Both CP5 and CP9, each containing 25% charged residues, were mixed with neutral CP1 in varying ratios to attain overall values of 10%, 5%, and 2% total charge (assuming co-assembly), which can be readily compared with CP3-5 and CP7-9, containing equivalent percentage of charges which are homogeneously distributed (**Table A5.3**). Theoretical fluorescence values were calculated for the case where no co-assembly took place, taking into account the fluorescence correction factor of CP1 and CP5 and their respective uptake as determined by the previous experiment. These values, reported in **Table A5.3**, were then compared with the values obtained for mixtures of the two compounds incubated with MDA-MB-231 cells for the same amount of time (20 hours).

For the mixtures of CP1 with CP5 (the ammonium derivative) a significant discrepancy between the theoretical and practical values was observed (**Figure 5.3A**). The results indicate that the 43.9 % decrease in fluorescence observed for the 40% CP5:CP1 mixture is not merely a feature of dilution of CP1. Instead, the results suggest that CP5 mixes and co-assembles with CP1, which in turns diminishes the propensity of the mixed system to self-assemble. In contrast, the phosphonium derivative mixture of CP9 and CP1 (**Figure 5.3B**) follows the theoretical values closely, indicating that in this case the decrease in intracellular fluorescence is due to a dilution of CP1. While these results do not allow for a definitive conclusion on the mechanism of co-assembly of charged and uncharged unimers, they indicate there is some difference between conjugates bearing ammoniums and conjugates bearing phosphoniums. In the present case, these discrepancies can be explained by considering the differences in size and electronegativity of nitrogen and phosphorous atoms. Phosphonium has a larger atomic radius and is more electronegative than its ammonium counterpart, thus its association to counter ions in solution is weaker.[58] Such enhanced electronegativity was previously reported in the literature, with phosphonium-based materials showing increased interaction with the negatively-charged membrane over ammonium analogues.[59] Additional electrostatic repulsion between the phosphonium would then lead to fewer phosphonium-bearing unimers inserting within existing nanotubes of uncharged compounds. Assuming than only one or less phosphonium-bearing unimers is able to insert in one uncharged nanotube (N_{agg} = 6), this would explain why self-assembly is seemingly not affected by the presence of phosphonium unimers in solution.

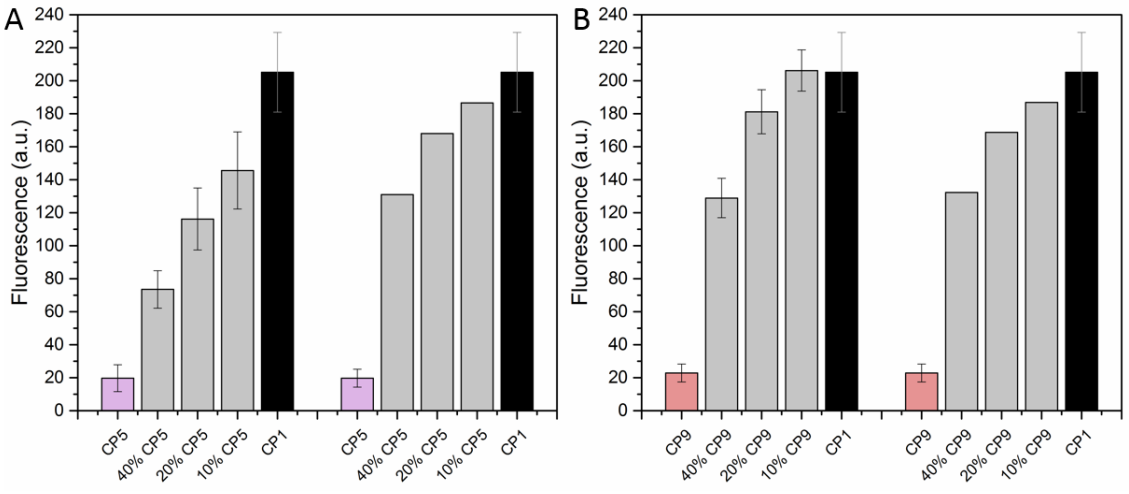

Figure 5.3: Intracellular fluorescence in MDA-MB-231 cells exposed to 50 μM of conjugates with various amount of charge, introduced from heterogeneous mixing of neutral CP1 with (A) ammonium derivative CP5 and (B) phosphonium derivative CP9.

5.3 Conclusion

Herein the effect of self-assembly *vs.* the molecular surface charge was compared for a library of CP-polymer conjugates on cellular uptake. RAFT polymerisation was used as an effective method by which a library of pPEGA-*stat*-pBEA copolymers were generated for direct conjugation to a self-assembling cyclic peptide core, in the absence of side reaction. The charged conjugates created from these precursor polymers, incorporating either an ammonium and phosphonium group, displayed unexpected results *in vitro*. Increasing quantities of charge did not result in additional cellular uptake, as the bulk of literature would suggest. Instead, self-assembly was found to be a far more effective property for improved cell penetration for polymeric nanotubes. In addition to this, the negative effect of charge on self-assembly was found in mixtures of assembling and unimeric conjugates and that ammonium and phosphonium analogues co-assembled differently. Charged ammonium conjugates, when mixed with assembling conjugates, resulted in less cellular uptake due to the co-assembly of the charged conjugates. In the case of phosphonium analogues however, no co-assembly was apparent. This indicates that despite structural similarities, the species of charges results in remarkably different self-assembly and therefore cell-uptake behaviours. The self-assembly properties of this

system, and the improved cell uptake it imparts, makes these materials an exciting potential material for drug delivery. With these encouraging results, further study should be undertaken in a less sterically hindered system to confirm these results.

5.4 Experimental

5.4.1 Materials

Triethylamine, dioxane and DMSO were purchased from Fisher Scientific. 4,4-Azobis(4-cyanovaleric acid) (ACVA) was purchased from MP Biomedicals. All other compounds were purchased from Sigma-Aldrich. All chemicals were used as received except PEGA monomer which was run through basic alumina to remove the inhibitor. All solvents were bought from commercial sources and used as received. Amicon Ultra-15 10K MWCO centrifugal filtration units were used as received for purification.

5.4.2 Methods & Instruments

^{1}H NMR spectra were recorded on a Bruker AV-300, HD-300 or AV-400 in $CDCl_3$, D_2O or DMSO-d_6. Shift values (δ) are reported in ppm. The residual proton signal of the solvent was used as an internal standard ($CDCl_3$ δ_H 7.26, D_2O δ_H 4.79, DMSO-d_6 δ_H 2.50). Size exclusion chromatography (SEC) was carried out on a Polymer Laboratories PL-GPC 50 Plus. DMF (0.1% LiBr) was used as eluent at 1.0 mL min^{-1} at 50 °C. Commercial narrow linear poly(methyl methacrylate) standards in range of 2.0 × 10^2 g mol^{-1} to 1.0 × 10^6 g mol^{-1} were used to calibrate the DMF SEC system. Analyte samples were filtered through polytetrafluoroethylene (PTFE) membrane with either 0.2 μm or 0.45 μm pore size before injection (100 μL). Analytical high performance liquid chromatography (HPLC) was performed on Agilent 1260 Infinity series stack equipped with an Agilent 1260 binary pump and degasser. 50 μL samples were injected using Agilent 1260 auto sampler with a flow rate of 1 mL· min^{-1}. The HPLC was fitted with an Agilent Eclipse Plus C18 column (100 × 4.6 mm) with 3.5 μm micron packing (95 Å). Detection was achieved using an Agilent 1260 variable wavelength detector monitoring at 220 nm and an Agilent 1260 fluorescence detector λ_{ex} = 490 nm, λ_{em} =525 nm. Mobile phase A consisted of 100 % water containing 0.05 % TFA as an additive. Mobile Phase B

consisted of 100 % methanol containing 0.05 % TFA as an additive. The column was equilibrated by washing with the starting % of mobile phase A for 10 minutes prior to injection for all conditions. The method gradient used for HPLC analysis: 15 % mobile phase B increasing to 100 % mobile phase B over 23 minutes, and remaining at 100% mobile phase B for 3 minutes, before resetting to the starting conditions in 1 minute and remaining in these conditions for 3 minutes to re-equilibrate the column before subsequent injections (30 min total run time). Zeta potential measurements were carried out using a Malvern nanoZS zetasizer instrument (scattering angle of 173°, 10mW He-Ne laser) in Malvern disposable folded capillary cell (DTS1070) cuvettes. Polymer solutions were prepared at ~ 2 mg· mL^{-1} in deionised water. Each sample was run in triplicate at 25 °C using the Malvern Zetasizer software. Centrifugal filtration was carried out using Vivaspin® 20, 3,000 MWCO centrifuge tubes. Experimental $M_{n,SEC}$ and $Đ$ values of synthesised polymers were determined using Agilent GPC software. PTFE 0.2 μm syringe filters were obtained from Fisherbrand for filtration of samples in organic solvents. Pall Gelman GHP Acrodisc 0.2 μm syringe filters were obtained from Sigma-Aldrich for filtration of aqueous samples.

5.4.3 Synthesis of Linear Peptide, Cyclic Peptide and Deprotection

Synthesis of the linear peptide was achieved by SPPS as described in Chapter 3.4.3. The cyclic peptide was generated by high dilution end-to-end amide bond formation as described in Chapter 3.4.4. Boc deprotection of the cyclic peptide was achieved as per the protocol in Chapter 3.4.5.

5.4.4 Copolymerisation of PEGA and BEA

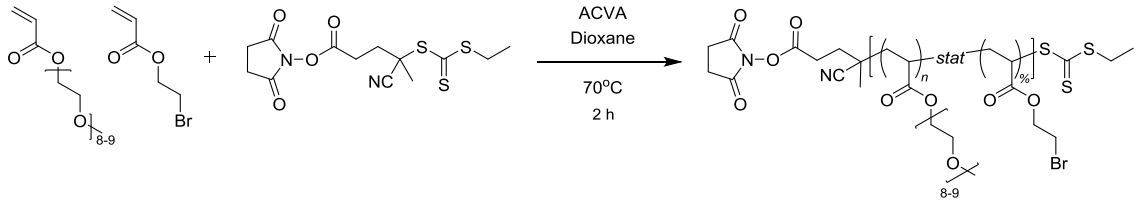

Polymerisation of PEGA was achieved using a protocol adapted from a previously reported procedure:[52] In a small vial with a magnetic stirrer; NHS-CPAETC (22.2 mg, 0.0616 mmol), PEGA (0.720 g, 1.50 mmol), BEA (91 mg, 0.508 mmol), ACVA (1.73 mg, 6.18 μmol), 1,3,5-trioxane (11 mg) as an internal standard and dioxane (1.25 mL) were combined and the vial sealed with a rubber septum. The vial and solution were deoxygenated by a stream of bubbled nitrogen for 10 min, then put in an oil bath that was pre-heated to 70 °C and allowed to stir until the desired conversion was reached. Conversion of monomer to polymer was followed by taking kinetic samples with a degassed syringe and analysed by ^{1}H NMR. Upon completion, the polymer was rapidly cooled to room temperature, opened to air and precipitated twice in hexane/diethyl ether (1:1, 50 mL). ^{1}H-NMR (300 MHz, 293K, $CDCl_3$, ppm): δ = 4.36 ($OC\underline{H}_2CH_2$, BEA), 4.15 ($C\underline{H}_2OCO$, PEGA), 3.76-3.35 ($C\underline{H}_2C\underline{H}_2O$, PEGA; $CH_2C\underline{H}_2Br$, BEA), 3.38 ($OC\underline{H}_3$, PEGA), 2.86 ($C\underline{H}_2$ -NHS end group), 2.32-1.43 ($CHC\underline{H}_2$, PEGA; $C\underline{H}C\underline{H}_2$, Backbone), 1.21 (-$C\underline{H}_3$, end group). See **Figure 5.4** for ^{1}H-NMR in $CDCl_3$. See **Figure 5.5** a typical SEC in DMF (0.1 % LiBr): p(PEGA-*stat*-pBEA)$_{29}$: M_n = 11000 g·mol^{-1}, M_w = 12400 g·mol^{-1}, $Đ$ = 1.13; p(PEGA-*stat*-pBEA)$_{22}$: M_n = 10600 g·mol^{-1}, M_w = 11900 g·mol^{-1}, $Đ$ = 1.13; p(PEGA-*stat*-pBEA)$_{26}$: M_n = 9900 g·mol^{-1}, M_w = 11100 g·mol^{-1}, $Đ$ = 1.13; p(PEGA-*stat*-pBEA)$_{28}$: M_n = 9100 g·mol^{-1}, M_w = 10100 g·mol^{-1}, $Đ$ = 1.10.

Table 5.1: Details of NHS-p(PEGA-*stat*-BEA) polymers synthesised.

Polymer	% BEA	DP	$\frac{[M]_0}{[CTA]_0}$	$\frac{[CTA]_0}{[I]_0}$	Conv. χ [a] (%)	$M_{n,th}$ [b] (g· mol^{-1})	$M_{n,SEC}$ [c] (g· mol^{-1})	$Đ$
p(PEGA-*stat*-pBEA)$_{29}$	2%	29	32	10	89	14300	11000	1.13
p(PEGA-*stat*-pBEA)$_{22}$	5%	22	32	10	77	12300	10600	1.13
p(PEGA-*stat*-pBEA)$_{26}$	10%	26	32	10	89	12900	9900	1.13
p(PEGA-*stat*-pBEA)$_{28}$	25%	28	32	10	85	9400	9100	1.10

[a] *Conversion determined by ^{1}H-NMR*

[b] *Theoretical number-average molecular weight*

[c] *DMF SEC, DRI detector, PMMA standards, number-average molecular weight*

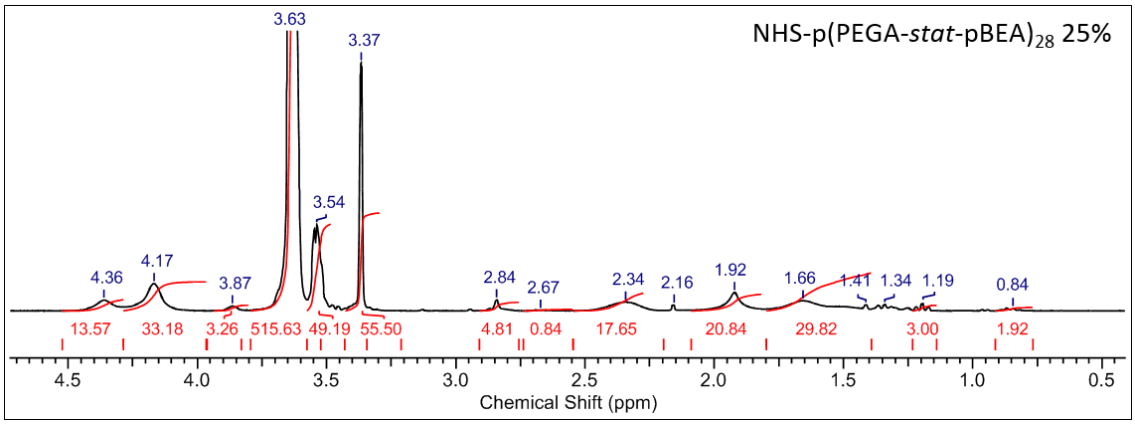

Figure 5.4: ^{1}H NMR of NHS-p(PEGA$_{75\%}$-*stat*-BEA$_{25\%}$)$_{28}$ in $CDCl_3$.

5.4.5 Conjugation of Polymer to Cyclic Peptide

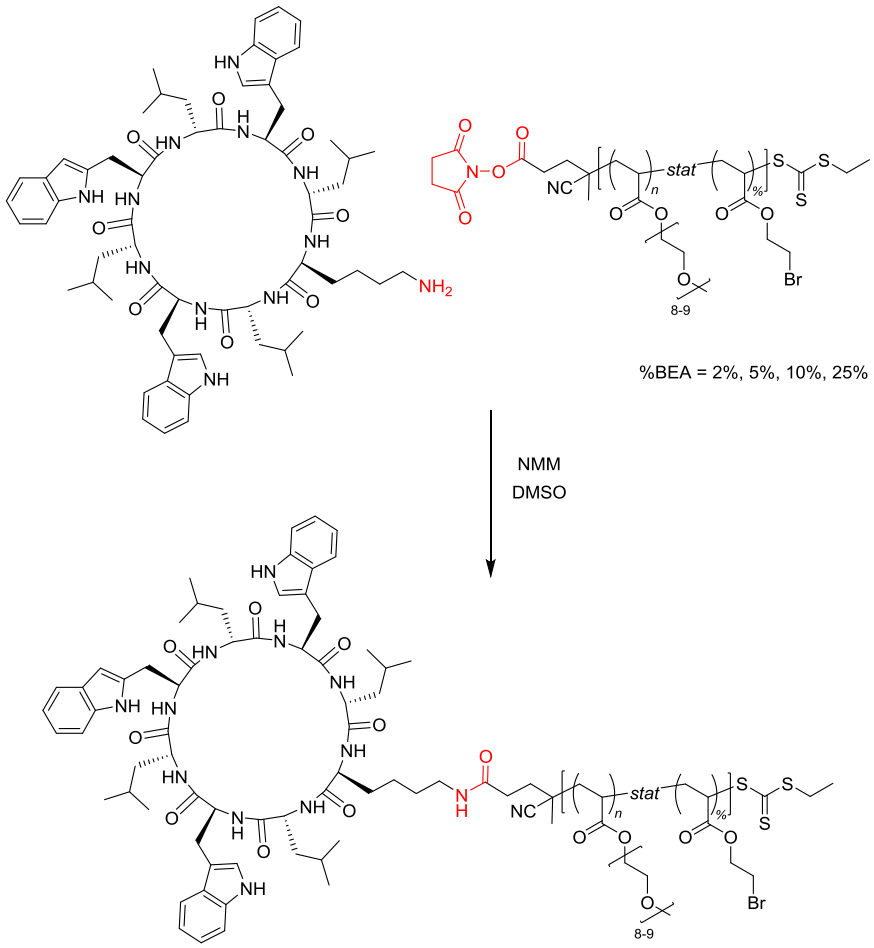

Scheme 5.2: Conjugation of NHS-p(PEGA-*stat*-pBEA)$_n$ copolymers to cyclic D-, L- α-octapeptide.

Conjugation of NHS-p(PEGA-*stat*-pBEA)$_n$ to 1-arm cyclic peptide was achieved as described in Chapter 3.4.8. See **Figure 5.5** a typical SEC in DMF (0.1 % LiBr): CP-p(PEGA-*stat*-pBEA)$_{29}$: M_n = 9500 g·mol^{-1}, M_w = 11400 g·mol^{-1}, $Đ$ = 1.20; CP-p(PEGA-*stat*-pBEA)$_{22}$: M_n = 11700 g·mol^{-1}, M_w = 14000 g·mol^{-1}, $Đ$ = 1.19; CP-p(PEGA-*stat*-pBEA)$_{26}$: M_n = 10900 g·mol^{-1}, M_w = 12800 g·mol^{-1}, $Đ$ = 1.18; CP-p(PEGA-*stat*-pBEA)$_{28}$: M_n = 100100 g·mol^{-1}, M_w = 1500 g·mol^{-1}, $Đ$ = 114.

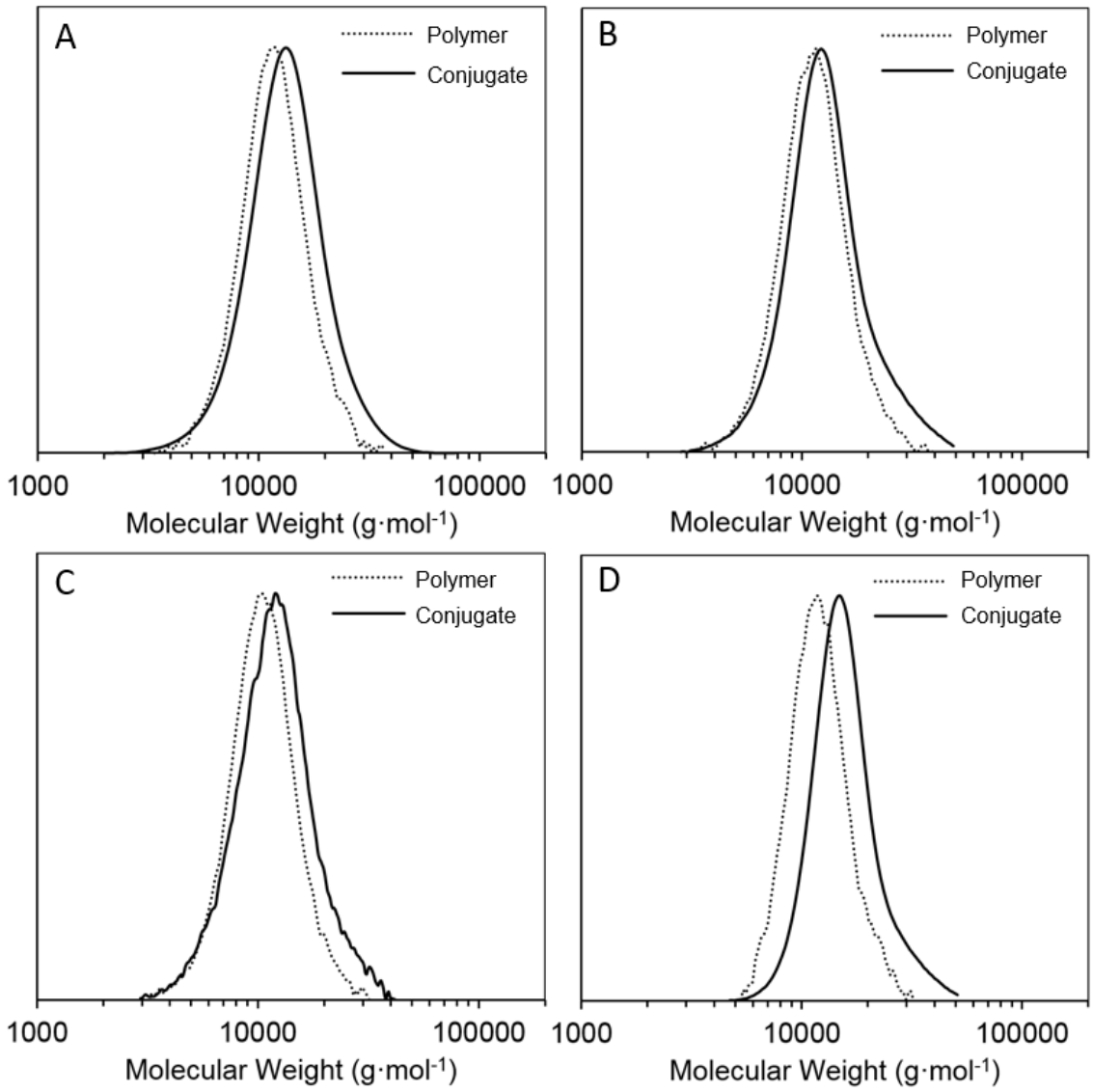

Figure 5.5: SEC analyses of NHS-p(PEGA-*stat*-pBEA)$_n$ polymers (dotted line) and following conjugation to the cyclic peptide (solid line) for (A) 2% BEA, (B) 5% BEA, (C) 10% BEA and (D) 25% BEA.

5.4.6 Synthesis of 3',6'-Dihydroxy-N-(2-mercaptoethyl)-3-oxo-3H-spiro[isobenzofuran-1,9'- xanthene]-4-carboxamide (Cystamidefluorescein)

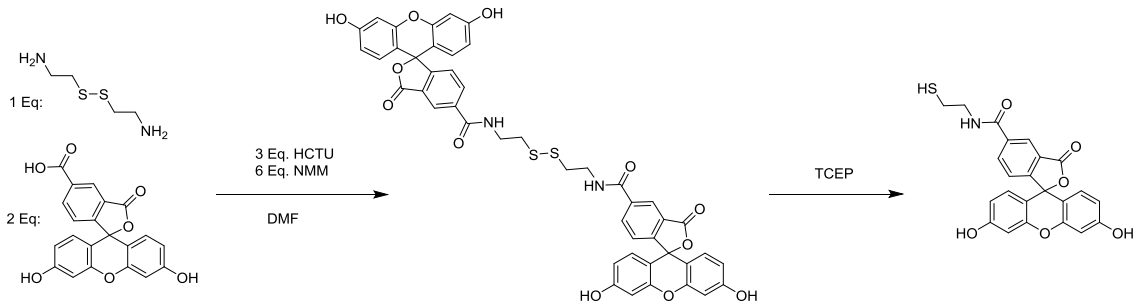

Scheme 5.3: Synthesis of cystamidefluorescein from cystamine.HCl and 5(6)-carboxyfluorescein *via* HCTU mediated amide bond formation. The disulfide intermediate product was treated with TCEP to give the desired free thiol cystamidefluorescein.

Cystamide fluorescein was prepared in a similar method to Buhl *et al*.[53] Cystamine.HCl (12.0 mg, 0.0534 mmol), 5(6)-Carboxyfluorescein (40.6 mg, 0.108 mmol), and HCTU (71.1 mg, 0.172 mmol) were suspended in DMF (1 mL) in a small vial with stirring and deoxygenated with a stream of N_2. While still under N_2 stream, NMM (80.3 μL, 73.9 mg, 0.730 mmol) was added to the reaction mixture and the solution was stirred at room temperature for a further 24 h. The reaction mixture was precipitated in water and purified by preparatory HPLC (t_R (min) = 23.3, 25.66, 26.98); ^{1}H-NMR (400 MHz, 293 K, DMSO-d_6, ppm): δ = 10.26 (2H, *br s*, -OH), 9.03 - 8.88 (1H, *d* of *m*, ArH), 8.44 (H, *d*, ArH), 8.25 - 8.05 (H, *m*, ArH), 7.87 (H, *m*, ArH), 7.68 - 7.61 (H, *m*, ArH), 7.38 - 7.27 (H, *m*, ArH); ESI-ToF (MeOH): $[M+H]^+$ calculated: 436.077; found: 436.1. See **Figure 5.6** for HPLC (t_R (min) = 23.3, 25.66, 26.98).

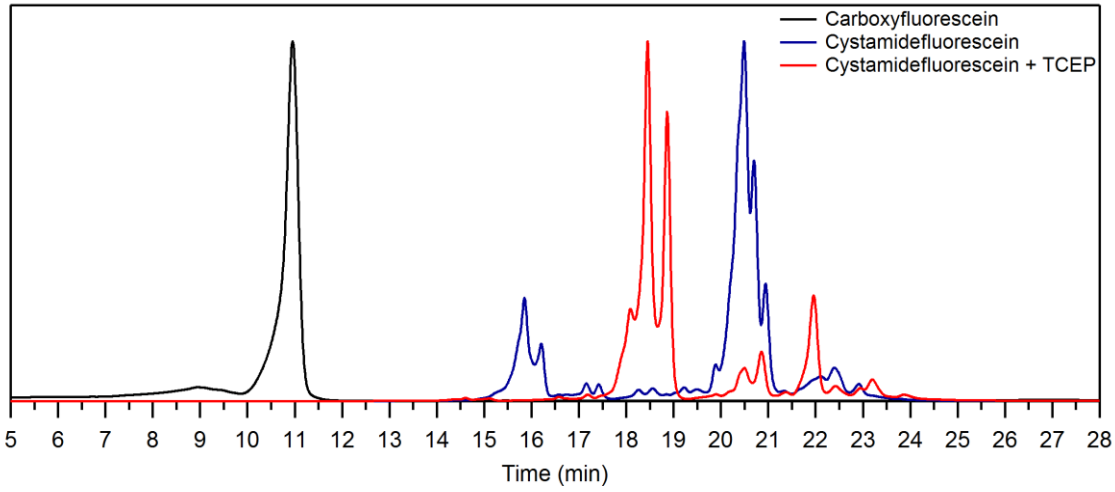

Figure 5.6: Overlay of HPLC traces for 5(6)-carboxyfluorescein starting material (black line), cystamidefluorescein product in the disulfide form (blue line) and desired free-thiol cystamidefluorescein product following addition of TCEP (red line). The trio of peaks in the cystamidefluorescein traces are due to isomerisation of the dye.

5.4.7 Post-modification of Polymers and Conjugates

5.4.7.1 Substitution with Cystamidefluorescein

Typical reaction of cystamidefluorescein with p(PEGA-*stat*-pBEA) polymer or conjugate: CP-p(PEGA-*stat*-BEA)$_n$ (0.090 g, 9.62 μmol) and DIPEA (1 μL, 0.742 mg, 4.59 μmol) were suspended in DMF (0.5 mL) in a small vial with stirrer bar. Separately fluorescein-SH (1 mg, 2.30 μmol) was suspended in DMF (0.5 mL) and added dropwise to the polymer solution over one hour. After 24 h the solution was halved without purification and directly substituted with trimethyl amine or trimethyl phosphine.

5.4.7.1.1 Substitution with Trimethyl amine

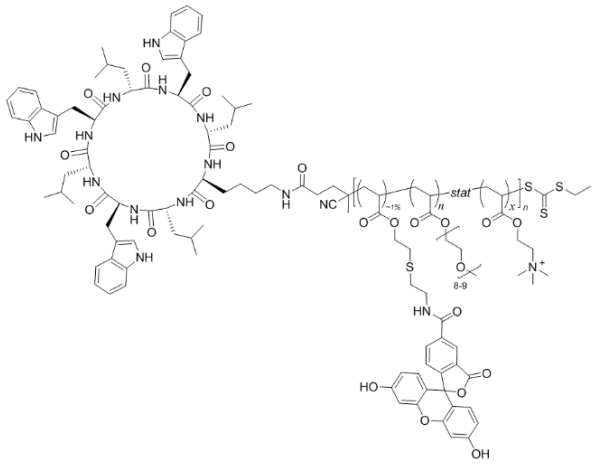

The reaction of trimethyl amine with p(PEGA-*stat*-pBEA)$_n$ polymer or conjugate without dye was conducted as per Chapter 4.

CP-[p(PEGA-*stat*-BEA)$_n$] (20 mg, 2.13 μmol) was suspended in 1 mL of DMSO in a small vial with stirrer bar, to which was added 2 equiv. of trimethyl amine per bromine (4.2 M in ethanol, 50 μL, 0.21 mmol) and stirred for 24 h. Upon completion, the conjugate was precipitated in a hexane:ether mixture (~4:1) to give the desired conjugate (CP-[p(PEGA-*stat*-pTMAEA)$_n$]).

Typical reaction of trimethyl amine with dye-substituted p(PEGA-*stat*-pBEA) polymer or conjugate: The reaction mixture from the cystamidefluorescein substitution (0.5 mL) of CP-p(PEGA-*stat*-BEA)$_n$ (0.045 g, 4.79 μmol) and 2 equiv. of trimethyl amine per bromine (4.2 M in ethanol, 35 μL, 0.147 mmol) were added to a small vial and stirred for 24 h under a N_2 atmosphere. Upon completion, the conjugate was purified by centrifugal filtration (10 kDa MWCO) with 1:1 brine/water mixtures at pH = 14 until washes were clear (3 - 5 × 15 mL)), then washed with deionised water (3 × 10 mL) to give the desired conjugate (CP-[p(PEGA-*stat*-pTMAEA)$_n$]). ^{1}H-NMR (400 MHz, 293 K, DMSO-d$_6$, ppm): δ = 8.31-6.92 (*m*, 10H, Trp), 4.41-4.58 (*m*, -CH$_2$- 2*x*H), 4.08 (br *s*, PEG 2*n*H), 3.91 (*m*, -CH$_2$- 2*x*H), 3.50 (br *s*, PEG -CH$_2$- ~16*n*H), 3.34 (br *m*, N-CH$_3$ 9*x*H), 2.41-1.61 (4*m*, 3*x*H), 0.85-0.65 (*m*, 24H, Leu), no other peptide peaks were observed. See **Figure 5.7** for ^{1}H NMR in DMSO-d$_6$. Dye conjugation and removal of free dye was confirmed by

HPLC: See **Figure A5.1** and **Figure A5.3** for CP2-5 and P2-5 respectively. CP2: t_R = 22.57 min; CP3: t_R = 22.53 min; CP4: t_R = 22.23 min; CP5: t_R = 21.53 min; P2: t_R = 21.02 min; P3: t_R = 21.03 min; P4: t_R = 20.24 min; P5: t_R = 17.77 min.

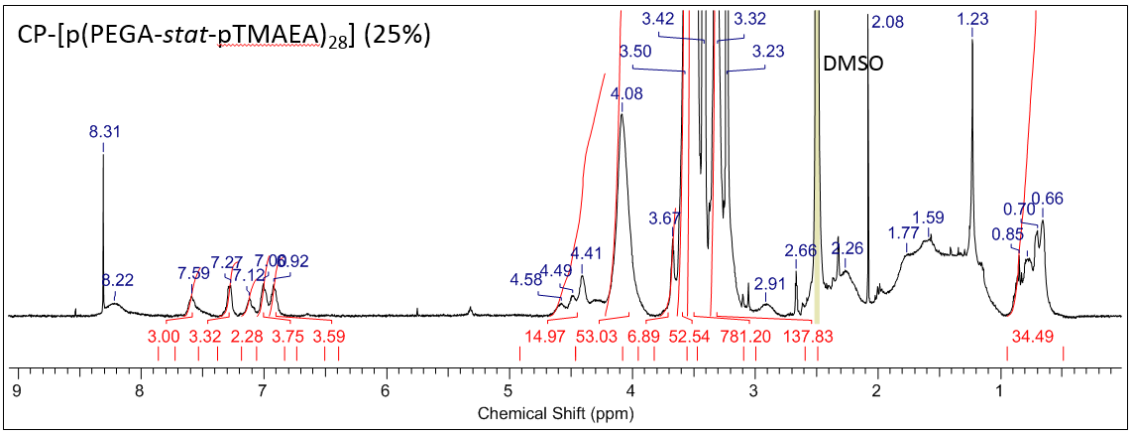

Figure 5.7: ^{1}H NMR of CP-[p(PEGA$_{75\%}$-*stat*-pTMAEA$_{25\%}$)$_{28}$] in DMSO-d$_6$ following substitution with trimethyl amine.

5.4.7.2 Substitution with Trimethyl phosphine

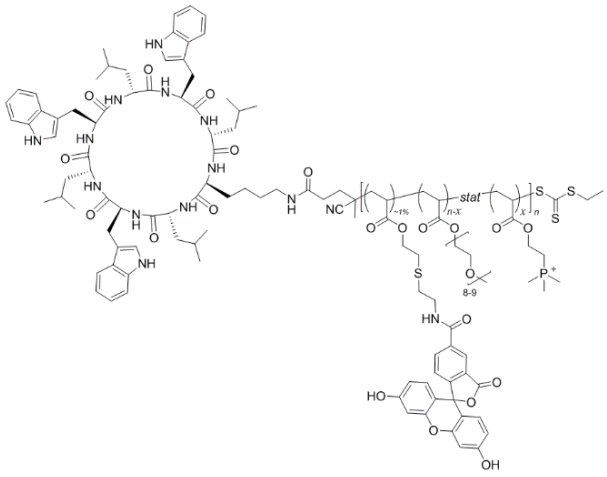

Typical reaction of trimethyl phosphine with p(PEGA-*stat*-pBEA)$_n$ polymer or conjugate: CP-[p(PEGA-*stat*-BEA)$_n$] (0.020 g, 2.13 μmol) was suspended in 250 μL of DMSO in a small vial with stirrer bar, to which was added 2 equiv. of trimethyl phosphine per bromine (1 M in THF, 250 μL, 0.250 mmol) and stirred for 24 h under a N_2 atmosphere.

Upon completion, the conjugate was precipitated in a hexane:ether mixture (~4:1) to give the desired conjugate (CP-[p(PEGA-*stat*-pTMPEA)$_n$]).

Typical reaction of trimethyl phosphine with dye substituted p(PEGA-*stat*-pBEA) polymer or conjugate: The reaction mixture from the cystamidefluorescein substitution (0.5 mL) of CP-[p(PEGA-*stat*-BEA)$_n$] (0.045 g, 4.79 µmol) and 2 equiv. trimethyl phosphine per bromine (1 M in THF, 200 µL, 0.2 mmol) were added to a small vial and stirred for 24 h under a N_2 atmosphere. Upon completion, the conjugate was purified by centrifugal filtration with 1:1 brine/water mixtures at pH = 14 until washes were clear (3 - 5 × 15 mL)), then washed with deionised water (3 × 10 mL) to give the desired conjugate (CP-[pPEGA-*stat*-pTMPEA$_n$]). ^{1}H-NMR (300 MHz, 293 K, DMSO-d$_6$, ppm): δ = 8.31-6.93 (*m*, 10H, Trp), 4.96 (br *s*, 2*x*H), 4.32-4.69 (*m*, -CH$_2$- 2*x*H), 4.09 (br *s*, PEG 2*n*H), 3.76 (*m*, -CH$_2$- 2*x*H), 3.501 (br *s*, PEG -CH$_2$- ~16*n*H), 2.29-1.61 (4*m*, 3*n*H + 9*x*H), 0.87-0.67 (*m*, 24H, Leu), no other peptide peaks were observed. See **Figure 5.8** for ^{1}H NMR in DMSO-d$_6$. Dye conjugation and removal of free dye was confirmed by HPLC: See **Figure A5.1** and **Figure A5.3** for CP6-9 and P6-9 respectively. CP6: t_R = 22.54 min; CP7: t_R = 22.51 min; CP8: t_R = 22.31 min; CP9: t_R = 22.02 min; P6: t_R = 21.30 min; P7: t_R = 21.33 min; P8: t_R = 21.18 min; P9: t_R = 21.07 min.

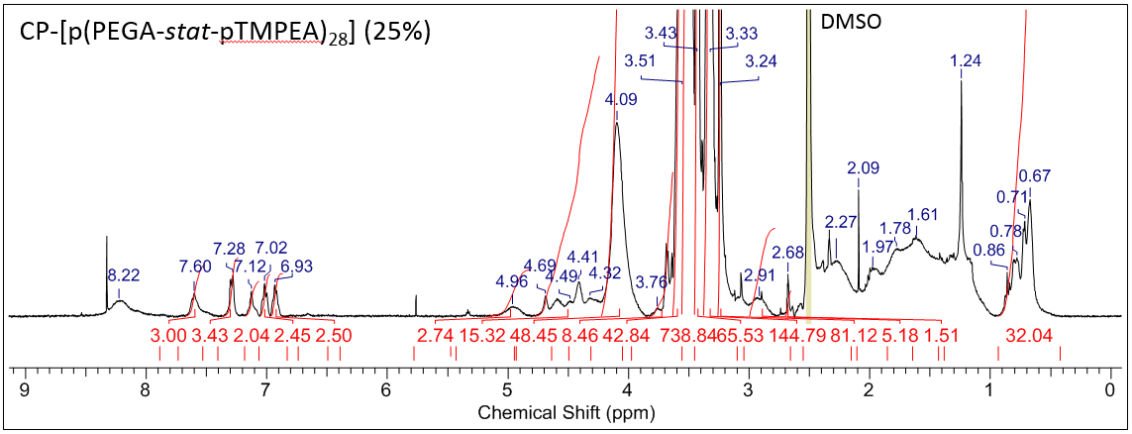

Figure 5.8: ^{1}H NMR of CP-[p(PEGA$_{75\%}$-*stat*-pTMAEA$_{25\%}$)$_{28}$] in DMSO-d$_6$ following substitution with trimethyl phosphine.

5.4.7.3 Substitution with Thioglycerol

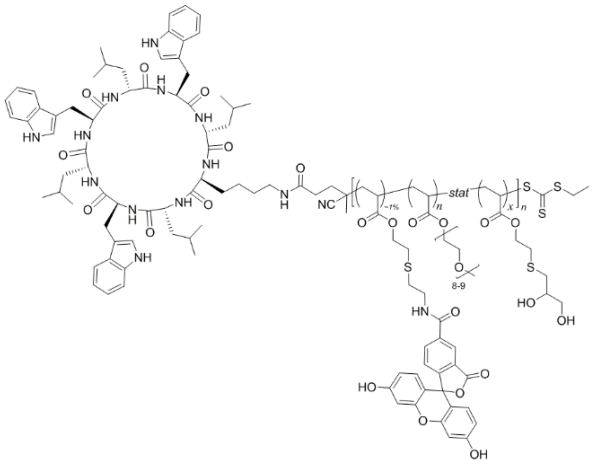

Typical reaction of thioglycerol with dye substituted p(PEGA-*stat*-pBEA)$_{29}$ polymer or conjugate: The reaction mixture from the cystamidefluorescein substitution (0.5 mL in DMSO) of CP-p(PEGA-*stat*-BEA)$_n$ (0.045 g, 4.79 μmol), thioglycerol (65 μL, 0.754 mmol) and DIPEA (131 μL, 0.754 mmol) were added to a small vial and stirred for 24 h under a N_2 atmosphere. Upon completion, the conjugate was purified by centrifugal filtration with 1:1 brine/water mixtures at pH = 14 until washes were clear (3 - 5 × 15 mL), then washed with deionised water (3 × 10 mL) to give the desired conjugate (CP-[p(PEGA-*stat*-p*Gly*EA)$_{29}$], CP1). ^{1}H-NMR (300 MHz, 293 K, DMSO-d$_6$, ppm): δ = 8.23-6.93 (*m*, 10H, Trp), 4.32-4.82 (*m*, -CH$_2$- 2*x*H), 4.10 (br *s*, PEG 2*n*H), 3.69 (*m*, -CH$_2$- 2*x*H), 3.51 (br *s*, PEG -CH$_2$- ~16*n*H), 2.41-1.61 (4*m*, 3*x*H), 0.78-0.66 (*m*, 24H, Leu), no other peptide peaks were observed. See **Figure 5.9** for ^{1}H NMR in DMSO-d$_6$. Dye conjugation was confirmed by HPLC: CP1: t_R = 22.93 min; P1: t_R = 22.12 min.

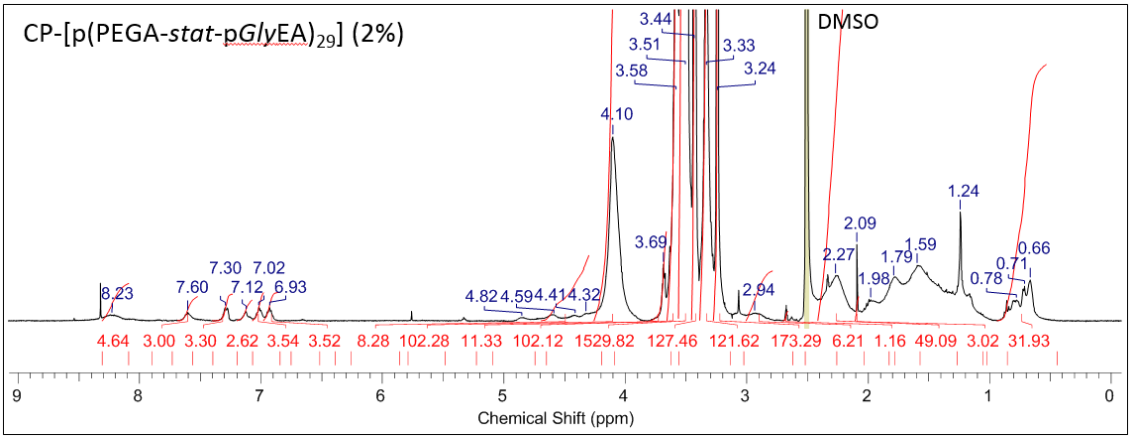

Figure 5.9: ^{1}H NMR of CP-[p(PEGA$_{98\%}$-*stat*-p*Gly*EA$_{2\%}$)$_{29}$] (CP1) in DMSO-d$_6$ following substitution with thioglycerol.

5.4.8 Static Light Scattering

SLS experiments were performed as discussed in Chapter 3.

5.5 References

1. Duncan, R.; Vicent, M. J. *Advanced Drug Delivery Reviews* **2013,** 65, (1), 60-70.

2. Ahmed, M.; Narain, R. *Biomaterials* **2011,** 32, (22), 5279-5290.

3. Synatschke, C. V.; Schallon, A.; Jérôme, V.; Freitag, R.; Müller, A. H. E. *Biomacromolecules* **2011,** 12, (12), 4247-4255.

4. Chen, Y.; Lord, M. S.; Piloni, A.; Stenzel, M. H. *Macromolecules* **2015,** 48, (2), 346-357.

5. He, C.; Hu, Y.; Yin, L.; Tang, C.; Yin, C. *Biomaterials* **2010,** 31, (13), 3657-3666.

6. Koschek, K.; Dathe, M.; Rademann, J. *ChemBioChem* **2013,** 14, (15), 1982-1990.

7. Shao, X.-R.; Wei, X.-Q.; Song, X.; Hao, L.-Y.; Cai, X.-X.; Zhang, Z.-R.; Peng, Q.; Lin, Y.-F. *Cell Proliferation* **2015,** 48, (4), 465-474.

8. Liu, J.; Bauer, H.; Callahan, J.; Kopečková, P.; Pan, H.; Kopeček, J. *Journal of Controlled Release* **2010,** 143, (1), 71-79.

9. Han, S.; Wan, H.; Lin, D.; Guo, S.; Dong, H.; Zhang, J.; Deng, L.; Liu, R.; Tang, H.; Dong, A. *Acta Biomaterialia* **2014,** 10, (2), 670-679.

10. Moraes, J.; Peltier, R.; Gody, G.; Blum, M.; Recalcati, S.; Klok, H.-A.; Perrier, S. *ACS Macro Letters* **2016,** 5, (12), 1416-1420.

11. Obata, M.; Kobori, T.; Hirohara, S.; Tanihara, M. *Polym. Chem.* **2015,** 6, (10), 1793-1804.

12. Mura, S.; Nicolas, J.; Couvreur, P. *Nat Mater* **2013,** 12, (11), 991-1003.

13. Kim, Y.; Pourgholami, M. H.; Morris, D. L.; Stenzel, M. H. *Biomacromolecules* **2012,** 13, (3), 814-825.

14. Perumal, O.; Khandare, J.; Kolhe, P.; Kannan, S.; Lieh-Lai, M.; Kannan, R. M. *Bioconjugate Chemistry* **2009,** 20, (5), 842-846.

15. Blunden , B. M.; Chapman, R.; Danial, M.; Lu, H.; Jolliffe, K. A.; Perrier , S.; Stenzel, M. H. *Chemistry – A European Journal* **2014,** 20, (40), 12745-12749.

16. Larnaudie, S. C. Supramolecular cyclic peptide-polymer nanotubes as drug delivery vectors. University of Warwick, 2017.

17. Couet, J.; Jeyaprakash, J. D.; Samuel, S.; Kopyshev, A.; Santer, S.; Biesalski, M. *Angewandte Chemie-International Edition* **2005,** 44, (21), 3297-3301.

18. ten Cate, M. G. J.; Severin, N.; Borner, H. G. *Macromolecules* **2006,** 39, (23), 7831-7838.

19. Chapman, R.; Koh, M. L.; Warr, G. G.; Jolliffe, K. A.; Perrier, S. *Chemical Science* **2013,** 4, (6), 2581-2589.

20. Albanese, A.; Tang, P. S.; Chan, W. C. W., The Effect of Nanoparticle Size, Shape, and Surface Chemistry on Biological Systems. In *Annual Review of Biomedical Engineering, Vol 14*, Yarmush, M. L., Ed. Annual Reviews: Palo Alto, 2012; Vol. 14, pp 1-16.

21. Mullner, M.; Dodds, S. J.; Nguyen, T. H.; Senyschyn, D.; Porter, C. J. H.; Boyd, B. J.; Caruso, F. *Acs Nano* **2015,** 9, (2), 1294-1304.

22. Li, Y.; Kroger, M.; Liu, W. K. *Nanoscale* **2015,** 7, (40), 16631-16646.

23. Sharifi, S.; Behzadi, S.; Laurent, S.; Laird Forrest, M.; Stroeve, P.; Mahmoudi, M. *Chemical Society Reviews* **2012,** 41, (6), 2323-2343.

24. Ghadiri, M. R.; Granja, J. R.; Buehler, L. K. *Nature* **1994,** 369, (6478), 301-304.

25. Danial, M.; Tran, C. M. N.; Jolliffe, K. A.; Perrier, S. *Journal of the American Chemical Society* **2014,** 136, (22), 8018-26.

26. Danial, M.; Perrier, S.; Jolliffe, K. A. *Organic & Biomolecular Chemistry* **2015,** 13, (8), 2464-73.

27. Rodriguez-Vazquez, N.; Ozores, H. L.; Guerra, A.; Gonzalez-Freire, E.; Fuertes, A.; Panciera, M.; Priegue, J. M.; Outeiral, J.; Montenegro, J.; Garcia-Fandino, R.; Amorin, M.; Granja, J. R. *Current topics in medicinal chemistry* **2014,** 14, (23), 2647-61.

28. Danial, M.; My-Nhi Tran, C.; Young, P. G.; Perrier, S.; Jolliffe, K. A. *Nature Communications* **2013,** 4, 2780.

29. Fei, L.; Ren, L.; Zaro, J. L.; Shen, W.-C. *Journal of Drug Targeting* **2011,** 19, (8), 675-680.

30. Mitchell, D. J.; Steinman, L.; Kim, D. T.; Fathman, C. G.; Rothbard, J. B. *The Journal of Peptide Research* **2000,** 56, (5), 318-325.

31. Matthias, H.; Elizabeth, G. L. W.; Agnès, K.; Sébastien, P.; Katherine, E. S. L. *Current Medicinal Chemistry* **2017,** 24, 1-26.

32. Kataoka, K.; Harada, A.; Nagasaki, Y. *Advanced Drug Delivery Reviews* **2001,** 47, (1), 113-131.

33. Chapman, R.; Warr, G. G.; Perrier, S.; Jolliffe, K. A. *Chemistry-a European Journal* **2013,** 19, (6), 1955-1961.

34. Catrouillet, S.; Brendel, J. C.; Larnaudie, S.; Barlow, T.; Jolliffe, K. A.; Perrier, S. *ACS Macro Letters* **2016,** 5, (10), 1119-1123.

35. She, W.; Luo, K.; Zhang, C.; Wang, G.; Geng, Y.; Li, L.; He, B.; Gu, Z. *Biomaterials* **2013,** 34, (5), 1613-1623.

36. Couet, J.; Biesalski, M. *Small* **2008,** 4, (7), 1008-1016.

37. Ghadiri, M. R.; Granja, J. R.; Milligan, R. A.; McRee, D. E.; Khazanovich, N. *Nature* **1993,** 366, (6453), 324-327.

38. Brea, R. J.; Reiriz, C.; Granja, J. R. *Chemical Society Reviews* **2010,** 39, (5), 1448-1456.

39. Knop, K.; Hoogenboom, R.; Fischer, D.; Schubert, U. S. *Angewandte Chemie International Edition* **2010,** 49, (36), 6288-6308.

40. Bays, E.; Tao, L.; Chang, C.-W.; Maynard, H. D. *Biomacromolecules* **2009,** 10, (7), 1777-1781.

41. Ryan, S. M.; Mantovani, G.; Wang, X.; Haddleton, D. M.; Brayden, D. J. *Expert Opin Drug Deliv* **2008,** 5, (4), 371-83.

42. Chang, C.-W.; Bays, E.; Tao, L.; Alconcel, S. N. S.; Maynard, H. D. *Chemical Communications* **2009**, (24), 3580-3582.

43. Chiefari, J.; Chong, Y. K.; Ercole, F.; Krstina, J.; Jeffery, J.; Le, T. P. T.; Mayadunne, R. T. A.; Meijs, G. F.; Moad, C. L.; Moad, G.; Rizzardo, E.; Thang, S. H. *Macromolecules* **1998,** 31, (16), 5559-5562.

44. Moad, G.; Rizzardo, E.; Thang, S. H. *Aust. J. Chem.* **2012,** 65, (8), 985-1076.

45. Perrier, S.; Takolpuckdee, P. *J. Polym. Sci. Pol. Chem.* **2005,** 43, (22), 5347-5393.

46. Barlow, T. R.; Brendel, J. C.; Perrier, S. *Macromolecules* **2016,** 49, (17), 6203-6212.

47. Fischer, D.; Li, Y.; Ahlemeyer, B.; Krieglstein, J.; Kissel, T. *Biomaterials* **2003,** 24, (7), 1121-1131.

48. Ornelas-Megiatto, C.; Wich, P. R.; Fréchet, J. M. J. *Journal of the American Chemical Society* **2012,** 134, (4), 1902-1905.

49. Loczenski Rose, V.; Shubber, S.; Sajeesh, S.; Spain, S. G.; Puri, S.; Allen, S.; Lee, D.-K.; Winkler, G. S.; Mantovani, G. *Biomacromolecules* **2015,** 16, (11), 3480-3490.

50. Loczenski Rose, V.; Mastrotto, F.; Mantovani, G. *Polym. Chem.* **2017,** 8, (2), 353-360.

51. Hemp, S. T.; Allen, M. H.; Green, M. D.; Long, T. E. *Biomacromolecules* **2012,** 13, (1), 231-238.

52. Larnaudie, S. C.; Brendel, J. C.; Jolliffe, K. A.; Perrier, S. *Journal of Polymer Science Part A: Polymer Chemistry* **2016,** 54, (7), 1003-1011.

53. Buhl, M.; Tesch, M.; Lamping, S.; Moratz, J.; Studer, A.; Ravoo, B. J. *Chemistry – A European Journal* **2016,** 23, (25), 6042-6047.

54. Adamczyk, M.; Fishpaugh, J. R.; Heuser, K. J. *Bioconjugate Chemistry* **1997,** 8, (2), 253-255.

55. Shaw, D. J., 7 - Charged interfaces. In *Introduction to Colloid and Surface Chemistry (Fourth Edition)*, Butterworth-Heinemann: Oxford, 1992; pp 174-209.

56. Petersen, H.; Fechner, P. M.; Martin, A. L.; Kunath, K.; Stolnik, S.; Roberts, C. J.; Fischer, D.; Davies, M. C.; Kissel, T. *Bioconjugate Chemistry* **2002,** 13, (4), 845-854.

57. von der Ehe, C.; Rinkenauer, A.; Weber, C.; Szamosvari, D.; Gottschaldt, M.; Schubert, U. S. *Macromolecular Bioscience* **2016,** 16, (4), 508-521.

58. Carvalho, P. J.; Ventura, S. P. M.; Batista, M. L. S.; Schröder, B.; Gonçalves, F.; Esperança, J.; Mutelet, F.; Coutinho, J. A. P. *The Journal of Chemical Physics* **2014,** 140, (6), 064505.

59. Xue, Y.; Xiao, H.; Zhang, Y. *International Journal of Molecular Sciences* **2015,** 16, (2), 3626-3655.

Conclusion, Perspectives and Outlook

The aim of this thesis was to develop a synthetic strategy by which complex polymeric cyclic-peptide nanotubes can be synthesised and further modified with a wide range of small molecules by post-polymerisation modification, and using these novel systems to determine if the self-assembly process can be manipulated and controlled on a molecular level.

Chapter 2 demonstrates that nucleophilic substitutions of a halogen side group polymer, a reaction that has been largely disregarded in polymer science to date, enables access to highly reactive and yet well-defined homopolymers. These polymers can be synthesised without the need of stringent polymerisation conditions nor at the cost of a low polymer yield. A convenient and versatile synthesis of an alkylbromo polymer, pBEA that can be readily synthesised under RAFT conditions was developed. A series of pBEA polymers were synthesised with varied molecular weights (2.0 – 26.2 kg mol $^{-1}$) and narrow dispersities (PDI = 1.10 – 1.17). Chain extension of these macro-CTAs proved that the majority of the chain ends remain active and no significant side reactions were observed despite the high reactivity of the bromine groups. The addition of the bromine residue on the polymer arm provides a highly reactive handle by which these polymers can be further modified by small molecules (such as charged moieties, or functional biomolecules) using simple post-polymerisation modification strategies.

The versatility of pBEA in nucleophilic substitutions allows for efficient production of a diverse library of functional polymers. A variety of nucleophiles were examined including well known nitrogen based substituents such as azides or tertiary amines, but also sulfites and sugars (which was previously unreported in the literature). Across all these nucleophilic species the substitution of pBEA proceeded with almost quantitative conversion (> 88%). A major advantage of this simple substitution is that only mild conditions are employed, *i.e.* room temperature and no need for additional catalysts. In concert with the high level of control provided by RAFT polymerisation, this strategy enables the synthesis of well-defined, highly charged polycations, permanently charged

polyanions, stable polythioethers, a highly reactive polyazide and even synthetically demanding glycopolymers with minimal synthetic effort. In particular, substitution using thiols is not limited to the demonstrated materials, but can be readily extended to encompass other available thiolates, allowing for the conjugation of even more molecules such as drugs, fluorescent tags, or cell targeting moieties. Considering the potential to create libraries of various materials with minimal effort and originating from a single precursor polymer, the synthetic route developed here is a unique and versatile tool.

Chapter 3 describes the development of an orthogonal reaction sequence for the synthesis of sugar-coated nanotubes. End-functionalised BEA polymers were synthesised by RAFT polymerisation as described in Chapter 2, however an NHS-modified CTA was used. The NHS- bearing pBEA polymers were conjugated to a self-assembling CP core without any unwanted side-reactions, resulting in a reactive nanotube precursor for subsequent post-modification. The self-assembly of these CP-pBEA conjugates was analysed by SANS and SLS, and found to form short nanotubes in THF-d_6 solutions; with longer polymer chain lengths found to decrease the size of nanotube. The brominated precursor conjugates were then modified post-conjugation *via* a thio-bromo "click" reaction with a glucose thiolate salt, which resulted in CP glycopolymer conjugates. The self-assembly of these glycopolymer conjugates was again assessed by SANS and were found to form longer tubes of 135 - 145 Å, in the more hydrogen bonding competitive environment of D_2O. The increase in length of the DP25 conjugate following post-modification, is an excellent demonstration that post-modification does not hinder self-assembly of the cyclic-peptide. Instead, post-modification is an advantageous route for enhancing nanotube formation by incorporating functional monomer units that can promote self-assembly, either by improving solubility, reducing steric hindrance or increasing the inter-molecular attractive-forces such as with additional hydrogen bonding or π-π stacking.

In Chapter 4, the synthesis and *in situ* characterisation of highly charged polyelectrolyte-CP conjugate self-assemblies using SANS was carried out. In pure D_2O, CP conjugates of both anionic pEASTEA and cationic pTMAEA exist as unimers. SANS scattering profiles of both conjugates were modelled to polyelectrolyte and cylinder form factors,

and the results are consistent with that of single unimers in solution. The presence of unimers was found to be due to the high electrostatic repulsion between polymer arms, preventing the inter-molecular hydrogen bond formation necessary for nanotube assembly. At high ionic strengths, the SANS profiles of anionic and cationic conjugates are very different, despite being synthesised from a single precursor and having the same number of charged monomers in the polymer chain. Guinier-Porod modelling revealed that the anionic conjugate formed an elongated spheroid structure, whereas the cationic analogue formed an extended cylindrical assembly. The scattering profile of anionic conjugates at high ionic strength (5 M NaCl) was modelled very effectively to a cylinder model, revealing that a mixture of unimeric conjugates and short stacks of peptides were formed. The SANS profile of the cationic conjugate was fitted with a Cylinder-Gaussian Coil combination model, which revealed that nanotubular structures of varying length are formed in high ionic strength solutions. The difference in assembly between the positively and negatively charged conjugates, despite the same polymer length, graft density and effective charge, is attributed to the difference in monomer size; with steric effects dominating the self-assembly once the electrostatic repulsions were shielded. This work presents a good step towards fine control of the self-assembly process for polymeric nanotubes, made possible by tuning the electrostatic interaction between polymer arms using salt to reduce the Debye radius and electrostatic repulsion.

Finally, in Chapter 5 the effect of self-assembly *vs*. the molecular surface charge was compared for a library of CP-polymer conjugates on cellular uptake. The RAFT polymerisation of BEA explored in Chapter 2, in conjunction with the pBEA conjugation method developed in Chapter 3, was used as an effective strategy by which a library of pPEGA-*stat*-pBEA copolymers were generated. The partially charged conjugates created incorporated either an ammonium or phosphonium group, and resulted in unexpected results *in vitro*. Increasing quantities of charge did not increase cellular uptake, as the bulk of literature would suggest, and instead remained in the cellular periphery without interacting with the lipid bilayer. In addition to this, the negative effect of charge on self-assembly *via* co-assembly was determined. Using mixtures of assembling and unimeric conjugates, it was found that ammonium and phosphonium analogues have different co-

assembly properties. Charged ammonium conjugates, when mixed with assembling conjugates of pPEGA, resulted in less cellular uptake due to the co-assembly of the charged unimers. In the case of phosphonium analogues however, no co-assembly was apparent. This indicates that despite structural similarities, the two different charged species results in a remarkably different self-assembly, and therefore cell-uptake behaviours. The self-assembly properties of this system, and the improved cell uptake it imparts, makes these materials an exciting potential material for drug delivery especially given the easy modification of the pBEA macromolecule. With these encouraging results, further study should be undertaken in a less sterically hindered system to confirm these results.

In summary, this thesis presents a new synthetic strategy with which a diverse library of materials based on self-assembling polymeric cyclic peptide nanotubes can be generated. The benefits of generating materials from a single precursor, is the possibility to study of the effect of different monomer types on the self-assembly process directly. In addition, this method provides access to complex functionalities such as polyelectrolytes and glycopolymers, which offer an exciting potential as antimicrobials, non-viral gene-delivery agents and drug delivery vehicles. Despite the scope of this work, there are many other avenues which can be further explored.

In Chapter 2, a more extensive library of polymers could be generated *via* nucleophilic substitution, such as zwitterionic compounds for antifouling applications. Additionally, a further study into the copolymerisation and chain extensions of BEA with other acrylate monomers would be an interesting insight.

The SANS and SLS of studies in Chapter 3 could be expanded to gain a better understanding of the effect of filtration and equilibration time in these systems. Additionally, the SLS of the glycopolymer conjugates, would give additional insight into the length of assemblies formed.

In Chapter 4, it would be beneficial to the study if the SANS profile of the polymer arms alone could be obtained (if additional SANS beam-time could be won!). This would give a greater insight into the interactions that are occurring in this highly complex system.

Additionally, SLS of these materials would potentially offer further insights into the self-assembly of these materials.

The glycopolymer conjugates generated in Chapter 3, are an exciting material that would make an excellent candidate for non-viral gene delivery and drug delivery applications. A library of glycopolymer conjugates could be synthesised, of varying DP, as well as different sugar moieties, such as galactose or mannose, and used to mimic complex glycosylation pathways found naturally *in vivo*, thus considerably expanding the potential application of these systems. Further, these glycopolymer conjugates would make a very interesting *in vitro* study for improving cell penetration. It would also be interesting to determine if the lectin binding properties of sugar-coated nanotubes is consistent with other sugars, by repeating the Con A study using different variations of sugar moieties. From the results of the studies in Chapter 5, self-assembly was highlighted as an important factor for improving cell penetration in polymeric cyclic peptide nanotubes. The extended nanotubular structure formed by glycopolymer conjugates in D_2O suggests these compounds have a very good potential in the field of drug delivery given their enhanced cell uptake.

Finally, to extend the work of Chapter 5, a series of copolymer-conjugates incorporating different charges should be synthesised that have a less sterically hindered co-monomer, such as the PEGA that was used in this study. Since the presence of PEGA chains likely shielded the charged monomers from interacting with the negative cell-membrane, a copolymer of charged units with a polymer comprising thioglycerol units would be an interesting material. Further to this a thioglycerol conjugate would be an interesting analogue to study alongside both glycopolymer conjugates and for the assessment of self-assembly *vs.* charge.

Appendix to Chapter 3

A3.1 Calculation of Conjugation Efficiency

The percentage of conjugated chains was determined using equation (1):

$$\%\ conjugated\ polymer\ chains = \frac{2 \times \%\ Area\ conjugate}{2 \times \%\ Area\ conjugate + \%\ Area\ free\ polymer} \quad (1)$$

If 2.2 equivalents of polymer were used, the theoretical maximum conjugation is:

$$\frac{2}{2.2} \times 100 = 91\%$$

Conjugation efficiency was calculated as a percentage relative to this maximum value, using equation (2):

$$Conjugation\ efficiency = \frac{\%\ conjugated\ polymer\ chains}{\%\ theoretical\ maximum\ conjugation} \quad (2)$$

Table A 3.1: Conjugation efficiencies of pBEA conjugations using equation 2.

Sample	Conjugation Efficiency
CP-$[pBEA_{10}]_2$	86%
CP-$[pBEA_{25}]_2$	94%

A3.2 Deconvolution of peptide-polymer conjugations

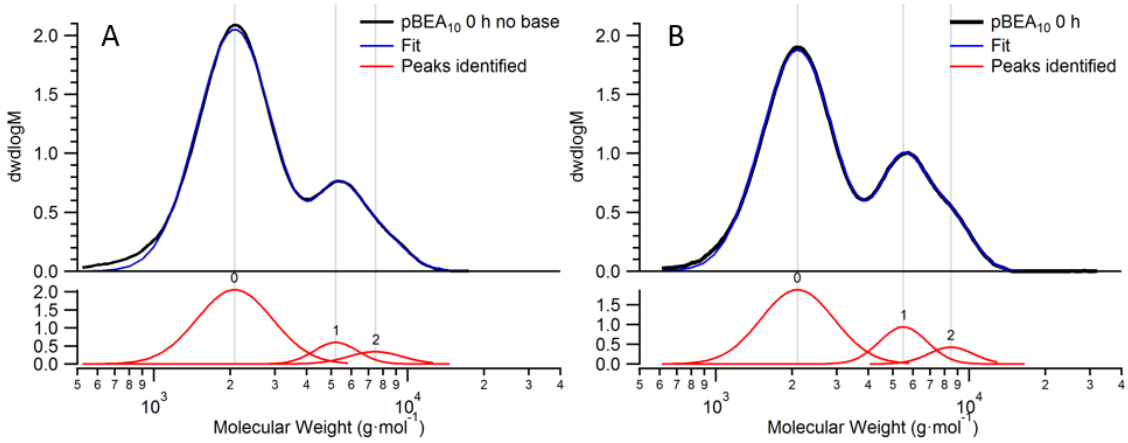

A 3.1: Deconvolution of dwdlogM of CP-[pBEA$_{10}$]$_2$ conjugation before and after addition of base.

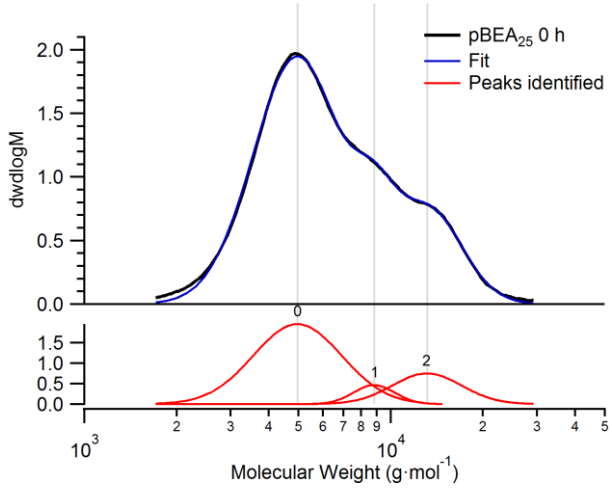

A 3.2: Deconvolution of dwdlogM of CP-[pBEA$_{25}$]$_2$ conjugation.

Table A 3.2: Deconvolution of CP-[pBEA$_{25}$]$_2$ conjugation area of peak fit.

	Log-Normal Peak Fit		
Time (h)	**Polymer**	**1-Arm**	**2-Arm**
0	100%	-	-
0.5	67%	9%	24%
1	60%	14%	26%
1.5	59%	9%	32%
3.5	48%	10%	42%
24	32%	-	68%

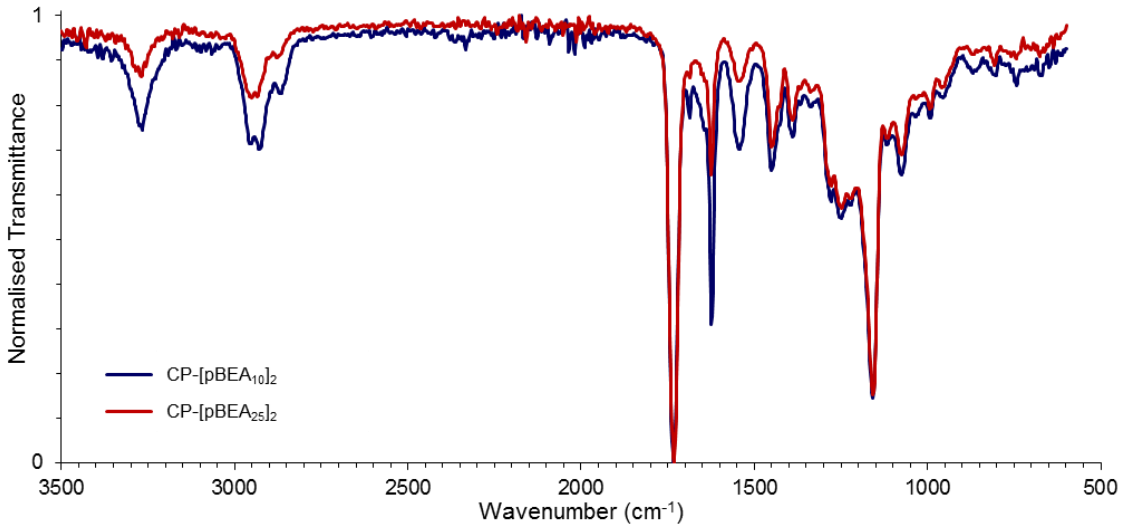

A 3.3: Normalised Infrared transmittance spectra of CP-[pBEA$_{10}$]$_2$ (blue line) and CP-[pBEA$_{25}$]$_2$ (red line).

A3.3 pBEA Conjugate SANS Analysis

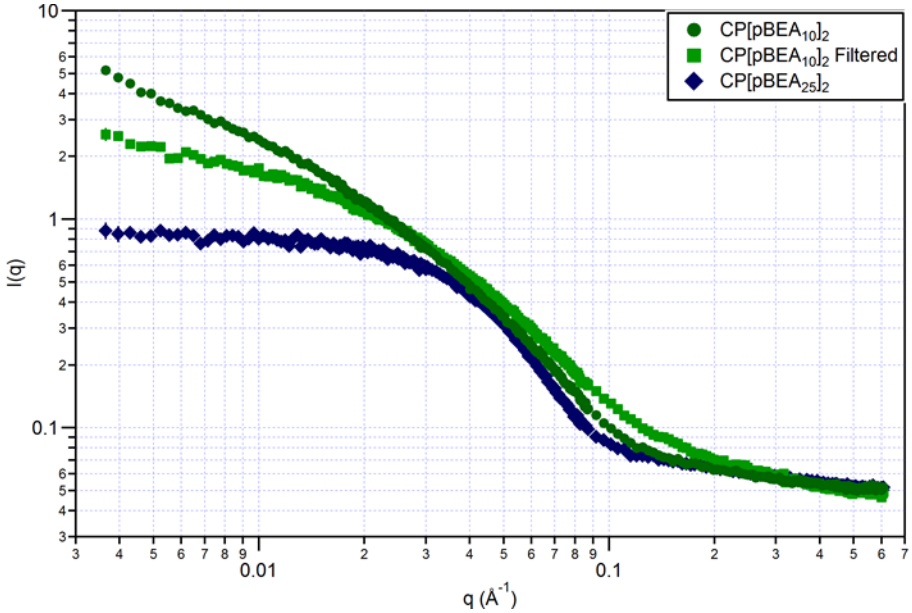

A 3.4: SANS profile of CP-[pBEA$_n$]$_2$ conjugates at 10 mg· mL^{-1} in THF-d$_8$: CP-[pBEA$_{10}$]$_2$ before (green circles) and after (green squares) filtration and CP-[pBEA$_{25}$]$_2$ (blue diamonds).

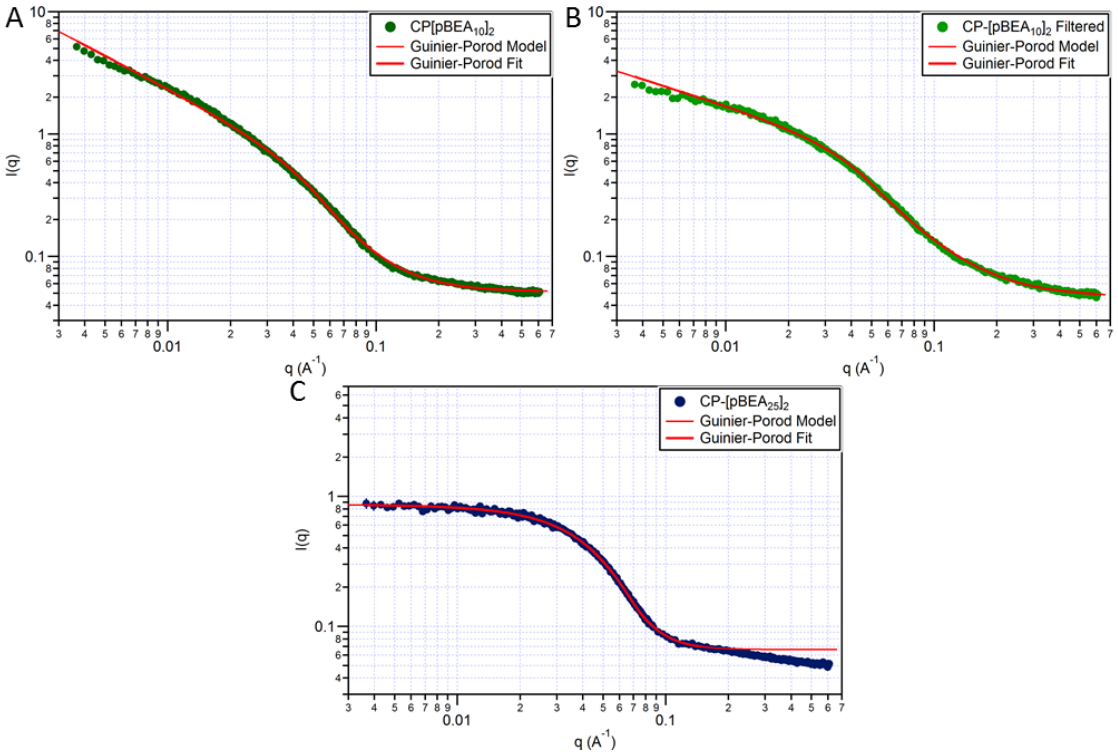

Guinier-Porod Model	CP-[pBEA$_n$]$_2$ in THF-d$_6$		
	***n* = 10**	***n* = 10 filtered**	***n* = 25**
Guinier Scale	0.0363	0.139	0.738
Dimension Variable (s)	0.902	0.541	0.013
R_g (Å)	22.8	26.5	36.6
Porod Exponent	2.42	1.93	4.27
Background (cm^{-1})	0.0515	0.0464	0.0663
$\sqrt{\chi^2/N}$	2.48	1.65	1.07

A 3.5: Guinier-Porod model fits of CP-[pBEA$_n$]$_2$ scattering profiles at 10 mg· mL^{-1} in THF-d$_8$ with different polymer arm DP: (A) DP10, (B) DP10 filtered, and (C) DP25.

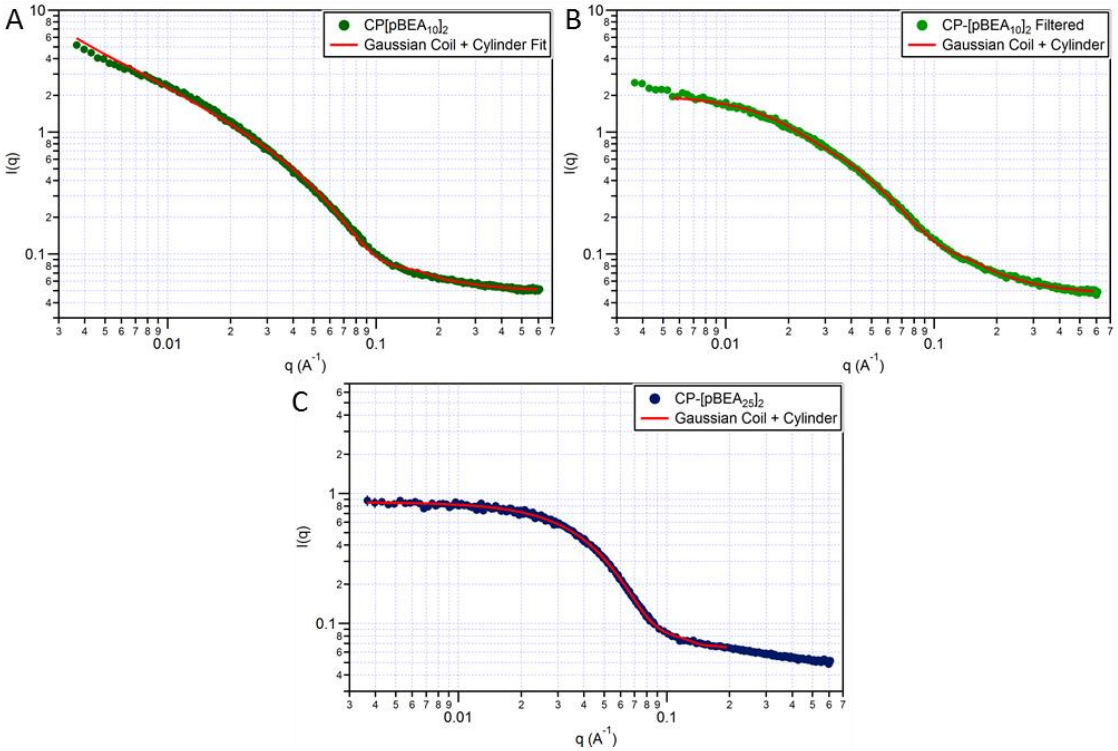

Cylinder-Gaussian Coil	CP-[pBEA$_n$]$_2$ in THF-d$_6$		
	***n* = 10**	***n* = 10 Filtered**	***n* = 25**
Scale	0.00102	0.000874	0.000764
Radius (Å)	31.8	32.9	46.5
Length (Å)	1480	259	50.7
$SLD_{cylinder}$ ($\times 10^{-6}$ Å^{-2})	9.46^{+}	9.46^{+}	9.00^{+}
$SLD_{solvent}$ ($\times 10^{-6}$ Å^{-2})	5.73^{+}	5.73^{+}	5.73^{+}
Background (cm^{-1})	0.0494	0.0464	0.0593
Scale	0.0757	0.194	0.180
R_g (Å)	15.5	19.5	44.0
Polydispersity	1^{+}	1^{+}	1^{+}
Background (cm^{-1})	0^{+}	0^{+}	0^{+}
$\sqrt{\chi^2/N}$	2.49	1.28	1.10
N_{agg}	314.8	55.2	10.8

A 3.6: Cylinder-Gaussian Coil model fits of CP-[pBEA$_n$]$_2$ scattering profiles at 10 mg·mL^{-1} in THF-d$_8$ with different polymer arm DP: (A) DP10, (B) DP10 filtered, and (C) DP25.

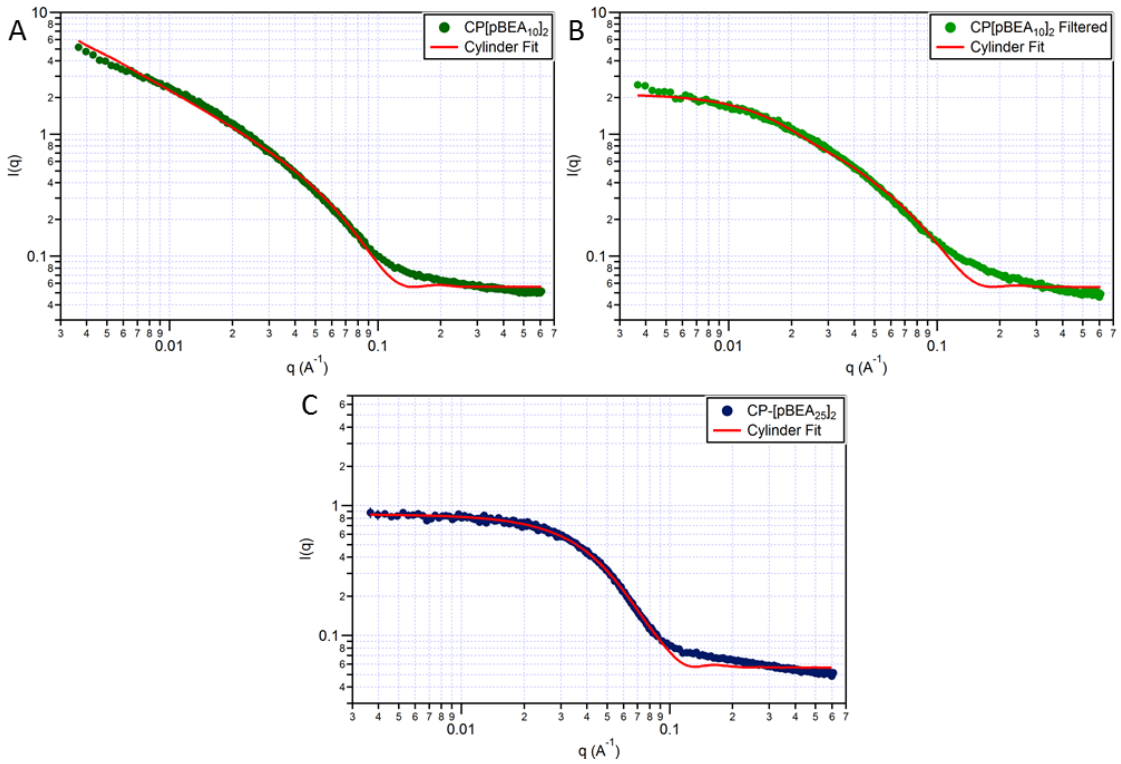

Cylinder Model	CP-[pBEA$_n$]$_2$ in THF-d$_6$		
	***n* = 10**	***n* = 10 Filtered**	***n* = 25**
Scale	0.00154	0.00238	0.00110
Radius (Å)	25.9	21.0	29.5
Length (Å)	1919.1	276.8	106.4
SLD$_{cylinder}$ (× 10^{-6} Å^{-2})	9.46†	9.46†	9.00†
SLD$_{solvent}$ (× 10^{-6} Å^{-2})	5.73†	5.73†	5.73†
Background (cm^{-1})	0.0558	0.0557	0.0567
$\sqrt{\chi^2/N}$	5.78	5.09	4.71

A 3.7: Cylinder model fits of CP-[pBEA$_n$]$_2$ scattering profiles at 10 mg· mL^{-1} in THF-d$_8$ with different polymer arm DP: (A) DP10, (B) DP10 filtered, and (C) DP25.

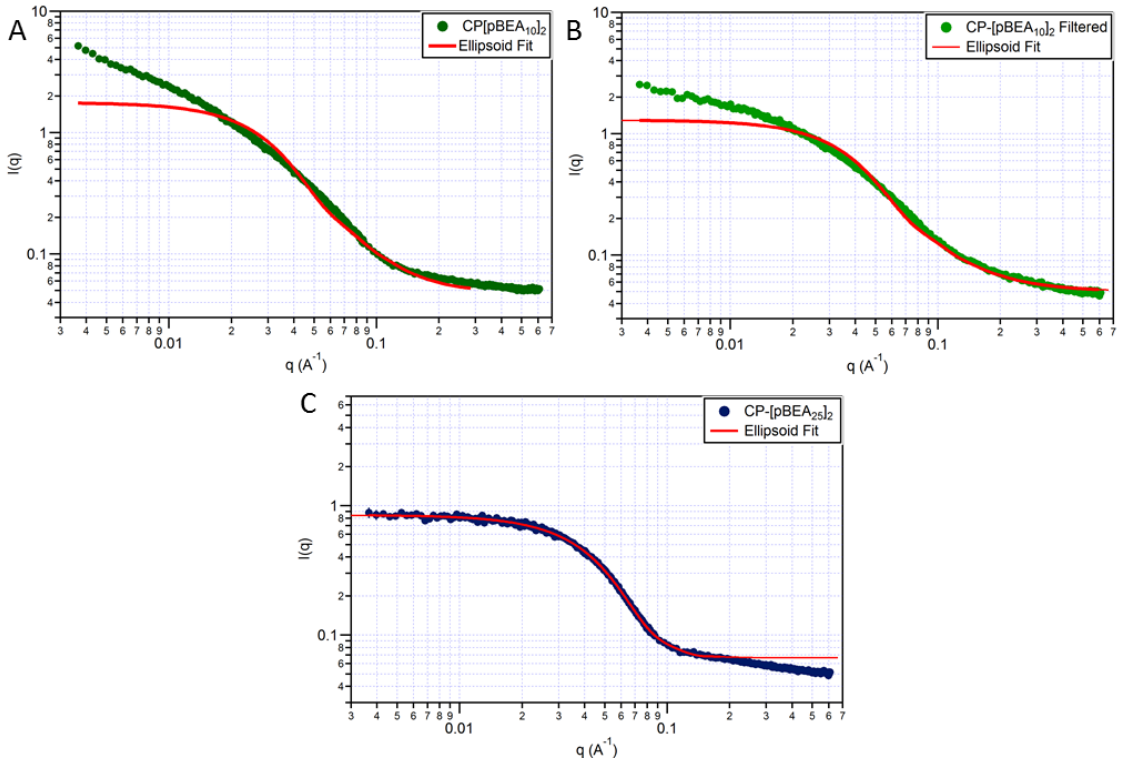

Ellipsoid Model	CP-[pBEA$_n$]$_2$ in THF-d$_6$		
	***n* = 10**	***n* = 10 Filtered**	***n* = 25**
Scale	0.00312	0.0173	0.00108
Radius *a* (Å)	8.71	1.87	23.9
Radius *b* (Å)	81.3	63.2	55.5
$SLD_{ellipsoid}$ (× 10^{-6} Å^{-2})	9.46†	9.46†	9.00†
$SLD_{solvent}$ (× 10^{-6} Å^{-2})	5.73†	5.73†	5.73†
Background (cm^{-1})	0.0505	0.0505	0.0665
$\sqrt{\chi^2/N}$	10.52	5.52	1.07

A 3.8: Ellipsoid model fits of CP-[pBEA$_n$]$_2$ scattering profiles at 10 mg· mL^{-1} in THF-d$_8$ with different polymer arm DP: (A) DP10, (B) DP10 filtered, and (C) DP25.

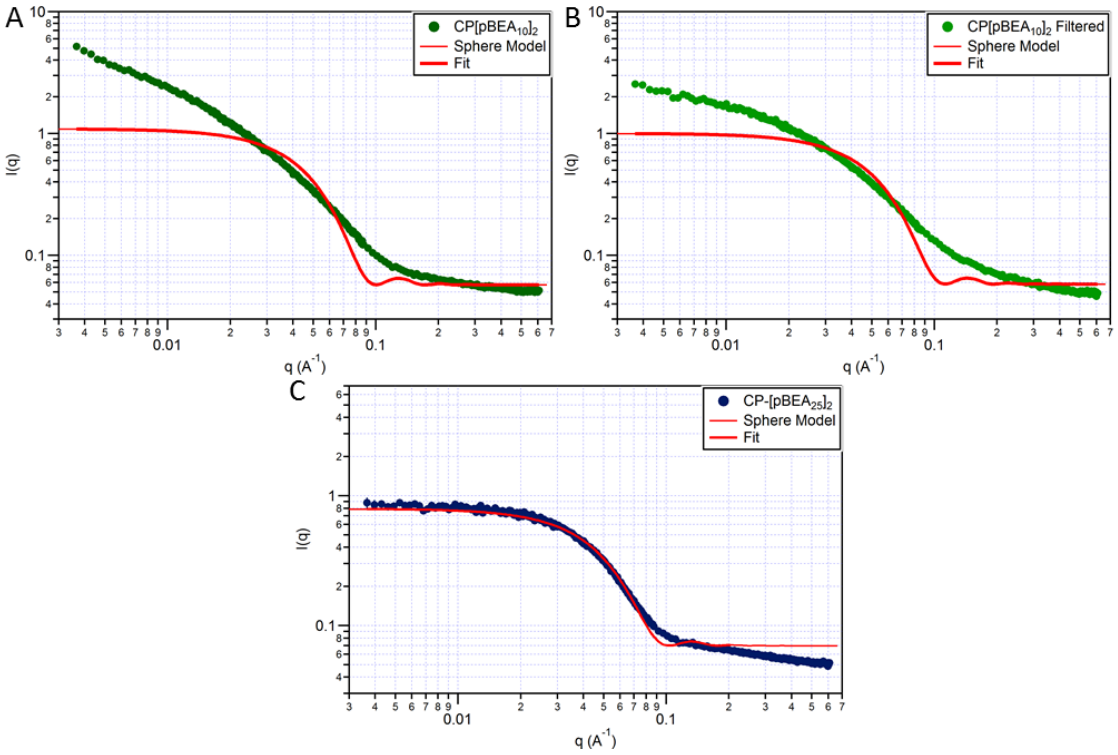

Sphere Model	CP-[pBEA$_n$]$_2$ in THF-d$_6$		
	***n* = 10**	***n* = 10 filtered**	***n* = 25**
Scale	0.00120	0.00154	0.000893
Radius (Å)	44.8	40.0	43.5
SLD_{sphere} (× 10^{-6} Å^{-2})	9.46†	9.46†	9.00†
$SLD_{solvent}$ (× 10^{-6} Å^{-2})	5.73†	5.73†	5.73†
Background (cm^{-1})	0.0572	0.0581	0.0697
$\sqrt{\chi^2/N}$	16.61	11.44	3.76

A 3.9: Sphere model fits of CP-[pBEA$_n$]$_2$ scattering profiles at 10 mg· mL^{-1} in THF-d$_8$ with different polymer arm DP: (A) DP10, (B) DP10 filtered, and (C) DP25.

A3.4 Thioglucose Conjugate SANS Analysis

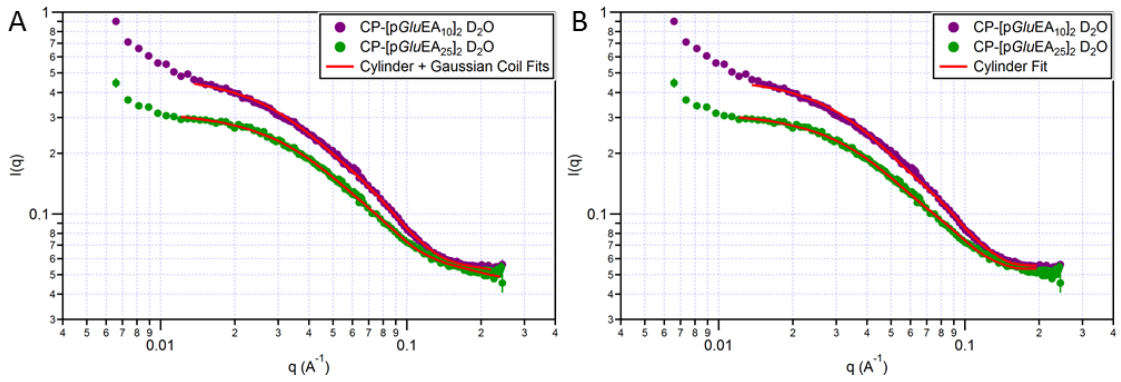

Cylinder-Gaussian Coil	CP-[p*Glu*EA$_n$]$_2$	
	***n* = 10**	***n* = 25**
Scale	0.000499	0.000164
Radius (Å)	23.8	26.8
Length (Å)	148.7	135.1
$SLD_{Cylinder}$ (× 10^{-6} Å^{-2})	1.14†	1.12†
$SLD_{Solvent}$ (× 10^{-6} Å^{-2})	6.34†	6.34†
Background (cm^{-1})	0.0470	0.0442
Scale	0.0861	0.1413
R_g (Å)	25.5	32.2
Polydispersity	1†	1†
Background (cm^{-1})	0†	0†
$\sqrt{\chi^2/N}$	1.59	1.02
N_{agg}	31.6	28.7

Cylinder Model	CP-[p*Glu*EA$_n$]$_2$	
	***n* = 10**	***n* = 25**
Scale	0.000855	0.000571
Radius (Å)	21.1	21.3
Length (Å)	131.0	119.2
$SLD_{Cylinder}$ (× 10^{-6} Å^{-2})	1.14†	1.12†
$SLD_{Solvent}$ (× 10^{-6} Å^{-2})	6.34†	6.34†
Background (cm^{-1})	0.0551	0.0532
$\sqrt{\chi^2/N}$	2.07	1.30
N_{agg}	27.9	25.4

A 3.10: Model fits of CP-[p*Glu*EA $_{10}$]$_2$ (purple circles) and CP-[p*Glu*EA $_{25}$]$_2$ (green circles) scattering profiles at 5 mg· mL^{-1} in D_2O: (A) fits to a Cylinder-Gaussian Coil model and (B) fits to a Cylinder model.

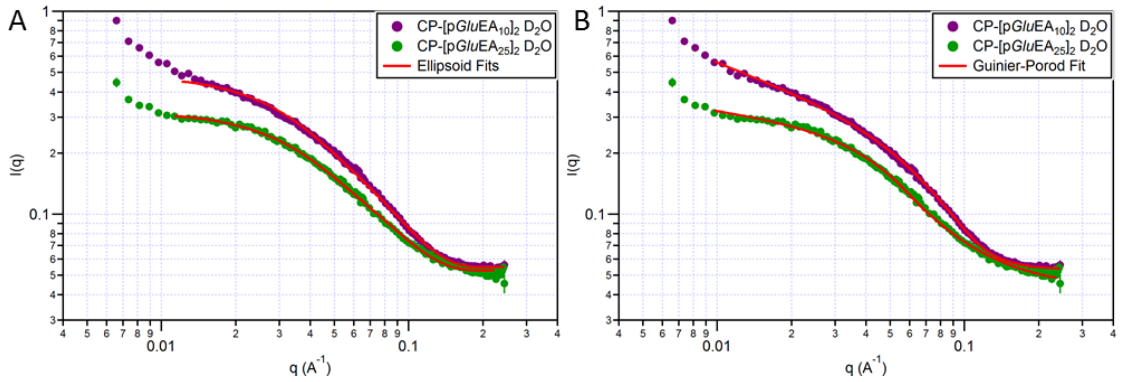

Ellipsoid Model	CP-[p*Glu*EA$_n$]$_2$	
	***n* = 10**	***n* = 25**
Scale	0.000902	0.000611
Radius *a* (Å)	88.9	80.9
Radius *b* (Å)	21.8	21.9
$SLD_{ellipse}$(× 10^{-6} Å^{-2})	1.14†	1.12†
$SLD_{solvent}$ (× 10^{-6} Å^{-2})	6.34†	6.34†
Background (cm^{-1})	0.0541	0.0522
$\sqrt{\chi^2/N}$	2.13	1.23

Guinier-Porod Model	CP-[p*Glu*EA$_n$]$_2$	
	***n* = 10**	***n* = 25**
Guinier Scale	0.0505	0.122
Dimension Variable (s)	0.50	0.19
R_g (Å)	20.3	26.8
Porod Exponent	4.29	1.93
Background (cm^{-1})	0.05	0.04
$\sqrt{\chi^2/N}$	1.48	1.51

A 3.11: Model fits of CP-[p*Glu*EA$_{10}$]$_2$ (purple circles) and CP-[p*Glu*EA $_{25}$]$_2$ (green circles) scattering profiles at 5 mg· mL^{-1} in D_2O: (A) fits to an Ellipsoid model and (B) to a Guinier-Porod model.

A3.5 SLS Analysis

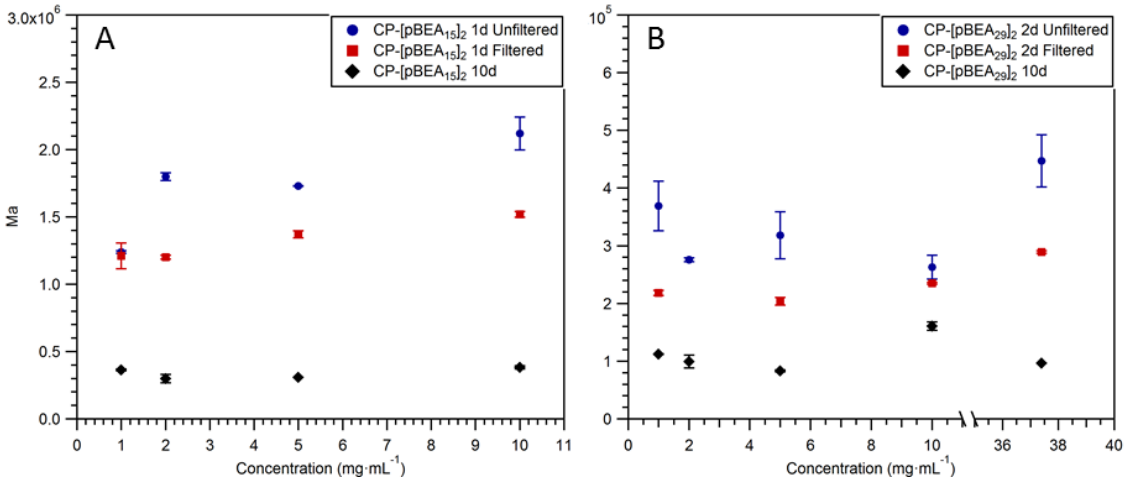

A 3.12: Concentration dependence of molecular weight (M_a) of (A) CP-[pBEA$_{15}$]$_2$ and (B) CP-[pBEA$_{29}$]$_2$ in THF obtained by light scattering.

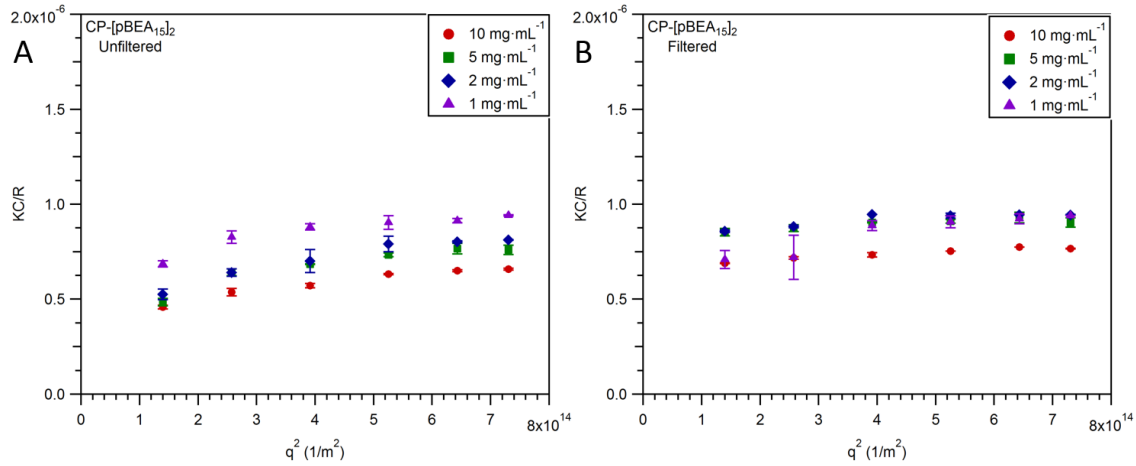

A 3.13: Evolution of KC/R as a function of q² obtained by light scattering for CP-[pBEA$_{15}$]$_2$ in THF before (A) and after (B) filtration.

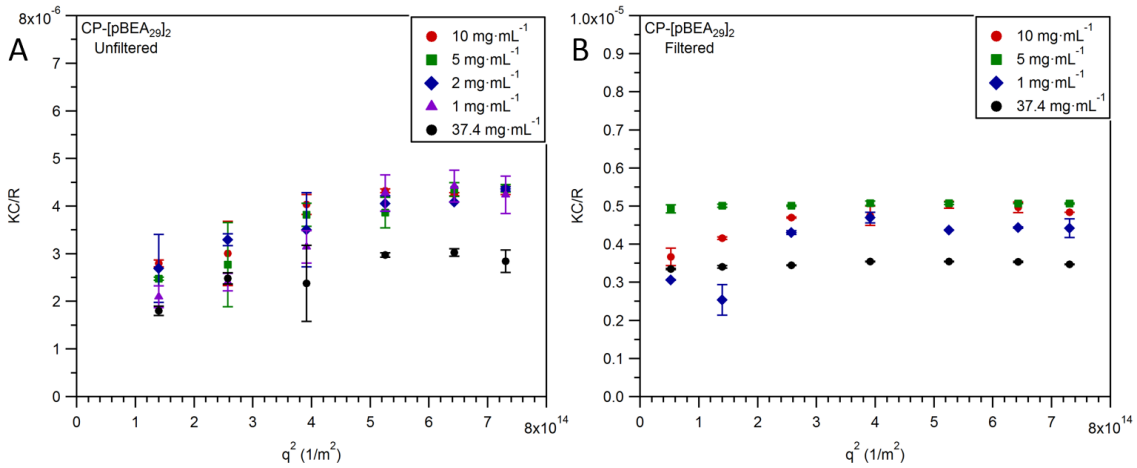

A 3.14: Evolution of KC/R as a function of q² obtained by light scattering for CP-[pBEA$_{29}$]$_2$ in THF before (A) and after (B) filtration.

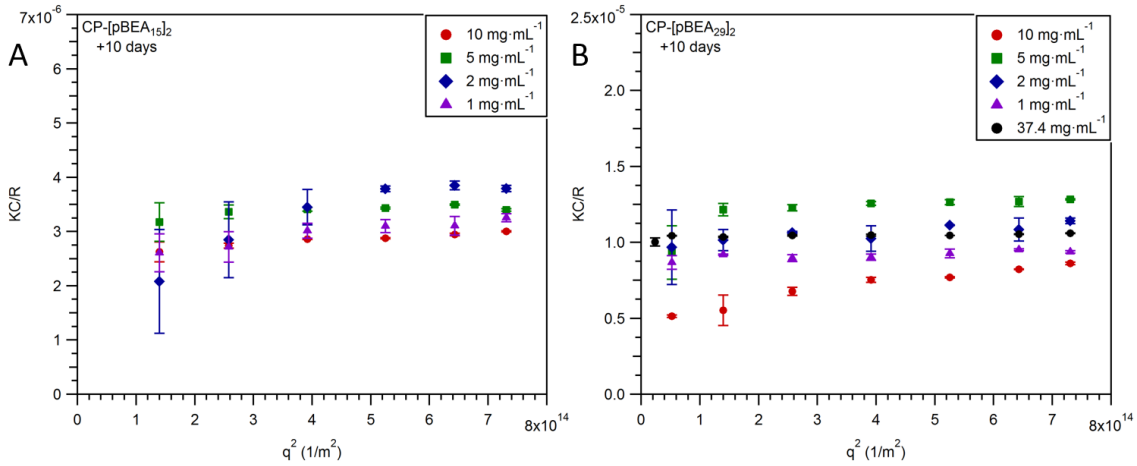

A 3.15: Evolution of KC/R as a function of q² obtained by light scattering for (A) CP-[pBEA$_{15}$]$_2$ and (B) CP-[pBEA$_{29}$]$_2$ in THF 10 days after filtration.

A3.6 Details used in Igor for the Cylinder + Gaussian-Coil model[1]

This was achieved using the model picking function in Igor Pro:

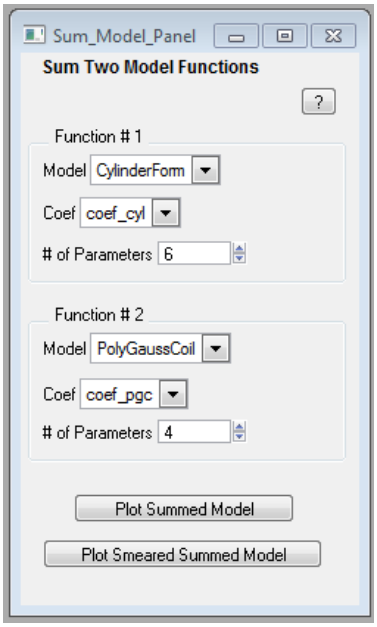

A 3.16: Screenshot of Cylinder + Gaussian-Coil sum model selected.

The summed model is a simple linear combination of the two models selected in **Figure A 3.16** based on the assumption that the two structures producing the scattering are non-interacting.

The coefficients for the summed model are a succession of the coefficients for the two individual models. For the two models, there are two independent scale factors that determine the scaling of each individual model. In real samples, this is often linked to how the material is distributed in the solution. The duplicated parameters (scale and background) were held fixed at appropriate values for curve fitting and are indicated by † following the held value.

A3.7 References

1. Kline, S. *Journal of Applied Crystallography* **2006,** 39, (6), 895-900.

Appendix to Chapter 4

A4.1 SANS Data Analysis

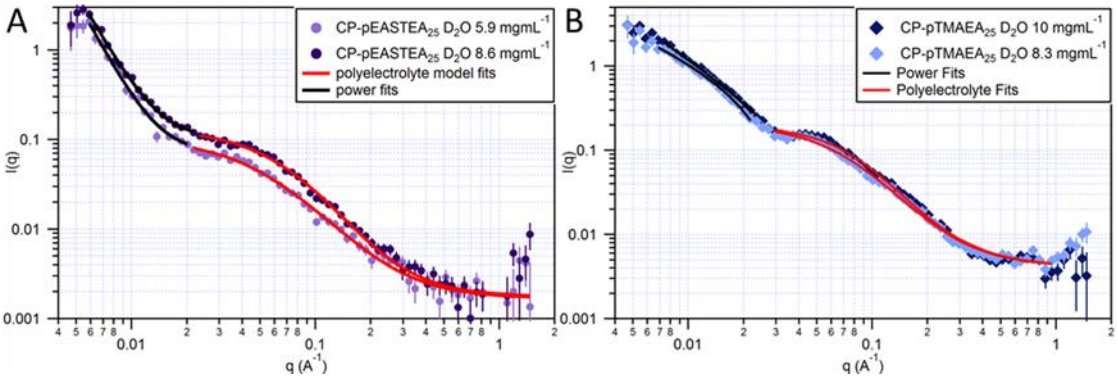

Polyelectrolyte Model	CP-[pEASTEA$_{25}$]$_2$ D_2O		CP-[pTMAEA$_{25}$]$_2$ D_2O	
	8.6 mgml^{-1}	**5.9 mgml^{-1}**	**10 mgml^{-1}**	**8.3 mgml^{-1}**
Contrast factor (barns)	5.840	16.15	21.74	24.52
Bjerrum length (Å)	7.12†	7.12†	7.12†	7.12†
Virial parameter (Å^{-3})	1589	1851	1951	1897
Monomer length (Å)	18.1	28.0	19.7	21.5
Salt conc. (mol/L)	0†	0†	0†	0†
Degree of ionisation	1†	1†	1†	1†
Polymer conc. (mol/L)	1.02	0.82	0.81	0.82
Background (cm^{-1})	0.00175	0.00169	0.00411	0.00411
Power Law Exponent	-3.62	-3.82	-1.47	-0.88
$\sqrt{\chi^2/N}$	1.30	1.06	2.16	1.95

A 4.1: BE_Polyelectrolyte fits of (A) CP-[pEASTEA$_{25}$]$_2$ at 8.6 mg· mL^{-1} and 5.9 mg· mL^{-1}; and (B) CP-[pTMAEA$_{25}$]$_2$ at 10 mg· mL^{-1} and 8.3 mg· mL^{-1} in D_2O (†=held parameter value).

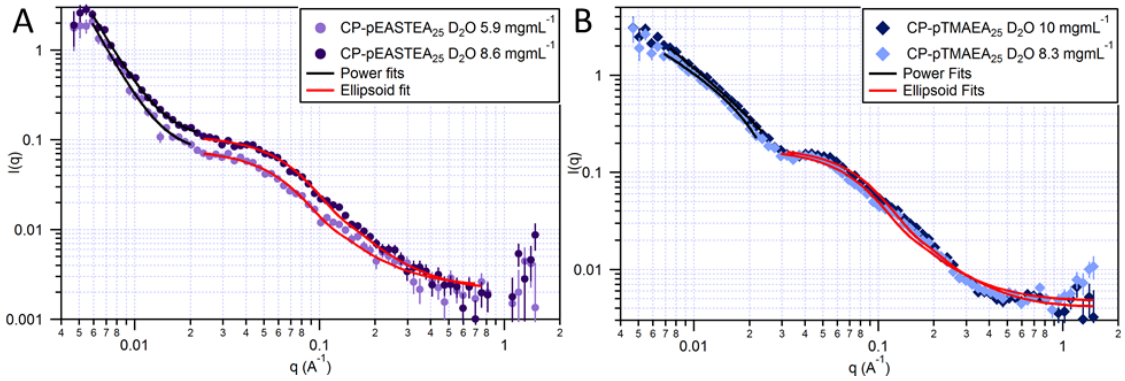

Ellipsoid Model	CP-[pEASTEA$_{25}$]$_2$ D_2O		CP-[pTMAEA$_{25}$]$_2$ D_2O	
	8.6 mgml^{-1}	**5.9 mgml^{-1}**	**10 mgml^{-1}**	**8.3 mgml^{-1}**
Scale	0.00214	0.00267	0.0080	0.0086
Radius *a* (Å)	2.7	1.2	1.8	1.3
Radius *b* (Å)	36.8	40.6	30.4	32.8
$SLD_{Ellipsoid}$ (× 10^{-6} Å^{-2})	0.56†	0.56†	0.65†	0.65†
$SLD_{Solvent}$ (× 10^{-6} Å^{-2})	6.34†	6.34†	6.34†	6.34†
Background (cm^{-1})	0.00234	0.00231	0.0041	0.0047
Power Law Exponent	-3.62	-3.82	-1.47	-0.88
$\sqrt{\chi^2/N}$	1.23	1.13	2.52	2.46

A 4.2: Ellipsoid fits of (A) CP-[pEASTEA$_{25}$]$_2$ at 8.6 mg· mL^{-1} and 5.9 mg· mL^{-1}; and (B) CP-[pTMAEA$_{25}$]$_2$ at 10 mg· mL^{-1} and 8.3 mg· mL^{-1} in D_2O (†=held parameter value).

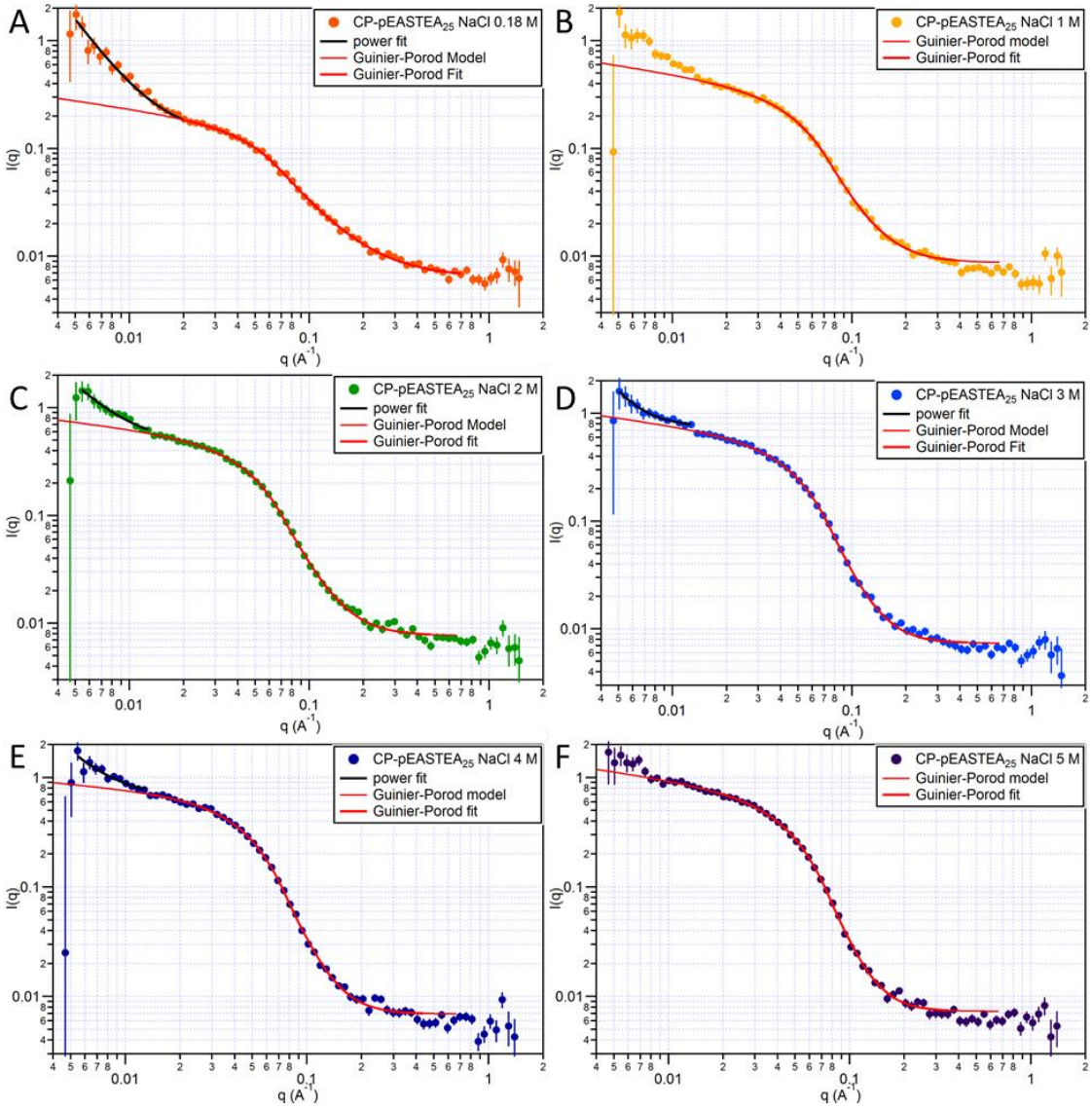

Guinier-Porod Model	0.18 M NaCl	1 M NaCl	2 M NaCl	3 M NaCl	4 M NaCl	5 M NaCl
Guinier Scale	0.0726	0.141	0.236	0.258	0.377	0.298
Dimension Variable (s)	0.25	0.27	0.21	0.23	0.16	0.25
R_g (Å)	22.9	26.6	29.0	29.5	31.2	30.7
Porod Exponent	2.03	3.12	3.29	3.79	3.88	4.15
Background (cm^{-1})	0.00638	0.00873	0.00767	0.00736	0.00693	0.00732
Power Law Exponent	-2.34	-2.09	-1.96	-3.19	-2.15	-1.98
$\sqrt{\chi^2/N}$	0.80	0.96	1.61	1.12	1.15	1.08

A 4.3: Guinier-Porod model fits of CP-[pEASTEA$_{25}$]$_2$ scattering profiles in D_2O with (A) 0.18 M NaCl, (B) 1 M NaCl, (C) 2 M NaCl, (D) 3 M NaCl, (E) 4 M NaCl, and (F) 5 M NaCl.

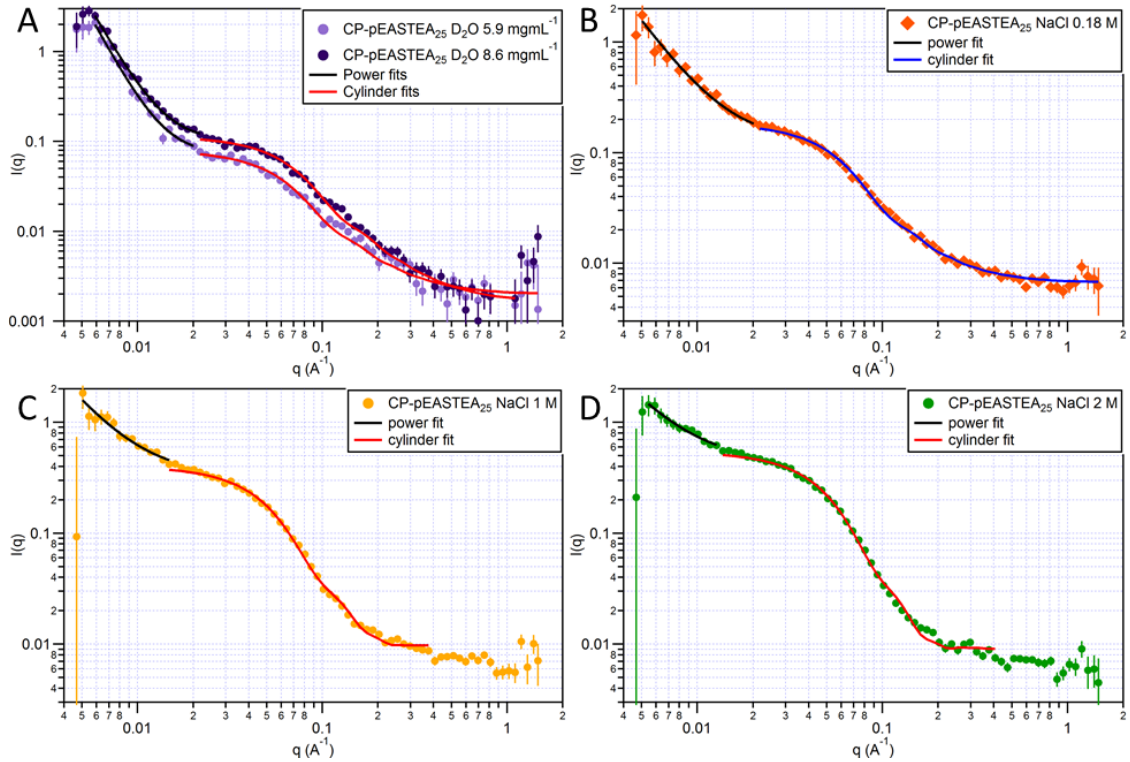

Cylinder Model	D_2O 8.6 mgml^{-1}	D_2O 5.9 mgml^{-1}	0.18 M NaCl	1 M NaCl	2 M NaCl
Scale	0.00425	0.00341	0.00561	0.000810	0.000874
Radius (Å)	32.6	35.9	37.7	43.9	45.3
Length (Å)	2.4	1.7	2.1	23.8	28.2
$SLD_{Cylinder}$ ($\times 10^{-6}$ Å^{-2})	0.56†	0.56†	0.56†	0.56†	0.56†
$SLD_{Solvent}$ ($\times 10^{-6}$ Å^{-2})	6.34†	6.34†	6.34†	6.34†	6.34†
Background (cm^{-1})	0.00170	0.00200	0.00672	0.00956	0.00895
Power Law Exponent	-3.62	-3.82	-2.34	-2.09	-1.96
$\sqrt{\chi^2/N}$	1.28	1.17	1.10	1.49	1.65

A 4.4: Cylinder model fits of CP-[pEASTEA$_{25}$]$_2$ scattering profiles in D_2O (A) at different concentrations: 5.9 and 8.5 mg· mL^{-1} (B) with 0.18 M NaCl, (C) 1 M NaCl, (D) 2 M NaCl (†=held parameter value).

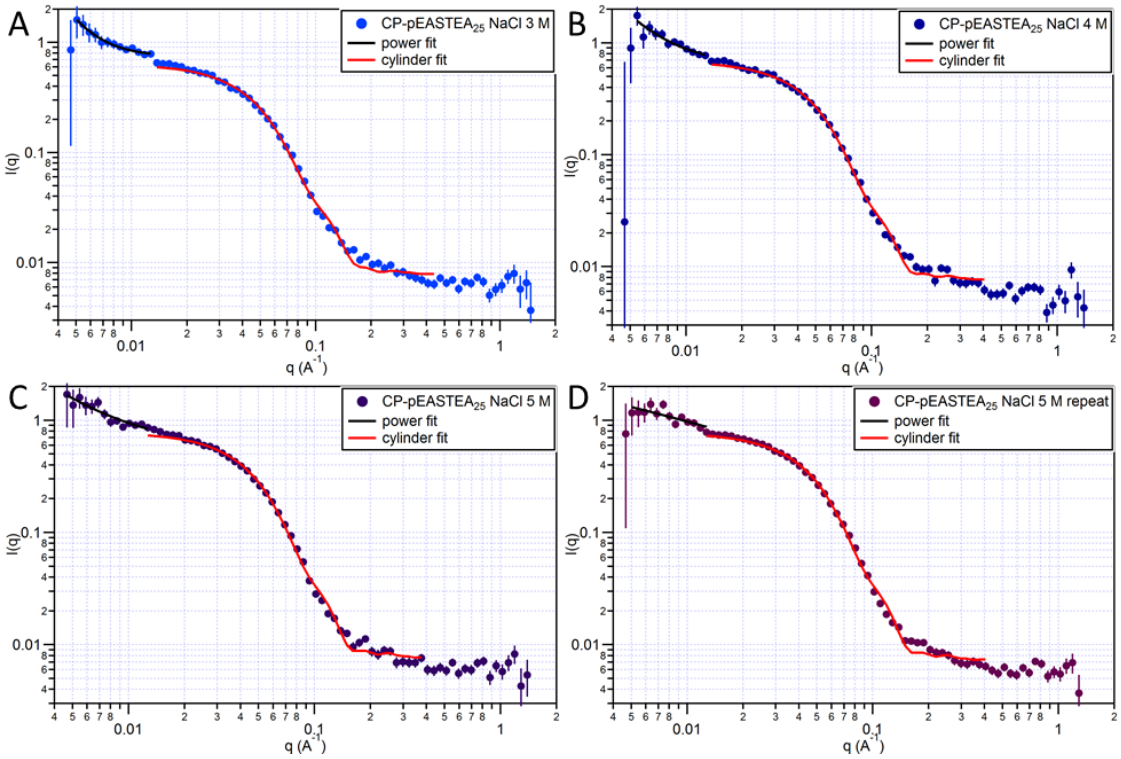

Cylinder Model	3 M NaCl	4 M NaCl	5 M NaCl	5 M repeat
Scale	0.000896	0.000911	0.000917	0.000923
Radius (Å)	45.6	45.5	47.3	47.1
Length (Å)	32.3	34.4	36.0	35.6
$SLD_{Cylinder}$ ($\times 10^{-6}$ Å^{-2})	0.56†	0.56†	0.56†	0.56†
$SLD_{Solvent}$ ($\times 10^{-6}$ Å^{-2})	6.34†	6.34†	6.34†	6.34†
Background (cm^{-1})	0.00784	0.00761	0.00764	0.00730
Power Law Exponent	-3.19	-2.15	-1.39	0.32
$\sqrt{\chi^2/N}$	1.91	1.68	1.98	1.81

A 4.5: Cylinder model fits of CP-[pEASTEA$_{25}$]$_2$ scattering profiles in D_2O with (A) 3 M NaCl, (B) 4 M NaCl,(C) 5 M NaCl, (D) 5 M NaCl re-run after 24 h (†=held parameter value).

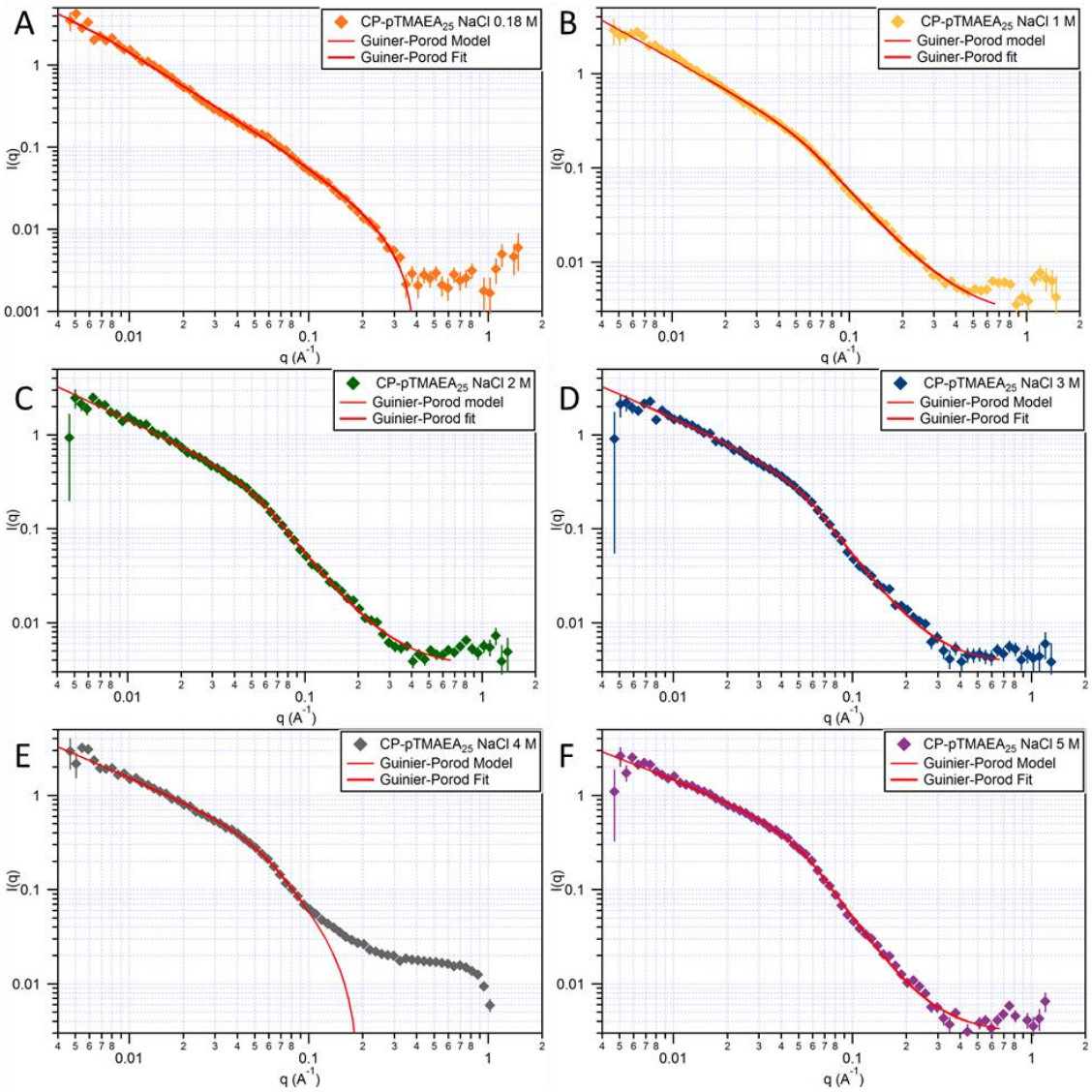

Guinier-Porod Model	0.18 M NaCl	1 M NaCl	2 M NaCl	3 M NaCl	4 M NaCl	5 M NaCl
Guinier Scale	0.0502	0.0122	0.0245	0.0325	0.0377	0.0509
Dimension Variable (*s*)	0.80	1.03	0.89	0.83	0.81	0.73
R_g (Å)	89.7	14.1	18.0	19.6	17.4	22.0
Porod Exponent	1.35	2.11	2.38	2.59	2.04	2.67
Background (cm^{-1})	0.000975	0.00258	0.00341	0.00407	-0.02161	0.00306
$\sqrt{\chi^2/N}$	1.84	1.28	1.30	1.53	1.27	1.59

A 4.6: Guinier-Porod model fits of CP-[pTMAEA$_{25}$]$_2$ scattering profiles in D_2O with (A) 0.18 M NaCl, (B) 1 M NaCl, (C) 2 M NaCl, (D) 3 M NaCl, (E) 4 M NaCl, and (F) 5 M NaCl.

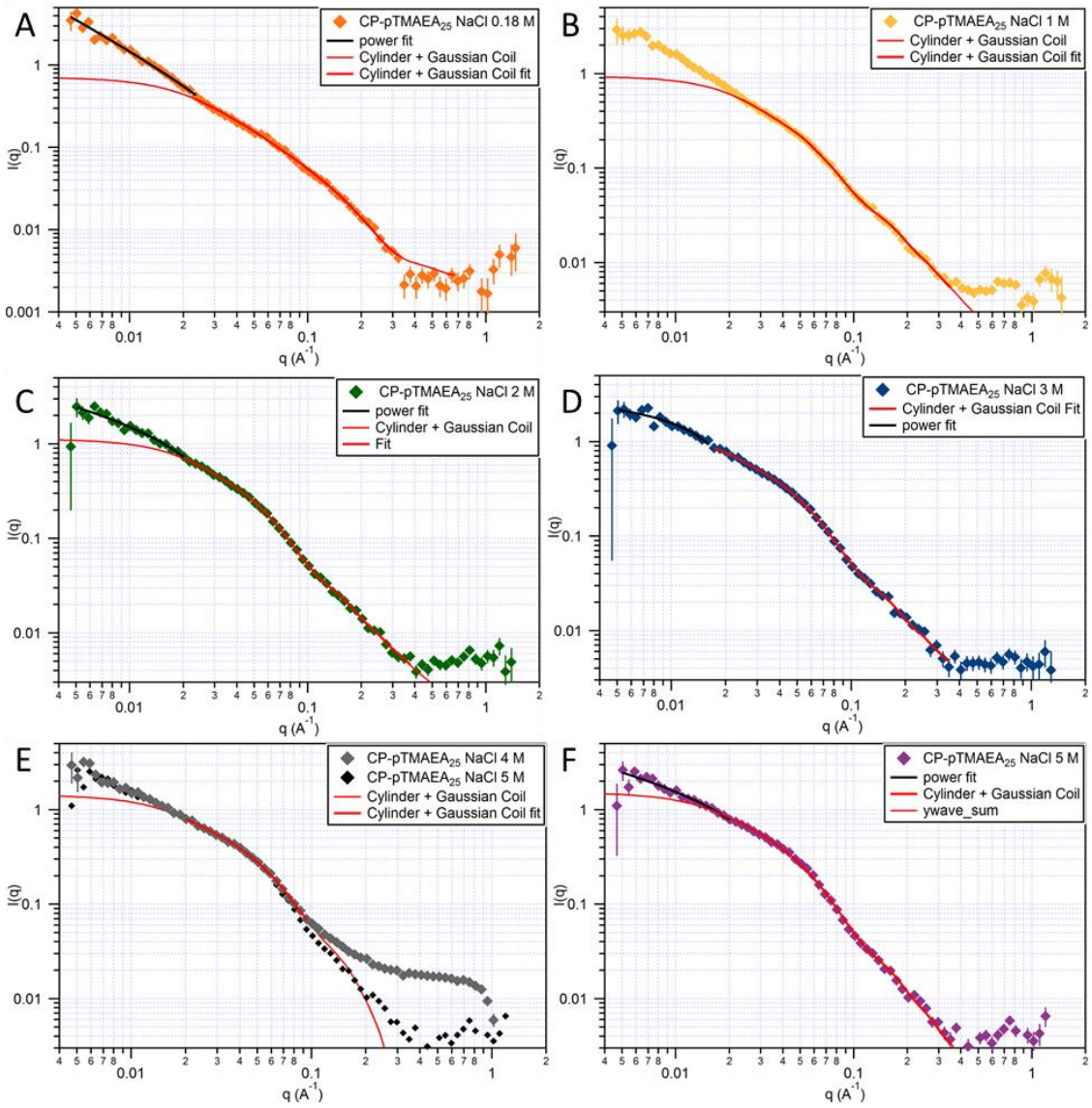

A 4.7: Cylinder-Gaussian Coil model fits of CP-[pTMAEA$_{25}$]$_2$ scattering profiles in D_2O with (A) 0.18 M NaCl, (B) 1 M NaCl, (C) 2 M NaCl, (D) 3 M NaCl, (E) 4 M NaCl, and (F) 5 M NaCl (†=held parameter value).

A 4.7: *Continued*

Cylinder-Gaussian Coil	0.18 M NaCl	1 M NaCl	2 M NaCl	3 M NaCl	4 M NaCl	5 M NaCl
Scale	0.00100	0.00041	0.00035	0.00037†	0.00037†	0.00037†
Radius (Å)	10.7	31.5	32.9	32.3	33.6	32.6
Length (Å)	199.8	285.9	223.8	258.1	268.1	284.1
$SLD_{Cylinder}$ (× 10^{-6} Å^{-2})	0.65†	0.65†	0.65†	0.65†	0.65†	0.65†
$SLD_{Solvent}$ (× 10^{-6} Å^{-2})	6.34†	6.34†	6.34†	6.34†	6.34†	6.34†
Background (cm^{-1})	0.002160	0.000629	0.000843	0.000387	0.00885	0.000818
Scale	0.498	0.107	0.229	0.294	0.292	0.368
R_g (Å)	75.3	17.6	29.0	35.6	29.3	40.3
Polydispersity	1†	1†	1†	1†	1†	1†
Background (cm^{-1})	0†	0†	0†	0†	0†	0†
$\sqrt{\chi^2/N}$	1.44	1.79	0.89	1.22	1.17	1.56

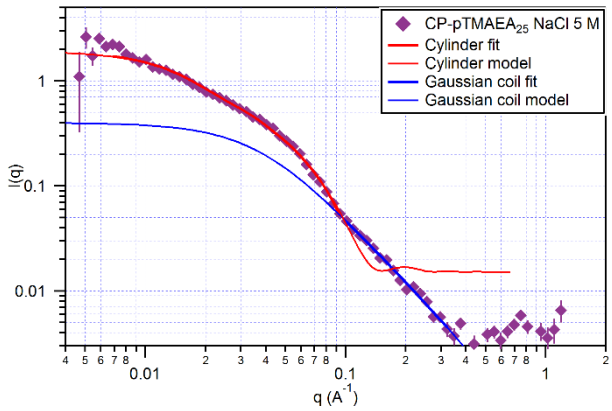

5 M NaCl			
Cylinder Model		**Gaussian Coil Model**	
Scale	0.00110	Scale	0.496
Radius (Å)	23.5	R_g (Å)	44.7
Length (Å)	312.1	Polydispersity	1†
$SLD_{Cylinder}$ (× 10^{-6} Å^{-2})	0.65†	Background (cm^{-1})	0.000219
$SLD_{Solvent}$ (× 10^{-6} Å^{-2})	6.34†	$\sqrt{\chi^2/N}$	0.83
Background (cm^{-1})	0.000216		
$\sqrt{\chi^2/N}$	1.97		

A 4.8: Cylinder fit and model (red lines) and Gaussian-Coil fit and model (blue lines) of CP-[pTMAEA$_{25}$]$_2$ in D_2O with 5 M NaCl (†=held parameter value).

Appendix to Chapter 5

A5.1 HPLC analyses

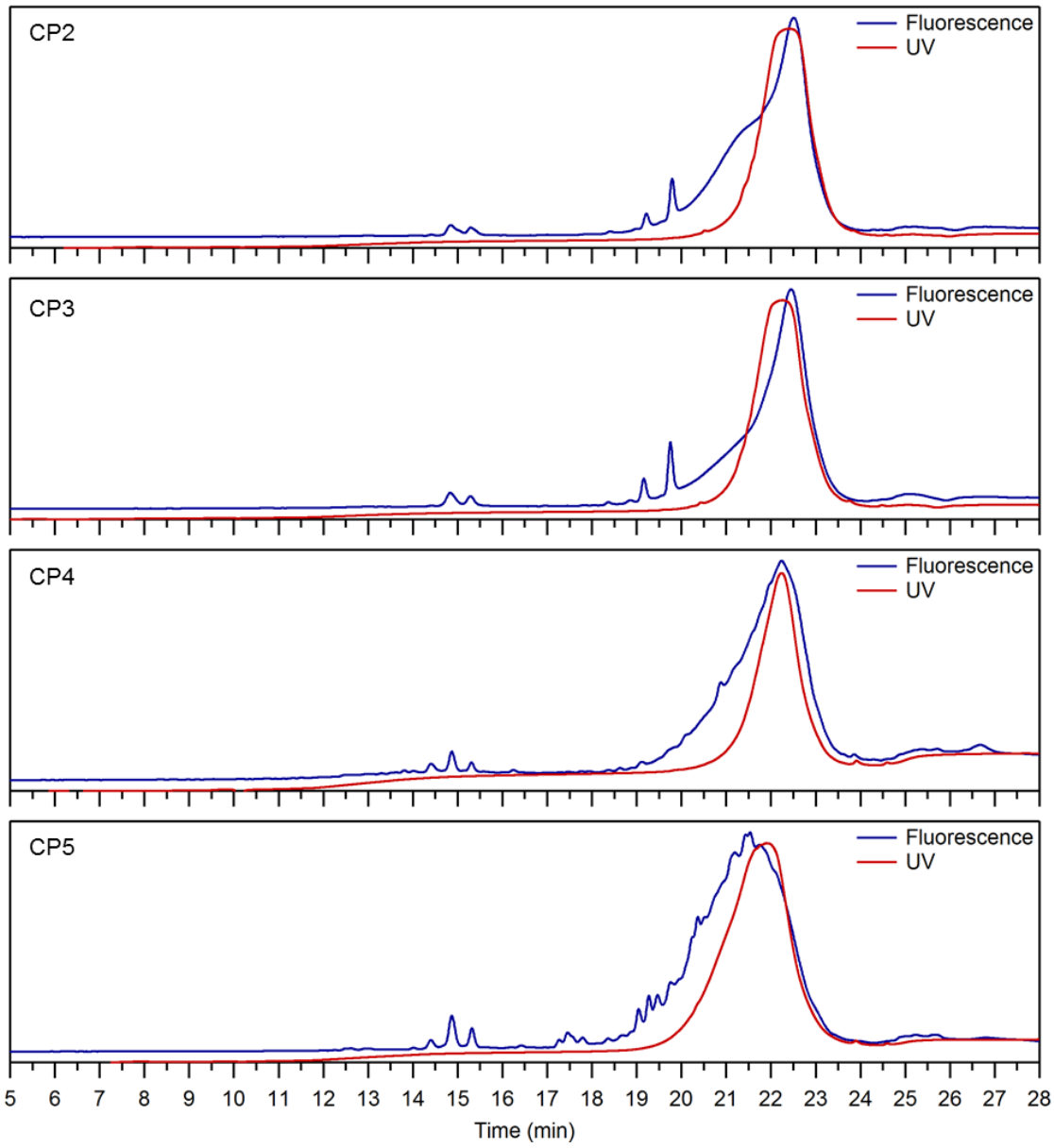

A 5.1: RP-HPLC traces of CP-polymer conjugates CP2-5: 15-100 % Methanol gradient over 30 min. The strong UV absorbance is due to the Tryptophan residues on the CP.

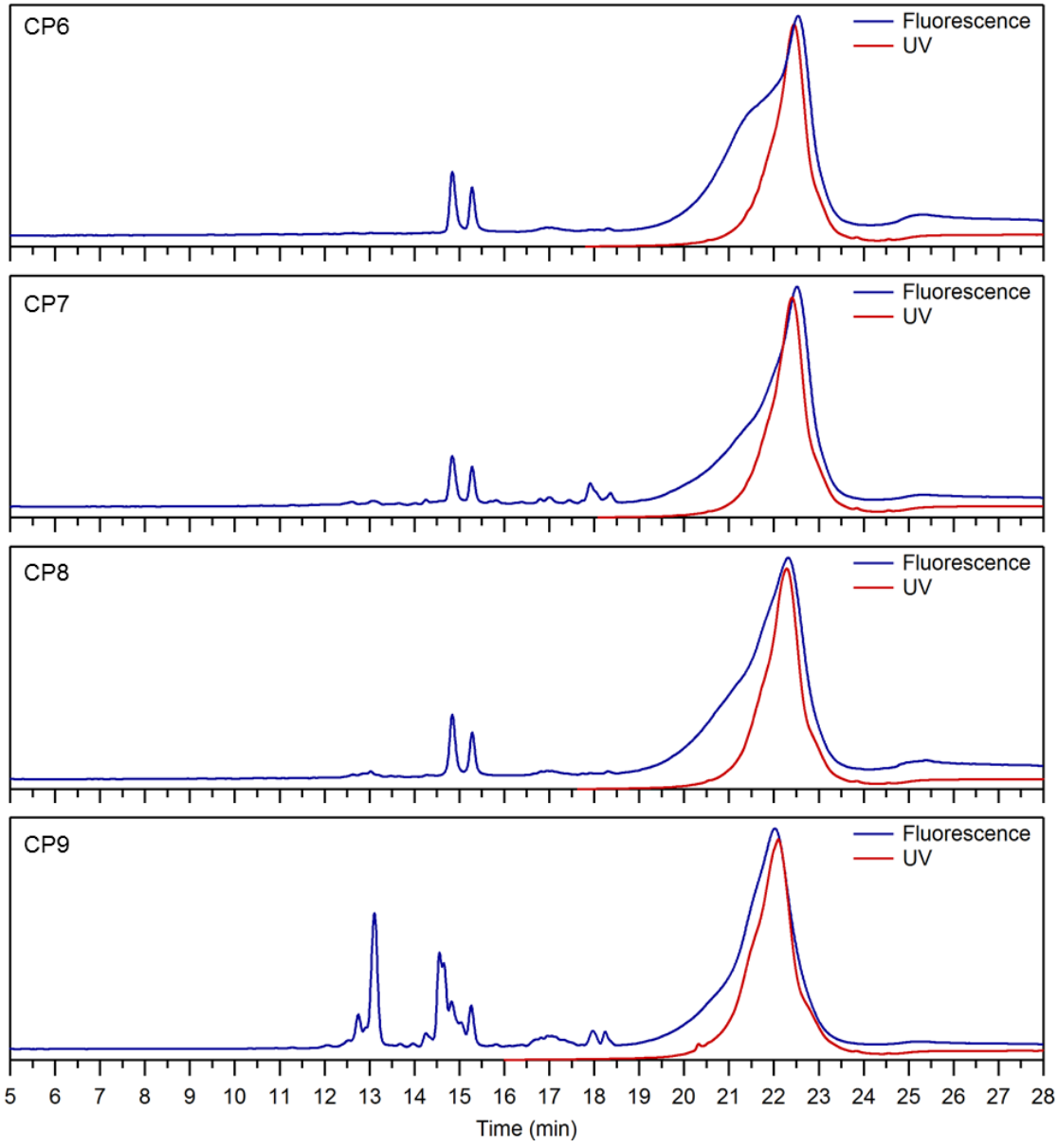

A 5.2: RP-HPLC traces of CP-polymer conjugates CP6 - 9: 15-100 % Methanol gradient over 30 min. The strong UV absorbance is due to the Tryptophan residues on the CP.

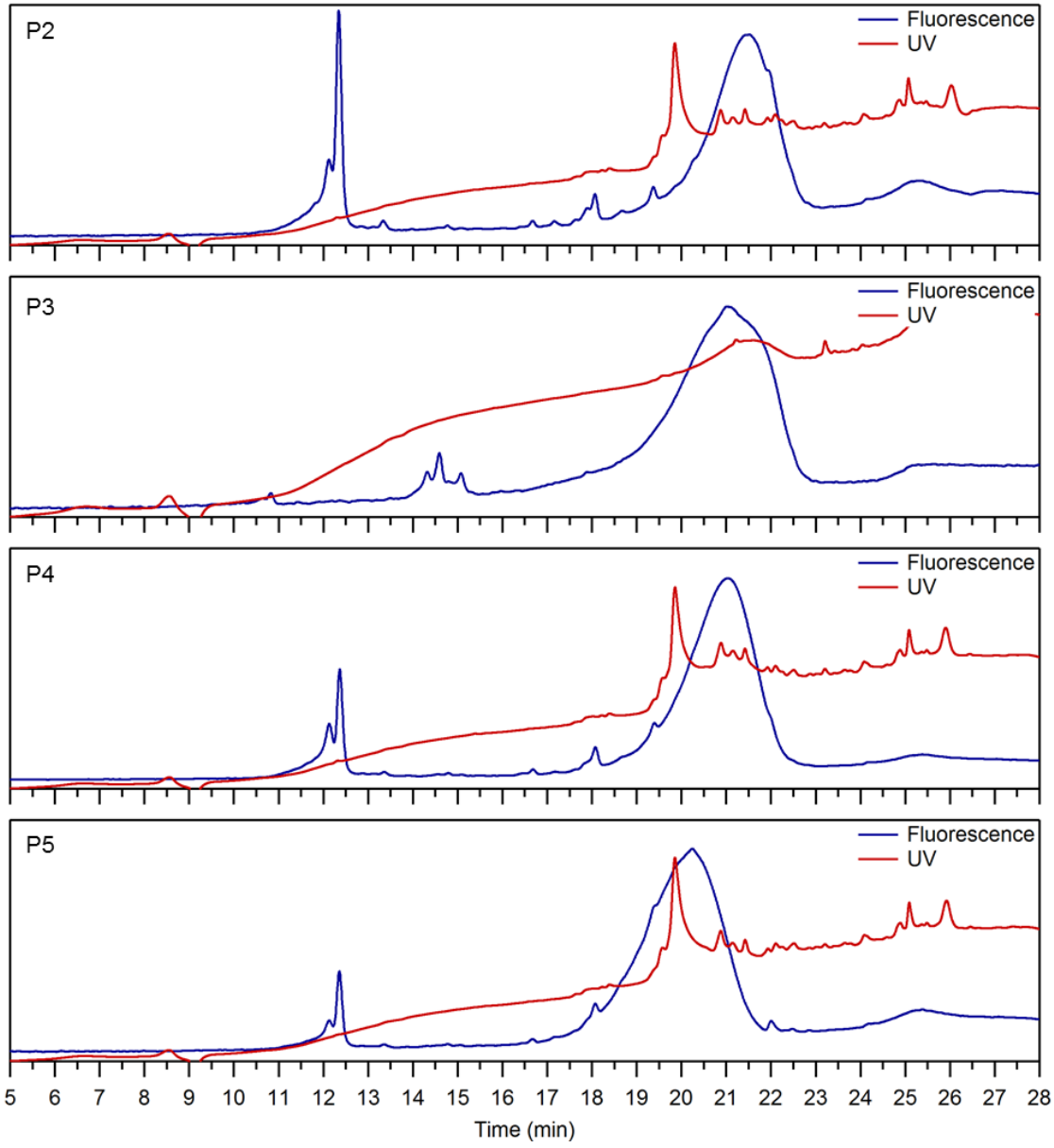

A 5.3: RP-HPLC traces of control polymers P2 - 5: 15-100 % Methanol gradient over 30 min. UV traces for the polymers are weak due to the absence of strongly UV active functionalities.

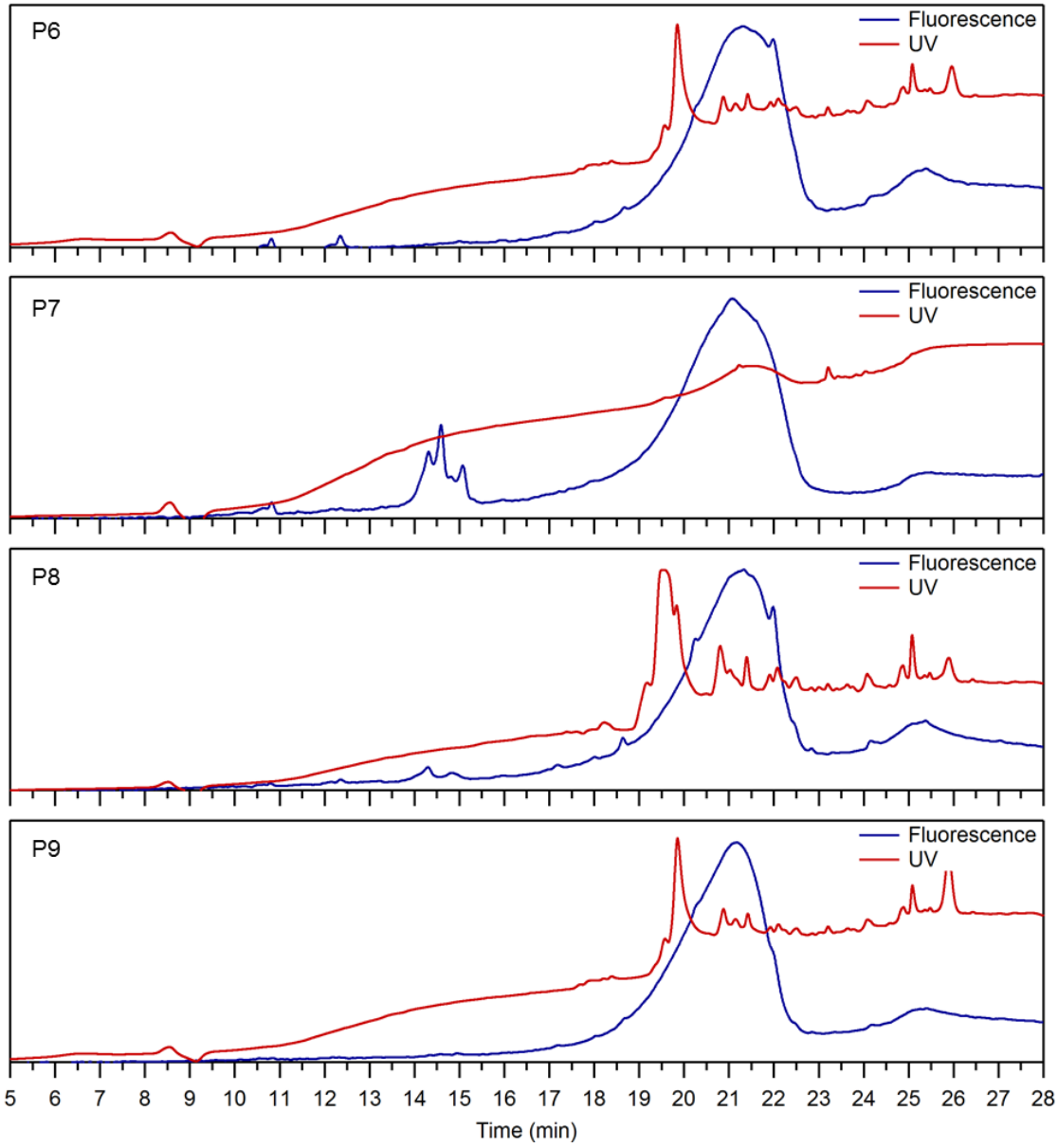

A 5.4: RP-HPLC traces of control polymers P6 - 9: 15 - 100 % Methanol gradient over 30 min. UV traces for the polymers are weak due to the absence of strongly UV active functionalities.

Table A 5.1: Zeta potential and electrophoretic mobility values for charged polymers and conjugates (P2 - 9 and CP2 - 9).

Sample	Charge (%)	Zeta Potential (mV)	Mobility (µmcm/Vs)	Δ Zeta Potential*	Δ Mobility**
CP1	0	-16.70	-1.31	0	0
P2	2	7.37	0.58	-	-
P3	5	6.85	0.54	-	-
P4	10	11.40	0.89	-	-
P5	25	18.93	1.49	-	-
CP2	2	-1.39	-0.11	15.31	1.20
CP3	5	4.59	0.36	21.29	1.67
CP4	10	7.26	0.57	23.96	1.88
CP5	25	27.17	2.13	43.87	3.44
P6	2	3.04	0.24	-	-
P7	5	4.26	0.29	-	-
P8	10	15.72	1.08	-	-
P9	25	28.43	2.23	-	-
CP6	2	-8.29	-0.65	8.41	0.66
CP7	5	3.81	0.30	20.51	1.61
CP8	10	9.68	0.76	26.38	2.07
CP9	25	10.77	0.84	27.47	2.15

* Difference in zeta potential from CP1 value

** Difference in electrophoretic mobility from CP1 value

A5.2 SLS Data

Table A 5.2: Summary of N_{agg} values obtained by static light scattering.

Compound	N_{agg}
CP1	6.2
CP2	2.4
CP3	2.8
CP4	2.3
CP6	2.6
CP7	2.1
CP8	1.9
CP9	0.8

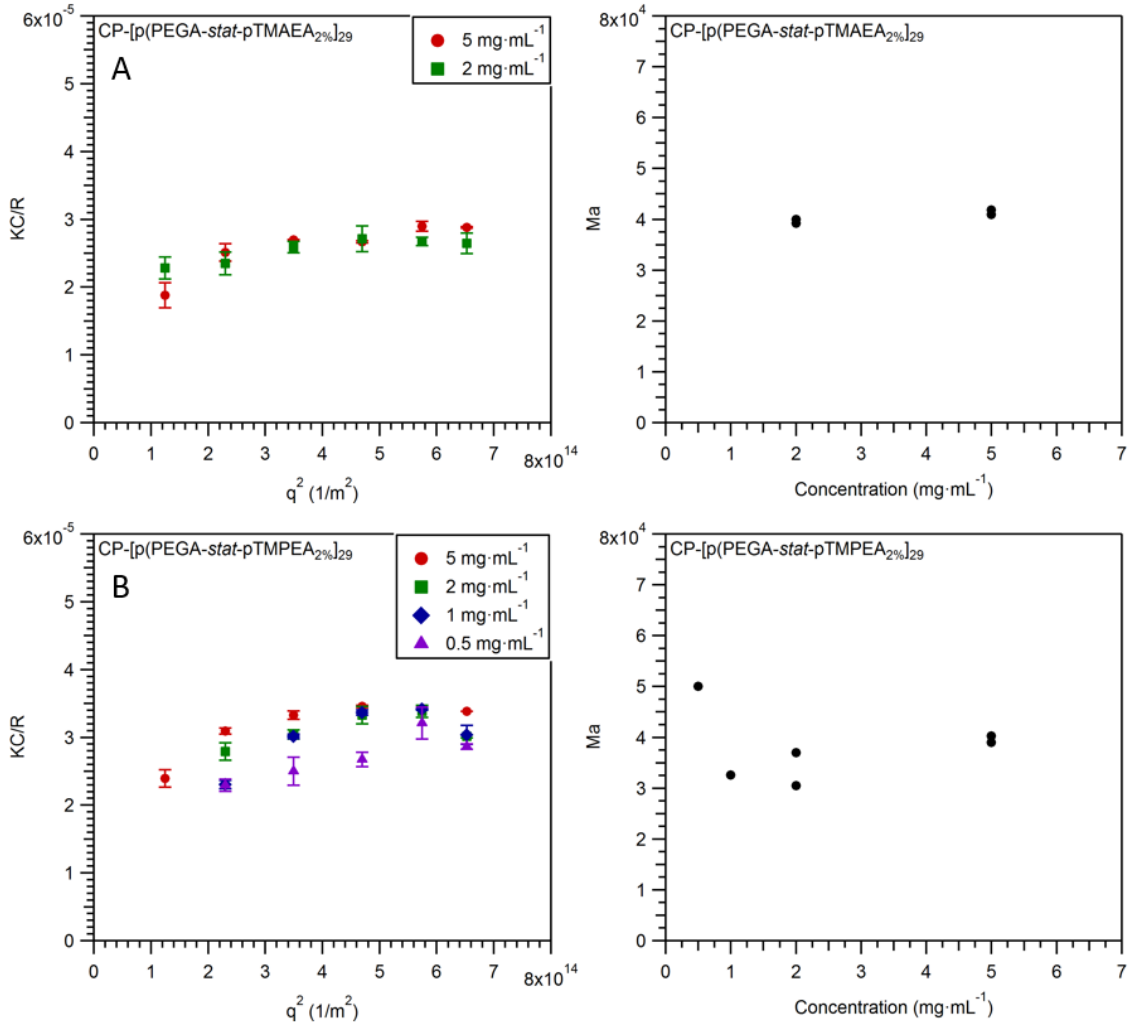

A 5.5: Zimm plots (KC/R) and concentration dependence of molecular weight for (A) CP-[p(PEGA-*stat*-pTMAEA$_{2\%}$]$_{29}$ and (B) CP-[p(PEGA-*stat*-pTMPEA$_{2\%}$]$_{29}$.

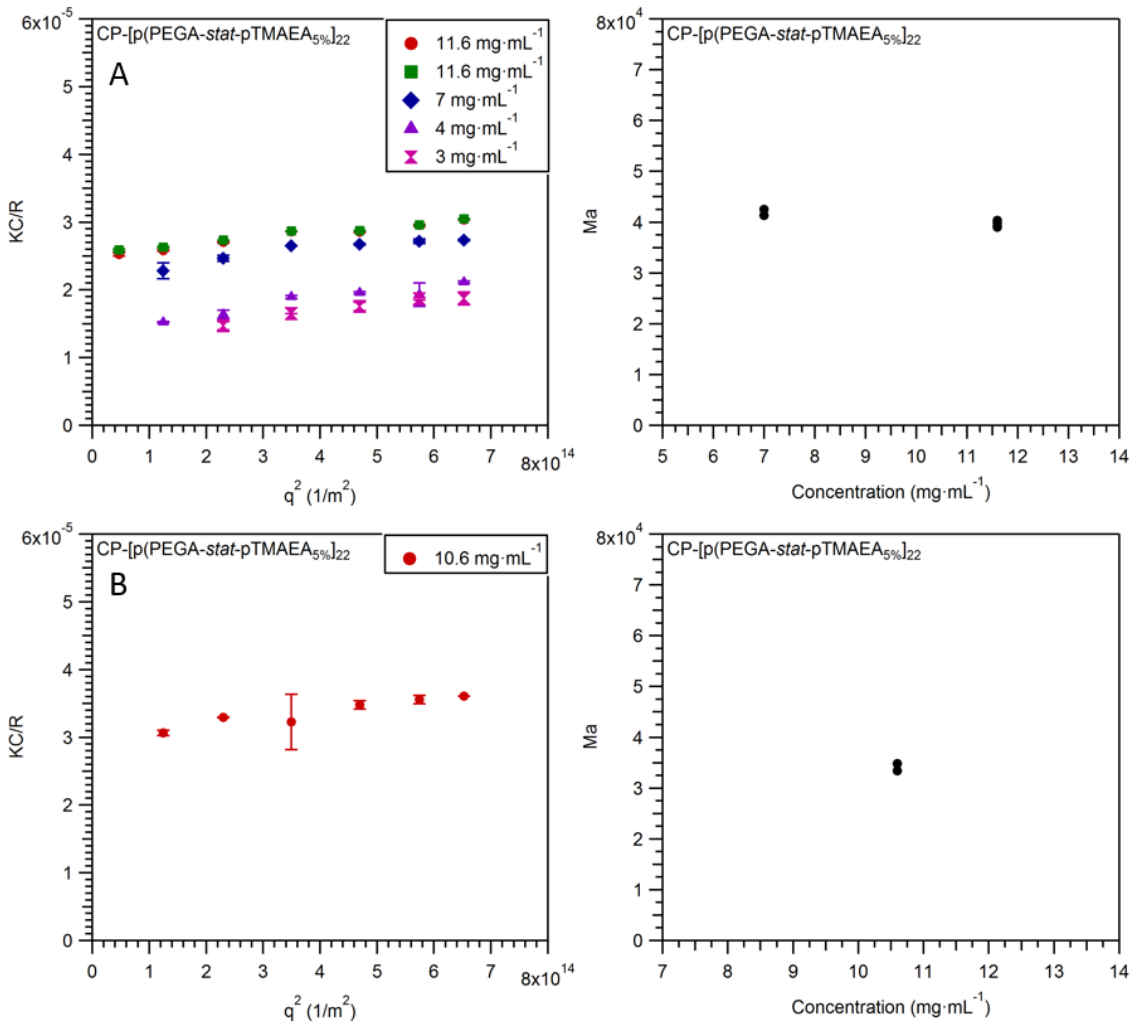

A 5.6: Zimm plots (KC/R) and concentration dependence of molecular weight for (A) CP-[p(PEGA-*stat*-pTMAEA$_{5\%}$]$_{22}$ and (B) CP-[p(PEGA-*stat*-pTMPEA$_{5\%}$]$_{22}$.

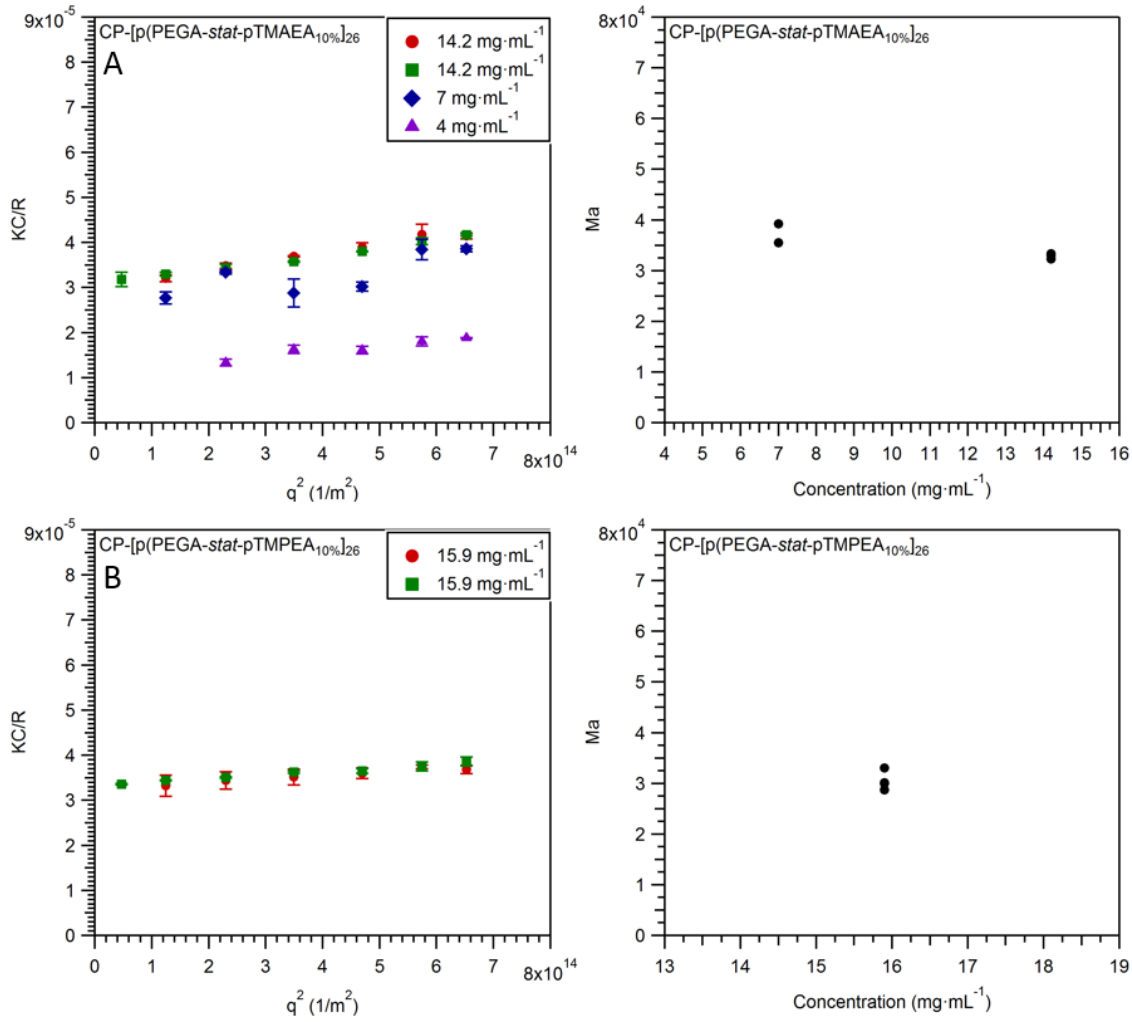

A 5.7: Zimm plots (KC/R) and concentration dependence of molecular weight for (A) CP-[p(PEGA-*stat*-pTMAEA$_{10\%}$]$_{26}$ and (B) CP-[p(PEGA-*stat*-pTMPEA$_{10\%}$]$_{26}$.

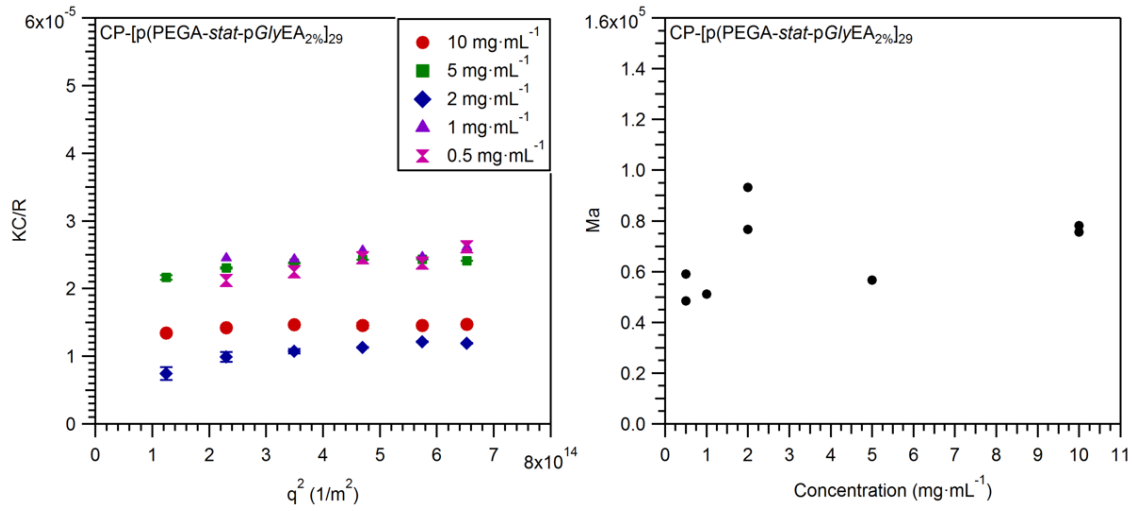

A 5.8: Zimm plots (KC/R) and concentration dependence of molecular weight for CP-[p(PEGA-*stat*-p*Gly*EA$_{2\%}$]$_{29}$.

A5.3 Cell Experiments

A5.3.1 Cell Lines

MDA-MB-231 cells were cultivated in DMEM medium supplemented with 10% foetal bovine serum and 2 mM L-glutamine.

A5.3.2 Cytotoxicity Assay

Cell viability was tested using a standard protocol for the XTT assay.[1] MDA-MB-231 cells were seeded into a 96 well plate at a density of 1×10^4 cells per well and allowed to grow for 24 h. The culture medium was replaced with fresh media containing a series of dilutions of polymer or conjugate (100, 50, 10, 1 and 0.1 μmol· L^{-1}) previously prepared from stock solutions in water at 500 μmol· L^{-1}. Following 24 h incubation, the media was replaced with fresh media and 25 μL of a solution of XTT (1 mg· mL^{-1}) containing *N*-methyl dibenzopyrazine methyl sulfate (PMS) (25 μmol· L^{-1}) in medium was added. Cells were further incubated for 16 h. Absorbance of samples were then measured using a Synergy HTX plate reader at 450 nm and 650 nm (background).

A5.3.3 Cellular Uptake Experiments

MDA-MB-231 cells were seeded into a 24 well plate at a density of 1×10^5 cells per well and allowed to grow for 24 h. The culture medium was replaced with fresh media containing the polymer or conjugate at 50 μmol· L^{-1} previously prepared from stock solutions in DMSO at 50 mmol· L^{-1}. Cells were then incubated for 20 h, after which the medium was removed, the cells were washed with PBS, trypsinised, centrifuged, redispersed in ice-cold PBS and filtered into FACS tube for analysis. Cells were kept in ice to minimise exocytosis of the compounds. For the heterogeneous mixing experiments, CP5 and CP1 or CP9 and CP1 were mixed previously from stock solutions in DMSO at 50 mmol· L^{-1}, vortexed, then water was slowly added (up to 500 μmol· L^{-1}) with frequent vortexing to allow good mixing of the unimers. These solutions were then allowed to mix for 30 minutes at room temperature before preparing the final solution at 50 μmol· L^{-1} in

cell culture media. The geometric mean fluorescence was used as the sample value. Uptake of fluorescein labelled polymers and conjugates was quantified using a Becton-Dickinson FACScan flow cytometer (λ_{ex} = 488 nm, λ_{em} = 530/30 nm). The data in Figure 2 and 3 are representative of two separate experiments where each sample was measured in duplicate (n = 4). All errors reported correspond to the standard deviation from the mean. Statistical analysis was performed using Student's *t*-test and **** $p < 0.0001$.

Table A 5.3: Relative fluorescence of fluorescein-modified compounds in PBS and fluorescence corrections of flow cytometry data.

Compound	Slope[a]	Correction Factor[b]	MDA-MB-231 24 h	
			Original	Corrected
P1	17.6	0.293	46.55	13.64
CP1	18.9	0.315	342.54	107.9
P2	255	4.250	2.32	9.88
P3	638	10.63	0.76	8.13
P4	501	8.350	1.31	10.96
P5	409	6.817	1.87	12.76
CP2	62.7	1.046	18.74	19.60
CP3	62.6	1.044	15.37	16.05
CP4	92.9	1.548	10.43	16.15
CP5	74.7	1.245	14.19	17.67
P6	53.6	0.893	16.32	14.57
P7	24.1	0.402	27.81	11.18
P8	78.7	1.311	7.85	10.29
P9	76.1	1.268	7.77	9.85
CP6	74.2	1.236	13.28	16.42
CP7	98.6	1.644	11.59	19.06
CP8	62.1	1.035	15.99	16.55
CP9	29.3	0.489	46.83	22.90

[a] Fluorescence intensity = $f_{(concentration)}$

[b] Slope/Average of slopes

Table A 5.4: Theoretical and experimental cellular fluorescence from mixtures of assembling and non-assembling conjugates.

Mix	CP1:	CP5	Charge	Theoretical Uptake*	Uptake	Difference
CP5	0	100	25%	19.78	19.78	-
CP1:CP5	60	40	10%	131.0	73.55	-43.9%
CP1:CP5	80	20	5%	168.1	116.2	-30.9%
CP1:CP5	90	10	2%	186.6	145.7	-22.0%
CP1	100	0	0%	205.2	205.2	-
CP9	0	100	25%	22.90	22.90	-
CP1:CP9	60	40	10%	132.3	129.0	-2.50%
CP1:CP9	80	20	5%	168.7	181.2	7.43%
CP1:CP9	90	10	2%	186.9	206.2	10.3%
CP1	100	0	0%	205.2	205.2	-

*Theoretical uptake calculated by multiplying the respective CP1, CP5, or CP9 by their respective ratio and added together.
i.e. CP1/CP5 = $90:10 = (205.2 \times 0.9) + (19.78 \times 0.1) = 186.6$

A5.4 References

1. Mosmann, T. *Journal of Immunological Methods* **1983,** 65, (1), 55-63.